Inflammatory processes and TLR4 signaling influenced by nitrated proteins and related substances

Kira Ziegler

(geb. Becker)

geb. am 25.03.1988
in Mainz

Dissertation

zur Erlangung des Grades eines 'Doctor rerum naturalium (Dr. rer. nat.)'
der Fachbereiche:

08 – Physik, Mathematik und Informatik,
09 – Chemie, Pharmazie und Geowissenschaften,
10 – Biologie,
Universitätsmedizin
der Johannes Gutenberg-Universität in Mainz
Max Planck Graduate Center

Mainz, Juli 2019

1. Berichterstatter:
2. Berichterstatter:

Declaration

I hereby declare that I wrote the dissertation submitted without any unauthorized external assistance and used only sources acknowledged in the work. All textual passages which are appropriated verbatim or paraphrased from published and unpublished texts as well as all information obtained from oral sources are duly indicated and listed in accordance with bibliographical rules. In carrying out this research, I complied with the rules of standard scientific practice as formulated in the statutes of Johannes Gutenberg-University Mainz to insure standard scientific practice.

Mainz, July 2019

Abstract

Inflammatory processes are involved in numerous acute and chronic diseases. In this context, the Toll-like receptor 4 (TLR4) plays a central role by detecting pathogen- and damage-associated molecular patterns such as lipopolysaccharides and various proteins. For example, the TLR4 can be stimulated by nutritional amylase trypsin inhibitors (ATI), nongluten proteins that are associated with gluten containing grains like wheat. In the gut, ATI can activate immune cells, especially myeloid cells (macrophages and dendritic cells), via TLR4, thereby initiating or enhancing intra- and extra-intestinal inflammation.

Upon stimulation of the TLR4 and in the course of inflammation, pro-inflammatory cytokines are secreted and reactive oxygen- and nitrogen species are generated. Among these reactive species is peroxynitrite, which is an anti-microbial and protein-nitrating agent. Proteins can also be nitrated by reactive species in the environment such as nitrogen oxides and ozone in polluted air. Either way, nitration leads to modifications in the chemical structure of proteins and can result in altered immune responses and allergic reactions.

This dissertation investigates the immunostimulatory effects of native and nitrated ATI and other TLR4 stimulating proteins. For this purpose, I developed and established a new stable monoclonal TLR4 reporter cell line to measure simultaneously TLR4 stimulation and toxic effects. Moreover, I optimized a method for the isolation and culturing of human primary macrophages tailored to the requirements of single molecule microscopy. This method revealed donor-dependent differences in TLR4 surface clustering on the nanoscale induced by nitrated ATI, which were not accessible to detection by conventional methods.

The key scientific findings of this dissertation can be summarized as follows: Nitrated ATI were found to enhance the immune response of primary human myeloid immune cells, resulting in increased nuclear translocation of NF-κB, secondary T cell proliferation, and pro-inflammatory cytokine secretion. Moreover, chemical modifications by peroxynitrite were found to amplify the inflammatory potential of several TLR4-stimulating proteins (ATI, α-synuclein, heat shock protein 60, high mobility group protein B1, grass pollen allergen Phl p 5). These findings suggest that protein nitration and related chemical modifications, such as oligomerization, may not only be a result of inflammation, but may also trigger or maintain inflammatory processes in a self-amplifying feedback cycle involving Toll-like receptors.

In addition to the above studies and results, the pro- and anti-inflammatory effects of herbal extracts and Cyanobacteria were investigated: Two herbal extracts with previously unknown anti-inflammatory toll like receptor 2 and 4 mediated activity were identified, and two species of Cyanobacteria were found to induce pro-inflammatory TLR4 signaling.

Overall, this dissertation provides new insights into the molecular mechanisms of inflammation, their potentiation by intrinsic and environmental factors, especially the process of protein nitration, and potential perspectives of medical anti-inflammatory treatment.

Zusammenfassung

Akute und chronische Entzündungen sind Bestandteil und Prozess vieler Krankheiten. Hierbei spielt der Toll-like-Rezeptor 4 (TLR4) eine zentrale Rolle, da er schadens- und pathogen-assoziierte Muster wie bakterielle Lipopolysaccharide und verschiedene Proteine erkennt. Beispielsweise kann der TLR4 durch Amylase-Trypsin-Inhibitoren (ATI) stimuliert werden, welche als Bestandteil von glutenhaltigem Getreide (zum Beispiel Weizen) über die Nahrung aufgenommen werden. Die durch ATI vermittelte TLR4-Stimulierung kann myeloide Immunzellen wie Makrophagen und dendritische Zellen im Darm aktivieren und intra- und extraintestinale Entzündungen auslösen.

Im Zuge der Entzündungsreaktionen werden entzündliche Zytokine ausgeschüttet und reaktive Sauerstoff- und Stickstoffspezies gebildet. Zu diesen reaktiven Spezies zählt Peroxynitrit, welches antimikrobiell wirkt und zudem Proteine nitrieren kann. Proteine können auch durch umweltbedingte reaktive Spezies wie Stickstoffoxide und Ozon nitriert werden. In beiden Fällen hat die Nitrierung Auswirkungen auf die chemische Struktur des Proteins, wodurch seine immunologische und allergene Reaktivität beeinflusst werden kann.

Im Rahmen dieser Doktorarbeit habe ich die immunstimulierende Wirkung von nativen und nitrierten ATI sowie von weiteren Proteinen, welche den TLR4 stimulieren können, untersucht. Zwecks simultaner Detektion von TLR4-Stimulierung und von toxischen Effekten wurde eine stabile, monoklonale Zelllinie entwickelt und etabliert. Zusätzlich wurde eine Methode zur Kultivierung von primären humanen Makrophagen optimiert, welche maßgeschneidert für die Einzelmolekül-Lokalisationsmikroskopie ist. Mit Hilfe dieser Methode konnte eine spenderabhängige TLR4-Cluster-Bildung im Nanobereich sichtbar gemacht werden, was mittels konventioneller Methoden nicht möglich gewesen wäre.

Die Hauptergebnisse dieser Arbeit können wie folgt zusammengefasst werden: Es wurde deutlich, dass nitrierte ATI eine erhöhte Immunreaktion bei primären humanen myeloiden Immunzellen hervorrufen. Dies zeigte sich in einer erhöhten Translokation von NF-κB in die Zellkerne, einer verstärkten sekundären T-Zell-Proliferation sowie einer gesteigerten Produktion von entzündlichen Zytokinen. Zusätzlich konnte für weitere TLR4-stimulierende Proteine (ATI, α-Synuclein, Hitzeschockprotein 60, High-Mobility-Group-Protein B1, Pollenallergen Phl p 5) nach der Behandlung mit Peroxyntirit eine erhöhte Entzündungsreaktion festgestellt werden. Die Ergebnisse deuten darauf hin, dass die Protein-Nitrierung und die damit verbundenen Mechanismen, wie zum Beispiel die Oligomerisierung, nicht nur ein Resultat entzündlicher Reaktionen sind. Vielmehr werden diese entzündlichen Reaktionen in einem selbstverstärkenden Prozess über Toll-like-Rezeptoren ausgelöst oder aufrechterhalten.

Über meine oben genannten Forschungen und die damit verbundenen Resultate hinausgehend wurden ethanolische Pflanzenextrakte sowie Cyanobakterien hinsichtlich ihrer

entzündungshemmenden und -auslösenden Wirkung untersucht. Dabei konnte bei zwei Pflanzenextrakten eine durch die Toll-like-Rezeptoren 2 und 4 vermittelte antientzündliche Wirkung identifiziert werden. Weiterhin wurden zwei Cyanobakterien-Spezies gefunden, die eine TLR4-vermittelte entzündliche Wirkung aufweisen.

Zusammenfassend bietet diese Dissertation neue Erkenntnisse über die molekularen Mechanismen entzündlicher Prozesse sowie über deren Potenzierung durch intrinsische und umweltbedingte Faktoren, insbesondere durch die Protein-Nitrierung. Sie zeigt außerdem mögliche Perspektiven der entzündungshemmenden medizinischen Behandlung auf.

Contents

1. Introduction and Motivation

1.1 Inflammatory Processes

Inflammation describes the body's own protective reaction upon damage. The protective reaction comprises defense, repair and restoration of the tissue, whereas damage can be induced by infectious bacteria, viruses, fungi, injury, radiation or chemical substances. Inflammatory reactions are primary driven by cells of the innate immune system like macrophages, dendritic cells (DC), granulocytes and natural killer cells. As inflammatory response they release toxic agents and signaling molecules to fight invading microbes, recruit further immune cells and initiate wound healing. If an acute inflammatory reaction is not timely and locally terminated the host develops a chronic inflammation, which is characterized by a cyclic and repetitive process between tissue damage and repair (Schett and Neurath, 2018; Lucas and Maes, 2013). Inflammation is part of many diseases such as rheumatoid arthritis, chronic obstructive pulmonary disease (COPD), Parkinson's and Alzheimer's disease, inflammatory bowel disease (IBD) or non-alcoholic steatohepatitis (Schett and Neurath, 2018; Chen *et al.*, 2018).

Sensing of damage and pathogen associated molecular patterns (DAMPs/PAMPs) is mainly performed by receptors of the four pattern recognition receptor families: Toll-like receptors (TLR), C-type lectin receptors, NOD-like receptors and RIG-I-like receptors (Jang *et al.*, 2015). Here especially the TLR-family, consisting of 10 receptor types, plays a central role as each receptor type is specialized sensing various DAMPs or PAMPs. One of the best studied TLRs is the TLR4 which recognizes a broad spectrum of agonists, such as bacterial lipopolysaccharides (LPS), several DAMPs, allergens (Kawasaki and Kawai, 2014) and also amylase trypsin inhibitors (ATI) (Junker *et al.*, 2012; Cuccioloni *et al.*, 2017). Upon stimulation TLR4 dimerizes and activates various intracytoplasmic kinases, causing the nuclear translocation of different transcription factors. Of special interest is the *nuclear factor kappa-light-chain-enhancer of activated B cells* (NF-κB, p50/p65), which controls about 250 mostly pro-inflammatory genes (Gilmore, 2018; Kawai and Akira, 2010; Kawasaki and Kawai, 2014).

Further triggers of inflammation are anthropogenic pollutants such as fine particulate matter and environmental factors, like ozone and nitrogen dioxide. Inhaled air particulate matter modifies the oxidant system in the lung which causes production of reactive oxygen species (ROS) and epithelial damage. In turn allergens or other substances can penetrate the epithelial barrier more easily, thereby triggering acute or chronic inflammation (Rao *et al.*, 2018; Reinmuth-Selzle *et al.*, 2017). Additionally, airborne bioparticles can be modified by anthropogenic pollutants. The modified bioparticles possess altered chemical and structural

properties, which induce or potentiate inflammation and immunogenic reactions in the body (Reinmuth-Selzle *et al.*, 2017)(Figure1).

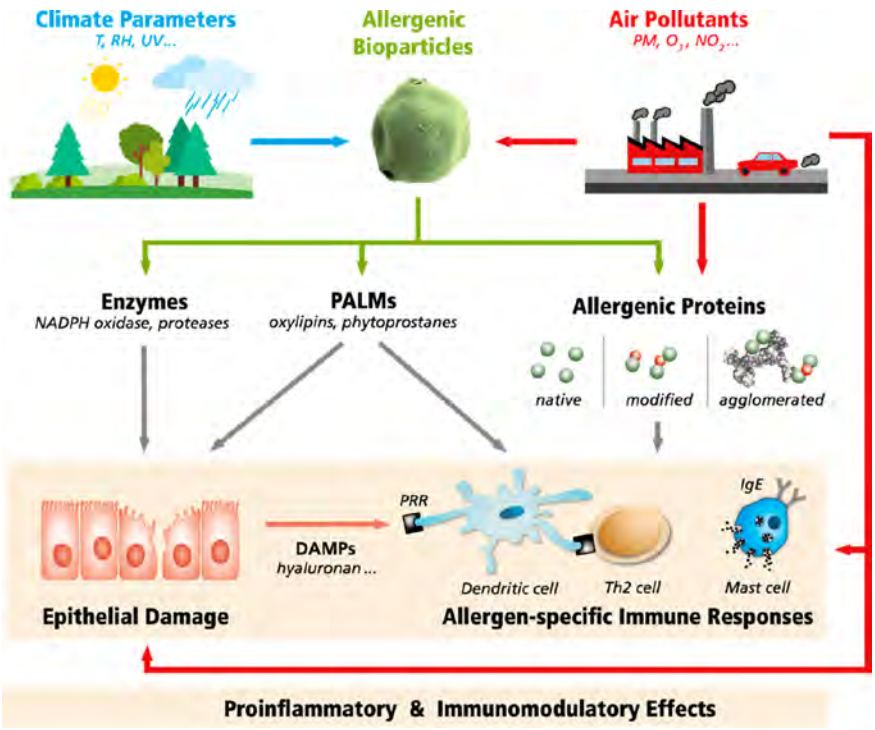

Figure 1: Sources and modifications of bioparticles which have pro-inflammatory and immunomodulatory effects.

Both, exogenous environmental factors and endogenous inflammation associated factors can modulate diverse immune reactions. Abbreviations: Temperature (T), relative humidity (RH), ultraviolet (UV) radiation, particulate matter (PM), ozone and nitrogen oxides (O3, NO_x), reduced nicotinamide adenine dinucleotide phosphate (NADPH) oxidase, pollen-associated lipid mediators (PALMs), damage-associated molecular patterns (DAMPs), pattern recognition receptors (PRR), type 2 T helper (Th2) cells, immunoglobulin E (IgE), allergenic proteins (green dots), and chemical modifications (red dots). Figure is adopted from (Reinmuth-Selzle et al., 2017).

For example, due to enhanced stabilization the modified bioparticles will be prolonged degraded in immune cells which causes enhanced antigen presentation inducing thereby increased immune stimulation (Untersmayr *et al.*, 2010; Karle *et al.*, 2012). Moreover, new epitopes can be introduced or binding properties of antibodies can be changed, due to amino acid modification such as nitrotyrosine or dityrosine formation during protein nitration. Due to modified ligand binding sites an adjuvant function may be introduced or an existing adjuvant function can be potentiated. Chemical modification of bioparticles or proteins induces also agglomeration or oligomerization, such as protein-protein cross linking by dityrosine formation, or agglomeration between proteins with other bioparticles, e.g. pollen particles or

soot. Both mechanisms can multiply or shield existing epitopes which in turn may enhance cross linking of effector cell receptors and immune reactivity (Scholl *et al.*, 2005; Rouvinen *et al.*, 2010; Ackaert *et al.*, 2014; Gruijthuijsen *et al.*, 2006; Reinmuth-Selzle *et al.*, 2017).

Accompanied with inflammatory conditions is the synthesis of reactive oxygen and nitrogen species (ROS/RNS). These bi-functional species serve as cellular signaling molecules as well as anti-microbial agents (Sies *et al.*, 2017). Major sources of superoxide are NADPH oxidases (NOX) and complex I of the respiratory chain in mitochondria by interaction with ubiquitinated ECSIT (Katsuyama, 2010; West *et al.*, 2011). Moreover, inducible *Nitric Oxide Synthase 2* (NOS2 or iNOS) provides during inflammation enhanced amounts of nitric oxide. Additionally, other reactive species are formed by secondary reaction, like peroxynitrite, hydrogen peroxide, nitrogen dioxide, hypochlorite and hydroxyl radical.

1.2 Protein Nitration

Nitration of proteins can be induced by two independent processes: Exogenously in the environment, or endogenously in the body. Causal agents in these mechanisms are reactive species like ozone, hydroxyl radicals, hydrogen peroxide, superoxide, nitric oxide or peroxynitrite. Exogenous nitration can happen during humid summer smog conditions, comprising high levels of ozone, nitrogen oxide, UV radiation and humidity (Franze *et al.*, 2005; Walcher *et al.*, 2003; Yang *et al.*, 2010; Zhang *et al.*, 2011; Shiraiwa *et al.*, 2012; Reinmuth-Selzle *et al.*, 2014). Endogenous nitration occurs under inflammatory conditions, where typically high concentrations of superoxide and nitric oxide are generated, what leads to the formation of peroxynitrite, a potent nitrating agent (Galinanes and Matata, 2002; Salvemini *et al.*, 2006; Reinmuth-Selzle *et al.*, 2014; Ferrer-Sueta *et al.*, 2018; Selzle *et al.*, 2013). Therefore, nitrotyrosine is an important biomarker for inflammatory and oxidative stress in the context of many diseases (Greenacre and Ischiropoulos, 2001; Murata and Kawanishi, 2004; Ghosh *et al.*, 2006; Ischiropoulos, 2009).

The oxidants react in a two-step mechanism at the aromatic ring of the amino acid tyrosine, resulting in the formation of a reactive oxygen intermediate (ROI), namely a tyrosyl radical (Figure 2). In the second step the free radical on the tyrosyl ring reacts either with nitrogen dioxide (NO_2) to 3-nitrotyrosine or with a second tyrosyl radical to dityrosine, whereby protein dimers or higher order oligomers are formed (Walcher *et al.*, 2003; Franze *et al.*, 2005; Ischiropoulos, 2009; Shiraiwa *et al.*, 2012; Radi, 2013; Reinmuth-Selzle *et al.*, 2014; Liu *et al.*, 2017; Kampf *et al.*, 2015). As during the reaction of protein nitration such as by peroxynitrite, not only nitrotyrosine but also intra- and inter-molecular dityrosine formation occurs, in the course of this thesis the term *peroxynitrite modified proteins* will refer to the aforementioned mechanisms.

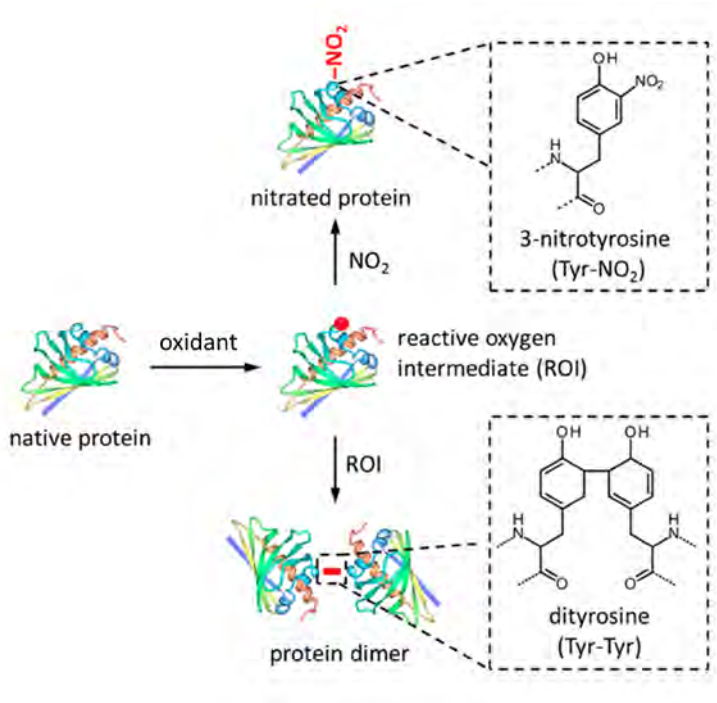

Figure 2: Nitrotyrosine and dityrosine formation.

A two-step reaction mechanism facilitates the formation of nitro- or dityrosine on the protein tyrosine residue. In the first step an oxidizing agent (such as ozone, hydroxyl radicals, hydrogen peroxide, superoxide, nitric oxide or peroxynitrite) reacts with the aromatic ring of tyrosine to a reactive oxygen intermediate (ROI). In the next step the ROI reacts either with NO_2 to nitrotyrosine or with a second ROI to dityrosine, forming thereby a protein dimer. Figure is modified from (Reinmuth-Selzle et al., 2017).

Protein nitration is an irreversible mechanism that has major impact on the structural and chemical features of the protein, as 3-nitrotyrosine lowers the pKa value, which in turn affects conformation and function of the protein (Turko and Murad, 2002; Hodara *et al.*, 2004). Moreover, dityrosine can be formed during the nitration process which causes protein cross linking (Kampf *et al.*, 2015) and thereby stabilization. Therefore, the nitrated and oligomerized proteins prolong degradation in APC and in turn promote antigen presentation on the MHCII (Untersmayr *et al.*, 2010; Karle *et al.*, 2012). Additionally, protein-aggregates may shield or multiply epitopes and enhance cross-linking of the effector cell receptors.

All together these altered conformational and functional changes of the nitrated proteins result in an increased immune reactivity, which was observed for different nitrated proteins (Gruijthuijsen *et al.*, 2006; Untersmayr *et al.*, 2010; Karle *et al.*, 2012; Ackaert *et al.*, 2014; Lang-Yona *et al.*, 2016; Ziegler *et al.*, 2019) that might contribute to the rise and prevalence of allergies.

1.3 Amylase Trypsin Inhibitors (ATI)

ATI are a family of mono-, di- and tetrameric non-gluten proteins with a monomer size range of 12-15 kDa which cause mainly extra-intestinal symptoms of non-celiac non-allergy wheat sensitivity (NCWS) (Fasano *et al.*, 2015; Schuppan *et al.*, 2015; Schuppan and Zevallos, 2015; Leccioli *et al.*, 2017). Especially the tetrameric CM3 and dimeric 0.19 ATI variants possess high immune stimulatory capacity by stimulation of the innate immune receptor TLR4 (Junker *et al.*, 2012; Cuccioloni *et al.*, 2017). Additionally, in Baker's Asthma, a classical IgE mediated allergy, ATI are major allergens (Walusiak *et al.*, 2004; Tatham and Shewry, 2008). ATI are part of the protein fraction of all gluten containing grains, like wheat, barley and rye where they represent 2-4% of the total protein (Dupont *et al.*, 2011). Their regular function in plants are the modulation of germination processes (Finnie *et al.*, 2002) and possibly defending of pathogens by blocking the amylase/trypsin activity in their salvia (Payan, 2004). As wheat is a major staple, the daily intake of an adult person is about 250 g, mainly as processed bread or pasta, which equals approximately 0.5 g to 1.0 g of ATI (Fasano *et al.*, 2015). Remarkably, ATI are resistant to food processing and to proteolysis in the gut where they stay biologically active and remain able to stimulate immune cells in the *lamina propria* of the gut lining that appear to emigrate to the surrounding and mesenteric lymph nodes after TLR4 stimulation (Zevallos *et al.*, 2017).

Several *in vivo* studies have demonstrated that an ATI-enriched diet induces and worsens intestinal and extra intestinal inflammation in an IgE and TLR4 mediated manner (Bellinghausen *et al.*, 2019; Zevallos *et al.*, 2017; Zevallos *et al.*, 2018). Moreover, ATI open intestinal tight junctions, explaining their pro-inflammatory activity via enhanced entry of potentially toxic luminal components and allergens (Caminero *et al.*, 2019). Especially monocytes and dendritic cells of the intestine are stimulated by ATI via TLR4 and release pro-inflammatory cytokines, which activate further immune cells and in turn initiate and fuel ongoing inflammation (Fasano *et al.*, 2015; Schuppan and Zevallos, 2015; Schuppan *et al.*, 2015) (Figure 3).

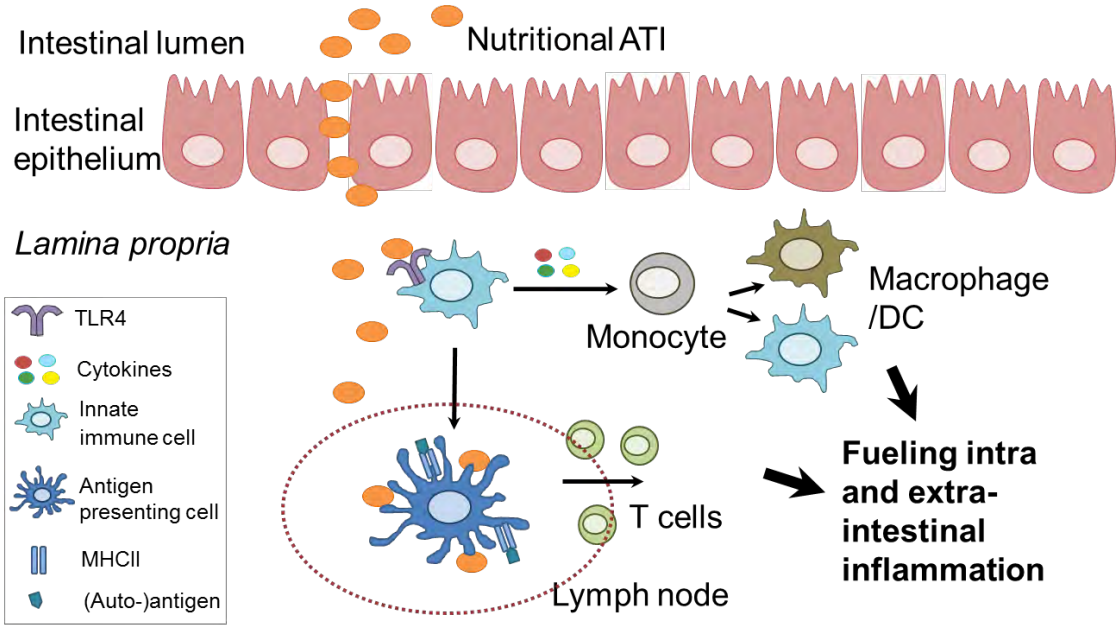

Figure 3: Schematic activation mechanisms of different immune cells by ATI in the gut.

ATI from food stay biologically active and pass active or passively the intestinal epithelium. In the lamina propria ATI stimulate TLR4 on innate immune cells e.g. macrophages and dendritic cells (DC) which subsequently release cytokines such as IL-8, IL-5 and MCP1. This leads to the recruitment and activation of further innate immune cells, especially monocytes from the blood, which differentiate into macrophages and dendritic cells. The activated immune cells possess an enhanced antigen presentation via major histocompatibility complex two (MHCII), mainly as mature DC. After migration to the surrounding draining lymph nodes, they activate T cells. In the case an autoimmune diseases or intestinal or pulmonary allergies, already autoantigen primed T cells will be further stimulated by the gut-emigrating ATI-activated myeloid cells. Thereby ATI possess an additional adjuvant effect by previous activation of macrophages and DC that represent the major antigen presenting cells for T cell activation. Together ATI stimulate innate and secondarily adaptive immune responses, which fuels intra and extra-intestinal inflammation. Figure is based on (Fasano et al., 2015).

1.4 Research Objectives

The focus of this work is the immunological process of inflammation, how it is triggered, enhanced and prevented. Therefore, the modulation of innate and adaptive pro-inflammatory reactions by natural compounds such as herbal extracts and Cyanobacteria as well as chemical modified proteins were studied. A central part of this work covers altered pro-inflammatory effects by nitrated proteins. Since nitration occurs under environmental and inflammatory conditions, protein nitration is a highly relevant mechanism and influences health aspects.

The topic of protein nitration was already initiated by Weller, Pöschl and colleagues (Franze *et al.*, 2005; Reinmuth-Selzle *et al.*, 2014; Kampf *et al.*, 2015) which observed changes in the structural properties of the nitrated birch pollen allergen Bet v 1a. Moreover, the modified Bet v 1a and other proteins were found to possess an altered immune reactivity (Gruijthuijsen *et al.*, 2006; Untersmayr *et al.*, 2010; Karle *et al.*, 2012; Ackaert *et al.*, 2014; Lang-Yona *et al.*, 2016), but the underlying mechanisms are still elusive. Based on this knowledge, my goal was to investigate to which degree nitration of TLR4 stimulating proteins alters their immune response. As ATI were intensively studied by Schuppan and colleagues (Junker *et al.*, 2012; Schuppan and Zevallos, 2015; Bellinghausen *et al.*, 2019; Caminero *et al.*, 2019) and exhibit strong immune stimulation via TLR4. My aim was to elucidate whether nitration of ATI affect or enhances this function. Various immunologic read outs, assessing cytokine release, secondary T cell proliferation, TLR4 stimulation and NF-kB translocation to the nucleus, demonstrated that nitrated ATI show an enhanced immunogenicity compared to native ATI (Ziegler *et al.*, 2019).

To test whether nitration also enhances the immunostimulatory function of other proteins, we modified TLR4-stimulating proteins by peroxynitrite from three different categories: DAMPs, disease related proteins and allergens. Indeed, we found for several such treated proteins (ATI, α-synuclein, heat shock protein 60, high mobility group protein B1, grass pollen allergen Phl p 5) an amplified inflammatory reaction. Protein nitration is often regarded as a side effect of inflammation. Here we find strong indications for a peroxynitrite driven, self-enhancing mechanism of inflammation, which may apply generally for many diseases.

2. Results and Conclusions

2.1 Overview

Altogether the work within my PhD study focused on pro- and anti-inflammatory immune reactions and especially the influence of protein nitration (Figure 3). The main results can be summarized as follows:

i. One important finding of my thesis are the enhanced immune reactions triggered by nitrated ATI. Therefore I developed a new HeLa TLR4 dual reporter cell line as fast and robust *in vitro* read out system detecting simultaneous TLR4 activation and toxicity, which enabled me to show that ATI induce enhanced TLR4 stimulation. Additional immunologic read outs based on human primary myeloid cells demonstrated that the nitrated ATI trigger enhanced secondary T cell proliferation and inflammatory cytokine release (Ziegler *et al.*, 2019)

ii. For the project “Nanoscale distribution of TLR4 on primary human macrophages stimulated with LPS and ATI”, I developed a protocol tailored to the needs of single molecule localization microscopy, regarding preparation and culturing of human primary macrophages. We found an increased number of TLR4 clusters after stimulation with LPS, ATI or nitrated ATI with strong donor dependent variations (Neumann *et al.*, 2019).

iii. My latest results are indicating that several TLR4 stimulating proteins induce enhanced NF-κB as well as TLR4 stimulation after peroxynitrite treatment. This suggests the existence of a so far unknown peroxynitrite driven feed forward mechanism in inflammation. Ongoing studies should provide a more comprehensive picture whether peroxynitrite induced protein nitration or oligomerization is the causative agent, and which receptors are most prone for sensing (Ziegler *et al.* in preparation).

iv. As TLR4 stimulation plays a central role in inflammatory reactions, also other compounds were tested using my newly developed HeLa TLR4 dual reporter cell line. This enabled me to contribute to two publications characterizing pro- or anti-inflammatory properties and toxicity of various herbal extracts and Cyanobacteria species (Schink *et al.*, 2018; Lang-Yona *et al.*, 2018).

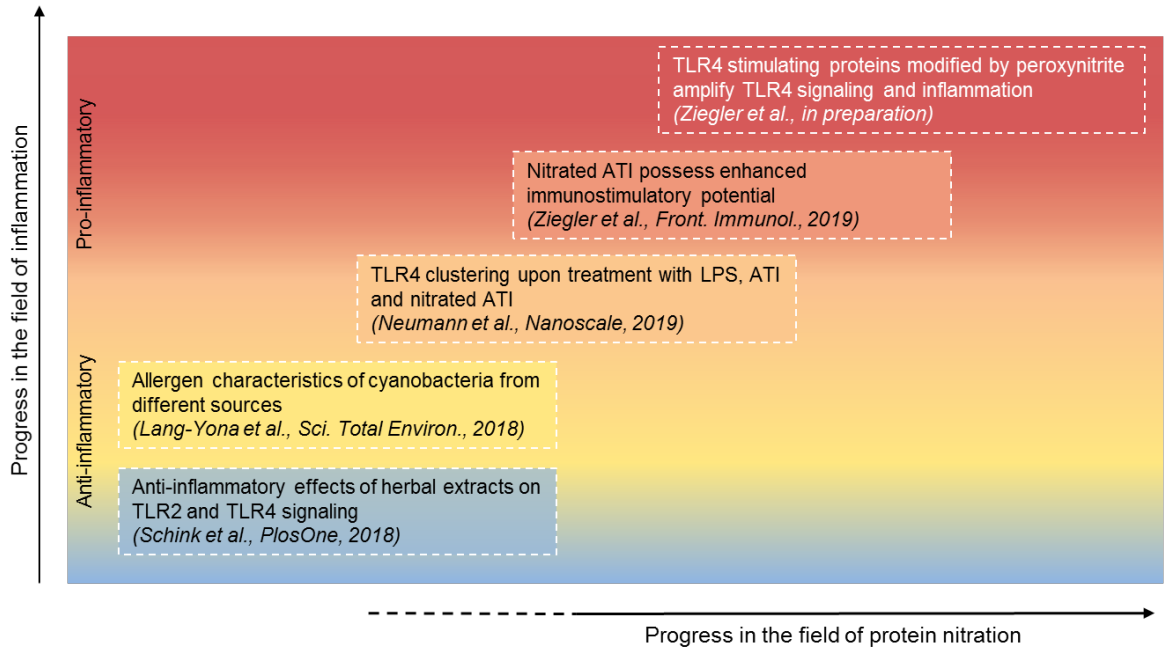

Figure 3: Visualization of five relevant publications to which I contributed during my PhD thesis.

Vertical axis from anti- to pro-inflammatory studies, horizontal axis from left to right studies contributing to the field of protein nitration.

2.2 Individual Studies

2.2.1 Nitration increases the immunostimulatory potential of amylase trypsin inhibitors

To elucidate the effect of nitration, we chemically modified amylase trypsin inhibitors from wheat (ATI) using three different methods simulating endo- (*in vivo*) and exogenous (environmental) nitration mechanisms. The aim of our study was to examine whether nitration of ATI alter their innate and adaptive immunostimulatory capacity. Modified ATI were quantified for their nitration degree using HPLC-DAD and ELISA. Furthermore, various *in vitro* studies were performed. The new HeLa TLR4 reporter cell line was generated and used for determination of innate immune stimulation. Adaptive immune reactions were analyzed in a mixed lymphocyte reaction by using primary immune cells which I isolated from whole blood of ten healthy donors. TLR4 activation, nuclear NF-κB translocation, expression of surface maturation markers, Th1, Th2 relevant cytokines and T cell proliferation were measured. We were able to demonstrate that ATI are potent immune stimulators which act even stronger after nitration. For details see Appendix B.1 Ziegler *et al.*, Front. Immunol, 2019.

2.2.2 Nanoscale distribution of TLR4 on primary human macrophages

In this study we investigated clustering of TLR4 on primary human macrophages from three healthy donors before and after stimulation with LPS, ATI or nitrated ATI. For this project we applied single molecule localization microscopy (SMLM) to observe changes in TLR4 distribution below the resolution limit of conventional fluorescence microscopy (<200 nm). For this study I developed a protocol tailored to the needs of SMLM regarding isolation and enrichment of human primary macrophages. In unstimulated cells we found remarkable donor dependent variations of pre-clustered TLR4 molecules, which may have clinical implications and should be further investigated in future studies. Thereafter cells were treated with LPS, ATI or nitrate ATI. Interestingly, although the clusters differed much in their pre-clustered state, there were no pronounced variations in cluster size and number of molecules within one cluster. Independently of treatment and donor, the cluster size remained unchanged at around ~57 nm containing ~25 molecules within a single cluster. Therefore, it can be concluded that TLR4 clusters have a fixed size but the percentage of pre-clustered TLR4 molecules varies largely between individuals. For details see Appendix B.2, Neumann *et al.*, Nanoscale, 2019.

2.2.3 Amplification of TLR4 signaling and NF-kB activation by peroxynitrite

Based on our previous findings for nitrated ATI we elucidated whether peroxynitrite modified TLR4 stimulating proteins generally can enhance their inflammatory potential. Therefore, we treated proteins from three different categories: DAMPs (high mobility group B1, heat shock protein 60), disease specific protein (α-synuclein) and allergens (grass pollen allergen Phl p 5, ATI) with peroxynitrite. The native and peroxynitrite treated proteins were tested for their capability to induce TLR4 stimulation, NF-κB activation, and transcription of inflammatory genes. For most of the tested TLR4 stimulating proteins we found a stronger immunostimulatory potential after nitration. By using THP-1 NF-κB reporter and HeLa TLR4 dual reporter cells we observed enhanced TLR4 stimulation and NF-κB activation. Moreover, upon TLR4 blocking by the antagonist TAK242, the NF-κB activation was significantly reduced, which indicates that peroxynitrite treated proteins stimulated specifically TLR4. Additionally the gene expression of tumor necrosis factor alpha, interleukin 1 beta was enhanced for all tested proteins and for some proteins also interleukin 8. Ongoing studies focus on pro-inflammatory cytokine release and stimulation of other receptors, which will contribute to a clear and more comprehensive picture. Moreover, we want to elucidate specifically whether nitrotyrosine or dityrosine formation is causative for enhanced receptor stimulation. For details see Appendix B.3, Ziegler *et al.*, in preparation, 2019.

2.2.4 Pro- and anti-inflammatory effects of herbal extracts and Cyanobacteria

Natural compounds which modulate inflammatory reactions are widely used as medication and food supplement. As TLR4 plays a central role in inflammatory reactions, I tested several herbal extracts and Cyanobacteria for their TLR4 stimulation and toxic effects, using my novel stable transfected monoclonal HeLa TLR4 dual reporter cell. Results obtained here contributed to two publications.

In the first study we screened 99 herbal extracts, which are known to have beneficial health effects. We screened the extracts for their potential to inhibit TLR2 and TLR4 induced pro-inflammatory responses. The ten most promising extracts were further tested for their ability to inhibit LPS induced nuclear translocation of NF-κB in HeLa TLR4 dual reporter cells using high content screening microscopy. Despite all extracts were found in pre-tests to be anti-inflammatory, surprisingly we found that three extracts did not inhibit LPS induced NF-κB translocation. This finding suggests that these three extracts induce the transcription of anti-inflammatory cytokines through NF-κB or counteract inflammation by other pathways. Further, we could show previously unknown anti-inflammatory TLR dependent effects for the extracts of sweet chestnut leaves (*Castanea sativa*) and common lady's mantle (*Alchemilla vulgaris*). Moreover, we proofed anti-inflammatory activity on TLR2- and TLR4-dependent signaling pathways for three whole extracts, such as bearberry leaves *(Arctostaphylos uva-ursi), cinchona bark (Cinchona pubescens)* and hops cones *(Humulus lupulus),* from which only single active compounds were known. For details see Appendix B.4, Schink *et al.*, PLoS ONE, 2018.

In the second study the focus was drawn on inflammatory effects of Cyanobacteria. Since Cyanobacteria are widely spread and used for biofuel production and as food supplements, they are considered to be a potential health hazard. In this study we tested Cyanobacteria species from different origins (marine, terrestrial, and fresh water) for their inflammatory and allergenic characteristics by various *in vitro* assays. Herein the first results generated with the use of the new HeLa TLR4 dual reporter assay system were published. Therefore, I tested seven different Cyanobacteria species for their TLR4 agonistic properties and their endotoxin levels. Interestingly, I found high levels of endotoxin in all samples but only two Cyanobacteria species (*Cylindrospermum siamensis* and *Anabaena ambigua*) stimulated TLR4. For details see Appendix B.5, A.1. Lang-Yona *et al.*, Sci Total Environ., 2018.

2.3 Conclusions and Outlook

This PhD study proceeds further along previous studies on nitrated proteins (Gruijthuijsen *et al.*, 2006; Karle *et al.*, 2012; Lang-Yona *et al.*, 2016; Untersmayr *et al.*, 2010; Ackaert *et al.*, 2014). In line with earlier findings, we observed for nitrated ATI an enhanced cytokine release and T cell proliferation. Additionally, we demonstrated enhanced TLR4 stimulation by using the new HeLa TLR4 dual reporter cell line. The observed enhanced immunogenicity provides a causative chain between stronger TLR4 agonistic effects leading to enhanced T cell proliferation and Th cytokine release upon nitration (Ziegler *et al.*, 2019).

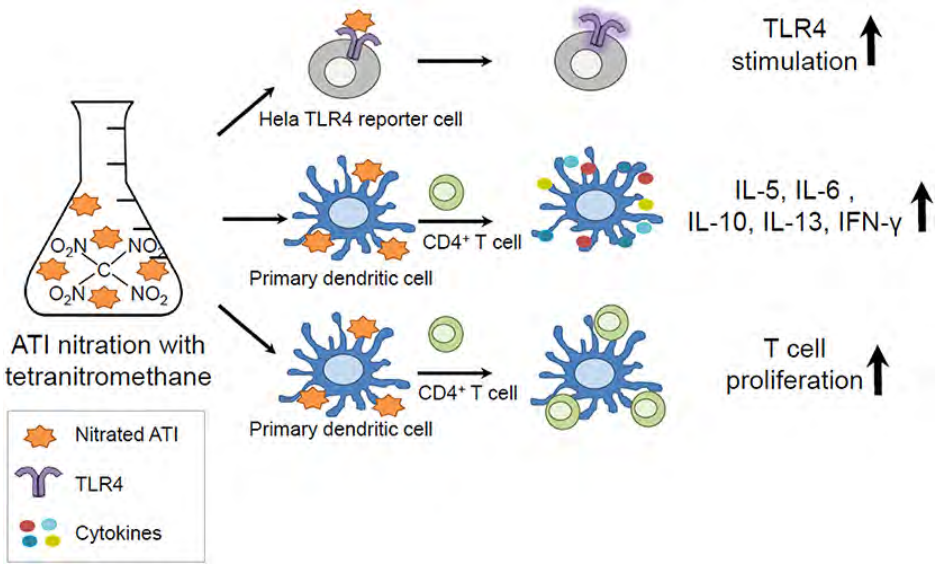

Figure 3: Illustration of increased immune reactions in vitro towards nitrated ATI

HeLa TLR4 dual reporter cells and human primary dendritic cells were treated with nitrated ATI. Increased TLR4 stimulation, cytokine secretion and T cell proliferation was observed. Figure is adopted from (Ziegler et al., 2019).

To prove our assumption that nitration amplifies the immune stimulant function of other proteins than ATI, we modified different TLR4 stimulating proteins with peroxynitrite. For several of the modified proteins tested, we found an increased TLR4 stimulation and inflammatory reaction. Ongoing studies focus on pro-inflammatory gene expression, cytokine release and stimulation of further receptors which induce NF-κB activation. Up to now it is not clear to which degree the formation of nitrotyrosine or dityrosine and thereby protein-oligomerization induces enhanced inflammation. The former would require a nitrotyrosine recognition function, whereas the latter may be explained by stabilizing receptor dimerization such as TLR4. All together these results will provide a comprehensive understanding, how peroxynitrite modified proteins affect immune reactions, contribute to inflammatory processes and related diseases.

3. Bibliography

Ackaert, C., Kofler, S., Horejs-Hoeck, J., Zulehner, N., Asam, C., von Grafenstein, S., Fuchs, J. E., Briza, P., Liedl, K. R., Bohle, B., Ferreira, F., Brandstetter, H., Oostingh, G. J., and Duschl, A.: The impact of nitration on the structure and immunogenicity of the major birch pollen allergen Bet v 1.0101, PloS one, 9, e104520, 10.1371/journal.pone.0104520, 2014.

Bellinghausen, I., Weigmann, B., Zevallos, V., Maxeiner, J., Reissig, S., Waisman, A., Schuppan, D., and Saloga, J.: Wheat amylase-trypsin inhibitors exacerbate intestinal and airway allergic immune responses in humanized mice, The Journal of allergy and clinical immunology, 143, 201-212.e204, 10.1016/j.jaci.2018.02.041, 2019.

Caminero, A., McCarville, J. L., Zevallos, V. F., Pigrau, M., Yu, X. B., Jury, J., Galipeau, H. J., Clarizio, A. V., Casqueiro, J., Murray, J. A., Collins, S. M., Alaedini, A., Bercik, P., Schuppan, D., and Verdu, E. F.: Lactobacilli Degrade Wheat Amylase Trypsin Inhibitors to Reduce Intestinal Dysfunction Induced by Immunogenic Wheat Proteins, Gastroenterology, 156, 2266-2280, 10.1053/j.gastro.2019.02.028, 2019.

Chen, L., Deng, H., Cui, H., Fang, J., Zuo, Z., Deng, J., Li, Y., Wang, X., and Zhao, L.: Inflammatory responses and inflammation-associated diseases in organs, Oncotarget, 9, 7204-7218, 10.18632/oncotarget.23208, 2018.

Cuccioloni, M., Mozzicafreddo, M., Bonfili, L., Cecarini, V., Giangrossi, M., Falconi, M., Saitoh, S. I., Eleuteri, A. M., and Angeletti, M.: Interfering with the high-affinity interaction between wheat amylase trypsin inhibitor CM3 and toll-like receptor 4: in silico and biosensor-based studies, Sci Rep, 7, 13169, 10.1038/s41598-017-13709-1, 2017.

Dupont, F. M., Vensel, W. H., Tanaka, C. K., Hurkman, W. J., and Altenbach, S. B.: Deciphering the complexities of the wheat flour proteome using quantitative two-dimensional electrophoresis, three proteases and tandem mass spectrometry, Proteome Sci, 9, 10, 10.1186/1477-5956-9-10, 2011.

Fasano, A., Sapone, A., Zevallos, V., and Schuppan, D.: Nonceliac gluten sensitivity, Gastroenterology, 148, 1195-1204, 10.1053/j.gastro.2014.12.049, 2015.

Ferrer-Sueta, G., Campolo, N., Trujillo, M., Bartesaghi, S., Carballal, S., Romero, N., Alvarez, B., and Radi, R.: Biochemistry of Peroxynitrite and Protein Tyrosine Nitration, Chemical reviews, 118, 1338-1408, 10.1021/acs.chemrev.7b00568, 2018.

Finnie, C., Melchior, S., Roepstorff, P., and Svensson, B.: Proteome analysis of grain filling and seed maturation in barley, Plant Physiol, 129, 1308-1319, 10.1104/pp.003681, 2002.

Franze, T., Weller, M. G., Niessner, R., and Poschl, U.: Protein nitration by polluted air, Environmental science & technology, 39, 1673-1678, 2005.

Galinanes, M., and Matata, B. M.: Protein nitration is predominantly mediated by a peroxynitrite-dependent pathway in cultured human leucocytes, The Biochemical journal, 367, 467-473, 10.1042/BJ20020825, 2002.

Ghosh, S., Janocha, A. J., Aronica, M. A., Swaidani, S., Comhair, S. A., Xu, W., Zheng, L., Kaveti, S., Kinter, M., Hazen, S. L., and Erzurum, S. C.: Nitrotyrosine proteome survey in asthma identifies oxidative mechanism of catalase inactivation, Journal of immunology (Baltimore, Md. : 1950), 176, 5587-5597, 2006.

NF-kB Target Genes: https://www.bu.edu/nf-kb/gene-resources/target-genes/, access: 11/08/2018, 2018.

Greenacre, S. A., and Ischiropoulos, H.: Tyrosine nitration: localisation, quantification, consequences for protein function and signal transduction, Free Radic Res, 34, 541-581, 2001.

Gruijthuijsen, Y. K., Grieshuber, I., Stocklinger, A., Tischler, U., Fehrenbach, T., Weller, M. G., Vogel, L., Vieths, S., Poschl, U., and Duschl, A.: Nitration enhances the allergenic potential of proteins, Int Arch Allergy Immunol, 141, 265-275, 10.1159/000095296, 2006.

Hodara, R., Norris, E. H., Giasson, B. I., Mishizen-Eberz, A. J., Lynch, D. R., Lee, V. M., and Ischiropoulos, H.: Functional consequences of alpha-synuclein tyrosine nitration: diminished binding to lipid vesicles and increased fibril formation, J Biol Chem, 279, 47746-47753, 10.1074/jbc.M408906200, 2004.

Ischiropoulos, H.: Protein tyrosine nitration--an update, Arch Biochem Biophys, 484, 117-121, 10.1016/j.abb.2008.10.034, 2009.

Jang, J. H., Shin, H. W., Lee, J. M., Lee, H. W., Kim, E. C., and Park, S. H.: An Overview of Pathogen Recognition Receptors for Innate Immunity in Dental Pulp, Mediators of inflammation, 2015, 794143, 10.1155/2015/794143, 2015.

Junker, Y., Zeissig, S., Kim, S. J., Barisani, D., Wieser, H., Leffler, D. A., Zevallos, V., Libermann, T. A., Dillon, S., Freitag, T. L., Kelly, C. P., and Schuppan, D.: Wheat amylase trypsin inhibitors drive intestinal inflammation via activation of toll-like receptor 4, J. Exp. Med, 209, 2395-2408, 2012.

Kampf, C. J., Liu, F., Reinmuth-Selzle, K., Berkemeier, T., Meusel, H., Shiraiwa, M., and Poschl, U.: Protein Cross-Linking and Oligomerization through Dityrosine Formation upon Exposure to Ozone, Environmental science & technology, 49, 10859-10866, 10.1021/acs.est.5b02902, 2015.

Karle, A. C., Oostingh, G. J., Mutschlechner, S., Ferreira, F., Lackner, P., Bohle, B., Fischer, G. F., Vogt, A. B., and Duschl, A.: Nitration of the pollen allergen bet v 1.0101 enhances the presentation of bet v 1-derived peptides by HLA-DR on human dendritic cells, PloS one, 7, e31483, 10.1371/journal.pone.0031483, 2012.

Katsuyama, M.: NOX/NADPH oxidase, the superoxide-generating enzyme: its transcriptional regulation and physiological roles, Journal of pharmacological sciences, 114, 134-146, 2010.

Kawai, T., and Akira, S.: The role of pattern-recognition receptors in innate immunity: update on Toll-like receptors, Nat Immunol, 11, 373-384, 10.1038/ni.1863, 2010.

Kawasaki, T., and Kawai, T.: Toll-like receptor signaling pathways, Frontiers in immunology, 5, 461, 10.3389/fimmu.2014.00461, 2014.

Lang-Yona, N., Shuster-Meiseles, T., Mazar, Y., Yarden, O., and Rudich, Y.: Impact of urban air pollution on the allergenicity of Aspergillus fumigatus conidia: Outdoor exposure study supported by laboratory experiments, The Science of the total environment, 541, 365-371, 10.1016/j.scitotenv.2015.09.058, 2016.

Lang-Yona, N., Kunert, A. T., Vogel, L., Kampf, C. J., Bellinghausen, I., Saloga, J., Schink, A., Ziegler, K., Lucas, K., Schuppan, D., Poschl, U., Weber, B., and Frohlich-Nowoisky, J.: Fresh water, marine and terrestrial cyanobacteria display distinct allergen characteristics, The Science of the total environment, 612, 767-774, 10.1016/j.scitotenv.2017.08.069, 2018.

Leccioli, V., Oliveri, M., Romeo, M., Berretta, M., and Rossi, P.: A New Proposal for the Pathogenic Mechanism of Non-Coeliac/Non-Allergic Gluten/Wheat Sensitivity: Piecing

Together the Puzzle of Recent Scientific Evidence, Nutrients, 9, 10.3390/nu9111203, 2017.

Liu, F., Reinmuth-Selzle, K., Lai, S., Weller, M. G., Poschl, U., and Kampf, C. J.: Simultaneous determination of nitrated and oligomerized proteins by size exclusion high-performance liquid chromatography coupled to photodiode array detection, J Chromatogr A, 1495, 76-82, 10.1016/j.chroma.2017.03.015, 2017.

Lucas, K., and Maes, M.: Role of the Toll Like receptor (TLR) radical cycle in chronic inflammation: possible treatments targeting the TLR4 pathway, Molecular neurobiology, 48, 190-204, 10.1007/s12035-013-8425-7, 2013.

Murata, M., and Kawanishi, S.: Oxidative DNA damage induced by nitrotyrosine, a biomarker of inflammation, Biochemical and biophysical research communications, 316, 123-128, 10.1016/j.bbrc.2004.02.022, 2004.

Neumann, J., Ziegler, K., Gelleri, M., Frohlich-Nowoisky, J., Liu, F., Bellinghausen, I., Schuppan, D., Birk, U., Poschl, U., Cremer, C., and Lucas, K.: Nanoscale distribution of TLR4 on primary human macrophages stimulated with LPS and ATI, Nanoscale, 11, 9769-9779, 10.1039/c9nr00943d, 2019.

Payan, F.: Structural basis for the inhibition of mammalian and insect alpha-amylases by plant protein inhibitors, Biochimica et biophysica acta, 1696, 171-180, 10.1016/j.bbapap.2003.10.012, 2004.

Radi, R.: Protein tyrosine nitration: biochemical mechanisms and structural basis of functional effects, Acc Chem Res, 46, 550-559, 10.1021/ar300234c, 2013.

Rao, X., Zhong, J., Brook, R. D., and Rajagopalan, S.: Effect of Particulate Matter Air Pollution on Cardiovascular Oxidative Stress Pathways, Antioxidants & redox signaling, 28, 797-818, 10.1089/ars.2017.7394, 2018.

Reinmuth-Selzle, K., Ackaert, C., Kampf, C. J., Samonig, M., Shiraiwa, M., Kofler, S., Yang, H., Gadermaier, G., Brandstetter, H., Huber, C. G., Duschl, A., Oostingh, G. J., and Poschl, U.: Nitration of the birch pollen allergen Bet v 1.0101: efficiency and site-selectivity of liquid and gaseous nitrating agents, J Proteome Res, 13, 1570-1577, 10.1021/pr401078h, 2014.

Reinmuth-Selzle, K., Kampf, C. J., Lucas, K., Lang-Yona, N., Frohlich-Nowoisky, J., Shiraiwa, M., Lakey, P. S. J., Lai, S., Liu, F., Kunert, A. T., Ziegler, K., Shen, F., Sgarbanti, R., Weber, B., Bellinghausen, I., Saloga, J., Weller, M. G., Duschl, A., Schuppan, D., and Poschl, U.: Air Pollution and Climate Change Effects on Allergies in the Anthropocene: Abundance, Interaction, and Modification of Allergens and Adjuvants, Environmental science & technology, 51, 4119-4141, 10.1021/acs.est.6b04908, 2017.

Rouvinen, J., Janis, J., Laukkanen, M. L., Jylha, S., Niemi, M., Paivinen, T., Makinen-Kiljunen, S., Haahtela, T., Soderlund, H., and Takkinen, K.: Transient dimers of allergens, PloS one, 5, e9037, 10.1371/journal.pone.0009037, 2010.

Salvemini, D., Doyle, T. M., and Cuzzocrea, S.: Superoxide, peroxynitrite and oxidative/nitrative stress in inflammation, Biochem Soc Trans, 34, 965-970, 10.1042/bst0340965, 2006.

Schett, G., and Neurath, M. F.: Resolution of chronic inflammatory disease: universal and tissue-specific concepts, Nature communications, 9, 3261, 10.1038/s41467-018-05800-6, 2018.

Schink, A., Neumann, J., Leifke, A. L., Ziegler, K., Frohlich-Nowoisky, J., Cremer, C., Thines, E., Weber, B., Poschl, U., Schuppan, D., and Lucas, K.: Screening of herbal extracts for

TLR2- and TLR4-dependent anti-inflammatory effects, PloS one, 13, e0203907, 10.1371/journal.pone.0203907, 2018.

Scholl, I., Kalkura, N., Shedziankova, Y., Bergmann, A., Verdino, P., Knittelfelder, R., Kopp, T., Hantusch, B., Betzel, C., Dierks, K., Scheiner, O., Boltz-Nitulescu, G., Keller, W., and Jensen-Jarolim, E.: Dimerization of the major birch pollen allergen Bet v 1 is important for its in vivo IgE-cross-linking potential in mice, Journal of immunology (Baltimore, Md. : 1950), 175, 6645-6650, 2005.

Schuppan, D., Pickert, G., shfaq-Khan, M., and Zevallos, V.: Non-celiac wheat sensitivity: differential diagnosis, triggers and implications, Best. Pract. Res. Clin. Gastroenterol, 29, 469-476, 2015.

Schuppan, D., and Zevallos, V.: Wheat amylase trypsin inhibitors as nutritional activators of innate immunity, Dig. Dis, 33, 260-263, 2015.

Selzle, K., Ackaert, C., Kampf, C. J., Kunert, A. T., Duschl, A., Oostingh, G. J., and Poschl, U.: Determination of nitration degrees for the birch pollen allergen Bet v 1, Analytical and bioanalytical chemistry, 405, 8945-8949, 10.1007/s00216-013-7324-0, 2013.

Shiraiwa, M., Selzle, K., Yang, H., Sosedova, Y., Ammann, M., and Poschl, U.: Multiphase chemical kinetics of the nitration of aerosolized protein by ozone and nitrogen dioxide, Environmental science & technology, 46, 6672-6680, 10.1021/es300871b, 2012.

Sies, H., Berndt, C., and Jones, D. P.: Oxidative Stress, Annual review of biochemistry, 86, 715-748, 10.1146/annurev-biochem-061516-045037, 2017.

Tatham, A. S., and Shewry, P. R.: Allergens to wheat and related cereals, Clin. Exp. Allergy, 38, 1712-1726, 2008.

Turko, I. V., and Murad, F.: Protein nitration in cardiovascular diseases, Pharmacol Rev, 54, 619-634, 2002.

Untersmayr, E., Diesner, S. C., Oostingh, G. J., Selzle, K., Pfaller, T., Schultz, C., Zhang, Y., Krishnamurthy, D., Starkl, P., Knittelfelder, R., Forster-Waldl, E., Pollak, A., Scheiner, O., Poschl, U., Jensen-Jarolim, E., and Duschl, A.: Nitration of the egg-allergen ovalbumin enhances protein allergenicity but reduces the risk for oral sensitization in a murine model of food allergy, PloS one, 5, e14210, 10.1371/journal.pone.0014210, 2010.

Walcher, W., Franze, T., Weller, M. G., Poschl, U., and Huber, C. G.: Liquid- and gas-phase nitration of bovine serum albumin studied by LC-MS and LC-MS/MS using monolithic columns, J Proteome Res, 2, 534-542, 2003.

Walusiak, J., Wiszniewska, M., Krawczyk-Adamus, P., and Palczynski, C.: Occupational allergy to wheat flour. Nasal response to specific inhalative challenge in asthma and rhinitis vs. isolated rhinitis: a comparative study, Int J Occup Med Environ Health, 17, 433-440, 2004.

West, A. P., Brodsky, I. E., Rahner, C., Woo, D. K., Erdjument-Bromage, H., Tempst, P., Walsh, M. C., Choi, Y., Shadel, G. S., and Ghosh, S.: TLR signalling augments macrophage bactericidal activity through mitochondrial ROS, Nature, 472, 476-480, 10.1038/nature09973, 2011.

Yang, H., Zhang, Y., and Poschl, U.: Quantification of nitrotyrosine in nitrated proteins, Analytical and bioanalytical chemistry, 397, 879-886, 10.1007/s00216-010-3557-3, 2010.

Zevallos, V. F., Raker, V., Tenzer, S., Jimenez-Calvente, C., Ashfaq-Khan, M., Russel, N., Pickert, G., Schild, H., Steinbrink, K., and Schuppan, D.: Nutritional Wheat Amylase-

Trypsin Inhibitors Promote Intestinal Inflammation via Activation of Myeloid Cells, Gastroenterology, 152, 1100-1113, 10.1053/j.gastro.2016.12.006, 2017.

Zevallos, V. F., Raker, V. K., Maxeiner, J., Scholtes, P., Steinbrink, K., and Schuppan, D.: Dietary wheat amylase trypsin inhibitors exacerbate murine allergic airway inflammation, Eur J Nutr, 10.1007/s00394-018-1681-6, 2018.

Zhang, Y., Yang, H., and Poschl, U.: Analysis of nitrated proteins and tryptic peptides by HPLC-chip-MS/MS: site-specific quantification, nitration degree, and reactivity of tyrosine residues, Analytical and bioanalytical chemistry, 399, 459-471, 10.1007/s00216-010-4280-9, 2011.

Ziegler, K., Neumann, J., Liu, F., Fröhlich-Nowoisky, J., Cremer, C., Saloga, J., Reinmuth-Selzle, K., Pöschl, U., Schuppan, D., Bellinghausen, I., and Lucas, K.: Nitration of Wheat Amylase Trypsin Inhibitors Increases Their Innate and Adaptive Immunostimulatory Potential in vitro, Frontiers in immunology, 9, 10.3389/fimmu.2018.03174, 2019.

A. Personal List of Publications

Journal Articles

Published

1. Ziegler K., Jan Neumann J., Fobang Liu F., Fröhlich-Nowoisky J., Christoph Cremer C., Saloga J., Reinmuth-Selzle K., Pöschl U., Schuppan D., Bellinghausen I. and Lucas K.: Nitration of wheat amylase trypsin inhibitors increases their innate and adaptive immunostimulatory potential *in vitro*, *Front. Immunol*, DOI:10.3389/fimmu.2018.03174, (2019).
2. Neumann J., Ziegler K., Gelléri M., Fröhlich-Nowoisky J., Liu F., Bellinghausen I., Schuppan D., Birk U., Pöschl U., Cremer C. and Lucas K.: Nanoscale distribution of TLR4 on primary human macrophages stimulated with LPS and ATI. *Nanoscale, 2019, 11, 9769 – 9779,* (2019).
3. Schink A., Neumann J., Leifke A. L., Ziegler K., Fröhlich-Nowoisky J., Cremer C., Thines E., Weber B., Pöschl U. and Schuppan D., Lucas K.: Screening of herbal extracts for TLR2- and TLR4-dependent anti-inflammatory effects. *PlosOne*, DOI: 10.1371/journal.pone.0203907, (2018).
4. Rosigkeit S., Meng M., Grunwitz C., Gomes P., Kreft A., Hayduk N., Heck R., Pickert G., Ziegler K., Abassi Y., Röder J., Kaps L., Vascotto F., Beissert T., Witzel S., Kuhn A., Diken M., Schuppan D., Sahin U., Haas H. and Bockamp E.: Monitoring Translation Activity of mRNA-Loaded Nanoparticles in Mice. *Mol Pharm.,* DOI: 10.1021/acs.molpharmaceut.8b00370 (2018).
5. Lang-Yona N., Kunert A. T., Vogel L., Kampf C. J., Bellinghausen I., Saloga J., Schink A., Ziegler K., Lucas K., Schuppan D., Pöschl U., Weber B. and Fröhlich-Nowoisky J.: Fresh water, marine and terrestrial cyanobacteria display distinct allergen characteristics. *Sci Total Environ.*, DOI: 10.1016/j.scitotenv.2017.08.069, (2018).
6. Kathrin Reinmuth-Selzle K., Christopher Kampf C. J., Lucas K., Lang-Yona N., Fröhlich-Nowoisky J., Shiraiwa M., Lakey P. S. J., Lai S., Liu F., Kunert A. T, Ziegler K., Shen F., Sgarbanti R., Weber B., Bellinghausen I., Saloga J., Weller M. G., Duschl A., Schuppan D. and Pöschl U.: Air Pollution and Climate Change Effects on Allergies in the Anthropocene: Abundance, Interaction, and Modification of Allergens and Adjuvants. *Environ. Sci. Technol.*, DOI: 10.1016/j.scitotenv.2017.08.069, (2017).

In preparation

7. Ziegler K., Kunert A. T., Widera D., Leifke A. L., Reinmuth-Selzle K. R., Maes M., Weller M., Schuppan D.,Fröhlich-Nowoisky J., Lucas K. and Pöschl U. (tentative authors list): TLR4 stimulating proteins modified by peroxynitrite amplify TLR4 signaling and inflammation. *In preperation*.

8. Ziegler K., Huffmann A., Davey R., Kunert A.T., Leifke A, Neumann J., Fröhlich-Nowoisky J, Pöschl U., and Lucas K. (tentative authors list): Native and nitrated Lactotransferrin samples from human milk induce biased immune responses. *In preparation*.
9. Kunert A.T, Ziegler K., Krevert C., Lucas K., Reinmuth-Selzle K., Pöschl U., Fröhlich-Nowoisky.(tentative authors list): Nitration of Phl p5 upon O_3/NO_2 exposure and $ONOO^-$ treatment. *In preparation*.
10. Reinmuth-Selzle K., Weller M., Kunert A.T, Ziegler K., Lucas K., Pöschl U., Fröhlich-Nowoisky (tentative authors list): Protein determination of challenging protein samples. *In preparation*.

Oral presentations

1. Ziegler K., Jan Neumann J., Fobang Liu F., Fröhlich-Nowoisky J., Christoph Cremer C., Saloga J., Reinmuth-Selzle K., Pöschl U., Schuppan D., Bellinghausen I. and Lucas K.: Nitration of wheat amylase trypsin inhibitors increases their innate and adaptive immunostimulatory potential in vitro, 31st Mainzer Allergy Workshop, Mainz, Germany (29th – 30th March 2019)
2. Schink A., Neumann J., Leifke A. L., Ziegler K., Fröhlich-Nowoisky J., Cremer C., Thines E., Weber B., Pöschl U., Schuppan D., Lucas K.: Screening of herbal extracts for TLR2- and TLR4-dependent anti-inflammatory effects, 31st Mainzer Allergy Workshop, Mainz, Germany (29th – 30th March 2019)
3. Ziegler K., Bellinghausen I., Neumann J., Liu F., Saloga J., Schuppan D., Pöschl U. and Lucas K.: Nitration of wheat derived alpha amylase trypsin inhibitors (ATIs) increases their immunostimulatory capacity, 30th Mainzer Allergy Workshop, Mainz, Germany (22nd – 23rd March 2018)
4. Ziegler K., Lucas K., Bellinghausen I., Liu F., Ashfaq-Khan M., Saloga J., Schuppan D. and Pöschl U.: The effect of nitration on the allergenicity of wheat derived alpha amylase trypsin inhibitors, 29th Mainzer Allergy Workshop, Mainz, Germany, (30th – 31st March 2017)
5. Kathrin Reinmuth-Selzle K., Christopher Kampf C. J., Lucas K., Lang-Yona N., Fröhlich-Nowoisky J., Shiraiwa M., Lakey P. S. J., Lai S., Liu F., Kunert A. T, Ziegler K., Shen F., Sgarbanti R., Weber B., Bellinghausen I., Saloga J., Weller M. G., Duschl A., Schuppan D. and Pöschl U.: Air Pollution and Climate Change Effects on Allergies in the Anthropocene: Abundance, Interaction, and Modification of Allergens and Adjuvants, 30th Mainzer Allergy Workshop, Mainz, Germany (22nd – 23rd March 2018)
6. Lang-Yona N., Kunert A. T., Vogel L., Kampf C. J., Bellinghausen I., Saloga J., Schink A., Ziegler K., Lucas K., Schuppan D., Pöschl U., Weber B. and Fröhlich-Nowoisky J.: Fresh water, marine and terrestrial cyanobacteria display distinct allergen characteristics, 29th Mainzer Allergy Workshop, Mainz, Germany, (30th – 31st March 2017)
7. Neumann J., Ziegler K., Zevallos, V. Birk, U., Lucas K., Schuppan D., Cremer C., and Pöschl, U.: Microscopic localization of molecules involved in chronic inflammatory processes, 29th Mainzer Allergy Workshop, Mainz, Germany, (30th - 31th March 2017)
8. Becker K., Lucas K., Bockamp E., Zevallos V., Ashfaq-Khan M., Bellinghausen I., Saloga J., Schuppan D. and Pöschl U.: Modulation of innate immune reactions upon interaction of the Toll like receptor 4 with chemically modified allergens, 28th Mainzer Allergy Workshop, Mainz, Germany, (17th – 18th March 2016)

Poster presentations

1. Ziegler K., Lucas K., Bellinghausen I., Liu F., Ashfaq-Khan M., Saloga J., Schuppan D. and Pöschl U.: The effect of nitration on the potential allergenicity of wheat derived alpha amylase trypsin inhibitors (ATIs), 4th TransMed Science Day, Mainz, Germany (24th August 2017)
2. Ziegler K., Lucas K., Bellinghausen I., Liu F., Ashfaq-Khan M., Saloga J., Schuppan D. and Pöschl U.: The effect of nitration on the potential allergenicity of wheat derived alpha amylase trypsin inhibitors (ATIs), 8th European Immunology Conference, Madrid, Spain (29th June – 1st July.2017)
3. Neumann J., Ziegler K., Szczurek A., Gourram A., Birk U., Lucas K., Zevallos V., Schuppan D., Cremer C. and Pöschl U.: Investigation of Molecules Involved in Chronic Inflammatory Processes Using Single Molecule Localization Microscopy in Cells, Focus on Microscopy, Bordeaux, France (09th – 12th April 2017)

B. Selected Publications

1. Ziegler K., Jan Neumann J., Fobang Liu F., Fröhlich-Nowoisky J., Christoph Cremer C., Saloga J., Reinmuth-Selzle K., Pöschl U., Schuppan D., Bellinghausen I. and Lucas K.: Nitration of wheat amylase trypsin inhibitors increases their innate and adaptive immunostimulatory potential *in vitro*, Front. Immunol. DOI: 10.3389/fimmu.2018.03174, (2019).
2. Neumann J., Ziegler K., Gelléri M., Fröhlich-Nowoisky J., Liu F., Bellinghausen I., Schuppan D., Birk U., Pöschl U., Cremer C. and Lucas K.: Nanoscale distribution of TLR4 on primary human ATI- and LPS- stimulated macrophages, Nanoscale*, 11, 9769 – 9779,* DOI: 10.1039/C9NR00943D, (2019).
3. Ziegler K., Kunert A. T., Widera D., Leifke A. L., Reinmuth-Selzle K. R., Maes M., Weller M., Schuppan D.,Fröhlich-Nowoisky J., Lucas K. and Pöschl U (tentative authors list): TLR4 stimulating proteins modified by peroxynitrite amplify TLR4 signaling and inflammation, *in preperation*, (2019).
4. Schink A., Neumann J., Leifke A. L., Ziegler K., Fröhlich-Nowoisky J., Cremer C., Thines E., Weber B., Pöschl U., Schuppan D., Lucas K.: Screening of herbal extracts for TLR2- and TLR4-dependent anti-inflammatory effects, PlosOne, DOI: 10.1371/journal.pone.0203907, (2018).
5. Lang-Yona N., Kunert A. T., Vogel L., Kampf C. J., Bellinghausen I., Saloga J., Schink A., Ziegler K., Lucas K., Schuppan D., Pöschl U., Weber B. and Fröhlich-Nowoisky J.: Fresh water, marine and terrestrial cyanobacteria display distinct allergen characteristics. Sci Total Environ., DOI: 10.1016/j.scitotenv.2017.08.069, (2018).

B.1 Ziegler *et al*., Front. Immunol., 2019

Nitration of wheat amylase trypsin inhibitors increases their innate and adaptive immunostimulatory potential *in vitro*

Ziegler K.[1], Neumann J.[1,2], Liu F.[1], Fröhlich-Nowoisky J.[1], Cremer C.[2], Saloga J.[3], Reinmuth-Selzle K.[1], Pöschl U.[1], Schuppan D.[4,5], Bellinghausen I.[3]*, and Lucas K.[1]*

[1]Max Planck Institute for Chemistry, Multiphase Chemistry Department, 55128 Mainz, Germany
[2]Institute of Molecular Biology, 55128 Mainz, Germany
[3]Department of Dermatology, University Medical Center of the Johannes Gutenberg University, 55131 Mainz, Germany
[4]Institute of Translational Immunology, University Medical Center of the Johannes Gutenberg University, 55131 Mainz, Germany
[5]Division of Gastroenterology, Beth Israel Deaconess Medical Center and Harvard Medical School, Boston, MA 02215, USA

Frontiers in Immunology, DOI: 10.3389/fimmu.2018.03174, (2019).

Author contributions.

DS, UP, KRS, IB, and KL designed the experiments. KZ, JN, FL, and IB performed the experiments. KZ, JN, FL, JFN, DS, UP, IB, and KL analyzed and interpreted the data. CC, FL, KRS, and IB contributed materials/methods/analysis tools. KZ, IB, and KL wrote the paper. All authors were involved in the editing and proof reading of the manuscript.

frontiers in Immunology

ORIGINAL RESEARCH
published: 21 January 2019
doi: 10.3389/fimmu.2018.03174

Nitration of Wheat Amylase Trypsin Inhibitors Increases Their Innate and Adaptive Immunostimulatory Potential *in vitro*

Kira Ziegler[1], Jan Neumann[1,2], Fobang Liu[1], Janine Fröhlich-Nowoisky[1], Christoph Cremer[1,2], Joachim Saloga[3], Kathrin Reinmuth-Selzle[1], Ulrich Pöschl[1], Detlef Schuppan[4], Iris Bellinghausen[3†] and Kurt Lucas[1†]*

[1] Multiphase Chemistry Department, Max Planck Institute for Chemistry, Mainz, Germany, [2] Institute of Molecular Biology, Mainz, Germany, [3] Department of Dermatology, University Medical Center of the Johannes Gutenberg University, Mainz, Germany, [4] Institute of Translational Immunology, University Medical Center of the Johannes Gutenberg University, Mainz, Germany

OPEN ACCESS

Edited by:
Zorica D. Juranic,
Institute of Oncology and Radiology of Serbia, Serbia

Reviewed by:
Julio Villena,
CONICET Centro de Referencia para Lactobacilos (CERELA), Argentina
Oscar J. Cordero,
University of Santiago de Compostela, Spain
Ivan Milos Stankovic,
University of Belgrade, Serbia

***Correspondence:**
Kurt Lucas
k.lucas@mpic.de

[†] These authors have contributed equally to this work and share senior authorship

Specialty section:
This article was submitted to Nutritional Immunology, a section of the journal Frontiers in Immunology

Received: 25 July 2018
Accepted: 24 December 2018
Published: 21 January 2019

Citation:
Ziegler K, Neumann J, Liu F, Fröhlich-Nowoisky J, Cremer C, Saloga J, Reinmuth-Selzle K, Pöschl U, Schuppan D, Bellinghausen I and Lucas K (2019) Nitration of Wheat Amylase Trypsin Inhibitors Increases Their Innate and Adaptive Immunostimulatory Potential in vitro. Front. Immunol. 9:3174. doi: 10.3389/fimmu.2018.03174

Amylase trypsin inhibitors (ATI) can be found in all gluten containing cereals and are, therefore, ingredient of basic foods like bread or pasta. In the gut ATI can mediate innate immunity via activation of the Toll-like receptor 4 (TLR4) on immune cells residing in the lamina propria, promoting intestinal, as well as extra-intestinal, inflammation. Inflammatory conditions can induce formation of peroxynitrite ($ONOO^-$) and, thereby, endogenous protein nitration in the body. Moreover, air pollutants like ozone (O_3) and nitrogen dioxide (NO_2) can cause exogenous protein nitration in the environment. Both reaction pathways may lead to the nitration of ATI. To investigate if and how nitration modulates the immunostimulatory properties of ATI, they were chemically modified by three different methods simulating endogenous and exogenous protein nitration and tested *in vitro*. Here we show that ATI nitration was achieved by all three methods and lead to increased immune reactions. We found that ATI nitrated by tetranitromethane (TNM) or $ONOO^-$ lead to a significantly enhanced TLR4 activation. Furthermore, in human primary immune cells, TNM nitrated ATI induced a significantly higher T cell proliferation and release of Th1 and Th2 cytokines compared to unmodified ATI. Our findings implicate a causative chain between nitration, enhanced TLR4 stimulation, and adaptive immune responses, providing major implications for public health, as nitrated ATI may strongly promote inhalative wheat allergies (baker's asthma), non-celiac wheat sensitivity (NCWS), other allergies, and autoimmune diseases. This underlines the importance of future work analyzing the relationship between endo- and exogenous protein nitration, and the rise in incidence of ATI-related and other food hypersensitivities.

Keywords: allergy, amylase trypsin inhibitors, dendritic cells, non-celiac wheat sensitivity, protein nitration, wheat

INTRODUCTION

Nitration of proteins can occur endogenously in the human body or exogenously in the environment. Air pollutants, like ozone and nitrogen oxides, are able to nitrate allergenic proteins, like the major birch pollen allergen Bet v 1, leading to an increased allergic potential and elevated immune reactions (1–6). In the human body, inflammatory conditions can lead

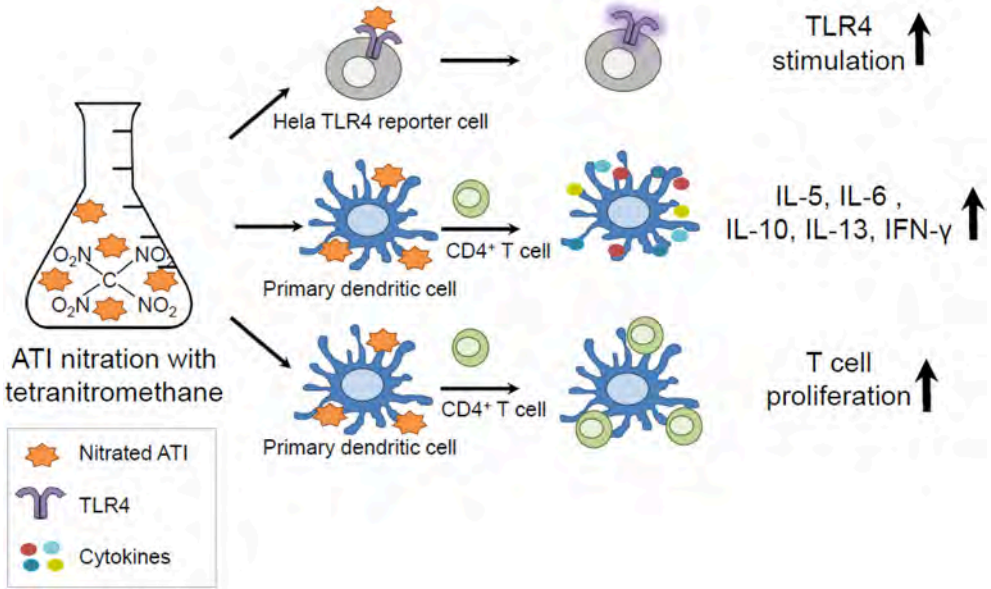

GRAPHICAL ABSTRACT | Amylase Trypsin Inhibitors (ATI) can be found in all gluten containing grains and are capable to mediate innate immunity by direct TLR4 stimulation. As protein nitration can occur during inflammatory processes in the body and under environmental conditions, ATI were nitrated and tested *in vitro*. The nitrated ATI induced increased innate and adaptive immune reactions.

to the formation of $ONOO^-$, which is the main agent for endogenous protein nitration (5, 7–9). Moreover, several air pollutants and pathogens can induce or favor inflammatory processes and related nitration processes (1, 3, 6). Diseases typically accompanied by a high degree of inflammation are, for example, autoimmune and other chronic inflammatory diseases, like chronic obstructive pulmonary disease (COPD), allergic asthma, inflammatory bowel diseases (IBD), or non-celiac non-allergy wheat sensitivity (NCWS) (10–12).

We previously showed that amylase trypsin inhibitors (ATI), a family of non-gluten proteins, are responsible for manifestations of mainly extra-intestinal symptoms of NCWS (10, 11, 13, 14). Moreover, ATI are major allergens in baker's asthma, a classical IgE mediated allergy (15, 16). ATI can be found in all gluten containing grains (wheat, barley, rye), and represent 2–4% of the total protein (17). In plants, ATI regulate the germination processes (18) and defense mechanisms by blocking the amylase and trypsin activity of parasites (19). The wheat intake of an adult person is about 250 g per day, mainly as processed bread or pasta which is equivalent to 0.5–1 g ATI (10). Remarkably, ATI are resistant to food processing and to proteolysis in the gastrointestinal tract where they stay biologically active (20). In the gut ATI are able to stimulate immune cells residing in the lamina propria and mesenteric lymph nodes through TLR4 binding and stimulation, and the emigration of the activated myeloid cells (20–22).

The innate immune receptor TLR4 recognizes damage and pathogen associated patterns (DAMPs/PAMPs), like lipopolysaccharides (LPS), which are major components in the outer membrane of gram negative bacteria. Upon stimulation, the receptor triggers an NF-κB dependent cascade leading to the release of pro-inflammatory cytokines (23, 24). Importantly, ATI can trigger TLR4 by direct interaction, and provoke innate immunity (21, 22). In a mouse model of inflammatory bowel disease, ATI enhanced the dextran sodium sulfate-induced intestinal inflammation by increasing the number of activated macrophages and dendritic cells in all sections of the intestine, the lamina propria, and especially in the mesenteric lymph nodes (20). Moreover, we showed in two mouse studies on experimental airway inflammation that ATI-enriched diets not only enhanced allergen-induced intestinal, but also lung allergic responses in an IgE- and TLR4-dependent manner (25, 26). Thus, the adjuvant effect of ATI is not limited to the intestine, but can also be observed for other organs, fueling ongoing inflammation. These inflammatory conditions might favor the formation of $ONOO^-$ and, thereby, protein nitration (7–9, 27), including ATI in the gut, apart from the environmental factors that may induce protein nitration.

To elucidate the effect of nitration, we chemically modified ATI using three different methods simulating endo- (*in vivo*) and exogenous (environmental) nitration mechanisms. These nitrating agents mainly induce the formation of 3-nitrotyrosine (1, 5, 27–31). The aim of our study was to examine whether nitrated ATI exhibit an altered innate and adaptive immunostimulatory capacity. Modified ATI were quantified for their nitration degree using HPLC-DAD and ELISA. Furthermore, various *in vitro* studies were performed. A novel HeLa TLR4 reporter cell line was established for determination of innate immune stimulation. Adaptive immune reactions were analyzed in a mixed lymphocyte reaction by the use of primary immune cells isolated from whole blood of healthy donors. TLR4

activation, NF-κB translocation, expression of surface maturation markers, Th1, Th2, relevant cytokines, and T cell proliferation were measured.

MATERIALS AND METHODS

Nitration and Analysis of Nitrated ATI

Nitration With Tetranitromethane (TNM) of ATI

ATI were obtained from Sigma Aldrich (α-Amylase Inhibitor from *Triticum aestivum* (wheat seed), Sigma-Aldrich, Darmstadt, Germany). Aliquots of aqueous ATI solutions (1 mg/mL, 0.5 mL) were mixed with 4.55 μL TNM/Methanol (4%, v/v) and stirred for 3 h at room temperature. To remove excess TNM after the reaction, a PD-25 size exclusion chromatography column (GE Healthcare, Little Chalfont, Great Britain) was used according to the manufacturer's instructions. Finally, the ATI were eluted with endotoxin free water (MilliQ, Biopak, Merck, Darmstadt, Germany).

Nitration With O_3/NO_2 of ATI

ATI aqueous solutions (0.5 mg/mL, 1 mL) were exposed to a gas mixture of O_3 and NO_2, as described previously (31). Briefly, O_3 was produced from synthetic air passed through a UV lamp (LOT-Quantum Design, Darmstadt, Germany) at ∼1.98 L/min. The air flow was then mixed with a N_2 flow (20 mL/min) containing ∼5 ppmV NO_2 (AirLiquide, Düsseldorf, Germany). The resulting air gas mixtures were bubbled directly through the aqueous ATI solutions at a flow rate of 60 mL/min using a Teflon tube (ID: 1.59 mm). The concentrations of O_3/NO_2 were monitored by commercial monitoring instruments (Ozone analyzer, 49i; NO_x analyzer, 42i-TL, Thermo Fisher Scientific, Darmstadt, Germany, respectively).

$ONOO^-$ Nitration of ATI

ATI solutions were prepared in 50 mM ammonium bicarbonate buffer at pH 7.8 (Carl Roth, Karlsruhe, Germany). For one reaction 300 μL of ATI solution [1 mg/mL] were mixed with 2.85 μL $ONOO^-$ (160–200 mM, Merck) in brown reaction vessels (Eppendorf, Hamburg, Germany) and incubated for 110 min on ice. Immediately after the reaction, the samples were desalted using a PD-10 size exclusion mini column (GE Healthcare), following the manufacturer manual with endotoxin free water.

HPLC-DAD Analysis

All nitrated ATI samples were analyzed using HPLC coupled to diode array detection (HPLC-DAD, 1,200 series, Agilent Technologies, Santa Clara, California, USA). Values were determined using peak areas of signals at wavelengths 280 and 357 nm. A detailed description of the analytical method can be found in Selzle et al. (30). The nitration degree is defined as the concentration of nitrotyrosine as a fraction of the sum of the concentrations of nitrotyrosine and tyrosine. For example, ATI 0.19 Chain D from *T. aestivum* comprises five tyrosine residues. A nitration degree of 20% reflects on average one nitrotyrosine per ATI 0.19 molecule.

Endotoxin Quantification

Endotoxin was quantified by Limulus Amebocyte Lysate chromogenic endotoxin quantitation kit (Thermo Fisher Scientific). ATI samples were tested at several dilutions and compared to an *Escherichia coli* endotoxin standard (011:B4) provided with the kit. The endotoxin levels in the final concentration used for all experiments were <20 Endotoxin units per mL.

Protein Analysis

To determine the ATI protein concentrations before and after nitration, a bicinchoninic acid assay (Thermo Fisher Scientific) was used according to the manufacturer's instructions. The optical density at 562 nm was determined using a Synergy Neo plate reader (Biotek, Bad Friedrichshall, Germany).

ATI oligomers were detected using sodium dodecyl sulfate polyacrylamide gel electrophoresis (5–20%, Bio-Rad, Munich, Germany), referring to the instruction manual. A 5 μg portion of each sample was prepared in 2x Laemmli buffer (Bio-Rad) containing 100 mM Dithiothreitol (Sigma Aldrich), heated on 96°C for 5 min, and loaded on the gel. After separation, the gel was stained for 3 h in Coomassie blue (Bio-Rad) and unstained in an aqueous solution containing 10% methanol (Merck) and 20% acetic acid (Carl Roth) over night. For image acquisition and for analysis, a ChemiDoc system and Image Lab software 5.2.1 (both Bio-Rad) were used, respectively.

Cell Culture

Hela TLR4 Dual Luciferase Reporter Cell Line (HeLa TLR4 Dual)

Cells were grown in Dulbecco's Modified Eagle's Medium (DMEM, Thermo Fisher Scientific) containing 25 mM D-glucose, 1 mM sodium pyruvate supplemented with 10% heat-inactivated fetal calf serum (FCS), (Biochrom, Berlin, Germany), 1% Penicillin/Streptomycin (Thermo Fisher Scientific), and 140 μg/mL Hygromycin B (Invivogen, Toulouse, France) in a humidified atmosphere of 5% CO_2 at 37°C.

For simultaneous determination of TLR4 stimulation and viability, a novel monoclonal dual reporter cell line was established. Therefore, the HeLa TLR4 cell line (Novusbio, Wiesbaden, Germany), expressing Renilla luciferase under the control of an IL-8 promotor reporting TLR4 activity, was stably transfected with a plasmid, constitutively expressing Firefly luciferase, and, thereby, measuring viability (pCMB-firefly-luc-hygro, kindly provided by Ernesto Bockamp, University Medical Center of the Johannes Gutenberg University). Lipofectamine 3000 (Thermo Fisher Scientific) was used as the transfecting reagent according to the manufacturer's protocol.

Combined TLR4 and viability assay

20,000 HeLa TLR4 dual reporter cells were seeded in a flat bottom 96-well plate (Greiner, Frickenhausen, Germany) in 100 μL complete DMEM. On the next day, the cells were treated with different nitrated ATI at a final concentration of 7.5 μg/mL. Mock nitrations and medium served as negative controls, and LPS EB (25 ng/mL, Invivogen) as a positive control. After 7 h, the plate was washed with 200 μL of warm PBS containing

calcium and magnesium (Thermo Fisher Scientific). Then the cells were lysed by adding passive lysis buffer (Dual-luciferase reporter assay, Promega, Mannheim, Germany) and frozen at −80°C. An analysis of both luciferase reporter activities in the cell lysate was performed according to the manufacturer's manual (Promega). The relative luciferase activity was calculated by dividing the Renilla luciferase (TLR4) signal by the Firefly luciferase (viability) signal. The resulting values were normalized to the value obtained for LPS treated cells.

To inhibit TLR4 signaling, HeLa TLR4 dual cells were pre-incubated with the TLR4 antagonist TAK242 (0.36 μg/mL, Merck), or, as a negative control, its solvent dimethylsulfoxide (4.4 μg/mL, Thermo Fisher Scientific) for 150 min.To provide a stronger stimulation, the doses of ATI were doubled in these experiments [15 μg/mL].

Generation of Monocyte Derived Dendritic Cells (DC)

Buffy coats from ten healthy donors were obtained from the Transfusion Center (University Medical Center of the Johannes Gutenberg University, Mainz, Germany) with approval from the local ethical committee (Landesärztekammer Rheinland-Pfalz). Peripheral blood mononuclear cells (PBMC) were isolated by Ficoll-Paque 1.077 g/mL (Biochrom) density centrifugation. The autologous plasma was heat-inactivated at 56°C for 30 min, centrifuged at 1,500 × g, and stored at 4°C. To enrich $CD14^+$ monocytes, 5×10^6 PBMC per well were incubated in a 12-well plate (Greiner) in 1.5 mL Iscove modified Dulbecco medium (IMDM, Lonza, Basel, Switzerland) enriched with 1% antibiotic/antimycotic solution (Sigma Aldrich) and 3% autologous plasma for 40 min in a cell incubator under 5% CO_2 atmosphere at 37°C. Cells were washed 3 times with warm PBS (without calcium magnesium, Thermo Fisher Scientific), and maintained in IMDM, supplemented with 10 ng/mL IL-4 (Miltenyi, Bergisch Gladbach, Germany), 200 U/mL granulocyte-macrophage colony-stimulating factor (GM-CSF, Leukine®, Immunex Corp., Seattle, WA, USA), and 2% autologous plasma. On day 6, immature DC were pulsed with ATI [15 μg/mL], TNM nitrated ATI [15 μg/mL], equivalent amounts of mock nitrated solution, or were left untreated. To induce DC maturation, the cells were additionally treated with tumor necrosis factor (TNF)-alpha, 10 ng/mL, Miltenyi Biotec), IL-1β (10 ng/mL, Miltenyi Biotec) and prostaglandin E_2 (1 μg/mL, Cayman Chemical, Ann Arbor, MI, USA). After 48 h, DC were harvested, washed twice in cold PBS, and used for T cell stimulation assays as well as for analysis of surface marker expression.

Surface marker staining and analysis by flow cytometry

5×10^4 DC or 5×10^5 T cells were stained with specific mouse anti-human monoclonal antibodies (mAbs) for 20 min at 4°C. The following antibodies were used: AlexaFluor 647-conjugated CD4 (MT310; Santa Cruz Biotechnology, Inc., Santa Cruz, CA, USA), fluorescein isothiocyanate (FITC)-conjugated human leukocyte antigen D-related (HLA-DR) (L243), phycoerythrin (PE)-conjugated CD80 (L307.4), and allophycocyanin-conjugated CD83 (HB15e, all from BD Biosciences). As a negative control, matured cells were used. Then, cells were washed, and analyzed by BD Accuri™ C6 Plus Flow Cytometer (BD Biosciences).

Isolation of $CD4^+$ T cells and co-culture with autologous native ATI- or TNM nitrated ATI-pulsed DC

Autologous $CD4^+$ T cells were obtained from PBMC using antibody-coated paramagnetic MicroBeads (MACS; Miltenyi Biotec) according to the manufacturer's protocol. Separation was confirmed by flow cytometry (purity, >98% $CD4^+$ T cells).

1×10^5 T cells and 1×10^4 mDC were co-cultured in 96-well plates (Greiner) in triplicates in 200 μL IMDM containing

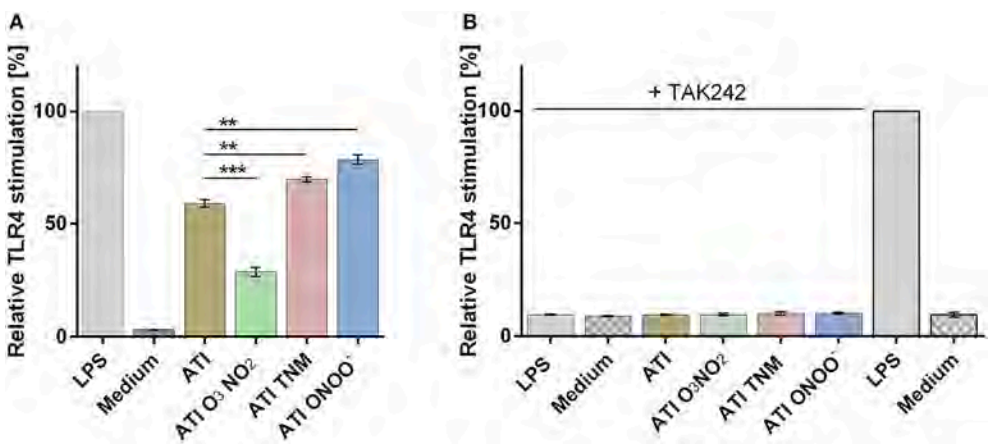

FIGURE 1 | Different nitrated ATI induce distinct TLR4 activation in HeLa TLR4 dual reporter cells. **(A)** HeLa TLR4 dual reporter cells were treated for 7 h with nitrated or unmodified ATI [7.5 μg/mL] or LPS [25 ng/mL] as a positive control. **(B)** Cells were pre-incubated for 2.5 h with TAK242 [0.36 μg/mL] or its solvent DMSO [4.4 μg/mL]. Then the cells were stimulated with nitrated or unmodified ATI [15 μg/mL], or LPS [25 ng/mL] for 7 h. The relative luciferase activity was calculated by dividing the Renilla luciferase (TLR4) signal by the Firefly luciferase (viability) signal. The resulting values were normalized to the value obtained for LPS- treated cells. Shown are the means ± SD of three independent experiments measured in triplicates using two independently nitrated probes. ***$P < 0.001$, **$P < 0.01$.

5% autologous plasma. Five days later, 50 µL of supernatant was taken for quantification of cytokine production. For the determination of proliferation, the co-culture was pulsed with 37 kBq/well of [^{3}H]-thymidine (ICN Biomedicals, CA, USA) for 6 h and [^{3}H]-TdR incorporation was measured using a beta counter (1205 Betaplate, LKB Wallac, Turku, Finland).

Quantification of soluble cytokines by magnetic multiplex assay

For quantification of cytokines, multiplex assay kits (R&D systems, Biotechne, Wiesbaden, Germany) were used. Supernatants from immature DC cultures were tested for TNF-alpha, IL-6, IL-8, IL-1β, and monocyte chemoattractant protein 1 (MCP1). Supernatants of mature DC-T cell co-cultures were analyzed for interferon gamma (IFN-gamma), IL-10, IL-17, IL-6, IL-4, IL-5, and IL-13. The samples were prepared according to the manufacturer's manual and analyzed on a MAGPIX device (Luminex, Austin, Texas, USA).

Quantification of ATI Induced NF-κB Translocation

Nuclear NF-κB translocation in macrophages was determined by fluorescence microscopy. Therefore, PBMCs were isolated and seeded in 12-well glass bottom plates (Cellvis, California, USA) at a concentration of $1.5 \times 10^6 - 2 \times 10^6$ cells per well in IMDM enriched with 200 U/mL GM-CSF and 2% autologous plasma. After 6 days, cells were stimulated for 2 h either with ATI, ATI TNM [12.5 µg/mL], or with LPS EB (100 ng/mL, Invivogen) as a positive control. Untreated cells (medium) served as a negative control. Next, cells were washed once in pre-warmed PBS and fixed using 4% formaldehyde solution (Thermo Fisher

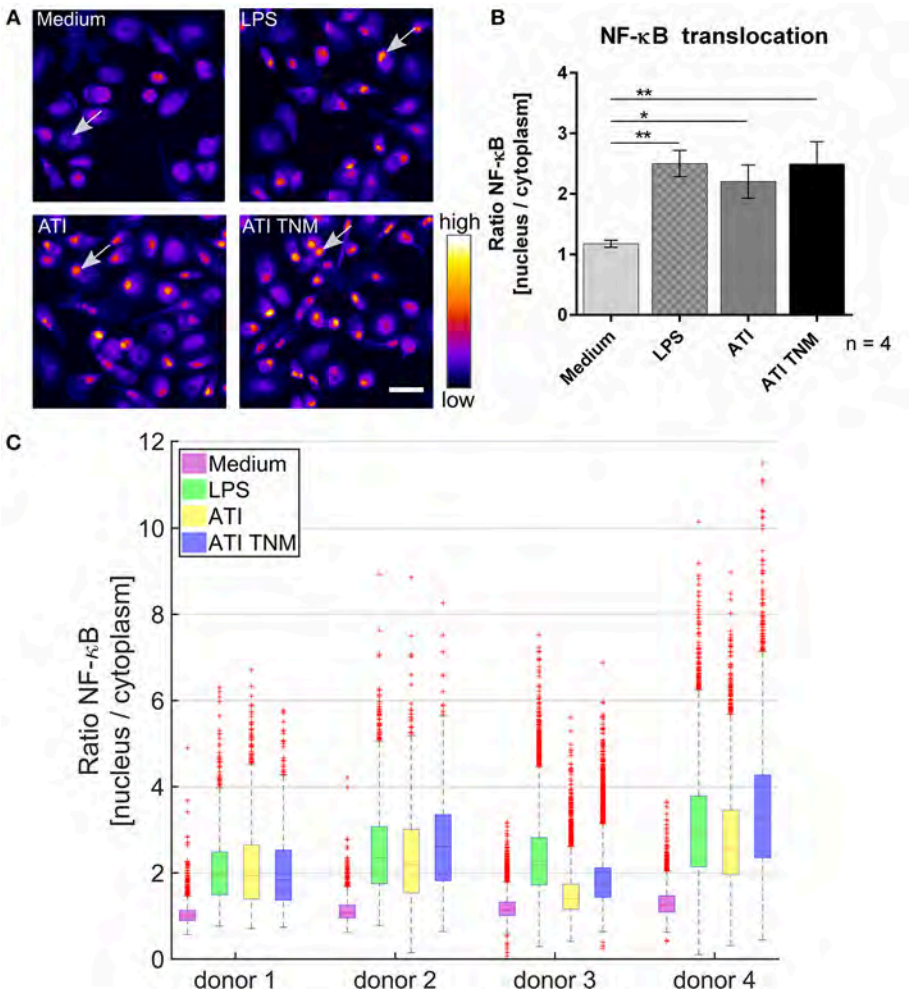

FIGURE 2 | Increased NF-κB p65 translocation into the cell nucleus in ATI and ATI TNM treated primary human macrophages. **(A)** Fluorescence microscopy images of macrophages treated for 2 h with LPS (positive control, 100 ng/mL), ATI or ATI TNM [12.5 µg/mL] and stained for NF-κB. In untreated conditions (medium) NF-κB resides mostly in the cytoplasm, whereas an increased translocation of NF-κB p65 into the nucleus can be observed for LPS, ATI, and ATI TNM treated cells (indicated by arrows). Brightness and contrast were adjusted to the same level for every image within the panel. Scale bar = 50 µm. **(B)** Quantitative evaluation of NF-κB translocation from the cell cytoplasm to the nucleus by Harmony high-content analysis software (Perkin Elmer). Shown are the means ± SEM from four independent experiments/donors, $^*P < 0.05$, $^{**}P < 0.01$. **(C)** Donor-dependent response to LPS (green), ATI (yellow), and ATI TNM (blue) treatment.

Scientific) in PBS for 10 min at 37°C. Subsequently, cells were rinsed three times with PBS, then blocked and permeabilized in PBS containing 0.3% Triton X-100 (Merck) and 5% bovine serum albumin (BSA, Cell Signaling Technology, Danvers, Massachusetts) for 1 h at room temperature. Afterwards, cells were incubated with primary rabbit anti-NF-κB p65 mAb (D14E12, Cell Signaling Technology) diluted in PBS comprising 1% BSA and 0.3% Triton X-100 (Merck) overnight at 4°C. Thereafter, cells were washed three times in PBS for 5 min each and incubated for 1 h at room temperature with anti-rabbit Alexa Fluor 568 antibody (A-11011, Thermo Fisher Scientific) diluted in PBS comprising 1% BSA and 0.3% Triton X-100. Cells were washed again three times in PBS for 5 min each and cell nuclei were counterstained using 4′,6-diamidino-2-phenylindole (DAPI, Thermo Fisher Scientific) according to the manufacturer's instructions. Imaging of stained macrophages was performed at an Opera Phenix High-Content Screening system (Perkin Elmer, Waltham, Massachusetts, USA). PBS was used as an imaging buffer. For image analysis, Harmony high-content analysis software (Perkin Elmer, Waltham, Massachusetts, USA)

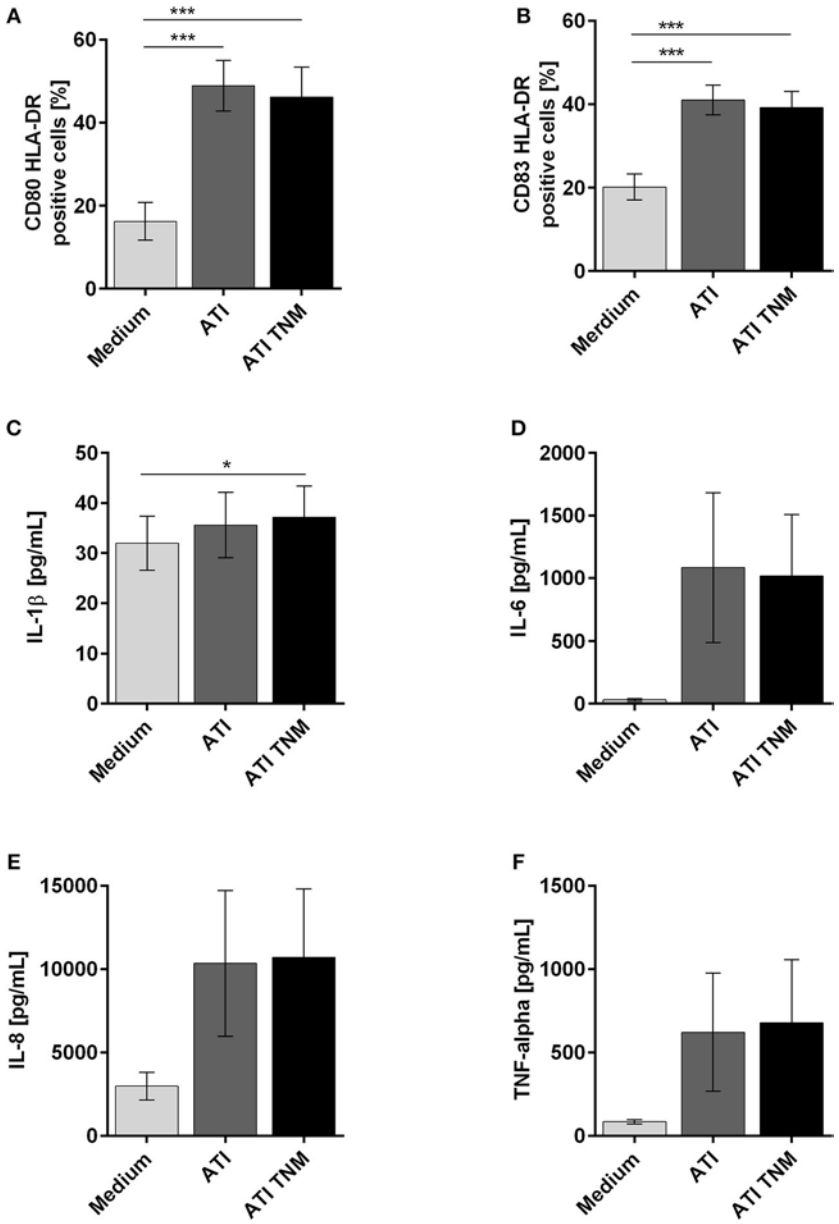

FIGURE 3 | Enhanced expression of maturation markers as well as pro-inflammatory cytokines by human immature DCs upon stimulation with ATI and ATI TNM. Immature DCs were pulsed with ATI or ATI TNM [15 μg/mL] on day 6. Forty-eight hours later cells were stained for expression of the indicated surface markers and analyzed by flow cytometry **(A,B)**. Before, supernatants were taken for determination of IL-1β, IL-6, IL-8, and TNF-alpha by magnetic multiplex assay **(C–F)**. Shown are the means ± SEM from ten independent experiments/donors, $^{*}P < 0.05$, $^{***}P < 0.001$.

was used. Nuclei were identified by DAPI staining, and a ring-like mask around each identified nucleus was created to obtain the corresponding cytoplasm area. Afterwards, the mean intensities of NF-κB within both masks were determined and the nuclear to cytoplasmic ratio of NF-κB was calculated. The described image processing steps are illustrated in **Figure S1**.

Statistics

GraphPad Prism version 6.07 (GraphPad, San Diego, California) was used for statistical analysis. To determine the standard deviation between the different treated groups, an ANOVA was performed. Unpaired *t*-tests were performed for TLR4 activation measurements using the Hela TLR4 dual reporter cell line. For all data sets based on primary immune cells, paired *t*-tests were carried out. Differences between groups were considered as significant when $^{*}p < 0.05$, $^{**}p < 0.01$, or $^{***}p < 0.001$. The number of experiments performed for each data set is described at the end of each figure legend.

RESULTS

Nitration of ATI by Different Nitrating Agents

The degree of ATI nitration varied for the different nitrating agents and methods used. High nitration was observed with TNM and $ONOO^-$. Lowest nitration was obtained for O_3/NO_2 (**Table 1**). All three nitration methods were able to modify ATI and induce about 3–13% of covalently linked ATI oligomers (**Figures S2A,B**).

Nitration of ATI Enhances TLR4 Stimulatory Activity

Compared to unmodified ATI, TNM, and $ONOO^-$, nitrated ATI induced a significantly higher TLR4 activation in HeLa TLR4 dual reporter cells. However, ATI nitrated with O_3 and NO_2 exhibited a lower TLR4 activation compared to native ATI (**Figure 1A**). All mock nitrations showed no TLR4 activation (**Figure S3**).

Administration of the TLR4 antagonist TAK242 completely diminished TLR4 activation induced by ATI or by the positive control LPS (**Figure 1B**).

TABLE 1 | Levels of ATI nitration by different nitrating agents.

Agent	Reaction condition	Nitration degree (%)[a]	Nitrotyrosine [μg/ml][b]
TNM	4.55 μL [4%], 3 h	19.5 ± 0.2	0.36 ± 0.03
O_3/NO_2	O_3 [200 ppb], NO_2 [50 ppb], 4 h	8.6 ± 0.5	7.8E-04 ± 2.4E-04
$ONOO^-$	2.85 μl [200mM], 1.8 h	26.2 ± 6,2	0.23 ± 0.12

[a] *The ND values here were corrected according to the background for pre-nitrated signals of native ATI (n = 2). Blank samples were conducted under the same nitration conditions, and no signal at 280 nm and 357 nm was detected for all the mock samples.*

[b] *The values are expressed in equivalents of nitrotyrosines [μg] nitrated BSA nBSA per 1 μg of nitrated ATI solution (n = 2). The values were corrected against unmodified ATI solution. Mock samples showed no nitration.*

Nitrated and Unmodified ATI Induce Similar Activation of Macrophages and Immature DC

In unstimulated primary human macrophages, NF-κB is mostly located in the cytoplasm. Upon treatment with ATI or TNM nitrated ATI, a significantly enhanced NF-κB translocation from cytoplasm to the cell nucleus was observed using fluorescence microscopy (**Figure 2A**). Nitrated ATI exhibited only slightly higher NF-κB translocation compared to native ATI, which was also observed in the individual donor dependent responses (**Figures 2B,C**).

Immature DC treated with unmodified or TNM nitrated ATI expressed significantly higher amounts of CD80, CD83, and HLA-DR on their surface in comparison to untreated cells (**Figures 3A,B**). For DC treated with mock nitrated samples, no changes were observed (**Figures S4A,B**). Furthermore, the release of the pro-inflammatory cytokines IL-1β, IL-6, IL-8, and TNF-alpha by immature DC was similarly elevated upon ATI or ATI TNM treatment compared to untreated cells (**Figures 3C–F**). No significant changes were observed for MCP-1 release or cells treated with mock nitrations (**Figures S4C–G**).

Nitrated ATI Enhance Proliferation and Induce an Enhanced Th1 and Th2 Cytokine Expression Profile in $CD4^+$ T Cells Stimulated With Autologous Mature DC

To analyze the immunogenicity of nitrated vs. unmodified ATI, $CD4^+$ T cells were co-cultured with autologous mature DC treated before with ATI or ATI-TNM. Proliferations as well as production of Th1 and Th2 cytokines were analyzed. In general, $CD4^+$ T cells from almost all donors showed an enhanced proliferative response and cytokine release after stimulation with ATI-pulsed compared to untreated DC. Only DC treated with nitrated ATI induced a significantly increased T cell proliferation (**Figure 4A**). Moreover, the release of the Th2 cytokines IL-5, IL-6, IL-10, and IL-13 as well as the Th1 cytokine IFN-gamma was significantly enhanced after stimulation with DC treated with ATI-TNM (**Figures 4B–F**). Comparing both ATI-treated groups, we found a significant higher release for IL-5, IL-6, IL-10, and IFN-gamma upon the ATI-TNM stimulus (**Figures 4B,D,F**). There were no significant changes in IL-4 and IL-17A release between all groups (**Figures S5A,B**). Mock nitration did neither influence cytokine release nor T cell proliferation (**Figures S5C–H**).

DISCUSSION

In the present study, we analyzed the impact of nitration on the immunogenicity of ATI, and could show that ATI can be nitrated by exogenous and endogenous nitrating agents. Furthermore, we demonstrated that nitration of ATI lead to enhanced innate and adaptive immune responses compared to unmodified ATI (**Graphical Abstract**).

By using a novel HeLa TLR4 dual luciferase reporter cell line, we could demonstrate that TNM and $ONOO^-$ mediated ATI nitration induced significant enhanced TLR4 stimulation,

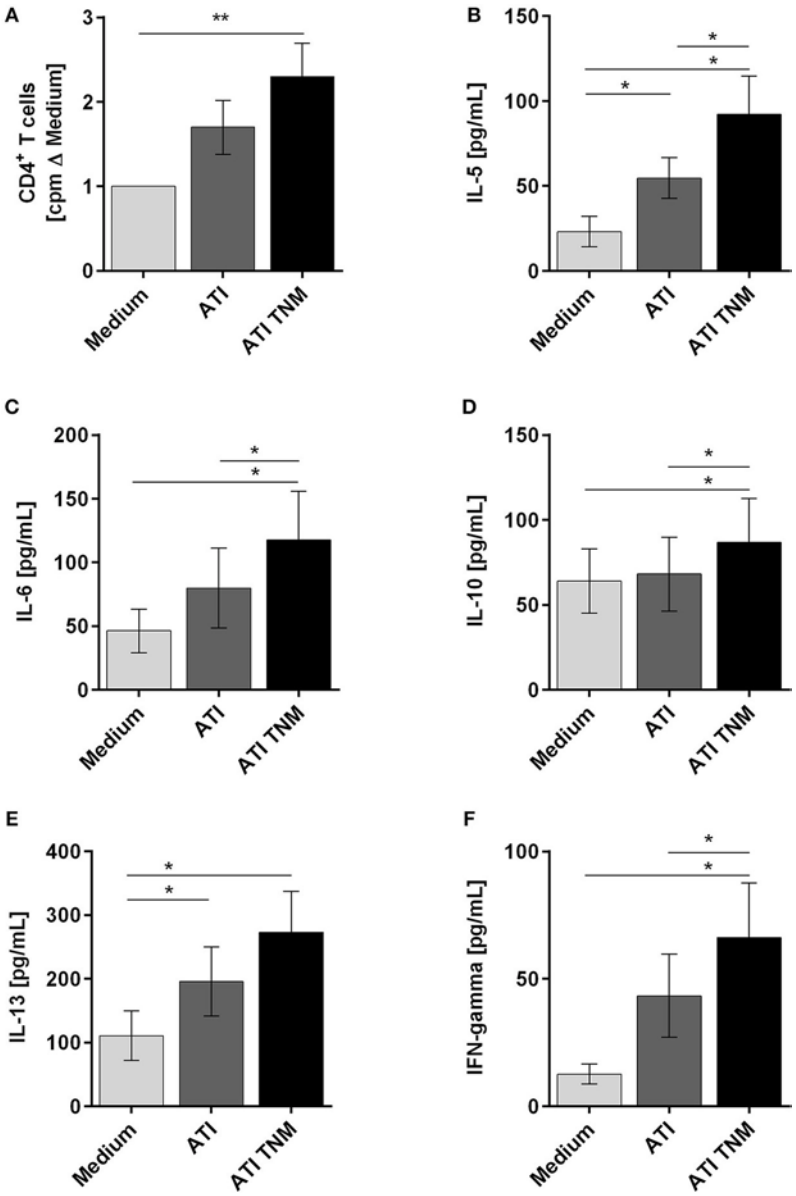

FIGURE 4 | Enhanced T cell proliferation as well as Th1 and Th2 cytokine production of $CD4^+$ T cells stimulated with autologous ATI TNM-pulsed mature DC. Immature DC were pulsed with ATI or ATI TNM [15 μg/mL] and matured with pro-inflammatory cytokines as described in Materials and Methods. After 48 h, mature DC were washed and co-cultivated with autologous $CD4^+$ T cells for 5 days. **(A)** T cell proliferation was measured by $[^3H]$-thymidine incorporation, and proliferation index was calculated related to untreated cells. **(B–F)** Supernatants (50 μL) were collected before thymidine administration to determine the production of IL-5, IL-6, IL-10, IL-13, and IFN-gamma by multiplex assay. Results are presented as means ± SEM from 10 independent experiments/donors. In some cases, cytokine concentrations were below the detection limit so that $n < 10$ (IL-5 $n = 8$, IL-13 $n = 5$, IFN-gamma $n = 9$), $^*P < 0.05$, $^{**}P < 0.01$.

which seems to correlate with the higher nitration degrees as determined by HPLC-DAD and ELISA. Pre-incubation of the cells with the TLR4 antagonist TAK242 inhibited ATI-induced TLR4 signaling, providing further evidence that ATI stimulate TLR4 directly, as reported in previous studies (21, 22). The complete abolishment of TLR4 activity by TAK242 furthermore allows the conclusion that nitrated ATI also impact the TLR4 agonistic properties directly. As nitration always induces the formation of nitrotyrosine (1, 5, 9, 27–31), it may be hypothesized that nitrotyrosine embedded into the ATI secondary structure itself serves as an amplifier. This hypothesis is supported by our results, showing the lack of enhanced TLR4 stimulation in HeLa TLR4 dual reporter cells upon treatment with unmodified ATI combined with pure nitrotyrosine (**Figure S6**).

Moreover, nitration of proteins is known to change their structure and function (29). Further investigations would be necessary to clarify to which degree nitration of ATI alters their

interaction with TLR4 (22), which may explain the observed enhanced TLR4 agonistic activity.

One essential step in TLR4 signaling is the nuclear translocation of the transcription factor NF-κB, controlling the expression of many genes relevant in innate and adaptive immunity (23, 24, 32). Therefore, we performed several studies on primary immune cells from healthy human donors *in vitro*. Using fluorescence microscopy, we visualized and quantified nuclear translocation of NF-κB in primary human macrophages after the addition of ATI or nitrated ATI. Under the conditions chosen, native and nitrated ATI provoked comparable nuclear translocation of NF-κB.

Previous studies showed that, not only NF-kB, but also the interferon regulatory factor (IRF-3) gets activated upon ATI treatment (21). Therefore, future investigations should also investigate whether nitrated ATI effect the IRF-3 pathway.

Moreover, we found that the NF-κB controlled cytokines IL-1β, IL-6, IL-8, TNF-alpha, and the DC maturation markers CD80 and CD83 (32) were strongly enhanced after treatment of immature DC with ATI and nitrated ATI, which is consistent with previous studies (21, 26). This finding indicates that ATI in general induce the maturation of DC, which is an essential step in the induction of T cell mediated immunity, both via Th1 and Th2 T helper cells, as occurs in autoimmunity and allergy, underpinning the intrinsic immune adjuvant function of (nutritional) ATI (20, 25, 26).

To investigate the modulation of adaptive immunity by nitrated ATI, we analyzed syngeneic DC-T cell co-cultures. Here, only TNM ATI treated DC induced significantly enhanced T cell proliferation. Moreover, treatment of DC with ATI or nitrated ATI caused a significantly higher release of Th2 relevant cytokines IL-5, IL-6, IL-10, and IL-13, and of the Th1 cytokine IFN-gamma. For unmodified ATI, this finding is in line with our prior studies on nutritional and inhalative allergies (25, 26). Remarkably, nitrated ATI significantly enhanced the production of both Th1 and Th2 cytokines compared to unmodified ATI.

Therefore, it can be concluded that nitrated ATI possess an overall enhanced immune stimulatory potential, including Th1 mediated diseases, as was shown by us before for unmodified ATI in murine inflammatory bowel disease (20). These results make it highly probable that nitrated ATI may more strongly promote inhalative wheat allergies (baker's asthma), NCWS, other allergies, and autoimmune diseases.

Similar findings were reported for other nitrated allergens in the context of allergic airway inflammation or anaphylaxis, but the exact underlying molecular mechanisms are still elusive (1–6). Allergen oligomerization as a side product during the nitration process (e.g., cross-linking of protein-bound tyrosine to form a dimer, or the formation of disulfide bridges) was observed for several proteins, and is discussed as one possible mechanism (4, 30, 31, 33). In this respect, it was suggested that one structural aspect of allergens is their capability to form dimers or oligomers, thereby enhancing their allergenicity (34). Ackaert et al. (4) reported two-fold higher stability for nitrated, as compared to unmodified, Bet v 1, making the allergen more resistant to proteolytic degradation, thus permitting enhanced and prolonged presentation on DC, followed by an enhanced T cell response (3, 4). Interestingly, higher molecular weight aggregates instead of oligomers of Bet v 1 (4), and the hypoallergenic Bet v 1d (35) were reported to favor Th1 immunogenicity. Indeed, for all nitration methods used, we found fractions of covalently linked ATI oligomers after the reaction.

Taken together, our results demonstrate that ATI are potent stimulators of innate and adaptive immune responses. In contrast to unmodified ATI, the nitrated ATI exhibit stronger immune stimulatory effects. The observed enhanced immunogenicity of ATI provides a causative chain between stronger TLR4 agonistic effects, leading to enhanced Th1 and Th2 cell activation upon nitration. Future investigations are needed to test how far the degrees of nitration obtained in our study match endogenous ATI nitration under inflammatory conditions, or exogenous nitration, which may occur under certain conditions of wheat growing and processing, e.g., via intensive fertilization, environmental pollution, or nitration during food processing.

DATA AVAILABILITY STATEMENT

All datasets analyzed for this study are included in the manuscript and the supplementary files.

AUTHOR CONTRIBUTIONS

DS, UP, KR-S, IB, and KL designed the experiments. KZ, JN, FL, and IB performed the experiments. KZ, JN, FL, JF-N, DS, UP, IB, and KL analyzed and interpreted the data. CC, JS, FL, KR-S, and IB contributed materials, methods, analysis tools. KZ, IB, and KL wrote the paper. All authors were involved in the editing and proofreading of the manuscript.

FUNDING

This work was supported by the Max Planck Graduate Center with the Johannes Gutenberg University Mainz (MPGC). DS was supported for ATI-related work by grants from the German Research Foundation (DFG) (DFG-Schu 646/17-1, DFG-Schu-646/20-1, the Collaborative Research Center TR128 Multiple Sclerosis project A08), and the Leibniz Foundation (project Wheatscan). IB was supported by DFG grant BE 4504/3-1.

ACKNOWLEDGMENTS

The authors acknowledge helpful discussions with the members of the Mainz Program for Chemical Allergology (MPCA) and support from the Max Planck Graduate Center with the Johannes Gutenberg University Mainz (MPGC). KZ and JN acknowledge the support by the IMB Microscopy and Histology Core Facility, as well as the DFG for funding the Opera Phenix High Content Spinning Disk Microscope (Project 402386039).

SUPPLEMENTARY MATERIAL

The Supplementary Material for this article can be found online at: https://www.frontiersin.org/articles/10.3389/fimmu.2018.03174/full#supplementary-material

REFERENCES

1. Franze T, Weller MG, Niessner R, Poschl U. Protein nitration by polluted air. *Environ Sci Technol.* (2005) 39:1673–8. doi: 10.1021/es0488737
2. Gruijthuijsen YK, Grieshuber I, Stocklinger A, Tischler U, Fehrenbach T, Weller MG, et al. Nitration enhances the allergenic potential of proteins. *Int Arch Allergy Immunol.* (2006) 141:265–75. doi: 10.1159/000095296
3. Karle AC, Oostingh GJ, Mutschlechner S, Ferreira F, Lackner P, Bohle B, et al. Nitration of the pollen allergen bet v 1.0101 enhances the presentation of bet v 1-derived peptides by HLA-DR on human dendritic cells. *PLoS ONE* (2012) 7:e31483. doi: 10.1371/journal.pone.0031483
4. Ackaert C, Kofler S, Horejs-Hoeck J, Zulehner N, Asam C, Von Grafenstein S, et al. The impact of nitration on the structure and immunogenicity of the major birch pollen allergen Bet v 1.0101. *PLoS ONE* (2014) 9:e104520. doi: 10.1371/journal.pone.0104520
5. Reinmuth-Selzle K, Ackaert C, Kampf CJ, Samonig M, Shiraiwa M, Kofler S, et al. Nitration of the birch pollen allergen Bet v 1.0101: eÿ ciency and site-selectivity of liquid and gaseous nitrating agents. *J Proteome Res.* (2014) 13:1570–7. doi: 10.1021/pr401078h
6. Reinmuth-Selzle K, Kampf CJ, Lucas K, Lang-Yona N, Frohlich-Nowoisky J, Shiraiwa M, et al. Air pollution and climate change effects on allergies in the anthropocene: abundance, interaction, and modification of allergens and adjuvants. *Environ Sci Technol.* (2017) 51:4119–41. doi: 10.1021/acs.est.6b04908
7. Galinanes M, Matata BM. Protein nitration is predominantly mediated by a peroxynitrite-dependent pathway in cultured human leucocytes. *Biochem J.* (2002) 367:467–73. doi: 10.1042/bj20020825
8. Salvemini D, Doyle TM, Cuzzocrea S. Superoxide, peroxynitrite and oxidative/nitrative stress in inflammation. *Biochem Soc Transl.* (2006) 34:965–70. doi: 10.1042/BST0340965
9. Ferrer-Sueta G, Campolo N, Trujillo M, Bartesaghi S, Carballal S, Romero N, et al. Biochemistry of peroxynitrite and protein tyrosine nitration. *Chem Rev.* (2018) 118:1338–408. doi: 10.1021/acs.chemrev.7b00568
10. Fasano A, Sapone A, Zevallos V, Schuppan D. Nonceliac gluten sensitivity. *Gastroenterology* (2015) 148:1195–204. doi: 10.1053/j.gastro.2014.12.049
11. Schuppan D, Zevallos V. Wheat amylase trypsin inhibitors as nutritional activators of innate immunity. *Dig Dis.* (2015) 33:260–3. doi: 10.1159/000371476
12. Zundler S, Neurath MF. Pathogenic T cell subsets in allergic and chronic inflammatory bowel disorders. *Immunol Rev.* (2017) 278:263–76. doi: 10.1111/imr.12544
13. Schuppan D, Pickert G, Shfaq-Khan M, Zevallos V. Non-celiac wheat sensitivity: differential diagnosis, triggers and implications. *Best Pract Res Clin Gastroenterol.* (2015) 29:469–76. doi: 10.1016/j.bpg.2015.04.002
14. Leccioli V, Oliveri M, Romeo M, Berretta M, Rossi P. A New proposal for the pathogenic mechanism of non-coeliac/non-allergic gluten/wheat sensitivity: piecing together the puzzle of recent scientific evidence. *Nutrients* 9:E1203. doi: 10.3390/nu9111203
15. Walusiak J, Wiszniewska M, Krawczyk-Adamus P, Palczynski C. Occupational allergy to wheat flour. Nasal response to specific inhalative challenge in asthma and rhinitis vs. isolated rhinitis: a comparative study. *Int J Occup Med Environ Health* (2004) 17:433–40.
16. Tatham AS, Shewry PR. Allergens to wheat and related cereals. *Clin Exp Allergy* (2008) 38:1712–26. doi: 10.1111/j.1365-2222.2008.03101.x
17. Dupont FM, Vensel WH, Tanaka CK, Hurkman WJ, Altenbach SB. Deciphering the complexities of the wheat flour proteome using quantitative two-dimensional electrophoresis, three proteases and tandem mass spectrometry. *Proteome Sci.* (2011) 9:10. doi: 10.1186/1477-5956-9-10
18. Finnie C, Melchior S, Roepstorff P, Svensson B. Proteome analysis of grain filling and seed maturation in barley. *Plant Physiol.* (2002) 129:1308–19. doi: 10.1104/pp.003681
19. Payan F. Structural basis for the inhibition of mammalian and insect alpha-amylases by plant protein inhibitors. *Biochim Biophys Acta* (2004) 1696:171–80. doi: 10.1016/j.bbapap.2003.10.012
20. Zevallos VF, Raker V, Tenzer S, Jimenez-Calvente C, Ashfaq-Khan M, Russel N, et al. Nutritional wheat amylase-trypsin inhibitors promote intestinal inflammation via activation of myeloid cells. *Gastroenterology* (2017) 152:1100–13. doi: 10.1053/j.gastro.2016.12.006
21. Junker Y, Zeissig S, Kim SJ, Barisani D, Wieser H, Leffler DA, et al. Wheat amylase trypsin inhibitors drive intestinal inflammation via activation of toll-like receptor 4. *J Exp Med.* (2012) 209:2395–408. doi: 10.1084/jem.20102660
22. Cuccioloni M, Mozzicafreddo M, Ali I, Bonfili L, Cecarini V, Eleuteri AM, et al. Interaction between wheat alpha-amylase/trypsin bi-functional inhibitor and mammalian digestive enzymes: Kinetic, equilibrium and structural characterization of binding. *Food Chem.* (2016) 213:571–8. doi: 10.1016/j.foodchem.2016.07.020
23. Kawai T, Akira S. The role of pattern-recognition receptors in innate immunity: update on Toll-like receptors. *Nat Immunol.* (2010) 11:373–84. doi: 10.1038/ni.1863
24. Kawasaki T, Kawai T. Toll-like receptor signaling pathways. *Front Immunol.* (2014) 5:461. doi: 10.3389/fimmu.2014.00461
25. Bellinghausen I, Weigmann B, Zevallos V, Maxeiner J, Reissig S, Waisman A, et al. Wheat amylase-trypsin inhibitors exacerbate intestinal and airway allergic immune responses in humanized mice. *J Allergy Clin Immunol.* (2018). doi: 10.1016/j.jaci.2018.02.041. [Epub ahead of print].
26. Zevallos VF, Raker VK, Maxeiner J, Scholtes P, Steinbrink K, Schuppan D. Dietary wheat amylase trypsin inhibitors exacerbate murine allergic airway inflammation *Eur J Nutr.* (2018). doi: 10.1007/s00394-018-1681-6. [Epub ahead of print].
27. Ischiropoulos H. Protein tyrosine nitration–an update. *Arch Biochem Biophys.* (2009) 484:117–21. doi: 10.1016/j.abb.2008.10.034
28. Walcher W, Franze T, Weller MG, Poschl U, Huber CG. Liquid- and gas-phase nitration of bovine serum albumin studied by LC-MS and LC-MS/MS using monolithic columns. *J Proteome Res.* (2003) 2:534–42. doi: 10.1021/pr034034s
29. Radi R. Protein tyrosine nitration: biochemical mechanisms and structural basis of functional effects. *Acc Chem Res.* (2013) 46:550–9. doi: 10.1021/ar300234c
30. Selzle K, Ackaert C, Kampf CJ, Kunert AT, Duschl A, Oostingh GJ, et al. Determination of nitration degrees for the birch pollen allergen Bet v 1. *Anal Bioanal Chem.* (2013) 405:8945–9. doi: 10.1007/s00216-013-7324-0
31. Liu F, Reinmuth-Selzle K, Lai S, Weller MG, Poschl U, Kampf CJ. Simultaneous determination of nitrated and oligomerized proteins by size exclusion high-performance liquid chromatography coupled to photodiode array detection. *J Chromatogr A.* (2017) 1495:76–82. doi: 10.1016/j.chroma.2017.03.015
32. Sakai J, Cammarota E, Wright JA, Cicuta P, Gottschalk RA, Li N, et al. Lipopolysaccharide-induced NF-kappaB nuclear translocation is primarily dependent on MyD88, but TNFalpha expression requires TRIF and MyD88. *Sci Rep.* (2017) 7:1428. doi: 10.1038/s41598-017-01600-y
33. Kampf CJ, Liu F, Reinmuth-Selzle K, Berkemeier T, Meusel H, Shiraiwa M, et al. Protein cross-linking and oligomerization through dityrosine formation upon exposure to ozone. *Environ Sci Technol.* (2015) 49:10859–66. doi: 10.1021/acs.est.5b02902
34. Scheurer S, Toda M, Vieths S. What makes an allergen? *Clin Exp Allergy* (2015) 45:1150–61. doi: 10.1111/cea.12571
35. Zaborsky N, Brunner M, Wallner M, Himly M, Karl T, Schwarzenbacher R, et al. Antigen aggregation decides the fate of the allergic immune response. *J Immunol.* (2010) 184:725–35. doi: 10.4049/jimmunol.0902080

Conflict of Interest Statement: The authors declare that the research was conducted in the absence of any commercial or financial relationships that could be construed as a potential conflict of interest.

frontiers

Supplementary Material

Nitration of Wheat Amylase Trypsin Inhibitors Increases Their Innate and Adaptive Immunostimulatory Potential *in vitro*

Kira Ziegler[1], Jan Neumann[1,2], Fobang Liu[1], Janine Fröhlich-Nowoisky[1], Christoph Cremer[2,1], Joachim Saloga[3], Kathrin Reinmuth-Selzle[1], Ulrich Pöschl[1], Detlef Schuppan[4], Iris Bellinghausen[3†], and Kurt Lucas[1†*]

[1]*Multiphase Chemistry Department, Max Planck Institute for Chemistry, Mainz, Germany*

[2]*Institute of Molecular Biology, Mainz, Germany*

[3]*Department of Dermatology, University Medical Center of the Johannes Gutenberg University, Mainz, Germany*

[4]*Institute of Translational Immunology, University Medical Center of the Johannes Gutenberg University, Mainz, Germany*

†equally contributing senior authors

*** Correspondence:**

Dr. Kurt Lucas

k.lucas@mpic.de

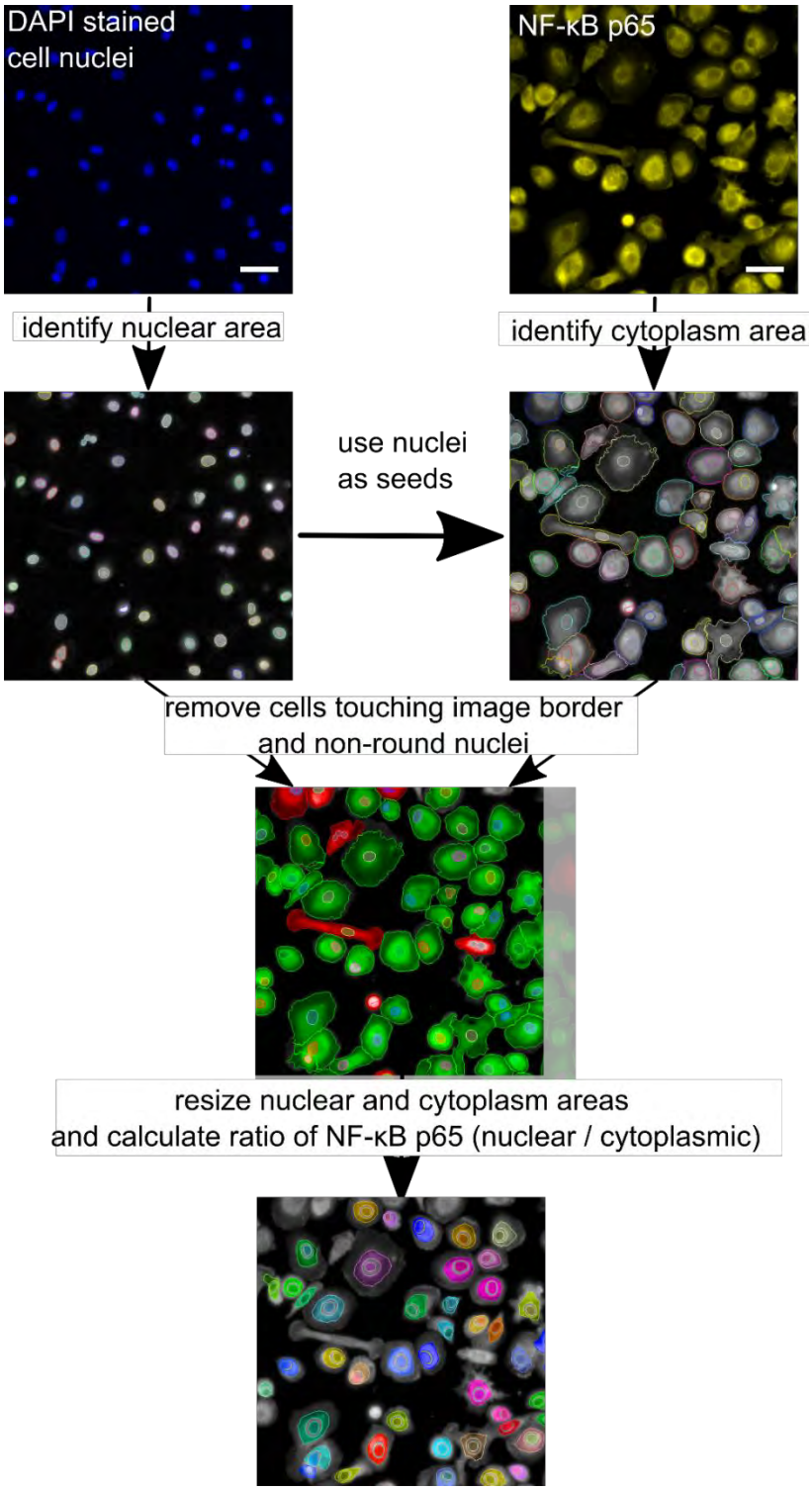

Supplementary Figure 1. Image processing steps to quantify nuclear translocation of NF-κB. DAPI (pseudocolor blue) and NF-κB (pseudocolor yellow) input images were taken at the Opera Phenix High-content screening system (Perkin Elmer, Waltham, Massachusetts, USA). The output image contains the nuclear and cytoplasm masks, which were used to calculate the mean NF-κB p65 intensities within the cytoplasm and the nucleus. Scale bar = 50 µm.

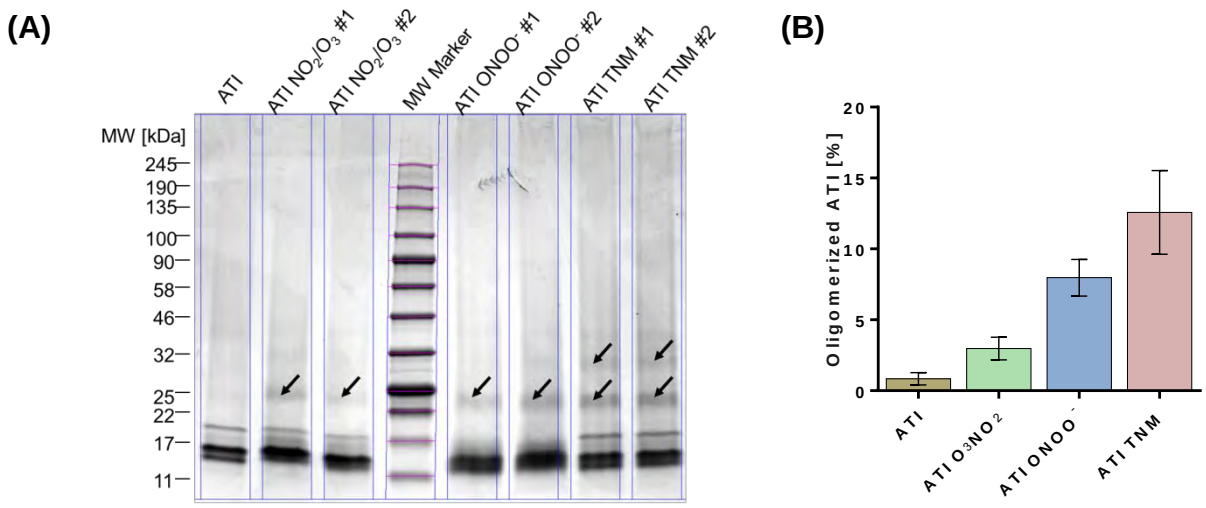

Supplementary Figure 2. SDS PAGE of unmodified ATI and nitrated ATI samples.
5 µg of each ATI sample was analyzed by sodium dodecyl sulfate polyacrylamide gel electrophoresis (SDS PAGE). Molecular weight (MW) is shown in kDa. A: Oligomers can be found for all nitrated ATI samples (indicated with arrows). B: Quantification of oligomers was carried out by Image lab software (Biorad). Results are presented as means ± SEM from n = 2 independent SDS PAGE and nitration experiments.

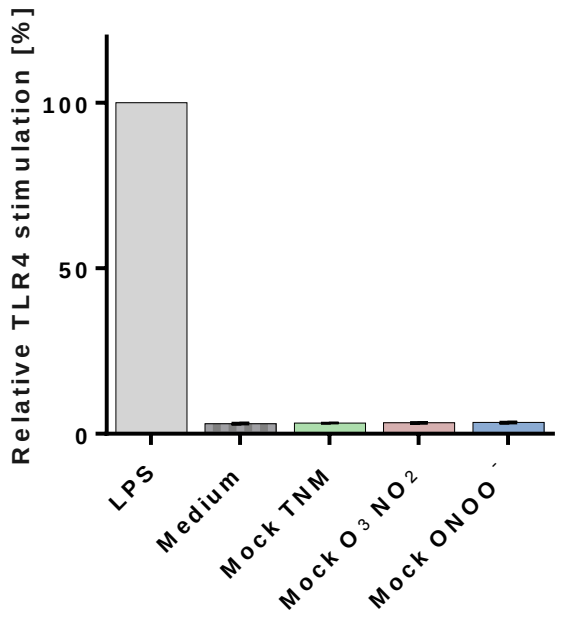

Supplementary Figure 3. TLR4 stimulation by Mock nitration on HeLa TLR4 dual reporter cells.

HeLa TLR4 dual reporter cells were treated for 7 h with equivalent volumes of mock nitrated solution, LPS [25 ng/mL] served as positive control. The relative luciferase activity was calculated by dividing the Renilla luciferase (TLR4) signal to the Firefly luciferase (viability) signal. The resulting values were normalized to the value obtained for LPS treated cells. Shown are the means ± SD of three independent experiments carried out in triplicates, using two independently nitrated probes.

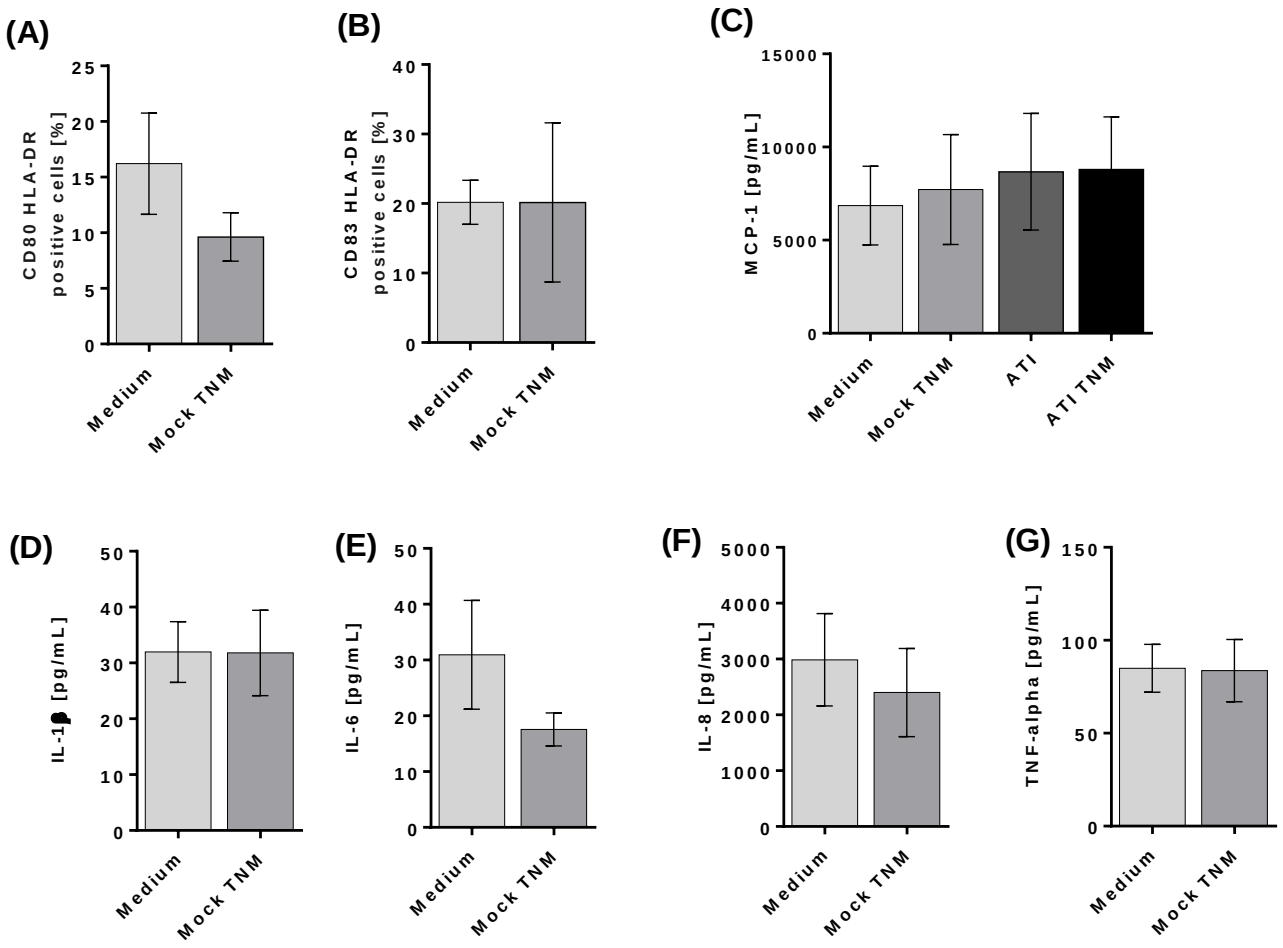

Supplementary Figure 4. Expression of maturation markers as well as pro-inflammatory cytokines by human immature DCs upon stimulation with Mock TNM

Immature DCs were left untreated or pulsed with ATI or ATI TNM [15 µg/mL] or equivalent volumes of mock nitrated solution on day 6. 48 h later the cells were stained for expression of the indicated surface markers and analyzed by flow cytometry (A+B). Before, supernatants were taken for determination of MCP-1, IL-1β, IL-6, IL-8 and TNF-alpha by magnetic multiplex assay (C-G). Shown are the means ± SEM from $n \geq 6$ independent experiments/donors, *P<0.05, ***P<0.001.

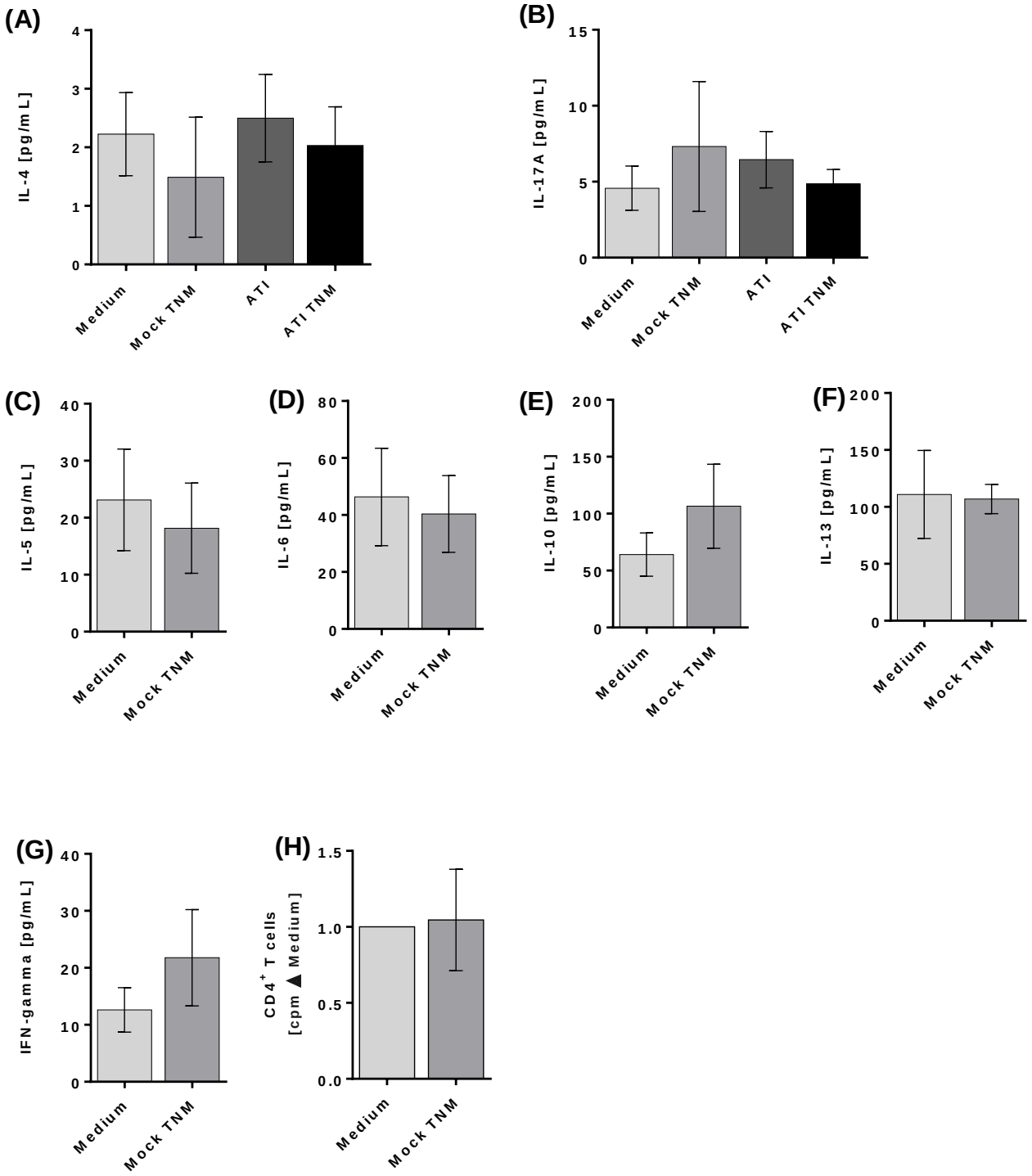

Supplementary Figure 5. T cell proliferation as well as Th1 and Th2 cytokine production of CD4$^+$ T cells stimulated with autologous Mock TNM pulsed mature DC.
Immature DC were left untreated or pulsed with ATI or ATI TNM [15 µg/mL] or equivalent volumes of mock nitrated sample and matured with pro-inflammatory cytokines as described in Materials and Methods. After 48 h, mature DC were washed and co-cultivated with autologous CD4$^+$ T cells for 5 days. A-G: Supernatants (50 µL) were collected before thymidine administration to determine the production of IL-4, IL-17A, IL-5, IL-6, IL-10, IL-13 and IFN-gamma by multiplex assay. H: T cell

proliferation was measured by [^{3}H]-thymidine incorporation and proliferation index was calculated related to untreated cells. Results are presented as means ± SEM from $n \geq 6$ independent experiments/donors.

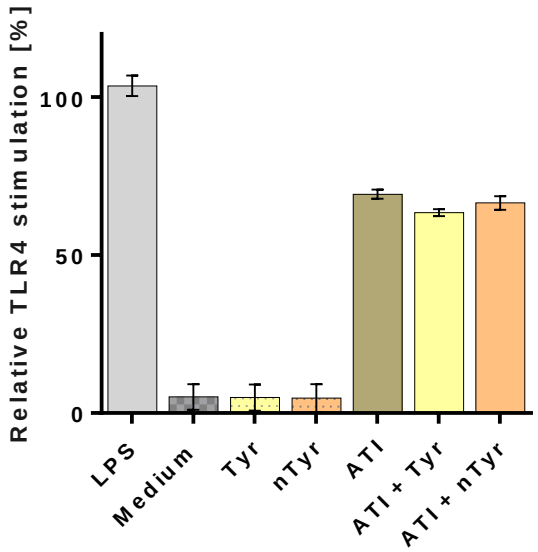

Supplementary Figure 6. TLR4 stimulation by ATI combined with pure nitrotyrosine.

HeLa TLR4 dual reporter cells were treated for 7 h with ATI [7.5 µg/ml] with or without addition of tyrosine or nitrotyrosine [30 µM], LPS [25 ng/mL]. The relative luciferase activity was calculated by dividing the Renilla luciferase (TLR4) signal to the Firefly luciferase (viability) signal. The resulting values were normalized to the value obtained for LPS treated cells. Shown are the means ± SD two independent experiments carried out in duplicates.

B.2 Neumann *et al.* , Nanoscale, 2019

Nanoscale distribution of TLR4 on primary human ATI- and LPS-stimulated macrophages

Neumann J.[1,2], Ziegler K.[1], Gelléri M.[2], Fröhlich-Nowoisky J.[1], Liu F.[1], Bellinghausen I.[3], Schuppan D.[4,5], Birk U.[2,†], Pöschl U.[1], Cremer C.[2,1] and Kurt Lucas[1]

[1]Max Planck Institute for Chemistry, Multiphase Chemistry Department, 55128 Mainz, Germany
[2]Institute of Molecular Biology, Ackermannweg 4, 55128 Mainz, Germany
[3]Department of Dermatology, University Medical Center of the Johannes Gutenberg University, 55131 Mainz, Germany
[4]Institute of Translational Immunology, University Medical Center of the Johannes Gutenberg University, 55131 Mainz, Germany
[5]Division of Gastroenterology, Beth Israel Deaconess Medical Center, Harvard Medical School, MA 02215, USA
[†]Current address: Hochschule für Technik und Wirtschaft Chur, 7000 Chur, Switzerland

Nanoscale, 11, 9769 – 9779 DOI: 10.1039/C9NR00943D (2019):

Author contributions.

UP, CC, KL, UB and JN designed the research. JN and KZ performed the experiments. JN, MG, KL and JFN analyzed and interpreted the data. FL, IB and DS contributed materials and methods. JN, MG and KL wrote the paper. All authors contributed in editing and proof reading of the manuscript.

Nanoscale

PAPER

View Article Online
View Journal

Cite this: DOI: 10.1039/c9nr00943d

Nanoscale distribution of TLR4 on primary human macrophages stimulated with LPS and ATI†

Jan Neumann, [a,b] Kira Ziegler, [a] Márton Gelléri, [b] Janine Fröhlich-Nowoisky, [a] Fobang Liu, [a] Iris Bellinghausen, [c] Detlef Schuppan, [d,e] Udo Birk, ‡[b] Ulrich Pöschl, [a] Christoph Cremer [b,a] and Kurt Lucas *[a]

Received 29th January 2019,
Accepted 27th April 2019

DOI: 10.1039/c9nr00943d

rsc.li/nanoscale

Toll-like receptor 4 (TLR4) plays a crucial role in the recognition of invading pathogens. Upon activation by lipopolysaccharides (LPS), TLR4 is recruited into specific membrane domains and dimerizes. In addition to LPS, TLR4 can be stimulated by wheat amylase-trypsin inhibitors (ATI). ATI are proteins associated with gluten containing grains, whose ingestion promotes intestinal and extraintestinal inflammation. However, the effect of ATI *vs.* LPS on the membrane distribution of TLR4 at the nanoscale has not been analyzed. In this study, we investigated the effect of LPS and ATI stimulation on the membrane distribution of TLR4 in primary human macrophages using single molecule localization microscopy (SMLM). We found that in unstimulated macrophages the majority of TLR4 molecules are located in clusters, but with donor-dependent variations from ~51% to ~75%. Depending on pre-clustering, we found pronounced variations in the *fraction of clustered molecules* and *density of clusters* on the membrane upon LPS and ATI stimulation. Although clustering differed greatly among the human donors, we found an almost constant cluster diameter of ~44 nm for all donors, independent of treatment. Together, our results show donor-dependent but comparable effects between ATI and LPS stimulation on the membrane distribution of TLR4. This may indicate a general mechanism of TLR4 activation in primary human macrophages. Furthermore, our methodology visualizes TLR4 receptor clustering and underlines its functional role as a signaling platform.

Introduction

Toll-like receptors (TLR) represent a family of pattern recognition receptors (PRRs) that are part of the innate immune system.[1,2] TLRs detect damage and pathogen associated molecular patterns (DAMPs, PAMPs), which subsequently triggers the production and release of inflammatory mediators. One of the best studied TLRs is TLR4, which is sensitive to lipopolysaccharide (LPS), a cell wall component of Gram-negative bacteria.[3,4] Moreover, TLR4 detects a broad spectrum of different molecules that are summarized as DAMPs, such as high-mobility group protein B1 (HMGB1) or heat-shock protein 60 (HSP60). TLR4 plays a central role in many acute and chronic inflammatory diseases such as chronic obstructive pulmonary disease (COPD), allergic asthma or non-celiac wheat sensitivity (NCWS).[5–8]

Stimulation of TLR4 through LPS is facilitated by a complex interaction between multiple molecules. First, LPS is bound by the soluble lipopolysaccharide binding protein (LBP), which transfers LPS to the co-receptor CD14. The LPS-CD14 complex in turn interacts with the TLR4-myeloid differentiation protein-2 (MD-2) heterodimer.[9–11] Binding of LPS leads to the dimerization of the TLR4/MD-2 complex followed by a change in receptor conformation and finally to the translocation of the transcription factor nuclear factor 'kappa-light-chain-enhancer' of activated B-cells (NF-κB) to the nucleus.[2]

Stimulation and subsequent downstream signaling of TLR4 is accompanied by a re-localization of TLR4 and its accessory molecules into specific domains of the cell membrane (reviewed in Płóciennikowska *et al.*,[12] Ruysschaert and Lonez[13]). Thereby, TLR4 is recruited into CD14 cholesterol-rich membrane microdomains after treatment with LPS.[14] Since these domains are smaller than 200 nm,[15,16] they are inaccessible by conventional microscopy. With the advent of super-resolution microscopy techniques,[17–26] various studies have

[a]Multiphase Chemistry Department, Max Planck Institute for Chemistry, Hahn-Meitner-Weg 1, 55128 Mainz, Germany. E-mail: k.lucas@mpic.de
[b]Institute of Molecular Biology, Ackermannweg 4, 55128 Mainz, Germany
[c]Department of Dermatology, University Medical Center of the Johannes Gutenberg University, 55131 Mainz, Germany
[d]Institute of Translational Immunology, University Medical Center of the Johannes Gutenberg University, Langenbeckstraße 1, 55131 Mainz, Germany
[e]Division of Gastroenterology, Beth Israel Deaconess Medical Center, Harvard Medical School, 330 Brookline Ave, Boston, MA 02215, USA

†Electronic supplementary information (ESI) available. See DOI: 10.1039/c9nr00943d

‡Current address: Hochschule für Technik und Wirtschaft Chur, Pulvermühlestrasse 57, 7000 Chur, Switzerland.

investigated the membrane distribution of TLR4 at the single molecule level. It has been reported that in human glioblastoma cells TLR4 clusters are present with a cluster size of ~50 nm.[27] In mouse macrophages, another study reported an increased TLR4 cluster size from ~380 nm to ~520 nm after simulation with LPS.[28] Moreover, it was shown that the oligomeric state of TLR4 in HEK 293 cells is affected, depending on the presence of the co-receptors MD2 and CD14 as well as on the LPS chemotype used.[29]

In general, it is assumed that the existence of receptor clusters and the recruitment of receptors into specific domains creates a local environment that facilitates downstream signaling and thus represents a functional or regulatory mechanism.[30,31] Thus, an increase in the cluster size or density of TLR4 on the membrane upon stimulation apparently promotes immune responses. Of note, in the course of stimulation the entire TLR4/MD-2/CD14 complex is endocytosed,[32] which might cause a depletion of TLR4 on the cell surface.

Our prior studies have shown that TLR4 can be stimulated by amylase trypsin inhibitors (ATI) from wheat and thus act as natural activators of innate immunity in monocytes, macrophages and dendritic cells.[7,33–39] Moreover, ATI are major allergens in Baker's asthma.[40] ATI are a family of non-gluten proteins found in different cereals containing gluten such as wheat, rye or barley.[35] With wheat as a major staple in modern societies, the daily intake of ATI is estimated at 0.5 g to 1.5 g per person.[35] Nutritional ATI are resistant to intestinal proteolysis and are major causes of non-celiac wheat sensitivity,[6,34,41] driving intestinal and extraintestinal inflammation.[33,35,37,38]

During inflammation, endogenous reactive oxygen and nitrogen species are formed that are capable of inducing protein nitration. Moreover, during highly polluted environmental conditions, proteins can be nitrated exogenously.[42–44] In a previous study, we have demonstrated that nitrated ATI induced enhanced TLR4 stimulation, pro-inflammatory cytokine secretion and T-cell proliferation.[39]

To investigate if the elevated immune reactions are caused by a change in TLR4 surface representation and distribution, we tested native and nitrated ATI as well as the natural TLR4 agonist LPS. We used single molecule localization microscopy (SMLM) to observe their effect on the spatial distribution of TLR4 in primary human macrophages.

Experimental

Cell culture

Primary human macrophages were derived from peripheral blood mononuclear cells (PBMC) isolated from leucocyte-enriched buffy coats from healthy donors (Transfusion Center, University Medical Center of the Johannes Gutenberg University, Mainz, Germany; for all donors: IgE < 20 kU l^{-1}, food- and aero-allergy negative, (CAP 0)) using Ficoll-Paque (1.077 g ml^{-1}, Biochrom) density centrifugation. After two washing steps with phosphate-buffered saline (PBS, Thermo Fisher Scientific), PBMC were diluted in Isocove's Modified Dulbecco's medium (IMDM, Lonza) containing 1% antibiotic antimycotic solution (Sigma Aldrich) and 3% heat-inactivated (30 min at 56 °C) autologous plasma. To enrich CD14+ monocytes, 2.5×10^6 PBMC were seeded per endotoxin-free glass coverslip (R. Langenbrinck GmbH, thickness of 0.17 mm ± 0.005 mm), which had been placed in a 6-well plate (Greiner Bio-One). After 30 min incubation at 37 °C and 5% CO_2, cells were washed three times with pre-warmed PBS and the remaining monocytes were incubated for 6 days in IMDM supplemented with granulocyte macrophage colony stimulating factor (GM-CSF, 200 Units ml^{-1}, Immunex) and 2% heat-inactivated autologous plasma.

Treatment with LPS, ATI or nitrated ATI

Primary human macrophages grown on glass coverslips were washed once with pre-warmed PBS. Next, cells were incubated with either 100 ng ml^{-1} lipopolysaccharide (LPS-EB; from *E. coli* O111:B4, Invivogen), 12.5 μg ml^{-1} ATI (α-amylase inhibitor from *Triticum aestivum*, Type I, Sigma Aldrich) or 12.5 μg ml^{-1} tetranitromethane (TNM)-nitrated ATI. All stimuli were diluted in complete cell culture medium and incubation was done at 37 °C and 5% CO_2 for 15 min and 30 min. Afterwards, cells were washed once in PBS followed by a two-step fixation process.[45,46] First, cells were fixed in cold PBS containing 4% formaldehyde (Thermo Fisher Scientific) and 0.2% glutaraldehyde (Sigma Aldrich). After 15 min at 4 °C, a second fixation step was performed with the same fixation buffer for 30 min at room temperature. Afterwards, cells were washed three times in PBS and stored at 4 °C in PBS until further use for immunostaining.

Immunostaining

Fixed cells were quenched for 7 min in 0.1% (w/v) sodium borohydride ($NaBH_4$, Sigma Aldrich). After three washing steps in PBS, cells were blocked in 2% bovine serum albumin (BSA, Cell Signaling Technology) dissolved in PBS for 60 min. Next, cells were incubated for 60 min at room temperature with 10 μg ml^{-1} mouse monoclonal anti-TLR4-antibody (ab22048, Abcam) diluted in blocking buffer. The performance of this TLR4 antibody has been validated in a previous study by Zeuner *et al.*,[27] which showed similar results in TLR4 imaging and clustering. Then, samples were washed three times with PBS and subsequently incubated with 20 μg ml^{-1} F(ab′)2 goat anti-mouse Alexa Fluor 647 secondary antibody (A-21237, Thermo Fisher Scientific) diluted in blocking buffer for 60 min at room temperature. After incubation, the sample was washed again three times in PBS and stained cells were post-fixed with 4% formaldehyde in PBS for 10 min at room temperature. After three additional washing steps in PBS, the sample was embedded in Vectashield H-1000 (Vector Laboratories) and sealed using picodent twinsil (picodent Dental Produktions- und Vertriebs GmbH).

Localization microscopy

Experiments were conducted on a custom-built localization microscope (for details see Fig. S1†). Alexa Fluor 647 was

excited using a 647 nm laser (Obis, Coherent). For SMLM imaging, the laser beam was expanded 3.125-fold, resulting in an illuminated area of ~640 μm^2 in the sample plane (area of $1/e^2$ width of Gaussian profile). The collimated laser beam was coupled into the back port of the microscope (DM RBE, Leica) and focused onto the back focal plane of the objective lens (100×/NA 1.49, Olympus). After passing an emission filter (bandpass 700/75 nm, Chroma Technology), emitted fluorescent light was collected on an electron multiplying charge-coupled device (EMCCD) camera (iXon 897 Ultra, Andor Technology) with an effective pixel size of 95 nm.

Imaging and data processing

A region of interest (ROI) was placed on a single cell selected for SMLM imaging. The ROI typically covered an area of ~50 μm^2 to ~400 μm^2 of the plasma membrane. From each ROI, 5000 frames were acquired with a laser intensity of 6.5 kW cm^{-2} (measured in the sample plane) and an exposure time of 40 ms.

To obtain the list of localizations, processing of the raw data stacks was done using Matlab (MathWorks) and the custom written software package Integrated Localization Environment (ILE; https://gitlab.com/microscopy/ILE). The localization algorithm of ILE, which accomplishes the extraction and position determination of single molecule signals from the raw data stacks, is based on fastSPDM.[47] In brief, an initial background image was created from the first eight frames of the raw data stack. The background image was subtracted from the frames of the raw data stack and while looping through the frames of the raw data stack the background image was continuously adjusted to account for changes in background intensities during imaging. Next, signal peaks were extracted from the resulting background corrected images. A 7 × 7 px ROI was centered around each signal peak exceeding a standard deviation of 2 times the noise. The noise was considered to follow a Poisson noise model. Extracted signal peaks were passed for subsequent position determination. Positions with subpixel accuracy were determined by calculating the center of mass of each input ROI, which corresponds in the absence of background (due to background subtraction) to a maximum likelihood estimation (MLE). Close-by signals were detected by searching each ROI from its center towards its boundaries for local intensity minima. In case of local minima, the ROI was clipped and the signal was recalculated or discarded when the clipping resulted in a loss of more than 30% of the ROI intensity. An initial list of localizations was returned by the algorithm, listing x- and y-coordinates of each detected single molecule as well as information about its photon count and localization precision. Next, the list of localization was post-processed using ILE by first joining localizations occurring in consecutive frames and within 2.5 times of the mean localization precision. Drift correction was done by splitting the list of localization in 5 subsets and correlating the reconstructions of the subsets.[48,49] The shift among the subsets was interpolated and used to correct the positions of the detected signals in the list of localizations. No further filtering of the list of localizations was applied. For reconstruction of SMLM images, the single molecule positions were blurred by a Gaussian with a standard deviation corresponding to the localization precisions of the respective signals.

Spatial point pattern analysis of SMLM data

A custom-written software package in Matlab (Localization Analyzer for Nanoscale Distributions (LAND), https://github.com/Jan-NM/LAND) was used to analyze spatial distribution of the detected single molecule signals. The list of localizations was pre-processed in a first step by reconstructing the images (*via* histogram binning) and cropping a rectangular ROI for each cell that showed a homogenous distribution on large scales; *i.e.* no visible gaps. For each cell, a new list of localizations was generated containing only the molecule signals within the rectangular ROI. The new list of localizations was used as experimental input data in the subsequent analysis, which was performed on the basis of the single molecule coordinates. Random data following complete spatial randomness (CSR) were generated using the density of signals of the experimental input data. In total, three different algorithms were used to characterize the point pattern:

Grid-based density analysis. Detected single molecule signals were binned on a uniform grid with a bin size of 10 nm, which corresponds to the average localization precision. For every bin, the density of signals per μm^2 was calculated. Each bin was subsequently divided by the mean density of the corresponding ROI. For better visualization, bin values larger than 20 times the ratio of bin density to mean density have been set to 2. Values lower than 20 times of the ratio were re-assigned between 0 and 2. Finally, bins were color-coded. Yellow colored areas indicate clustering, whereas blue areas indicate dispersion.

Ripley's *H*-function. Ripley's H-function[50] up to a distance of 1 μm was calculated to estimate the typical domain size of the point pattern. To account for edge effects, molecule signals with a minimum distance of 1 μm from the image border were extracted from the input data. A distance matrix between the extracted point pattern and the input data was pre-computed. The distance matrix contained only entries of distances smaller than 1 μm. Using the distance matrix, Ripley's K-function was calculated:[51]

$$K(r) = \frac{1}{N}\sum_{i=1}^{N}\frac{n_{p_i}(r)}{\lambda}.$$

Here N denotes the total number of molecule signals that are investigated, n is the number of molecule signals within a distance r of a point p_i and λ the density of molecule signals. The K-function was later transformed to obtain Ripley's H-function:

$$H(r) = \sqrt{\frac{K(r)}{\pi}} - r.$$

Subsequently, the Ripley's H-functions obtained from different donors from the same treatment were averaged and

the maximum of Ripley's *H*-function was used as an estimate of the characteristic cluster size. Only maxima within a distance of 200 nm were considered.

Density-based spatial clustering of applications with noise (DBSCAN). Further cluster analysis was done using DBSCAN,[52] which allows identification and visualization of individual clusters of any shape (Fig. S2†). DBSCAN requires two user input parameters – the radius (ε) and the minimum number of neighboring molecule signals (minPts) within this radius. Together, these values form a local density threshold that determines whether the point under investigation is part of a cluster. Initial DBSCAN parameter selection was done as follows: the 4th nearest neighbor distances of the detected molecules from the list of localizations for a few experimental data sets were calculated. The nearest neighbor distances were sorted in ascending order and plotted against the number of molecule signals within the corresponding data set. The distance where the bend in the plot occurs was used as a starting value for the radius parameter of DBSCAN. Next, DBSCAN was executed with those starting parameters and further iterative adjustment of the parameters was done by visualizing the clusters and comparing the distance distribution obtained from the molecule signals outside of clusters with a random distribution (Fig. S3†). Using this parameter estimation pipeline, a value of 30 nm for the radius (ε) and a value of 6 for the minimum number of molecule signals (minPts) were determined. With these input parameters and the list of localizations, the implemented DBSCAN algorithm first calculated a sparse distance matrix, which contains for every molecule signal (= single molecule) entries to molecule signals that lie within the specified distance (ε = 30 nm). DBSCAN was applied to the distance matrix and points were assigned to a specific cluster or as noise. Next, for every detected cluster the algorithm generated a table containing its area, diameter, center of mass, density, the number of molecules and the distance to the next neighboring cluster as well as an assignment list for every point to which cluster it belongs. This assignment list was used to calculate the distances of molecule signals outside of the clusters as shown in Fig. S3.† The maximum allowable cluster diameter was set to 1 μm. If a cluster larger than 1 μm was detected, its molecule signals were assigned as noise.

Wide-field fluorescence microscopy of TLR4

Primary human macrophages were derived and isolated from PBMC as described before. Instead of glass coverslips, 2.5×10^6 cells per well were seeded in a glass bottom 12-well plate (Cellvis). Fixation and immunostaining of TLR4 was done in the same way as for the localization microscopy experiments. Nuclei were counterstained using 4′,6-diamidino-2-phenylindole (DAPI; Thermo Fisher Scientific) at a concentration of 300 nM in PBS for 3 min. After incubation, cells were washed three times in PBS. Instead of Vectashield H-1000, cells were imaged in PBS on the Opera Phenix High-Content Screening system (PerkinElmer). TLR4 stained cells (excitation 640 nm, emission 650 nm–760 nm) and DAPI stained nuclei (excitation 405 nm, emission 435 nm–480 nm) were imaged in non-confocal mode using a 20×/1.0 water immersion objective.

Nitration of ATI with tetranitromethane (TNM) and endotoxin quantification

ATI were diluted in ultra-pure water to a final concentration of 1 mg ml^{-1}. 4.55 μl TNM/methanol (4% v/v) were added to 500 μl of diluted ATI. The mixture was stirred for 3 h at room temperature. Residual TNM was removed using a PD-25 size exclusion column (GE Healthcare). The endotoxin content was quantified using a limulus amebocyte lysate (LAL) assay (Thermo Fisher Scientific). Nitrated ATI solutions with a final endotoxin content of less than 20 endotoxin units per ml (1.3 EU μg^{-1} protein) were used for experiments.

Sample size

Experiments were conducted on primary human macrophages obtained from three different healthy donors. A total of at least 25 cells were evaluated per treatment. All values refer to the median. Number of cells used for Ripley's *H*-function and DBSCAN analysis can be found in Tables S1–S3.†

Ethics statement

Buffy coats from healthy donors were obtained anonymously from the local blood bank (Transfusion Center, University Medical Center of the Johannes Gutenberg University, Mainz, Germany). The local ethical committee (Landesärztekammer Rheinland-Pfalz, Mainz, Germany) approved all experiments according to the guidelines of the 1964 Declaration of Helsinki (9th revision, 2013). Consent of participants was given in written form.

Results and discussion

TLR4 is pre-clustered in unstimulated primary human macrophages

To investigate the large and small-scale distribution of TLR4 on the cell membrane, unstimulated macrophages stained for TLR4 were imaged by conventional fluorescence and localization microscopy (Fig. 1A + B). Conventional fluorescence images show that macrophages express TLR4. In line with other studies,[53,54] we observed differences in TLR4 surface representation between cells and variations on individual cells (Fig. 1A, Fig. S4†). Using SMLM, finer structural details become visible compared to conventional fluorescence microscopy (Fig. 1B, Fig. S5†). An accumulation of TLR4 molecules in domains at the nanometer range was detected (Fig. 1C, ROI). To quantitatively evaluate the observed pattern, a grid-based density analysis was performed (Fig. 1D, ROI). It reveals that in unstimulated cells TLR4 clusters are present that are embedded in regions reduced in TLR4 surface representation. These regions contain small isolated clustered regions that can be associated with fluorophores belonging to a single TLR4 receptor. Normally, a single fluorophore may blink several times during SMLM imaging. This results in mul-

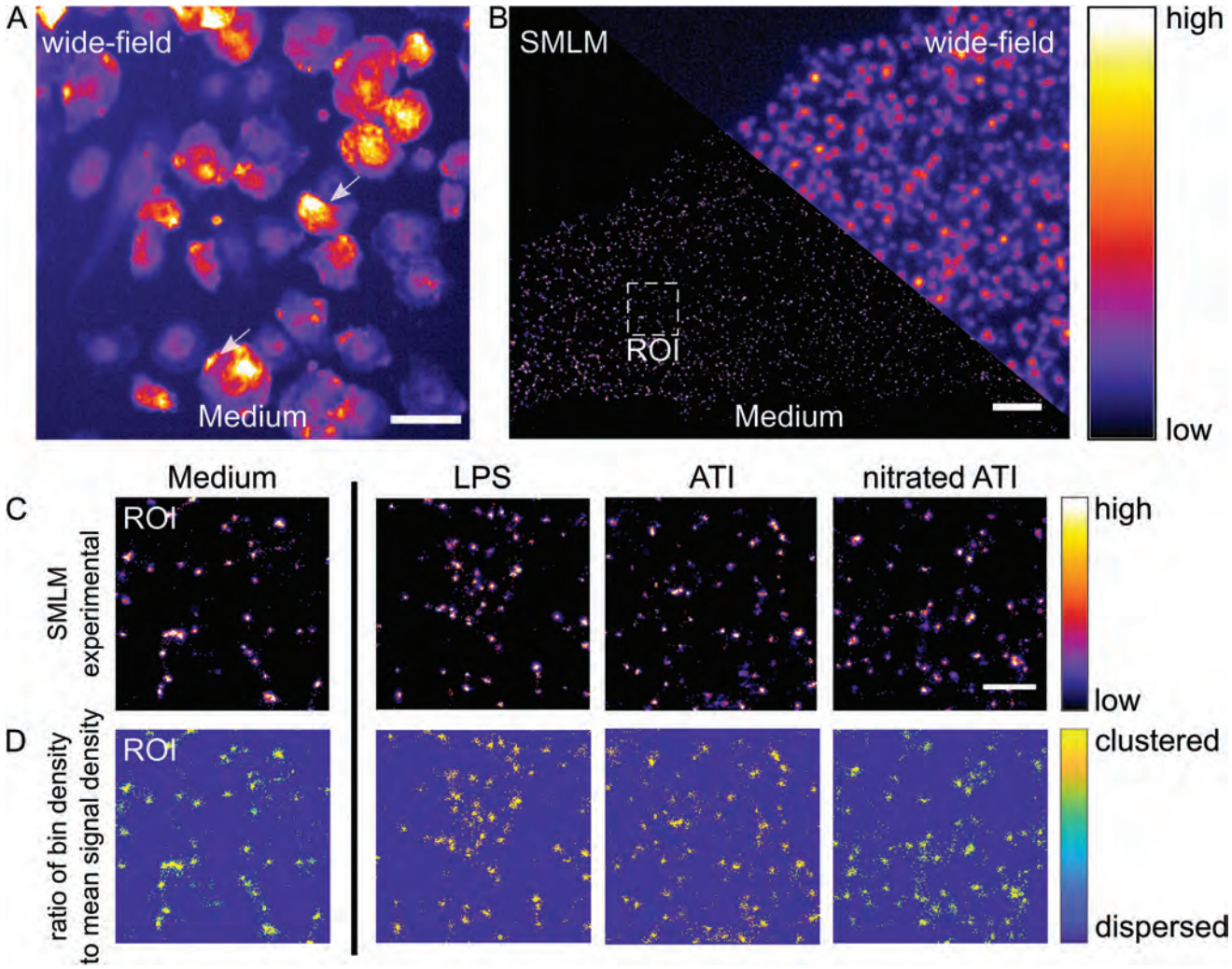

Fig. 1 TLR4 clusters on the cell membrane of primary human macrophages. (A) Conventional fluorescence microscopy image of unstimulated macrophages stained for TLR4. Intensity-coded visualization reveals differences in TLR4 expression levels between cells and variations in its surface representation on individual cells (white arrows). Scale bar = 50 μm. (B) Combined SMLM and wide-field image of an untreated macrophage stained for TLR4. Scale bar = 2 μm. (C) TLR4 SMLM image sections of macrophages treated with LPS-EB (100 ng ml^{-1}), ATI (12.5 μg ml^{-1}) or nitrated ATI (12.5 μg ml^{-1}) for 15 min compared to medium control. The image section of the medium control was taken from the region of interest (ROI) indicated in panel 1B. SMLM images are intensity-coded, *i.e.* high intensity areas correspond to an accumulation of single molecule signals. Scale bar = 500 nm. (D) Grid-based density analysis of SMLM images from panel 1C. Blue areas indicate a dispersed distribution, whereas yellow areas show clustering of TLR4.

tiple detected signals per fluorophore, whose positions are distributed within the localization precision. Therefore, several fluorophores coupled to a single antibody generate small pseudo-clusters (Fig. S6, ESI Note 1†). Overall, our findings show that TLR4 molecules are present in a pre-clustered state on unstimulated macrophages, which confirms previous investigations on receptor clustering.[55–57]

Next, we investigated whether ATI and tetranitromethane (TNM)-nitrated ATI have an effect on the membrane distribution of TLR4. Therefore, macrophages were stimulated with ATI or nitrated ATI for 15 min and 30 min, respectively (ESI Note 2 + 3, Fig. S7†). LPS served as a positive control. Visual inspection and grid-based density analysis of SMLM images from the stimulated cells revealed a clustered distribution of TLR4 as observed in the unstimulated samples (Fig. 1C + D, Fig. S8†).

Donor-dependent TLR4 cluster formation upon stimulation with LPS and ATI

To analyze the effect of LPS and ATI further, the density of molecules on the membrane was calculated for the different donors (Fig. 2, Fig. S9A†). Already in the unstimulated state, the donors exhibit different levels of density of molecules on the membrane (Fig. 2A). With ~80 signals per μm^2, the lowest density of molecules was observed for donor 2, while the other donors showed densities 4 times higher in the unstimulated state. Differences among donors were also detected in response to LPS, ATI and nitrated ATI (Fig. 2B–D). Donor 2 in

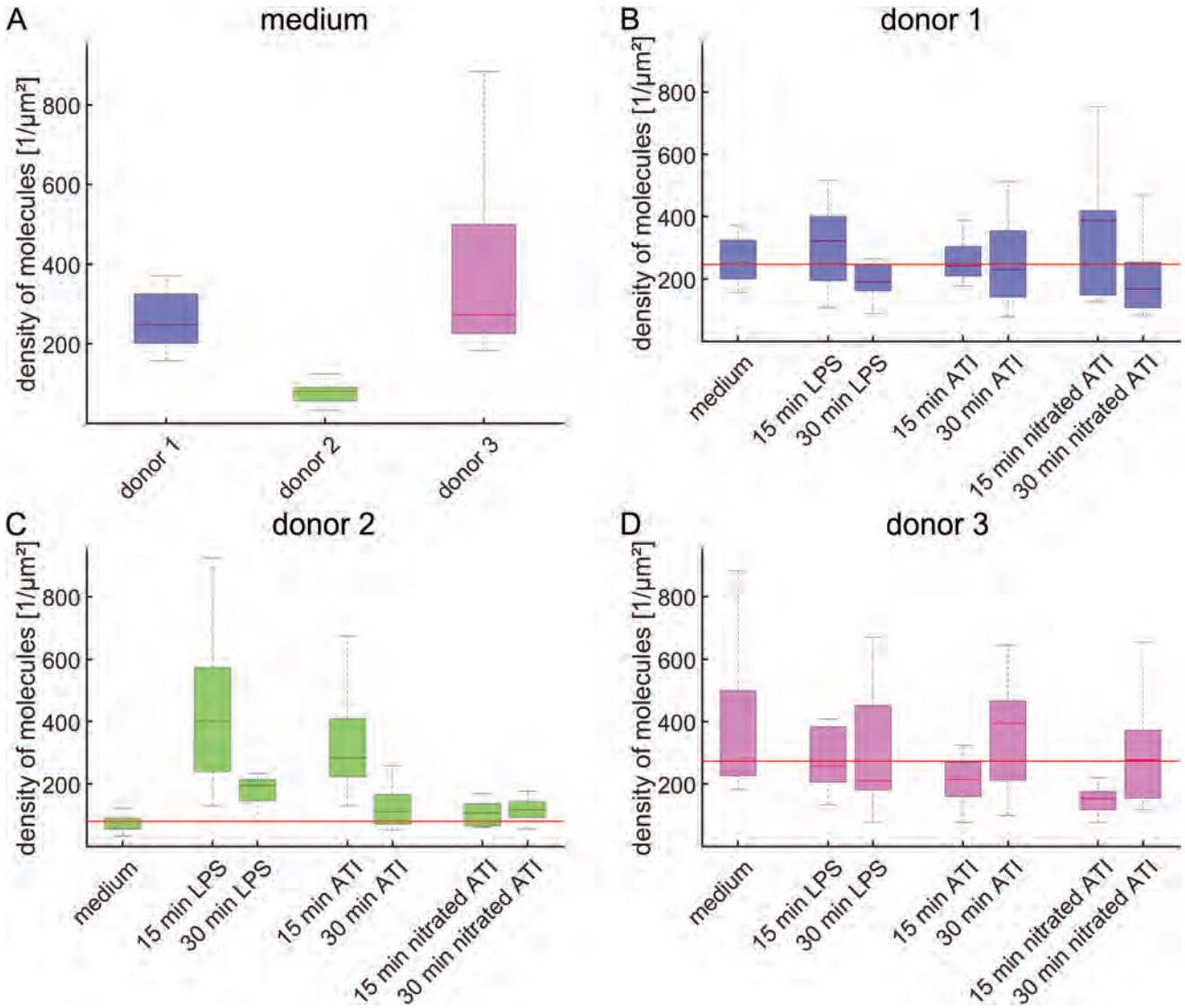

Fig. 2 Molecule densities on the cell membrane are specific to the individual donors. (A) Density of molecules on unstimulated macrophages. The colors of the boxes represent the three different donors. (B–D) Density of molecules after stimulation with LPS, ATI or nitrated ATI, categorized according to the various donors. The boxes represent the median and the 25th to 75th percentile of the donors, whereas the whiskers cover 99.3% of the data. The horizontal red line indicates the median value of the medium control.

particular showed an increase in the density of molecules by about 390% and 250% compared to unstimulated cells after treatment with LPS and ATI for 15 min (Fig. 2C). In contrast, no change in molecule densities was found after treatment of macrophages from donor 2 with nitrated ATI. The substantial changes in the density of molecules seen for donor 2 after stimulation with LPS and ATI was not observed for the other donors (Fig. 2B + D). Apparently, these donors already had an elevated level in the density of molecules in the unstimulated state, suggesting that the ground state may influence later response to external stimuli.

To analyze the clustering behavior of TLR4, the fraction of clustered molecules and the density of clusters was calculated for each donor separately (Fig. 3, Fig. S9B + C†). Similar to the density of the molecules on the cell membrane, strong differences were present in the fraction of clustered molecules among the donors in the unstimulated state (Fig. 3A). These range from ~51% for donor 2 to ~75% for donor 1. For donor 2, a pronounced increase in the fraction of clustered molecules was found after stimulation, with LPS and ATI showing the highest increase of about 40% and nitrated ATI the lowest with ~10%. After 15 min ATI stimulation, donor 1 showed an increase of about 7%, whereas donor 3 showed the strongest increase after 30 min stimulation with ATI and nitrated ATI. Furthermore, the cluster analysis revealed that on unstimulated cells, approximately 2 clusters per μm^2 to 4.4 clusters per μm^2 were present (Fig. 3B). This can be translated to a distance of neighboring clusters between 200 nm and 320 nm, respect-

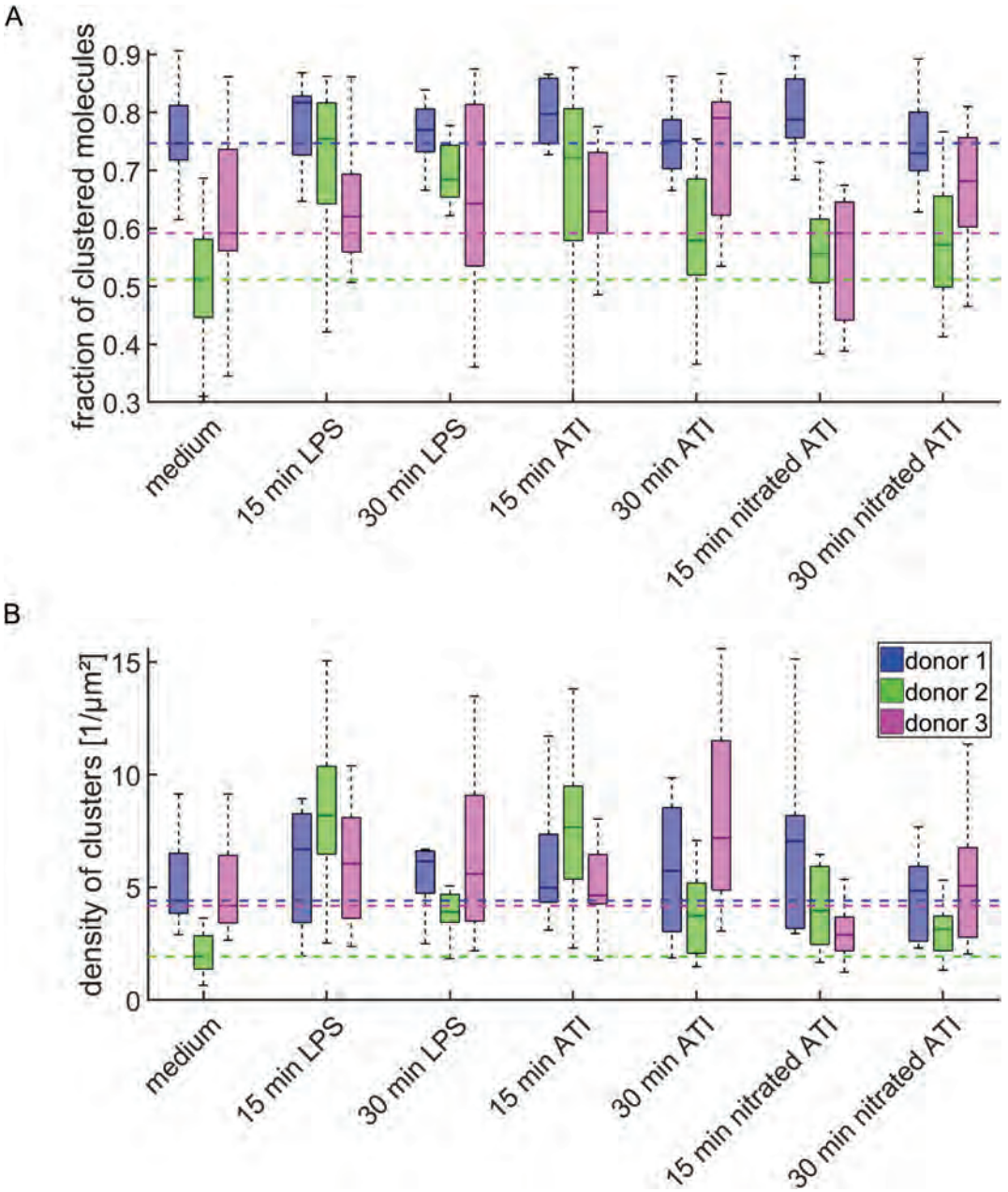

Fig. 3 Donor dependent clustering of TLR4 as analyzed by DBSCAN. The fraction of clustered molecules (A) and the density of clusters on the membrane (B) for the three different donors is shown. The color-coded boxes indicate the median and the 25th to 75th percentile for the individual donors. The dashed lines represent the median values of the medium control from the respective donors. The whiskers cover 99.3% of the data. In total 264 cells were evaluated.

ively. Comparing the density of clusters *vs.* the density of molecules on the membrane, a positive correlation between both variables can be found (Fig. S10†). As a result, an increase in the density of clusters on the membrane was most pronounced for donor 2, forming about 8 clusters per μm^2 after 15 min of stimulation with LPS and ATI. For donor 3, a broadening of the cluster density distribution was recognizable after 30 min stimulation, which may suggest a heterogeneous response to the stimuli. The observed densities of clusters on the membrane are in agreement with previous investigations on LPS stimulated glioblastoma cells.[27]

TLR4 cluster sizes remain unchanged after LPS or ATI stimulation

The clusters were further analyzed by extracting their diameter, the absolute number of molecules per cluster and the density of molecules within the clusters (Fig. 4). A median cluster diameter of about 44 nm was found (Fig. 4A). No significant

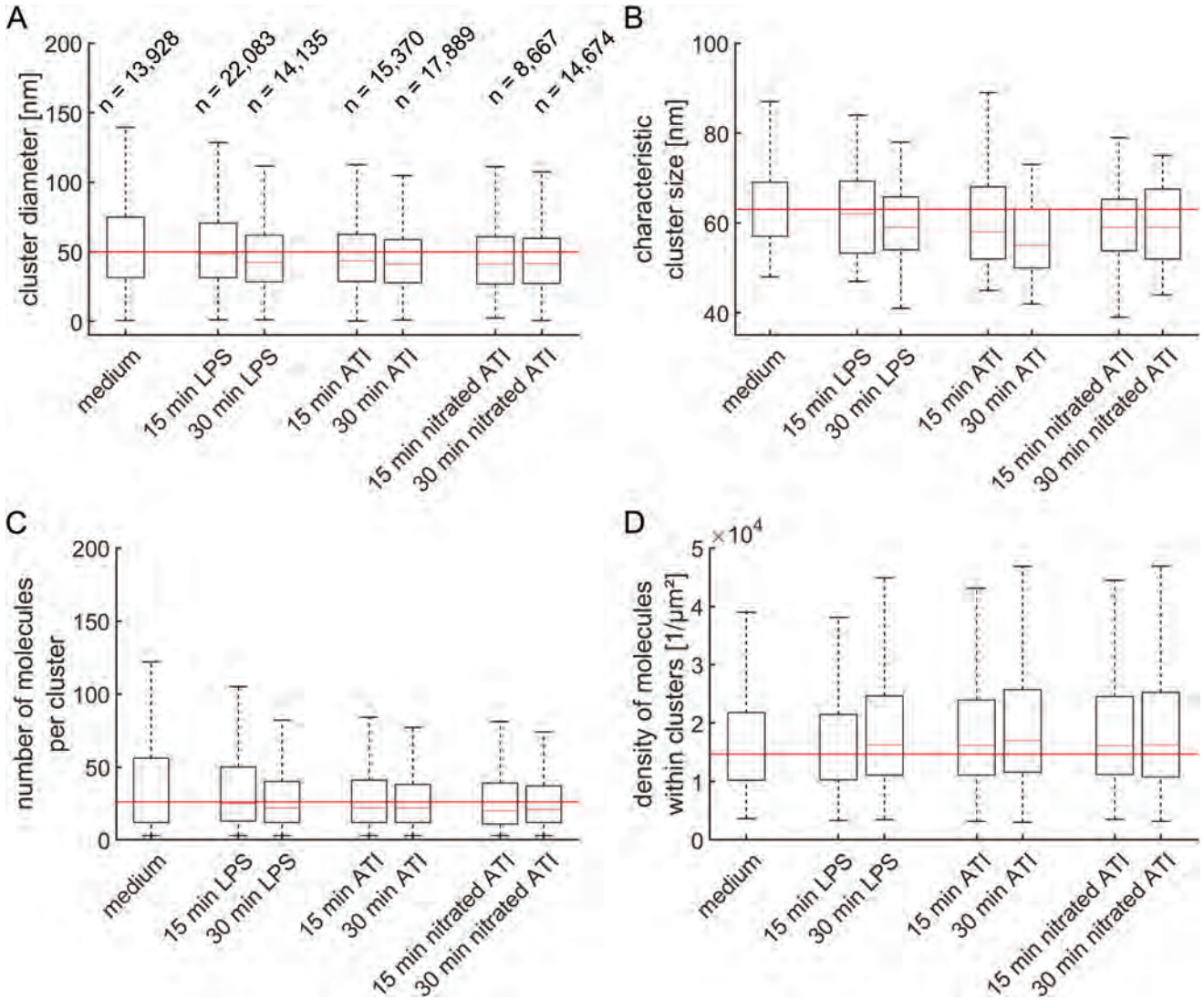

Fig. 4 Unchanged cluster characteristics of TLR4 revealed by DBSCAN and Ripley's *H*-function. (A) Cluster diameter as obtained from DBSCAN analysis. The numbers above the boxes denote the number of identified clusters for panels A, C and D. (B) Average cluster size of TLR4 obtained from the maximum of Ripley's *H*-function of individual cells (Fig. S11†). (C) Number of molecules per cluster and (D) density of molecules within the clusters as obtained from DBSCAN analysis. All data are presented as box plots, showing the median and the 25th to 75th percentile as boxes. The whiskers cover 99.3% of the data.

changes in the median cluster diameter could be observed, as the variations for each condition stayed close to the median of unstimulated cells, within the interquartile range. To verify the results, Ripley's *H*-function was calculated (Fig. S11†) and the maximum of the function was used to derive the characteristic cluster size (Fig. 4B). Moreover, simulations were carried out to verify that the characteristic cluster size corresponds to the cluster diameter (Fig. S12†). As already found in the previous analysis, cluster size remained unchanged among the samples. Similar findings were made by Zeuner *et al.*,[27] where the authors observed a cluster size of ~50 nm on glioblastoma cells independent of the LPS stimuli applied. In contrast, Aaron *et al.*[28] reported a TLR4 cluster size of ~380 nm in unstimulated mouse macrophages, which increased to ~520 nm after stimulation with LPS. Discrepancies between the studies could be attributed to the use of different cell lines, especially a different behavior of TLR4 in mouse cells compared to human cells.[27] Alternatively, these discrepancies may be the result of inefficient photoswitching during localization imaging,[27] which can lead to an apparently larger cluster size. It must be also noted that our measured cluster diameter is larger than actual diameters due to the indirect labeling system. This system consists of primary antibody and fluorescently labeled secondary F(ab′)2 fragments, which increases the distance between protein and detection molecule. Therefore, the measured cluster diameter represents an upper limit.

Regarding the absolute signals per cluster, on average 22 molecule signals were detected (Fig. 4C), resulting in an

average density within the clusters of 1.6×10^4 molecules per μm^2 (Fig. 4D). As already observed for the cluster diameter, no significant changes were observed.

Model of TLR4 receptor clustering

In our study, we have demonstrated that the majority of TLR4 molecules are already located in clusters in unstimulated primary human macrophages. Upon stimulation, donor-dependent variations in the fraction of clustered molecules accompanied by changes in the density of receptors and clusters on the membrane were observed. These changes may result from the superposition of TLR4 recruitment and endocytosis processes (Fig. 5). On the one hand, TLR4 receptors can be recruited into or around pre-existing clusters. On the other hand, new clusters can be generated by recruitment of receptors around monomers or pre-existing lower order oligomers. Moreover, any recruitment of receptors increases the local density of detected single molecule signals during SMLM imaging, thus exceeding the threshold beyond which DBSCAN detects a cluster. For both processes, replenishment of TLR4 receptors can happen from the Golgi apparatus[58,59] or by translocation of receptors present on the membrane following stimulation, *i.e.* recruitment into cholesterol-rich microdomains, also referred as lipid rafts.[14] These recruitment processes can also be assumed to take place continuously in unstimulated cells, but the rate might differ after stimulation.

Moreover, the TLR4 receptor complex can be endocytosed from the membrane after stimulation.[60,61] Altogether, these processes determine the density of clusters on the membrane and the fraction of clustered molecules.

A recent study elucidated the ligand-specific receptor dimerization of TLR4 using stoichiometric labeling of TLR4 together with quantitative single molecule localization microscopy.[29] In that study, the authors were able to determine the proportion of monomeric and dimeric TLR4 complexes depending on the LPS chemotype used. An extension of these experiments to ATI might help to understand whether the formation of clusters is accompanied by a change in the ratio of monomers to dimers upon ATI stimulation. Such effects would indicate stronger and focused signaling events, which would underline together with our results the importance of receptor clusters as signaling platforms.

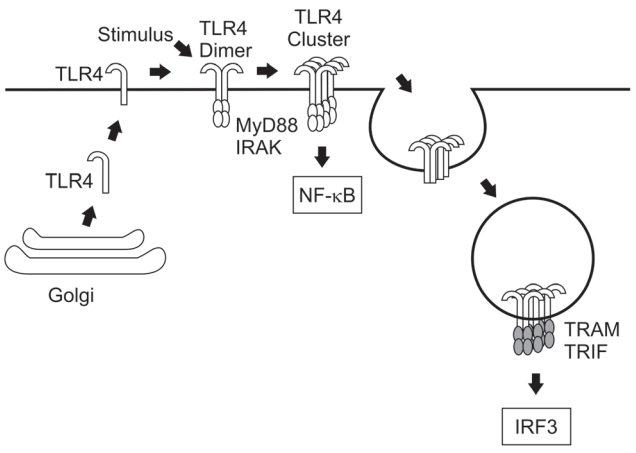

Fig. 5 Schematic diagram of recruitment, clustering and depletion of membranous TLR4. TLR4 is glycosylated in the Golgi apparatus and subsequently recruited on the cell membrane.[58,59] Upon stimulation, TLR4 molecules may be recruited into pre-existing clusters or form new clusters by re-arrangement of TLR4 monomers. Subsequently, TLR4 receptors are endocytosed,[60,61] thus leading to a depletion of TLR4 from the membrane.

Conclusions

In our study, we investigated the membrane distribution of TLR4 on primary human macrophages using SMLM. We focused on ATI and nitrated ATI, which have been identified as stimulating the TLR4/NF-κB pathway in macrophages and dendritic cells.[33,39] Using different quantitative analysis methods, we found that the majority of TLR4 molecules are already located in clusters, whereby pronounced differences existed among the donors already in the unstimulated state. Upon stimulation with LPS or ATI, the overall fraction of clustered TLR4 molecules increased. Moreover, we observed an overall increase in the density of clusters up to ~8 clusters per μm^2 compared to ~2 clusters per μm^2 in the unstimulated state. Furthermore, we found that the clusters have a median diameter of about 44 nm, which did not change significantly after treatment. The donor-dependent differences underline the individuality of human samples and the need for future experiments on a larger cohort of donors to get a better understanding and comprehensive picture of TLR4 clustering and activation, as well as to extract possible patterns of different response types.

Altogether, our findings suggest a donor-dependent formation of clusters before and after stimulation with LPS and ATI. This structural change could further affect functional or regulatory processes of the TLR4 downstream cascade inducing finally enhanced inflammation. Regardless of the TLR4 agonist used, we found similar structural changes suggesting a general mechanism of TLR4 cluster formation upon stimulation.

Author contributions

UP, CC, KL, UB and JN designed the research. JN and KZ performed the experiments. JN, MG, KL and JFN analyzed and interpreted the data. FL, IB and DS contributed materials and methods. JN, KZ, MG and KL wrote the paper. All authors contributed to the discussion, editing and proofreading of the manuscript.

Funding disclosure

This work was supported by the Max Planck Graduate Center with the Johannes Gutenberg University Mainz (MPGC). DS

was supported for ATI-related work by grants from the German Research Foundation (DFG) (DFG-Schu 646/17-1, DFG-Schu-646/20-1, the Collaborative Research Center TR128 "Multiple Sclerosis" project A08), and the Leibniz Foundation (project Wheatscan). IB was supported by DFG grant BE 4504/3-1.

Conflicts of interest

The authors have no conflicting financial interests to disclose. UB and CC are also affiliated with LuciaOptics Forschungszentrum, a non-profit company based in Karlsruhe, Germany. The founding sponsors had no role in the design of the study; in the collection, analyses, or interpretation of data; in the writing of the manuscript or in the decision to publish the results.

Acknowledgements

We thank Dr Sandra Ritz, Dr Maria Hanulova, Dr Jonas Schwirz, Dr Aleksander Szczurek, Florian Schock and Amine Gourram for continuous support and helpful discussions. Support by the Max Planck Graduate Center, the Mainz Program for Chemical Allergology and the joint Laboratory of Inflammation and Microscopy is gratefully acknowledged. We also acknowledge the IMB Microscopy and Histology Core Facility for support and the Deutsche Forschungsgemeinschaft (DFG) for funding the Opera Phenix High Content Spinning Disk Microscope (Project 402386039). We thank Dr Frank Helleis, Dr Thomas Klimach and the workshop of the MPI for Chemistry as well as the E-lab of IMB for help and support in the construction of the SMLM setup. Open Access funding provided by the Max Planck Society.

References

1 E. M. Y. Moresco, D. LaVine and B. Beutler, *Curr. Biol.*, 2011, **21**, R488–R493.
2 T. Kawasaki and T. Kawai, *Front. Immunol.*, 2014, **5**, 1–8.
3 J. C. Chow, D. W. Young, D. T. Golenbock, W. J. Christ and F. Gusovsky, *J. Biol. Chem.*, 1999, **274**, 10689–10692.
4 B. Beutler, X. Du and A. Poltorak, *J. Endotoxin Res.*, 2001, **7**, 277–280.
5 L. Zuo, K. Lucas, C. A. Fortuna, C.-C. Chuang and T. M. Best, *Front. Physiol.*, 2015, **6**, DOI: 10.3389/fphys.2015.00312.
6 A. Fasano, A. Sapone, V. Zevallos and D. Schuppan, *Gastroenterology*, 2015, **148**, 1195–1204.
7 D. Schuppan and V. Zevallos, *Dig. Dis.*, 2015, **33**, 260–263.
8 S. Zundler and M. F. Neurath, *Immunol. Rev.*, 2017, **278**, 263–276.
9 J. da Silva Correia, K. Soldau, U. Christen, P. S. Tobias and R. J. Ulevitch, *J. Biol. Chem.*, 2001, **276**, 21129–21135.
10 T. L. Gioannini, A. Teghanemt, D. Zhang, N. P. Coussens, W. Dockstader, S. Ramaswamy and J. P. Weiss, *Proc. Natl. Acad. Sci. U. S. A.*, 2004, **101**, 4186–4191.
11 B. S. Park, D. H. Song, H. M. Kim, B.-S. Choi, H. Lee and J.-O. Lee, *Nature*, 2009, **458**, 1191–1195.
12 A. Płóciennikowska, A. Hromada-Judycka, K. Borzęcka and K. Kwiatkowska, *Cell. Mol. Life Sci.*, 2014, **72**, 557–581.
13 J.-M. Ruysschaert and C. Lonez, *Biochim. Biophys. Acta, Biomembr.*, 2015, **1848**, 1860–1867.
14 M. Triantafilou, K. Miyake, D. T. Golenbock and K. Triantafilou, *J. Cell Sci.*, 2002, **115**, 2603–2611.
15 L. J. Pike, *J. Lipid Res.*, 2006, **47**, 1597–1598.
16 M. Schürmann, N. Frese, A. Beyer, P. Heimann, D. Widera, V. Mönkemöller, T. Huser, B. Kaltschmidt, C. Kaltschmidt and A. Gölzhäuser, *Small*, 2015, **11**, 5781–5789.
17 S. W. Hell and J. Wichmann, *Opt. Lett.*, 1994, **19**, 780–782.
18 R. Heintzmann and C. Cremer, *Proc. SPIE*, 1999, **3568**, 185–196.
19 M. G. Gustafsson, *J. Microsc.*, 2000, **198**, 82–87.
20 K. A. Lidke, B. Rieger, T. M. Jovin and R. Heintzmann, *Opt. Express*, 2005, **13**, 7052–7062.
21 E. Betzig, G. H. Patterson, R. Sougrat, O. W. Lindwasser, S. Olenych, J. S. Bonifacino, M. W. Davidson, J. Lippincott-Schwartz and H. F. Hess, *Science*, 2006, **313**, 1642–1645.
22 S. T. Hess, T. P. K. Girirajan and M. D. Mason, *Biophys. J.*, 2006, **91**, 4258–4272.
23 M. J. Rust, M. Bates and X. Zhuang, *Nat. Methods*, 2006, **3**, 793–795.
24 A. Sharonov and R. M. Hochstrasser, *Proc. Natl. Acad. Sci. U. S. A.*, 2006, **103**, 18911–18916.
25 M. Heilemann, S. Van De Linde, M. Schüttpelz, R. Kasper, B. Seefeldt, A. Mukherjee, P. Tinnefeld and M. Sauer, *Angew. Chem., Int. Ed.*, 2008, **47**, 6172–6176.
26 P. Lemmer, M. Gunkel, D. Baddeley, R. Kaufmann, A. Urich, Y. Weiland, J. Reymann, P. Müller, M. Hausmann and C. Cremer, *Appl. Phys. B*, 2008, **93**, 1–12.
27 M.-T. Zeuner, C. L. Krüger, K. Volk, K. Bieback, G. S. Cottrell, M. Heilemann and D. Widera, *Biochim. Biophys. Acta, Mol. Cell Res.*, 2016, **1863**, 3084–3095.
28 J. S. Aaron, B. D. Carson and J. A. Timlin, *Small*, 2012, **8**, 3041–3049.
29 C. L. Krüger, M. T. Zeuner, G. S. Cottrell, D. Widera and M. Heilemann, *Sci. Signaling*, 2017, **10**(503), DOI: 10.1126/scisignal.aan1308.
30 T. Lang and S. O. Rizzoli, *Physiology*, 2010, **25**, 116–124.
31 M. F. Garcia-Parajo, A. Cambi, J. A. Torreno-Pina, N. Thompson and K. Jacobson, *J. Cell Sci.*, 2014, **127**, 4995–5005.
32 N. Tanimura, S. Saitoh, F. Matsumoto, S. Akashi-Takamura and K. Miyake, *Biochem. Biophys. Res. Commun.*, 2008, **368**, 94–99.
33 Y. Junker, S. Zeissig, S.-J. Kim, D. Barisani, H. Wieser, D. A. Leffler, V. Zevallos, T. A. Libermann, S. Dillon, T. L. Freitag, C. P. Kelly and D. Schuppan, *J. Exp. Med.*, 2012, **209**, 2395–2408.

34 D. Schuppan, G. Pickert, M. Ashfaq-Khan and V. Zevallos, *Best Pract. Res., Clin. Gastroenterol.*, 2015, **29**, 469–476.
35 V. F. Zevallos, V. Raker, S. Tenzer, C. Jimenez-Calvente, M. Ashfaq-Khan, N. Rüssel, G. Pickert, H. Schild, K. Steinbrink and D. Schuppan, *Gastroenterology*, 2017, **152**, 1100–1113.e12.
36 M. Cuccioloni, M. Mozzicafreddo, L. Bonfili, V. Cecarini, M. Giangrossi, M. Falconi, S. I. Saitoh, A. Maria Eleuteri and M. Angeletti, *Sci. Rep.*, 2017, **7**, 4–6.
37 V. Zevallos, V. K. Raker, J. Maxeiner, P. Scholtes, K. Steinbrink and D. Schuppan, *Eur. J. Nutr.*, 2018, DOI: 10.1007/s00394-018-1681-6.
38 I. Bellinghausen, B. Weigmann, V. Zevallos, J. Maxeiner, S. Reißig, A. Waisman, D. Schuppan and J. Saloga, *J. Allergy Clin. Immunol.*, 2019, **143**, 201–212.e4.
39 K. Ziegler, J. Neumann, F. Liu, J. Fröhlich-Nowoisky, C. Cremer, J. Saloga, K. Reinmuth-Selzle, U. Pöschl, D. Schuppan, I. Bellinghausen and K. Lucas, *Front. Immunol.*, 2019, **9**, DOI: 10.3389/fimmu.2018.03174.
40 A. S. Tatham and P. R. Shewry, *Clin. Exp. Allergy*, 2008, **38**, 1712–1726.
41 V. Leccioli, M. Oliveri, M. Romeo, M. Berretta and P. Rossi, *Nutrients*, 2017, **9**, 1203.
42 T. Franze, M. G. Weller, R. Niessner and U. Pöschl, *Environ. Sci. Technol.*, 2005, **39**, 1673–1678.
43 Y. K. Gruijthuijsen, I. Grieshuber, A. Stöcklinger, U. Tischlera, T. Fehrenbach, M. G. Weller, L. Vogel, S. Vieths, U. Pöschl and A. Duschl, *Int. Arch. Allergy Immunol.*, 2006, **141**, 265–275.
44 K. Reinmuth-Selzle, C. J. Kampf, K. Lucas, N. Lang-Yona, J. Fröhlich-Nowoisky, M. Shiraiwa, P. S. J. Lakey, S. Lai, F. Liu, A. T. Kunert, K. Ziegler, F. Shen, R. Sgarbanti, B. Weber, I. Bellinghausen, J. Saloga, M. G. Weller, A. Duschl, D. Schuppan and U. Pöschl, *Environ. Sci. Technol.*, 2017, **51**, 4119–4141.
45 K. A. K. Tanaka, K. G. N. Suzuki, Y. M. Shirai, S. T. Shibutani, M. S. H. Miyahara, H. Tsuboi, M. Yahara, A. Yoshimura, S. Mayor, T. K. Fujiwara and A. Kusumi, *Nat. Methods*, 2010, **7**, 865–866.
46 P. Sengupta, T. Jovanovic-Talisman, D. Skoko, M. Renz, S. L. Veatch and J. Lippincott-Schwartz, *Nat. Methods*, 2011, **8**, 969–975.
47 F. Grüll, M. Kirchgessner, R. Kaufmann, M. Hausmann and U. Kebschull, in Proceedings – 21st International Conference on Field Programmable Logic and Applications, *IEEE*, 2011, pp. 1–5.
48 M. J. Mlodzianoski, J. M. Schreiner, S. P. Callahan, K. Smolková, A. Dlasková, J. Šantorová, P. Ježek and J. Bewersdorf, *Opt. Express*, 2011, **19**, 15009–15019.
49 Y. Wang, J. Schnitzbauer, Z. Hu, X. Li, Y. Cheng, Z.-L. Huang and B. Huang, *Opt. Express*, 2014, **22**, 15982–15991.
50 B. D. Ripley, *J. R. Stat. Soc. Ser. B*, 1977, **39**, 172–212.
51 M. A. Kiskowski, J. F. Hancock and A. K. Kenworthy, *Biophys. J.*, 2009, **97**, 1095–1103.
52 M. Ester, H.-P. Kriegel, J. Sander and X. Xu, Proc. Second Int. Conf. Knowl. Discov. Data Min., 1996, pp. 226–231.
53 K.-H. Tse, K. B. S. Chow, W. K. Leung, Y. H. Wong and H. Wise, *Neuroscience*, 2014, **279**, 10–22.
54 N. Rashidi, M. Mirahmadian, M. Jeddi-Tehrani, S. Rezania, J. Ghasemi, S. Kazemnejad, E. Mirzadegan, S. Vafaei, M. Kashanian, Z. Rasoulzadeh and A.-H. Zarnani, *J. Reprod. Infertil.*, 2015, **16**, 72–81.
55 R. Kaufmann, P. Müller, G. Hildenbrand, M. Hausmann and C. Cremer, *J. Microsc.*, 2011, **242**, 46–54.
56 Y. S. Hu, H. Cang and B. F. Lillemeier, *Proc. Natl. Acad. Sci. U. S. A.*, 2016, **113**, 7201–7206.
57 P. S. Boyd, N. Struve, M. Bach, J. P. Eberle, M. Gote, F. Schock, C. Cremer, M. Kriegs and M. Hausmann, *Nanoscale*, 2016, **8**, 20037–20047.
58 E. Latz, A. Visintin, E. Lien, K. A. Fitzgerald, B. G. Monks, E. A. Kurt-Jones, D. T. Golenbock and T. Espevik, *J. Biol. Chem.*, 2002, **277**, 47834–47843.
59 T. Ohnishi, M. Muroi and K. Tanamoto, *Clin. Diagn. Lab. Immunol.*, 2003, **10**, 405–410.
60 H. Husebye, Ø. Halaas, H. Stenmark, G. Tunheim, Ø. Sandanger, B. Bogen, A. Brech, E. Latz and T. Espevik, *EMBO J.*, 2006, **25**, 683–692.
61 J. C. Kagan, T. Su, T. Horng, A. Chow, S. Akira and R. Medzhitov, *Nat. Immunol.*, 2008, **9**, 361–368.

Supplementary Material

Nanoscale distribution of TLR4 on primary human macrophages stimulated with LPS and ATI

Jan Neumann[a,b], Kira Ziegler[a], Márton Gelléri[b], Janine Fröhlich-Nowoisky[a], Fobang Liu[a], Iris Bellinghausen[c], Detlef Schuppan[d,e], Udo Birk[b,†], Ulrich Pöschl[a], Christoph Cremer[b,a], and Kurt Lucas[a]

[a]*Multiphase Chemistry Department, Max Planck Institute for Chemistry, Hahn-Meitner-Weg 1, 55128 Mainz, Germany*
[b]*Institute of Molecular Biology, Ackermannweg 4, 55128 Mainz, Germany*
[c]*Department of Dermatology, University Medical Center of the Johannes Gutenberg University, 55131 Mainz, Germany*
[d]*Institute of Translational Immunology, University Medical Center of the Johannes Gutenberg University, Langenbeckstraße 1, 55131 Mainz, Germany*
[e]*Division of Gastroenterology, Beth Israel Deaconess Medical Center, Harvard Medical School, 330 Brookline Ave, Boston, MA 02215, USA*

Correspondence to K. Lucas (k.lucas@mpic.de)

[†]Current address: Hochschule für Technik und Wirtschaft Chur, Pulvermühlestrasse 57, 7000 Chur, Switzerland

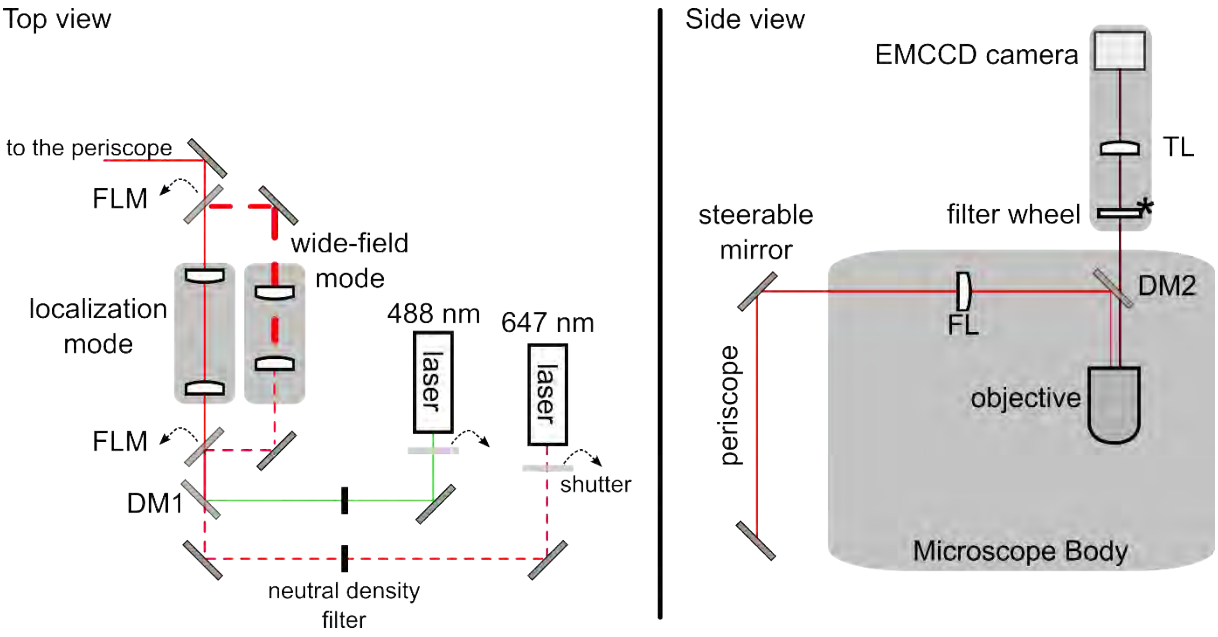

Fig. S1: Schematic diagram of the custom-built localization microscope setup. The setup was equipped with a 647 nm laser (Obis, Coherent) and a 488 nm laser (Sapphire, Coherent). Selection of laser lines was done with custom-built shutters and neutral density filters allowed adjustment of laser intensities. Both laser lines were combined using a dichromatic mirror (DM1; HC BS 580, AHF Analysetechnik). With two motorized flipping mirrors (FLM; Radiant Dyes), the laser beam could be switched between two beam paths consisting of beam expanders for localization or wide-field acquisitions. In wide-field mode, the laser beam was expanded 10-fold, illuminating the whole field of view of the camera (49.15 µm x 49.15 µm) homogenously. For localization measurements, the beam was expanded 3.125-fold. This led to an illuminated area of ~640 µm² in the sample plane (area derived from $1/e^2$ width of Gaussian profile). The collimated laser beams were coupled into the back port of the microscope (DM RBE, Leica) using a periscope. The mirror in the top unit was placed in the focal plane of the focusing lens and piezoelectric actuators (Thorlabs) attached to the mirror allowed the beam to be steered between epi-illumination and total internal reflection (TIR) illumination. The collimated laser beam was focused on the back focal plane of a 100x/NA 1.49 objective lens (Olympus) using a f = 300 mm focusing lens (FL, Thorlabs) mounted on a xyz-translator. The objective lens was attached to a piezo objective scanner (Physik Instrumente) for z-focusing of the sample. The sample was mounted on a xy-stepper stage, guided by a commercial controller (Corvus-2 eco TT, ITK Dr. Kassen GmbH). Fluorescence discrimination was done with a dichroic mirror (dual line zt488/647 rpc, AHF Analysetechnik) incorporated into a filter cube (DM2).

The filter cube also contained a laser clean-up filter (ZET488/640, AHF Analysetechnik) and a dual-notch filter (488/647 nm, AHF Analysetechnik) to remove remaining excitation light. Emitted fluorescent light was collected on an EMCCD camera (iXon 897 Ultra, Andor Technology) mounted on a custom-built camera adapter, which included an emission filter wheel. The emission filter wheel contained a 500 nm long pass filter (Chroma Technology) for 488 nm illumination and a 700/75 nm bandpass filter for 647 nm illumination. For astigmatism-based 3D localization microscopy,[1] a weak cylindrical lens (f = 1,000 mm, Thorlabs) could be placed between the tube lens (TL; f = 300 mm, Thorlabs) and the camera. Interfacing with all hardware devices and data acquisitions was done with μManager.[2]

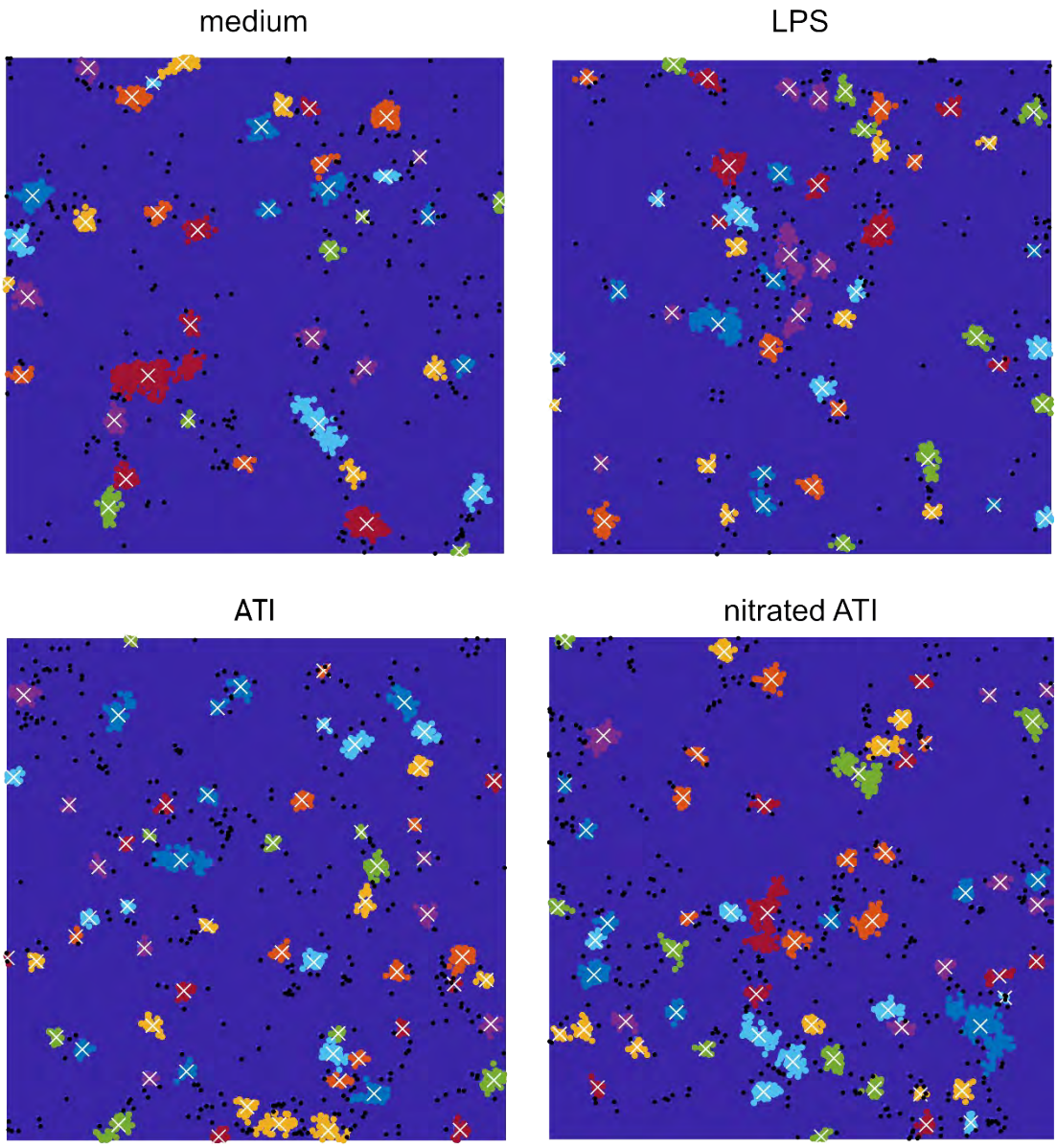

Fig. S2: Visualization of clusters as detected by DBSCAN. Representation of the detected clusters from the SMLM images from Fig. 1C. A color was randomly assigned to each identified cluster. The white cross indicates the center of mass of the cluster. Black dots represent detected molecules that are not part of a cluster.

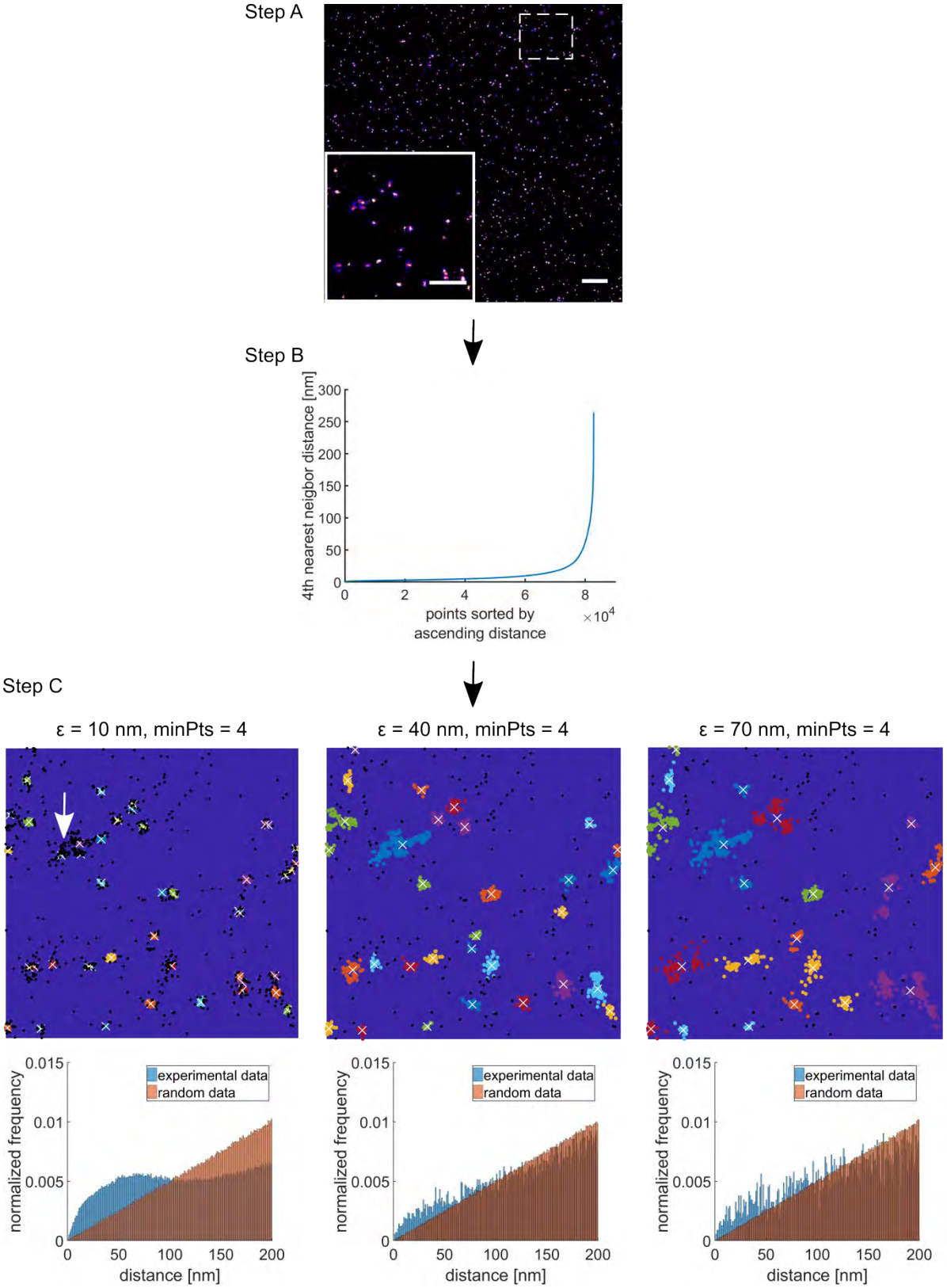

Fig. S3: Iterative determination of DBSCAN parameters. Different TLR4 sample data sets were selected for determination of DBSCAN parameters. Step A shows an 11.6 µm x 11.6 µm SMLM image from such a dataset containing approximately 80,000 detected single molecule signals (scale bar = 1 µm, inset scale bar = 500 nm). To

estimate the DBSCAN parameters (minPts and ε), a similar approach as shown in Ester et al (1996)[3] was used in a first step. The detected molecule coordinates from the list of localizations were used to determine the 4th nearest neighbor distances. These distances were sorted in ascending order and plotted against the number of detected signals. The distance value where the first strong bend in the curve occurs, was taken as a starting point for ε (step B, indicated by the black arrow). Next, DBSCAN was applied using minPts = 4 and the estimated ε obtained from step B. The clusters obtained by DBSCAN were visualized (step C). Every detected cluster is represented by a different color. Black dots correspond to molecules that are not part of a cluster or which belong to a cluster with a diameter larger than 1 µm. The white cross indicates the center of mass of the cluster. For better visibility, only the ROI from step A is shown, but calculations were done for all molecule signals of the dataset. In addition to the visualization, distances between all molecule signals outside of the detected clusters were calculated and plotted in a histogram (blue histogram). The obtained frequency distribution of distances was then compared to the one expected from a random distribution. To account for edge effects, distances originating from molecule signals that are located within the cut-off distance of 200 nm from the image border, were not calculated. The result of different combinations of ε and fixed minPts for DBSCAN is depicted in step C. Using an ε value of 10 nm, DBSCAN identified some small clusters that are surrounded by non-clustered molecule signals (assigned as noise, white arrow). By visual inspection, it appears that these noise signals belong to the clusters. This can be also seen in the frequency distribution of the distances from the molecule signals outside of the cluster (= noise points). At shorter distances, points deviate from the random distribution indicating clustering. If parameter for DBSCAN were correctly selected, these molecule signals should follow a random distribution. As a result, the ε parameter was set in this case to small. If ε is set to 40 nm, more molecule signals are assigned to a cluster and the frequency distribution of the distances from the residual noise signals approximates a random distribution. If ε is set too large, i.e. 70 nm, well separated clusters will be detected as one large cluster. The final parameters were found by iteratively adjusting minPts and ε such that the frequency distribution of distances from molecule signals outside of a cluster approximates a random distribution, supported by visual inspection of the clusters obtained from DBSCAN.

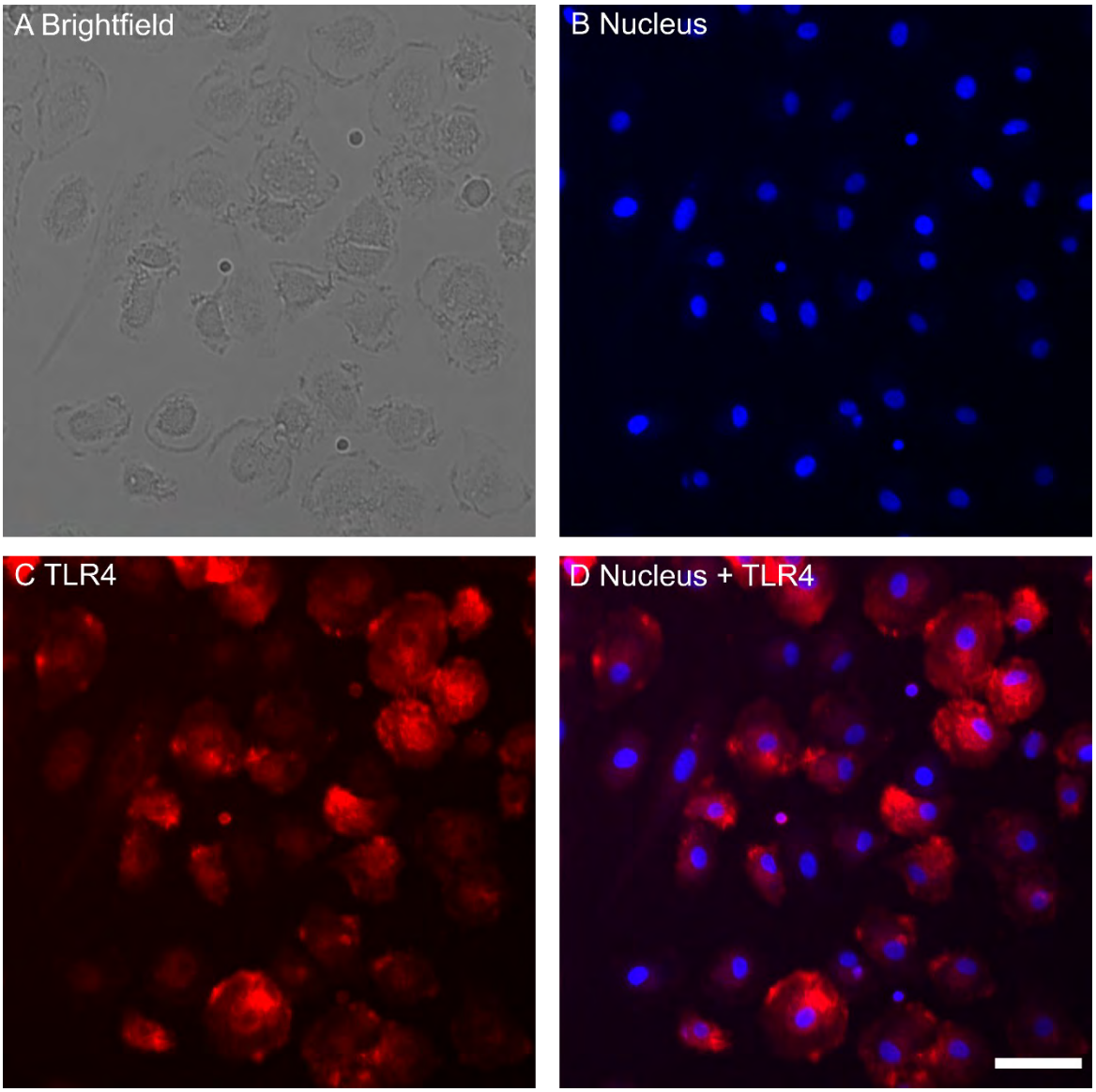

Fig. S4: Wide-field images of untreated primary human macrophages. Bright field (**A**) and fluorescence microscopy images of macrophages stained for the cell nucleus (**B**, pseudocolor blue) and TLR4 (**C**, pseudocolor red). (**D**) Overlay of nucleus and TLR4 image. Scale bar = 50 µm.

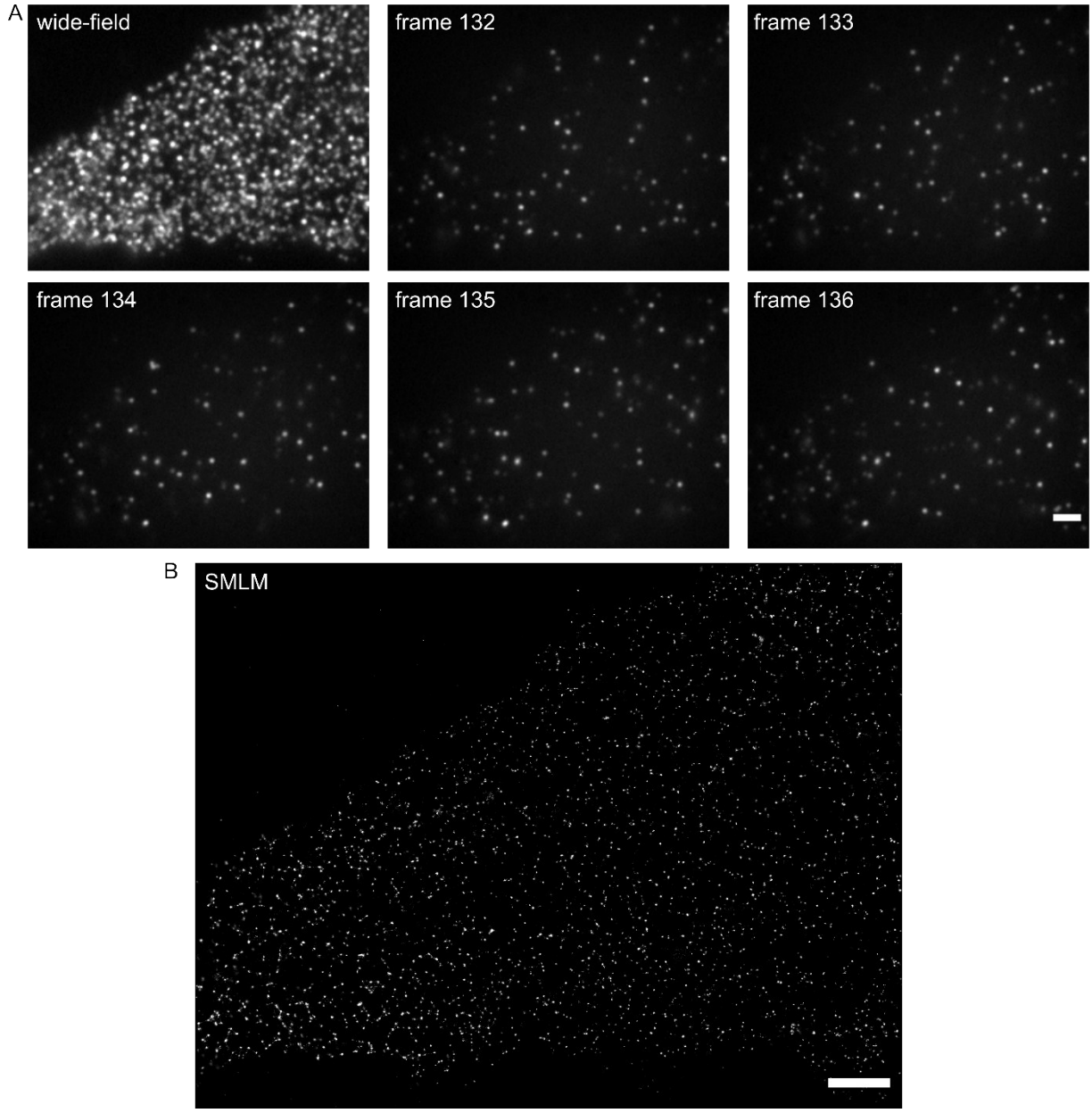

Fig. S5: Raw data images of the cell membrane of a TLR4 stained macrophage. (**A**) Wide-field image and frames 132 to 136 of the raw SMLM image data stack. A total of 5,000 frames was recorded for each cell. Scale bar = 2 µm. (**B**) Reconstructed SMLM image, where each detected signal had been blurred with a Gaussian function whose standard deviation is equal to the localization precision of the corresponding signal. Scale bar = 2 µm.

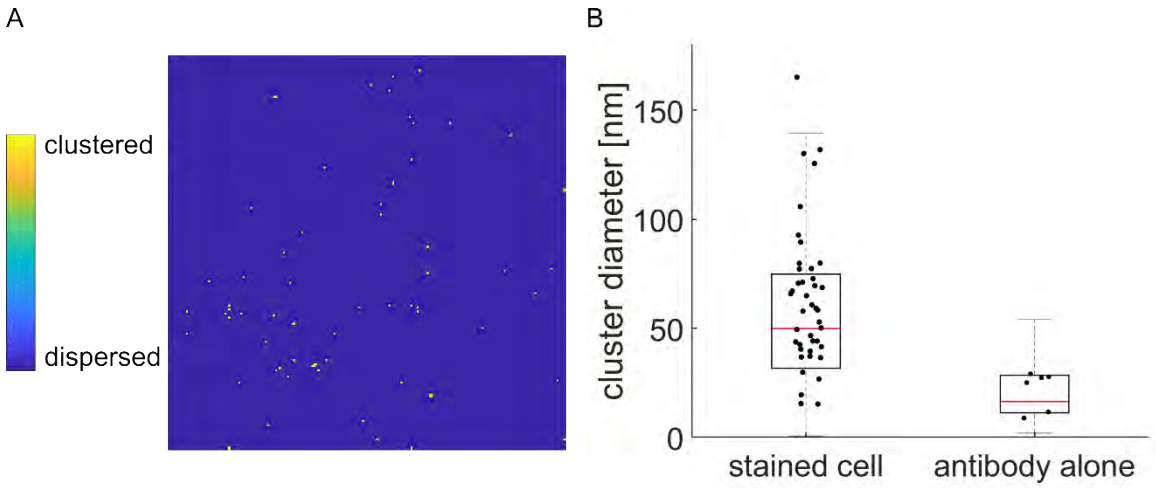

Fig. S6: Cluster size due to multiple blinking of the same fluorophore. (**A**) Grid-based density analysis of sparsely distributed secondary antibodies on a coverslip. 2 µm x 2 µm region of interest (ROI) showing the level of clustering. Yellow areas indicate clusters on the order of a few pixels. The pixel size is 10 nm. (**B**) Average cluster diameter obtained by DBSCAN. Every point corresponds to the average cluster diameter obtained from a stained cell or a field of sparsely distributed secondary antibodies on a coverslip (antibody alone). Of note, the cluster diameter obtained from the stained cell is the result of using a labeling system consisting of primary and secondary antibody. Furthermore, the mean localization precision in the cell sample was about 11 nm, whereas the mean localization precision in the antibody sample was about 16 nm. This could adversely influence the cluster diameter measured for the antibody sample.

Supplementary Note 1: Sample preparation to estimate size of clusters due to multiple blinking.

To estimate the size of clustering due to multiple blinking of the same fluorophore, coverslips containing sparsely distributed secondary antibodies were prepared. Glass coverslips (R. Langenbrinck GmbH) were coated with poly-l-lysine (Sigma Aldrich) for 15 min to 30 min and then rinsed in ddH_2O. Meanwhile, secondary antibodies (A-21237, Thermo Fisher Scientific) were diluted 1 to 10,000 in ddH_2O. After vortexing, 100 µl of diluted antibody solution were pipetted on parafilm. The coverslip was placed on top of it with the coated side facing downwards. The sample was incubated for 1 h to 2 h. Next, the sample was rinsed with PBS (Thermo Fisher Scientific), embedded in Vectashield H-1000 (Vector Laboratories) and sealed using picodent twinsil (picodent

Dental Produktions- und Vertriebs GmbH). Imaging and data evaluation were performed in the same way as for the cell samples.

Supplementary Note 2: Choice of stimulation time

The chosen stimulation times are based on previous studies with LPS as agonist, where it was shown that within 10 min after stimulation TLR4 is recruited into lipid rafts.[4] Furthermore, it was observed that TLR4 co-localizes with endosomes within 15 min of LPS stimulation.[5] Additionally, our measurements on macrophages revealed, that an LPS-induced translocation of NF-κB from the cytoplasm into the nucleus occurs within 30 minutes of stimulation (Fig. S7).

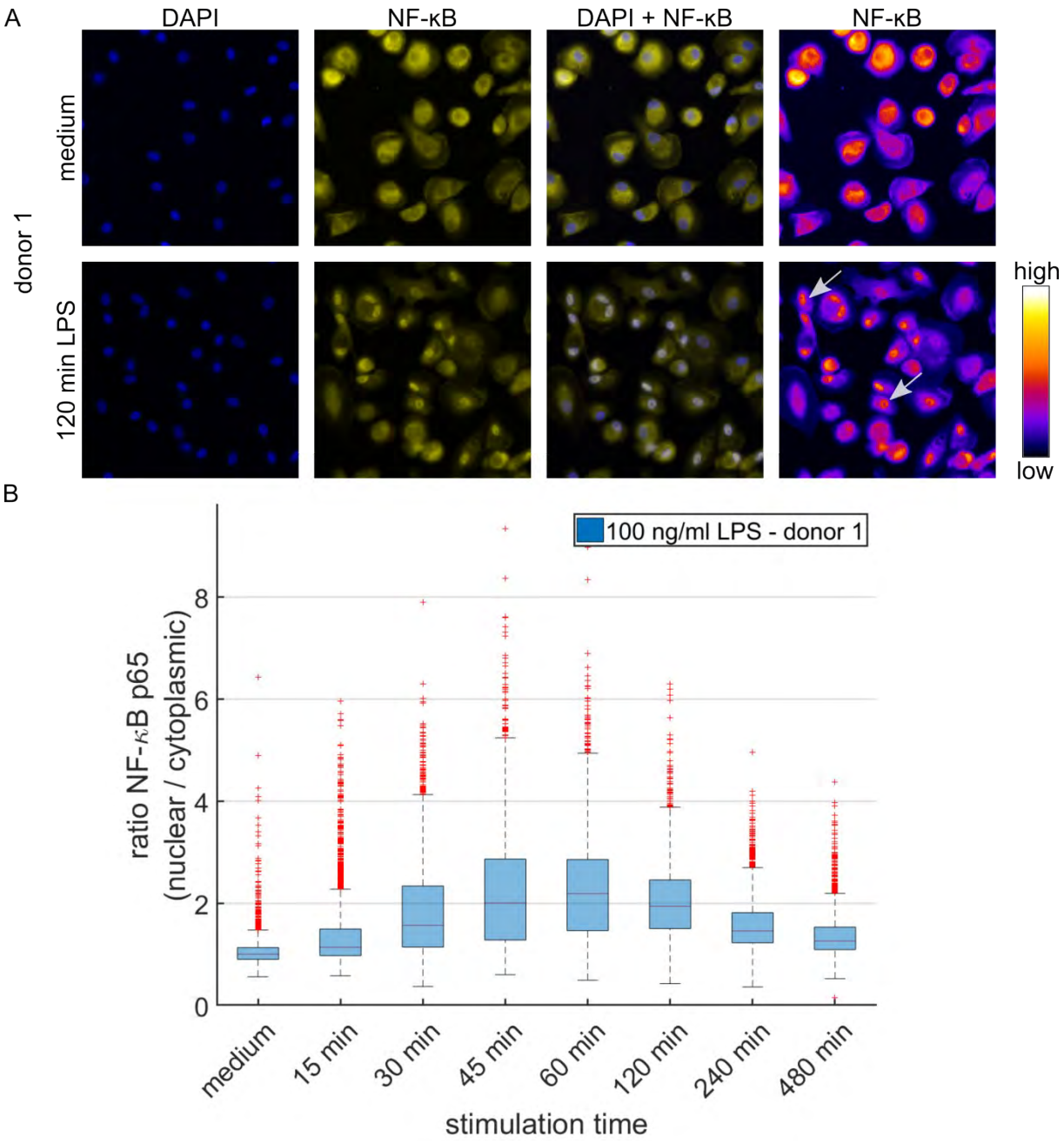

Fig. S7: Time-dependent translocation of NF-κB induced by LPS. (**A**) Fluorescence microscopy images of human primary macrophages stimulated for 120 min with LPS-EB (100 ng/ml). After fixation, cells were stained for NF-κB (pseudocolor yellow). The nucleus is counterstained using DAPI (pseudocolor blue). In the medium control NF-κB is mostly located in the cytoplasm, whereas in LPS-stimulated samples NF-κB is enriched in the nucleus (indicated by arrows). Scale bar = 50 µm. (**B**) Quantitative evaluation of NF-κB translocation for cells fixed at indicated time points. The ratio of nuclear to cytoplasmic NF-κB is plotted against the stimulation time. Nuclear translocation of NF-κB is visible within 30 min of LPS stimulation.

Supplementary Note 3: Treatment, immunofluorescence staining and imaging of NF-κB p65.

Treatment

Primary human macrophages were isolated and differentiated as described in the experimental section. Cells were seeded on 12-well glass bottom plates (Cellvis). After 6 days of differentiation, cells were stimulated with 100 ng/ml LPS-EB for 15 min to 480 min. Cells were then washed once in pre-warmed PBS and subsequently fixed using 4 % formaldehyde in PBS for 10 min at 37 °C. Next, cells were washed three times in PBS before proceeding with immunostaining of NF-κB.

Immunofluorescence staining

For immunostaining, cells were permeabilized and blocked for 1 h in PBS containing 5 % bovine serum albumin (BSA; Cell Signaling Technology) and 0.3 % Triton X-100 (Merck). Primary antibody (D14E12, Cell Signaling Technology), directed against human p65 subunit of NF-κB, was diluted 1 to 400 in antibody dilution buffer (1 % BSA and 0.3 % Triton X-100 in PBS). Cells with primary antibody were incubated overnight at 4 °C. Afterwards, cells were washed three times in PBS, followed by incubation with goat anti-rabbit Alexa Fluor 568 conjugated secondary antibody (Thermo Fisher Scientific, cat. no. A-11011), diluted 1 to 400 in the same buffer as the primary antibody. After 1 h of incubation at room temperature, cells were again washed three times in PBS. Counterstaining of cell nuclei was done using 4’,6-diamidino-2-phenylindole (DAPI; Thermo Fisher Scientific) at a concentration of 300 nM in PBS for 3 min. After three washing steps in PBS, stained cells were immediately imaged. PBS was used as the imaging buffer.

Imaging

Imaging was done using the Opera Phenix High-Content Screening system (PerkinElmer). Samples were imaged through a 20x/1.0 water immersion objective. Cells stained for NF-κB p65 and DAPI were excited using 561 nm and 405 nm laser lines, respectively. Emitted light was collected on two sCMOS cameras through specific emission filters for NF-κB p65 (570 nm to 630 nm) and DAPI (435 nm to 480 nm). 2 x 2 binning was used for the two cameras and the microscope was operated in

a non-confocal mode. Intensity and exposure time were set to obtain sub-saturating pixels. In each well, images from 72 different ROIs were taken.

Image processing was done using Harmony software (PerkinElmer). First, stained cell nuclei were identified by segmenting the DAPI channel. Identified nuclei were used as seeds to identify their corresponding cytoplasm masks using the NF-κB p65 channel. Masks were resized to avoid overlapping between them and to stay within the boundaries of the cell. Finally, a nuclear mask with a corresponding ring-like cytoplasm mask was obtained. Mean NF-κB p65 intensities within both masks were determined and the ratio of nuclear to cytoplasmic NF-κB p65 was calculated.

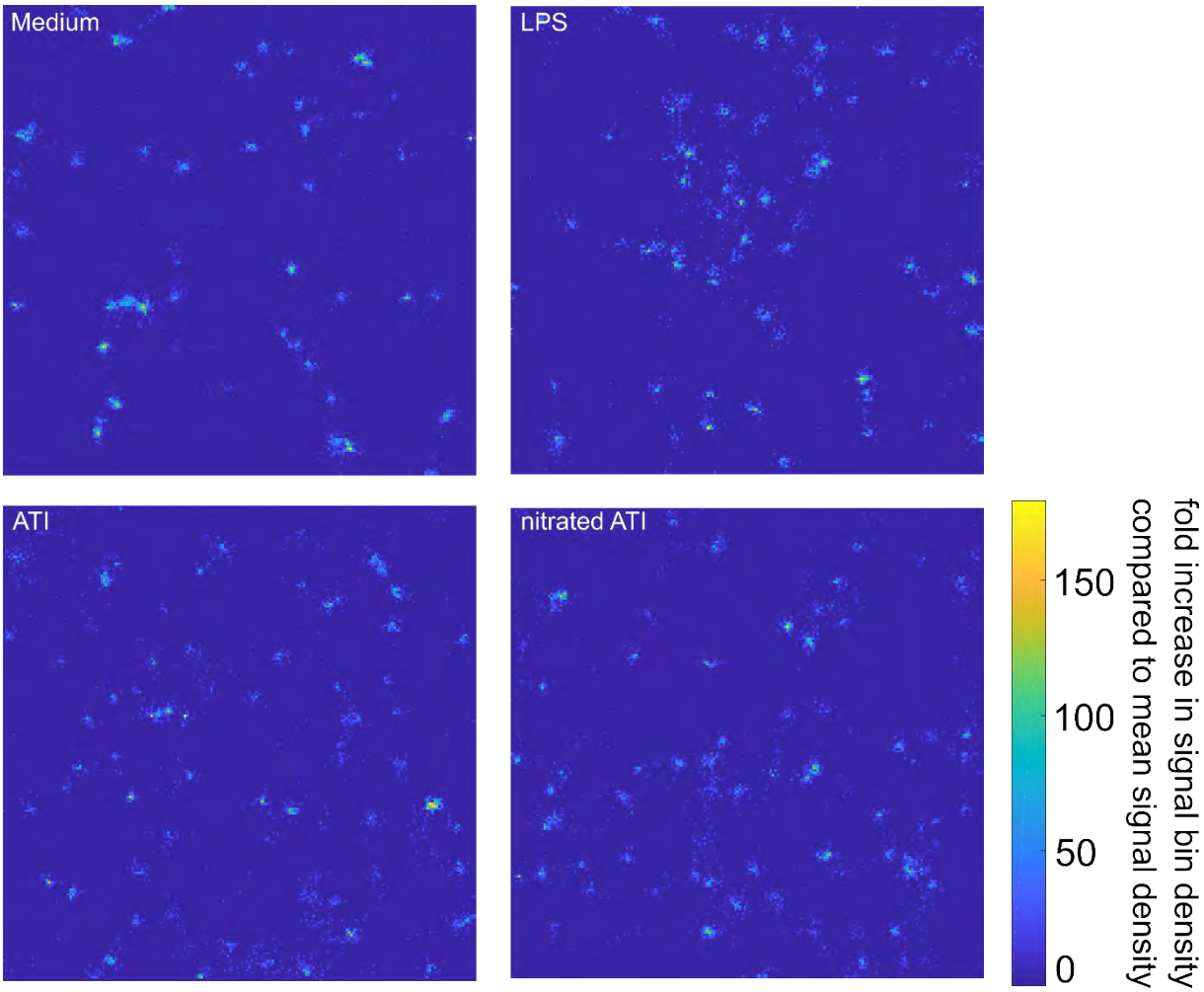

Fig. S8: Grid-based density analysis reveals the local level of clustering. Representation of the grid-based density analysis depicted in Figure 1D with absolute values. Detected signals were binned on a 10 nm x 10 nm grid and the signal density of each bin was divided by the mean signal density of the corresponding ROI.

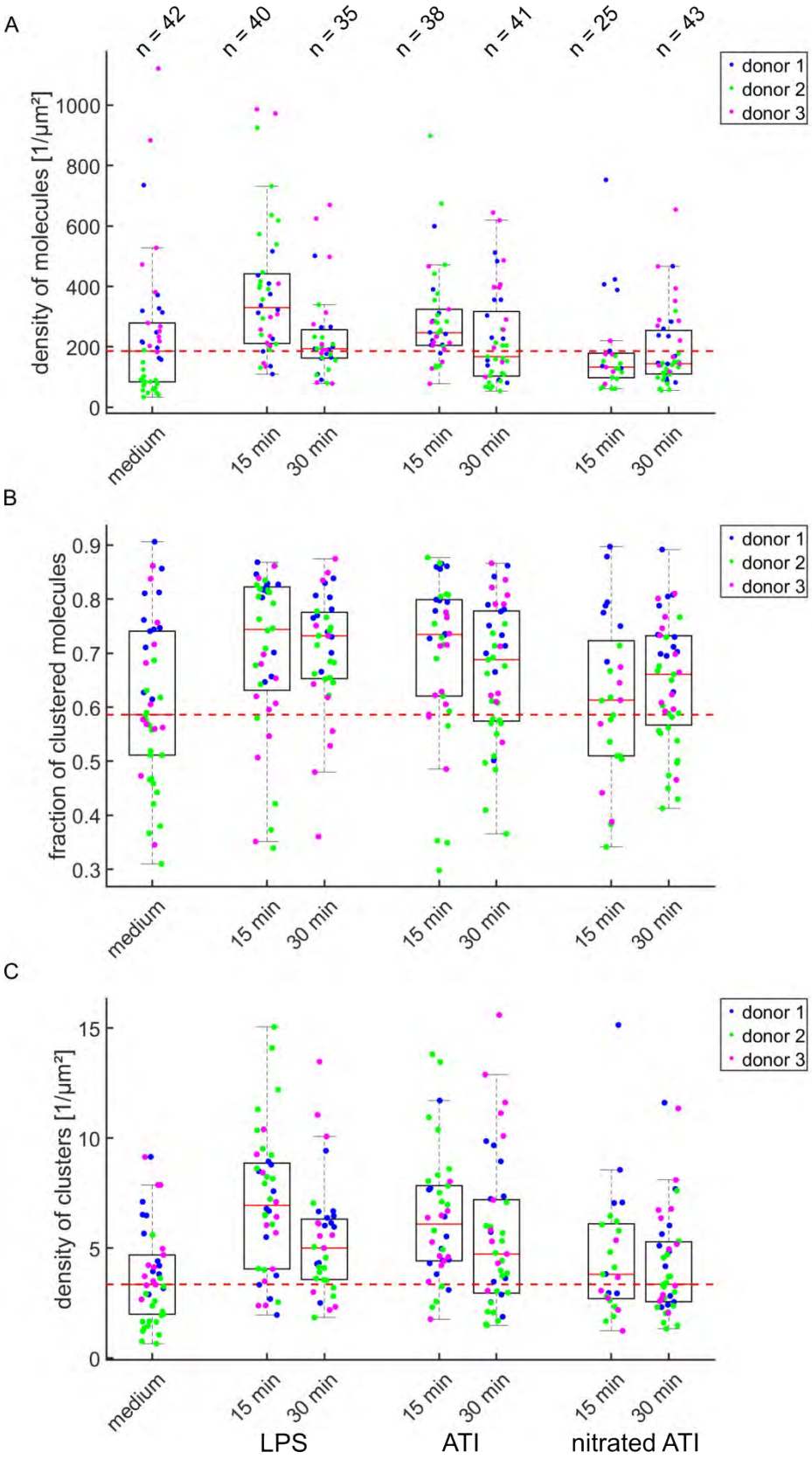

Fig. S9: TLR4 membrane clustering upon LPS and ATI stimulation. The mean density of detected molecules on the cell membrane (**A**) as well as the fraction of clustered molecules (**B**) and the density of clusters (**C**) as analyzed by DBSCAN is shown. The boxes represent the median and the 25th to 75th percentile, whereas the

whiskers cover 99.3 % of the data. The horizontal red line indicates the median value of the medium control. Overlaid dots represent mean values obtained from different cells. The color of the dots corresponds to the respective donors and the number above each treatment denotes the number of measured cells.

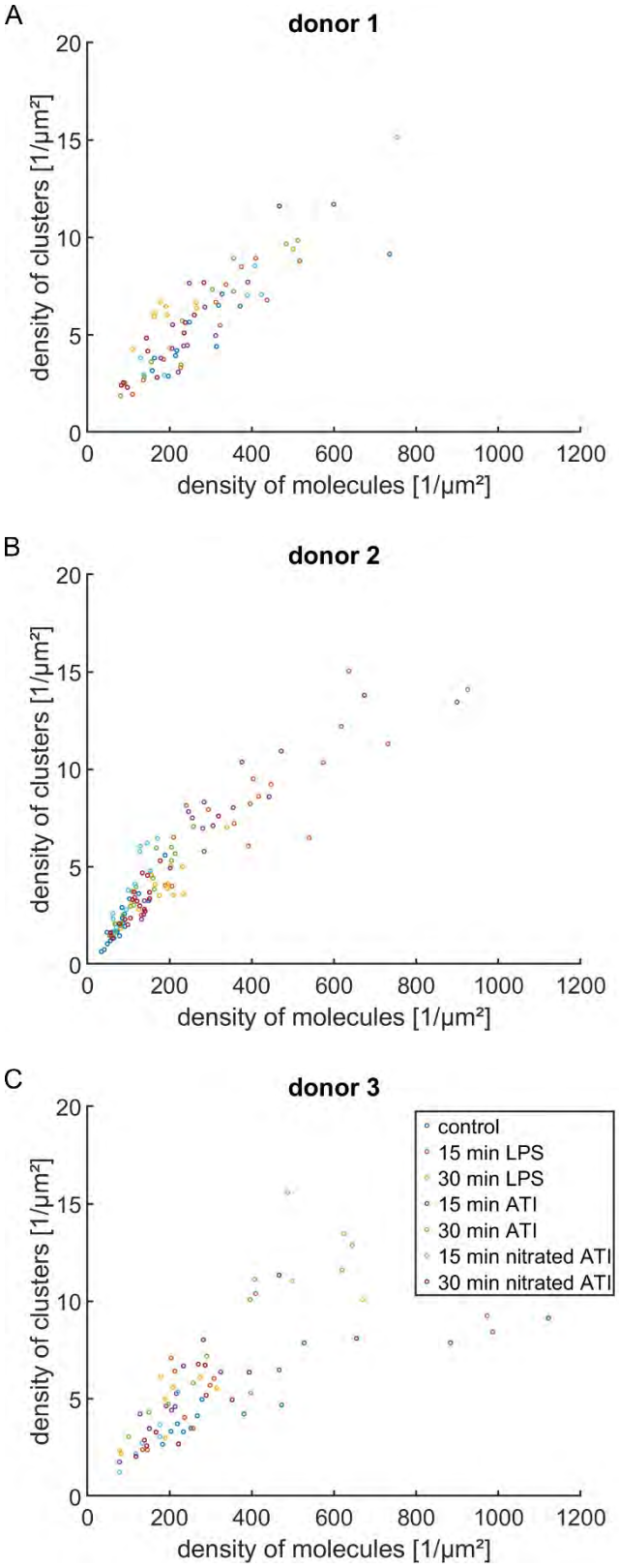

Fig. S10: Correlation between TLR4 surface representation and TLR4 clustering. For donor 1 (A), donor 2 (B) and donor 3 (C) the density of molecules vs. the density of clusters on the cell membrane is shown. All plots indicate a positive correlation between both variables. Each point represents a cell and the color of the point corresponds to the respective treatment.

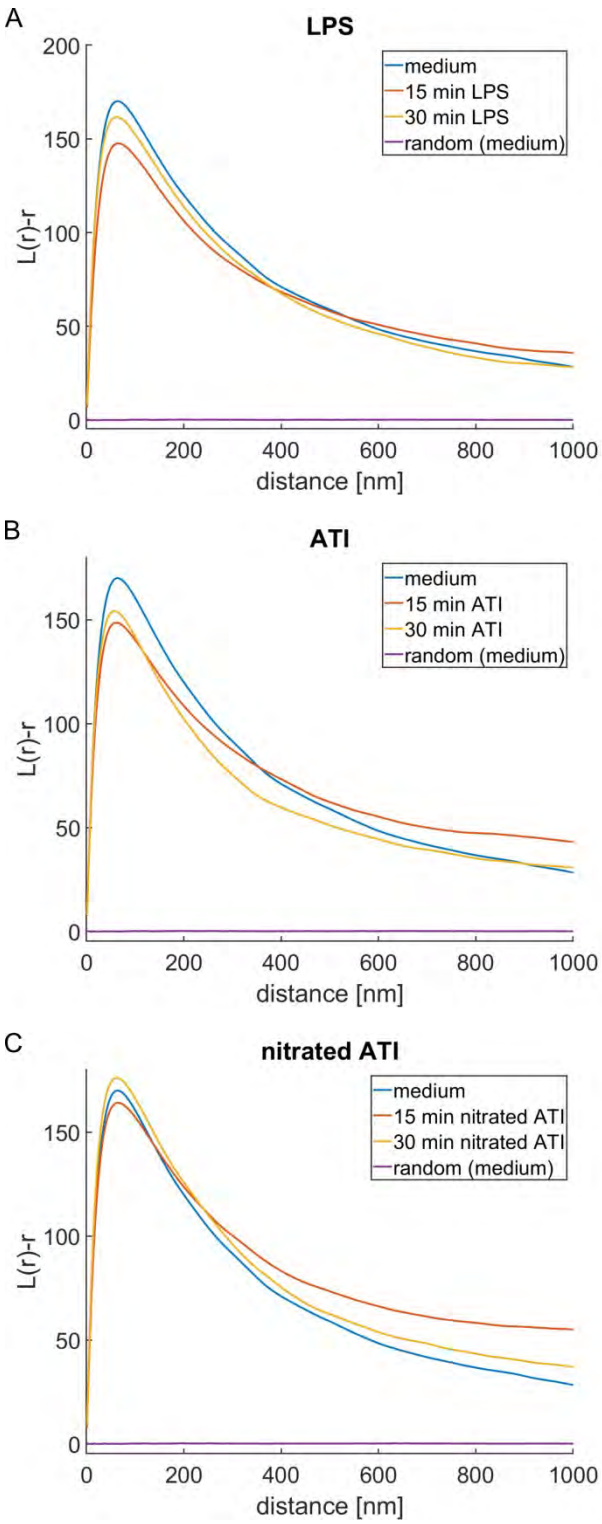

Fig. S11: Average of Ripley's H-function for the different treatments. Ripley's H-function of macrophages stimulated for 15 min and 30 min with (**A**) 100 ng/ml LPS, (**B**) 12.5 µg/ml ATI or (**C**) 12.5 µg/ml nitrated ATI. Each function displays the average obtained from three healthy donors. All plots also show Ripley's H-function, which was obtained from the random data of the medium sample.

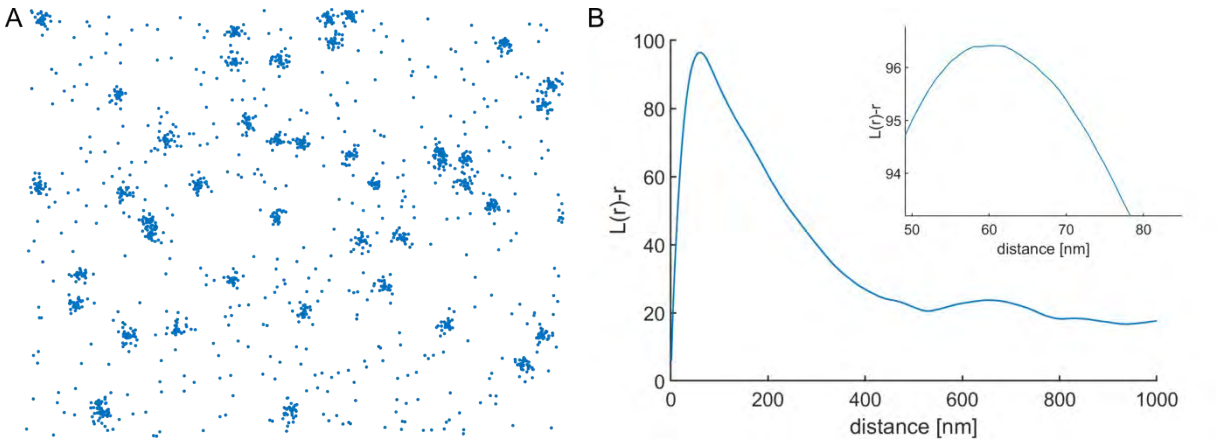

Fig. S12: Simulation of clusters. (**A**) Section of a 10 µm x 10 µm simulated image. Simulation parameters were set to represent experimental data. The average density is 300 molecule signals/µm², with 70 % of molecule signals being part of a simulated Gaussian-shaped cluster. Simulated clusters were randomly distributed over the randomly simulated point pattern with an average density of 6 cluster/µm². Cluster diameter was set to 60 nm. (**B**) Ripley's H-function of the simulated point pattern. The maximum of Ripley's function is approximately 60 nm.

Table S1: TLR4 cluster size obtained by Ripley's H-function. Values denote mean ± standard deviation.

	donor	number of cells	Maximum Ripley's H function [nm]
medium	donor 1	11	58 ± 5
	donor 2	19	67 ± 11
	donor 3	12	66 ± 9
15 min LPS	donor 1	11	66 ± 15
	donor 2	18	62 ± 14
	donor 3	10	75 ± 44
30 min LPS	donor 1	11	58 ± 8
	donor 2	13	64 ± 7
	donor 3	11	67 ± 29
15 min ATI	donor 1	11	61 ± 10
	donor 2	16	69 ± 37
	donor 3	11	62 ± 15
30 min ATI	donor 1	11	64 ± 10
	donor 2	19	55 ± 7
	donor 3	11	51 ± 5
15 min nitrated ATI	donor 1	7	62 ± 8
	donor 2	12	53 ± 8
	donor 3	6	79 ± 25
30 min nitrated ATI	donor 1	11	58 ± 9
	donor 2	20	58 ± 10
	donor 3	12	65 ± 14

	number of cells			density of molecules on the membrane [1/µm²]			fraction of clustered molecules			number of molecules per cluster		
Buffycoat	Donor 1	Donor 2	Donor 3	Donor 1	Donor 2	Donor 3	Donor 1	Donor 2	Donor 3	Donor 1	Donor 2	Donor 3
medium	11	19	12	300 ± 160	80 ± 40	420 ± 300	0.7 ± 0.1	0.5 ± 0.1	0.6 ± 0.1	48 ± 46	21 ± 19	59 ± 87
15 min LPS	11	18	11	300 ± 130	430 ± 210	380 ± 300	0.8 ± 0.1	0.7 ± 0.2	0.6 ± 0.1	44 ± 42	37 ± 45	54 ± 99
30 min LPS	11	13	11	210 ± 110	190 ± 65	300 ± 210	0.8 ± 0.1	0.7 ± 0.1	0.7 ± 0.2	28 ± 26	31 ± 30	40 ± 47
15 min ATI	11	16	11	280 ± 120	340 ± 200	230 ± 105	0.8 ± 0.1	0.7 ± 0.2	0.7 ± 0.1	39 ± 34	33 ± 47	30 ± 36
30 min ATI	11	19	11	270 ± 150	130 ± 60	360 ± 180	0.7 ± 0.1	0.6 ± 0.1	0.7 ± 0.1	37 ± 37	23 ± 21	32 ± 35
15 min nitrated ATI	7	12	6	350 ± 220	110 ± 40	150 ± 50	0.8 ± 0.1	0.5 ± 0.1	0.6 ± 0.1	43 ± 42	15 ± 12	29 ± 31
30 min nitrated ATI	11	20	12	200 ± 110	120 ± 60	290 ± 160	0.7 ± 0.1	0.6 ± 0.1	0.7 ± 0.1	30 ± 28	23 ± 20	42 ± 57

	cluster diameter [nm]			density of molecules within clusters [x10^4 1/µm²]			distance to next neighboring cluster [nm]			density of clusters [1/µm²]		
Buffycoat	Donor 1	Donor 2	Donor 3	Donor 1	Donor 2	Donor 3	Donor 1	Donor 2	Donor 3	Donor 1	Donor 2	Donor 3
medium	57 ± 29	38 ± 20	65 ± 41	2.3 ± 16	2.4 ± 4.3	2.1 ± 23	230 ± 120	360 ± 230	230 ± 120	5 ± 2	2 ± 1	5 ± 2
15 min LPS	57 ± 27	52 ± 32	59 ± 43	1.9 ± 4.5	2.0 ± 2.7	2.0 ± 2.6	220 ± 110	190 ± 90	230 ± 130	6 ± 3	8 ± 3	6 ± 3
30 min LPS	43 ± 24	46 ± 25	55 ± 32	2.4 ± 4.6	2.4 ± 3.9	1.9 ± 2.0	220 ± 120	270 ± 150	200 ± 110	6 ± 2	4 ± 1	6 ± 3
15 min ATI	53 ± 25	48 ± 32	45 ± 27	2.1 ± 17	3.3 ± 85	2.5 ± 3.6	220 ± 120	200 ± 120	230 ± 130	6 ± 3	8 ± 3	5 ± 2
30 min ATI	52 ± 28	39 ± 22	46 ± 24	2.1 ± 7.3	2.7 ± 5.3	2.2 ± 1.9	230 ± 130	260 ± 150	190 ± 100	6 ± 3	4 ± 2	8 ± 4
15 min nitrated ATI	58 ± 29	31 ± 16	45 ± 27	1.7 ± 1.5	2.9 ± 4.1	2.4 ± 2.7	200 ± 110	260 ± 160	290 ± 170	7 ± 4	4 ± 2	3 ± 1
30 min nitrated ATI	47 ± 26	39 ± 21	56 ± 34	2.5 ± 19	3.1 ± 23	2.1 ± 4.7	240 ± 140	300 ± 180	240 ± 140	5 ± 3	3 ± 2	5 ± 3

Table S2: Donor-specific results from TLR4's density-based clustering analysis. Values denote mean ± standard deviation.

	number of cells	density of molecules on the membrane [1/µm²]	fraction of clustered molecules	number of molecules per cluster
medium	42	240 ± 230	0.6 ± 0.2	48 ± 68
15 min LPS	40	380 ± 220	0.7 ± 0.1	43 ± 62
30 min LPS	35	230 ± 140	0.7 ± 0.1	33 ± 37
15 min ATI	38	290 ± 160	0.7 ± 0.1	34 ± 41
30 min ATI	41	230 ± 160	0.7 ± 0.1	31 ± 32
15 min nitrated ATI	25	180 ± 160	0.6 ± 0.1	31 ± 35
30 min nitrated ATI	43	190 ± 130	0.6 ± 0.1	31 ± 38

	cluster diameter [nm]	density of molecules within clusters [x10^4 1/µm²]	distance to next neighboring cluster [nm]	density of clusters [1/µm²]
medium	57 ± 36	2.2 ± 19	260 ± 150	4 ± 2
15 min LPS	55 ± 34	2.0 ± 3.3	200 ± 110	7 ± 3
30 min LPS	48 ± 28	2.2 ± 3.6	230 ± 130	5 ± 3
15 min ATI	49 ± 29	2.7 ± 57	220 ± 120	6 ± 3
30 min ATI	46 ± 25	2.3 ± 5.3	230 ± 130	6 ± 3
15 min nitrated ATI	47 ± 28	2.2 ± 2.8	240 ± 140	5 ± 3
30 min nitrated ATI	47 ± 28	2.6 ± 18	260 ± 150	4 ± 2

Table S3: Averaged results from TLR4's density-based clustering analysis. Values denote mean ± standard deviation.

References

1 B. Huang, W. Wang, M. Bates and X. Zhuang, *Science*, 2008, **319**, 810–813.

2 A. Edelstein, N. Amodaj, K. Hoover, R. Vale and N. Stuurman, *Curr. Protoc. Mol. Biol.*, 2010, **92**, 1–17.

3 M. Ester, H.-P. Kriegel, J. Sander and X. Xu, *Proc. Second Int. Conf. Knowl. Discov. Data Min.*, 1996, 226–231.

4 J. Cuschieri, E. Bulger, J. Billgrin, I. Garcia and R. V. Maier, *Surg. Infect. (Larchmt).*, 2007, **8**, 91–106.

5 H. Husebye, Ø. Halaas, H. Stenmark, G. Tunheim, Ø. Sandanger, B. Bogen, A. Brech, E. Latz and T. Espevik, *EMBO J.*, 2006, **25**, 683–692.

B.3 Ziegler *et al.*, in preparation, 2019

TLR4 stimulating proteins modified by peroxynitrite amplify TLR4 signaling and inflammation

Tentative author list. To be extended/adjusted.

Ziegler K.[1], Kunert A. T. [1], Widera D. [2], Leifke A. L. [1], Reinmuth-Selzle K. R. [1], Maes M. [3], Weller M. [4], Schuppan D. [5,6],Fröhlich-Nowoisky J. [1], Lucas K. [1] and Pöschl U[1]

[1]Max Planck Institute for Chemistry, Multiphase Chemistry Department, 55128 Mainz, Germany

[2]Stem Cell Biology and Regenerative Medicine Group, School of Pharmacy, University of Reading, RG6 6AP Reading, UK

[3]Maes Clinics Tria, 10310 Bangkok, Thailand

[4] Bundesanstalt für Materialforschung und -prüfung,12205 Berlin, Germany

[5]Institute of Translational Immunology, University Medical Center of the Johannes Gutenberg University, 55131 Mainz, Germany

[6]Division of Gastroenterology, Beth Israel Deaconess Medical Center, Harvard Medical School, MA 02215, USA

TLR4 stimulating proteins modified by peroxynitrite amplify TLR4 signaling and inflammation

(Tentative author list. To be extended/adjusted)

Ziegler K.[1], Kunert A. T. [1], Widera D. [2], Leifke A. L. [1], Reinmuth-Selzle K. R. [1], Maes M. [3], Weller M. [4], Schuppan D. [5,6],Fröhlich-Nowoisky J. [1], Lucas K. [1]* and Pöschl U[1]*

[1]Max Planck Institute for Chemistry, Multiphase Chemistry Department, 55128 Mainz, Germany

[2]Stem Cell Biology and Regenerative Medicine Group, School of Pharmacy, University of Reading, RG6 6AP Reading, UK

[3]Maes Clinics Tria, 10310 Bangkok, Thailand

[4] Bundesanstalt für Materialforschung und -prüfung,12205 Berlin, Germany

[5]Institute of Translational Immunology, University Medical Center of the Johannes Gutenberg University, 55131 Mainz, Germany

[6]Division of Gastroenterology, Beth Israel Deaconess Medical Center, Harvard Medical School, MA 02215, USA

*correspondence to: k.lucas@mpic.de, u.poschl@mpic.de

Abstract

In the course of inflammatory processes reactive species such as peroxynitrite are formed and lead to protein modification by nitration and oligomerization. So far, however, the question whether these modified proteins are markers or mediators of inflammation remaines elusive. Here, we show that modification by peroxynitrite enhances the pro-inflammatory reaction of prominent disease-related, damage-associated and allergenic proteins.

Methods:

To mimic inflammatory conditions, proteins were modified with peroxynitrite. The degree of protein nitration was determined by HPLC and protein oligomerization identified by gel electrophoresis and silver stain. General pro-inflammatory properties of the native and modified proteins were assessed by measuring the stimulation of TLR4 and activation of NF-κB by specific reporter cell lines. Furthermore, pro-inflammatory cytokine expression was determined on mRNA and protein level of THP-1 monocytes.

Results:

We find enhanced TLR4 and NF-κB stimulation, as well enhanced TNF-α and IL-1 β expression after modification with peroxynitrite for most of the tested proteins. These are, the Parkinson disease associated protein *alpha-Synuclein* (α-Synuclein) the DAMPs: *Heat shock protein 60* (HSP60) and *high mobility group 1* (HMGB1) and the allergens: Grass pollen allergen *Phl p 5* and bakers' asthma allergen *amylase trypsin inhibitors* (ATI) from wheat. Based on our findings, we suggest a model, in which the process of protein modification by peroxynitrite contributes to inflammation and disease in a TLR4, NF-kB, IL-1 and TNF-alpha mediated positive feedback loop. This suggested molecular pathomechanism might be relevant in many diseases and especially in Parkinson's disease.

1. Introduction

Protein nitration occurs exogenously in the environment and endogenously in the body by independent mechanisms. Exogenous nitration can happen under summer smog conditions, where the main causing agents are ozone, nitrogen dioxide, UV radiation, and humidity (Franze *et al.*, 2005; Shiraiwa *et al.*, 2011; Shiraiwa *et al.*, 2012; Selzle *et al.*, 2013). Endogenous nitration frequently takes place during inflammatory processes in the body. Thereby immune cells produce locally high concentrations of reactive oxygen and nitrogen species (RS) to kill invading pathogens. However, RS also causes damage in sterile inflammation. Reactive species such as superoxide and nitric oxide can lead to the formation of peroxynitrite, which is the main nitrating agent in endogenous nitration (Radi, 2013; Reinmuth-Selzle *et al.*, 2014).

Exogenous and endogenous protein nitration are irreversible processes, which are facilitated in a two-step mechanism. First forms a tyrosine residue RS intermediate. In a second step, the RS-Tyrosine residue is reacting with nitrogen oxide to nitrotyrosine. (Selzle *et al.*, 2013; Shiraiwa *et al.*, 2012) Alternatively, the RS-Tyrosine residue can react with a second RS-Tyrosine residue and form a dityrosine. Thereby protein dimers or higher oligomers can be formed (Kampf *et al.*, 2015; Liu *et al.*, 2017; Kanwar and Balasubramanian, 2000). Summarized, during the reaction of proteins with peroxynitrite nitration and oligomerization can take place. To cover both aspects, in the following collectively term *nitration modified proteins* (n-proteins) is used.

Indeed, nitrotyrosine is frequently used as a marker for inflammation and oxidative stress (Greenacre and Ischiropoulos, 2001;Ghosh et al., 2006;Ischiropoulos, 2009) (Murata and Kawanishi, 2004). Here we investigate how peroxynitrite treatment alters pro-inflammatory potential of proteins, which are described as TLR4 agonists. We tested proteins from three different categories: *disease related proteins, damage associated molecular pattern* (DAMPs), and *allergens* for their inflammatory reactivity. We mimicked endogenous protein-nitration using peroxynitrite and determined the degree of nitration by HPLC and oligomerization by gel electrophoresis followed by silver stain. As NF-κB (p50/p65) signaling is a key pathway to induce the transcription of many pro-inflammatory cytokines, we tested the modified proteins in comparison to their native forms for their ability to induce NF-κB activation in THP-1 NF-κB reporter cells. As second measure of pro-inflammatory effects, we analyzed TLR4 stimulation in HeLa TLR4 dual reporter cells. To obtain a more precise pattern of the single pro-inflammatory markers, we assessed mRNA expression of TNF-α, IL-1 β IL-6, IL-8, IFN-γ, CCL5 and TGF-β as well as cytokine secretion of IL-6, IL-8 and IL-1β from THP-1 monocytes treated with native and modified proteins.

2. Material and Methods

2.1 Selected proteins

Table 1: Overview proteins tested and their main functions

Category	Protein	Source & Supplier	Concentration applied	Main function
Control	Keyhole limpet haemocyanine (KLH)	Chicken egg white, Invivogen	50.0 µg/mL	Immune stimulant and carrier for haptens
Control	Ovalbumin (OVA)	*Megathura crenulata*, Sigma	50.0 µg/mL	Model allergen in asthma mouse models
Disease specific	Amyloid beta (β-Amyloid), human peptide 1-42	Recombinant *E.coli*, Genscript	45.0 µg/mL	Associated to the pathology of Alzheimer´s disease
Disease specific	Alpha Synuclein (α-Synuclein), human	Recombinant *E.coli*, Merck Millipore	50.0 µg/mL	Associated to the pathology of Parkinson´s disease
DAMP	High Mobility group 1 (HMGB1), human	Recombinant *E.coli*, Sigma Aldrich	3.6 µg/mL	Nuclear DAMP
DAMP	Heat Shock Protein 60 (HSP 60), human	Recombinant *E.coli*, Abcam	14.3 µg/mL	Mitochondrial DAMP
Allergen	Amylase trypsin inhibitors (ATI), wheat seed type I	*Triticum aestivum,* Sigma Aldrich	15.0 µg/mL	Major allergen in baker´s asthma and TLR4 stimulant
Allergen	*Phleum pratense*, timothy grass pollen allergen 5 (Phl p 5)	Recombinant *E.coli*, Biomay	30.0 µg/mL	Major grass pollen allergen
Allergen	*Betula verrucosa*, allergen isoform 1a (Bet v 1a)	Recombinant *E.coli*, Biomay	30.0 µg/mL	Major birch pollen allergen
Allergen	*Betula verrucosa*, allergen isoform 1d (Bet v 1d)	Recombinant *E.coli*, Biomay	30.0 µg/mL	Isoform of the major birch pollen allergen Bet v 1a

2.1.1 Control proteins

Ovalbumin (OVA) is a 45 kDa glycoprotein and the most abundant protein in avian egg white. Through its high accessibility, OVA is widely used in protein chemistry and in experimental mouse models of allergy when combined with adjuvants. In a mouse model of food allergy nitrated OVA induced enhanced IgE reactions (Untersmayr *et al.*, 2010), whereas a second study demonstrated enhanced immunogenicity for nitrated OVA in general (Gruijthuijsen *et al.*, 2006). In our study OVA served as negative control for human TLR4 and NF-κB.

Keyhole limpet haemocyanine (KLH) provokes unspecific innate and adaptive immune responses. Therefore, it is frequently used as a carrier for haptens to induce immune reactions. Here it served as unspecific positive control, as it is described to stimulate TLR4 and other receptors.

2.1.2 Damage associated molecular patterns (DAMPs)

DAMPs play a crucial role in innate immunity, stimulating pattern recognition receptors (PRRs) such as TLR4. Naturally, TLR4 senses lipopolysaccharides of gram-negative bacteria and DAMPs, which induces pro-inflammatory cytokine production via NF-κB and IRF3/IRF7 (Kawasaki and Kawai, 2014) and RS (Park *et al.*, 2004). One classical DAMP is HMGB1, which interacts with the advanced glycosylation end product-specific receptor (RAGE or AGER) (Chandramouleeswaran *et al.*, 2016; Liu *et al.*, 2014), TLR2 (Yu *et al.*, 2006) and TLR4. HMGB1 induces the production of nitric oxide and RS, the stimulation of TLR4, and nitrotyrosine formation (Chandrashekaran *et al.*, 2017). Other classical DAMPs are Heat shock proteins (HSP), which are chaperones and relevant for correct protein folding. Moreover, secreted HSP60 can act as danger signal and can stimulate TLR2, TLR4 and TREM2 (Zanin-Zhorov *et al.*, 2018; Stefano *et al.*, 2009; Cohen-Sfady *et al.*, 2005).

2.2.3 Disease specific proteins

Amyloid Beta (β-Amyloid) is formed by β-Amyloid peptides and involved in Alzheimer´s disease. The β-Amyloid oligomers are major component in plaques (Glenner and Wong, 2012), related to synaptic and cognitive dysfunctions, and act as TLR4 agonists (Balducci *et al.*, 2017). To obtain bioactive Amyloid beta oligomers, dissolving of the β-Amyloid peptide in to monomers is a crucial step (Ryan *et al.*, 2013). To receive comparable results, we used synthesized β-Amyloid peptides (amino acids 1-42) comprising normal tyrosine in its native form, or nitrotyrosine in the nitrated form.

A different prominent disease specific protein is alpha-Synuclein (α-Synuclein) which is highly relevant in Parkinson's disease. Interestingly, an enrichment of nitrated α-Synuclein is found in Lewy bodies and during neuroinflammation (He *et al.*, 2018). Benner et al. demonstrated a

robust T cell response by immunization with nitrated α-Synuclein in mice (Benner *et al.*, 2008). Moreover, α-Synuclein can stimulate TLR4, inducing the nuclear translocation of NF-κB, the release of pro-inflammatory cytokines and the production of RS in microglia and astroglia (Fellner *et al.*, 2013).

2.2.4 Allergens

Allergic reactions are characterized by a hypersensitivity towards a non-pathogenic protein or epitope, leading to a strong adaptive immune response (Scheurer *et al.*, 2015). Here we tested the major allergen in baker´s asthma, amylase trypsin inhibitors from wheat (ATI) (Walusiak *et al.*, 2004; Tatham and Shewry, 2008). ATI can are associated to gluten containing grains and can be adsorbed through gluten containing food. In the intestine ATI can trigger TLR4 stimulation and thereby intra and extra-intestinal inflammatory reactions (Junker *et al.*, 2012; Zevallos *et al.*, 2018; Bellinghausen *et al.*, 2018). In a previous study, we found an increased immune reaction towards nitrated ATI, exhibited by enhanced T-cell proliferation, cytokine secretion and TLR4 stimulation (Ziegler *et al.*, 2019).

Moreover, we used the pollen allergen of Common timothy grass (*Phleum pretense*) Phl p 5, which induces high IgE reactions in grass pollen allergic patients (Bastl *et al.*, 2016).

In addition we tested, major birch pollen allergen (Bet v 1a) and its isoform d (Bet v 1d). The major allergen Bet v 1a is known to provoke immunoglobulin E (IgE) reactions in birch allergic patients (Bastl *et al.*, 2016; Scholl *et al.*, 2005) whereas Isoform d induces low IgE but high T-cell proliferation (Zaborsky *et al.*, 2010).

2.2 Protein Analysis

2.2.1 Concentration determination

To determine the protein concentrations before and after nitration, a *Take3 trio micro-volume plate* (Biotek, Bad Friedrichshall, Germany) was used, measuring the absorption at 260 nm / 280 nm in a Synergy Neo plate reader (Biotek). The amount of proteins given by the suppliers were used as starting point for concentration calculation. Dilution series of the native proteins served as reference for the determination of their nitrated counterparts.

2.2.2 Protein- and oligomer quantification

To validate that equal amounts of each native its modified counterpart was applied and to quantify the oligomerization degree, the proteins were visualized by silver stain (Thermo Fisher Scientific, Darmstadt, Germany). Therefore, 50 ng of each protein was prepared in 2x Laemmli buffer, containing 65.8 mM Tris-HCl (pH 6.8, Carl Roth, Karlsruhe, Germany), 26.3% glycerol (w/v, Carl Roth), 2.1% SDS (Carl Roth), 0.02% bromphenol blue (Sigma Aldrich) and

5.0% 2-mercaptoethanol (Sigma, #M3148-100ml). The samples were applied on protein gels (4-20% mini-protean TGX, Bio-Rad, Munich, Germany) together with a molecular weight marker (broad range, New-England Biolabs, Frankfurt, Germany) and stained with using a silver stain kit (Thermo Fisher Scientific) referring to the instruction manual. For image acquisition a ChemiDoc (Bio-Rad) system and for quantification of protein monomers, dimers and oligomers Image Lab software 5.2.1 (Bio-Rad) was used. The values of protein monomers, dimers and oligomers were quantified in two independent experiments. Except Phl p 5 which was analyzed once. As the size of KLH (>391.5 kDa) and ß-Amyloid (<5 kDa) were beyond the detection limits, both were not analyzed.

Table 2: Oligomerization of native and peroxynitrite modified Proteins

Protein	**Monomers [%]**	**Dimers [%]**	**Oligomers [%]**	**Total di- & oligomers [%]**
OVA	83.8 ± 4.3	16.2 ± 4.3	0	16.2 ± 4.3
nOVA	87.6 ± 0.5	12.5 ± 0.6	0.3 ± 0.3	12.7 ± 0,3
α-Synuclein	100	0	0	0
nα-Synuclein	77.5 ± 3.6	19.7 ± 3.0	2.8 ±0.5	22.5 ± 3.5
HMGB1	96.7 ± 3.4	3.4 ± 3.4	0	3.4 ± 3.4
nHMGB1	95.8 ± 4.2	4.2 ± 4.2	0	4.2 ± 3.0
HSP60	100	0	0	0
nHSP60	54.8 ± 3.1	14.6 ± 14.6	30.7 ±11.5	45.25 ±3.1
ATI	100	0	0	0
nATI	94.6 ± 5.5	2.6 ± 2.6	2.9 ± 2.9	5.5 ± 5.5
Phl p 5	100	0	0	0
nPhl p 5	56.4 ± 4.8	25.8 ±1.7	17.7 ±6.4	43.5 ± 4.7
Bet v 1a	100	0	0	0
nBet v 1a	77.5 ± 5.6	18.8 ± 2.5	3.7 ± 3.2	22.5 ± 5.5

2.2.3 Endotoxin quantification

The amount of endotoxin was quantified by Pierce LAL chromogenic endotoxin quantitation kit (Thermo Fisher Scientific). Therefore, the protein samples were tested at several dilutions and compared to an *E. coli* endotoxin standard (011:B4) provided with the kit. The endotoxin level in all protein samples was less than 1 EU per µg of protein.

2.3 Protein nitration

2.3.1 Nitration of proteins with peroxynitrite

Protein solutions were prepared in PBS (Thermo Fisher Scientific) containing 50 mM ammonium bicarbonate buffer at pH 7.8 (Carl Roth). For each reaction 300 µL – 500 µL of protein solution (1 mg/mL) was used. After being thawed on ice, sodium peroxynitrite ($ONOO^-$, 160-200 mM, Merck, Darmstadt, Germany) was added to yield a molar ratio of $ONOO^-$ to Tyr of 5/1, except for KLH 9/1. Reaction was performed in brown reaction tubes (Eppendorf, Hamburg, Germany) on ice for 110 minutes. Thereafter, the buffer was replaced with fresh PBS using a 10 kDa centrifugal filter (Amicon®, Merck). Briefly, the sample was pipetted into the filter device, centrifuged at 14,000 x g for two minutes (Eppendorf) and 200 µL PBS were added. This procedure was repeated five times. For sample recovery, the filter was turned upside down, transferred into a clean microcentrifuge tube, and centrifuged at 1,000 x g for two minutes. To remove possible sample residues, the filter was washed with 200 µL fresh PBS and centrifuged upside down at 1,000 x g for two minutes into the concentrated protein sample. Equivalent amounts of PBS were treated under the same peroxynitrite conditions and used as Mock samples.

For ß-Amyloid synthetic peptides 1-42 with Tyr respective nitro-Tyr were used (GenScript, NJ, USA).

2.3.2 HPLC-DAD Analysis

The nitration degree for each protein sample was determined as described previously (Selzle et al. 2013) (Table 2). Briefly, an HPLC−DAD system (Agilent Technologies 1200 series, Waldbronn, Germany) was equipped with a monomerically bound C_{18} column (Vydac 238TP, 250 mm x 2.1 mm i.d., 5 µm, Grace Vydac, Alltech, Mainz, Germany) for chromatographic separation. Gradient elution was performed with 0.1 % (v/v) trifluoroacetic acid in water and acetonitrile. Absorbance was measured at wavelength of 280 nm and 357 nm. Injection volume was 10 µL, and each chromatographic run was repeated twice. For system control and data analysis, ChemStation Software was used (Rev. B.03.01, Agilent).

The nitration degree (ND) was calculated using Equation (1).

$$ND = \frac{A_{NTyr,357}}{A_{NTyr,357} + \frac{f}{k}\left(A_{all,280} - k\, A_{NTyr,357}\right)} \quad (1)$$

with scaling factors f = 2.93 ± 0.06 and k = 1.79 ± 0.06, absorbance signal of NTyr at 357 nm ($A_{NTyr,357}$), and absorbance signal of Tyr and NTyr at 280 nm ($A_{all,280}$).

Table 3: Properties of native and peroxynitrite modified proteins

Protein	Size [kDa]	Length [AA]	Tyrosine residues	Nitration degree [%]
KLH	391.5	3408	141	nd
OVA	42.8	386	10	17.3
β-Amyloid	4.5	42	1	100
α-Synuclein	19.5	140	4	33.2
HMGB1	25.0	215	7	63.5
HSP60	60.0	573	7	82.5
ATI	19.0	124	5	38.4
Phl p 5	30.7	309	14	40.1
Bet v 1a	17.5	160	7	31.8
Bet v 1d	17.5	160	7	21.9

2.4 Cell culture

2.4.1 THP-1 NF-κB reporter cells and specific receptor antagonists

To assess the NF-κB activity of cells treated with different native and modified proteins, THP-1 NF-κB reporter cells (Invivogen, Toulouse, France) were used. Per well 100.000 cells were seeded into an flat-bottom 96-well plate (Greiner, Frickenhausen, Germany) in RPMI medium (Thermo Fisher Scientific) supplemented with 10% heat-inactivated fetal calf serum (FCS, Lot #0973F; Biochrom, Berlin, Germany), 100 µg/mL Zeocin (Invivogen), and 1% Penicillin/Streptomycin (Thermo Fisher Scientific) in a humidified atmosphere of 5% CO_2 at 37 °C. To inhibit TLR4 or RAGE signaling, THP-1 NF-κB reporter cells were pre-incubated with the TLR4 specific antagonist TAK242 (0.36 µg/mL, Merck Millipore, Darmstadt, Germany) or the RAGE antagonist FPS-ZM1 (1 µM, Merck Millipore) for four hours. As a negative control served dimethylsulfoxide (4.4 µg/mL, Thermo Fisher Scientific). Subsequently, cells were incubated for 24 hours with the respective protein sample (see Table 1). Activity of NF-κB was measured by Quantiluc reagent (Invivogen) according to the manufacturer`s instructions. Briefly, each 10 µL of cell culture supernatant were transferred into a white plate (Lumitarc, Greiner, Frickenhausen, Germany), and mixed with 50 µL of Quanitluc reagent (Invivogen). The luminescence was detected in a Synergy Neo plate reader (Biotek). Values were normalized to the mean of the positive control LPS EB UP (25ng/mL, Invivogen), which was set to 100%.

Assessment of viability was performed using the Alamar blue assay (Thermo Fisher Scientific), according to the manufacturer protocol. Excitation was performed at 560 nm and emission was measured at 590 nm in a Synergy Neo plate reader plate reader (Biotek).

2.4.2 HeLa TLR4 dual reporter cells:

Based on the HeLa TLR4 reporter cells (Novusbio, Wiesbaden, Germany) we determined simultaneously TLR4 stimulation and viability by a HeLa TLR4 dual luciferase reporter cell line (Ziegler *et al.*, 2019). Cells were grown in Dulbecco's Modified Eagle's Medium (DMEM, Thermo Fisher Scientific) containing 25 mM D-glucose, 1 mM sodium pyruvate supplemented with 10% heat-inactivated fetal calf serum (Lot #0973F, Biochrom, Berlin, Germany), 1% Penicillin/Streptomycin (Thermo Fisher Scientific) and 140 µg/mL Hygromycin B (Invivogen) in a humidified atmosphere of 5% CO_2 at 37 °C.

In a flat bottom 96-well plate (Greiner) 10.000 HeLa TLR4 dual reporter cells per well were seeded. On the next day, the cells were incubated with the respective protein samples (see Table 1) for seven hours. Thereafter, cells were washed with PBS (Thermo Fisher Scientific) and lysed using passive lysis buffer (Promega, Mannheim, Germany) over night at -80°C. The

read out was performed using a dual luciferase kit (Promega) according to the manufacturer manual. Both luminescence signals were measured in a Synergy Neo plate reader (Biotek). The relative luciferase activity was calculated by dividing the Renilla luciferase (TLR4) signal by the Firefly luciferase (viability) signal. The resulting values were normalized to the value of LPS-treated cells, which was set to 100%.

2.4.3 mRNA extraction and qPCR analysis

Quantification of mRNA expression was performed using real time quantitative PCR (qPCR). Therefore, human THP-1 monocyte cells (ATCC, #TIB-202, Manassas, Virginia) were grown in RPMI medium 1640 (Thermo Fisher Scientific, #A1049101) supplemented with 10% heat inactivated fetal bovine serum (Lot #0973F, Biochrom), 0.05 mM 2-mercaptoethanol (Sigma, #M3148-100ml) and 1x penicillin-streptomycin (Thermo Fisher Scientific, #15140122). For qPCR analysis, 400.000 cells/well were seeded into a 6-well cell culture plate (Greiner, #657160). On the next day cells were stimulated for one hour and four hours with the different native or nitrated proteins (see Table 1). As positive control cells were exposed to LPS (25 ng/mL, InvivoGen, #tlrl-eblps). Mock nitrated PBS served as negative control. Cells were harvested by centrifugation for 5 minutes at 500 x g for qPCR analysis and supernatant was analyzed by multiplex ELISA.

Total RNA was extracted from cells using RNeasy mini kit (Qiagen, #74104) following the spin technology protocol. Total RNA yield was determined using a *Take3 trio micro-volume plate* in *Synergy Neo plate reader* (Biotek). Using the high capacity cDNA reverse transcription kit (Thermo Fisher Scientific, # 4374966) 500 ng of total RNA per sample were transcribed into cDNA. Afterwards qPCR was performed using 5 µL of cDNA mixed with SsoAdvanced Universal SYBR Green Supermix (Bio-Rad, #1725274) to a final concentration of 5 µM for each primer (see Table 4). As reference genes served TBP and PPIA. Reactions were performed at 98°C for 30 seconds followed by 37 cycles of 98°C for 10 seconds and 60°C for 25 seconds.

Table 4: Sequence of Real Time-PCR primers

Gene	Accession number	Sequence 5´→ 3´
CCL5	NM_001278736.1	fw ACCCAGCAGTCGTCCACAGG rev CTTGCCCTTGTTCAGCCGGGA
IFN-γ	NM_000619.3	fw ATGGCTGAACTGTCGCCAGCA rev AGGCAGGACAACCATTACTGGGAT
IL-1 β	NM_000576.2	fw GCCCTAAACAGATGAAGTGCTC rev GAACCAGCATCTTCCTCAG
IL-6	NM_000600.5	fw ACCCCTGACCCAACCACAAAT rev AGCTGCGCAGAATGAGATGAGTT
IL-8	NM_000584.3	fw AGTCCTTGTTCCACTGTGCCTTGG rev TGCTTCCACATGTCCTCACAACATC
IL-10	NM_001565.4	fw CTGTACGCTGTACCTGCATCAGCA rev ACACGTGGACAAAATTGGCTTGC
PPIA	NM_021130.4	fw TCTGCACTGCCAAGACTGAG rev TGGTCTTGCCATTCCTGGAC
TBP	NM_001172085.1	fw TGAGCCAGAGTTATTTCCTGGT rev AATTTCTGCTCTGACTTTAGCACC
TGF-β	NM_000660.6	fw CGGCATCAAGGCACAGGGGA rev TCCCTGCATCTCAGAGTGTTGCT
TNF-α	NM_000594.4	fw GCCCAGGCAGTCAGATCATCTT rev CCTCAGCTTGAGGGTTTGCTACA

2.4.4 Cytokine secretion

To assess the amount of pro-inflammatory cytokines, THP-1 monocytes were treated for 1 hour or 4 hours with the respective protein, as described in the qPCR section. The supernatant of the cells was analyzed for IL-6, IL-8 and IL-1 beta by a multiplex assay kit (R&D systems, Biotechne, Wiesbaden, Germany), prepared according to the manufacturer's manual and analyzed on a MAGPIX device (Luminex, Austin, Texas, USA).

2.5 Statistic

For statistical analysis GraphPad Prism version 6.07 (GraphPad, San Diego, California) was used. Unpaired t-tests were performed to observe differences between the native and nitrated protein. The results were considered as significant when *$p<0.05$, **$p<0.01$, ***$p<0.005$, ****$p<0.001$. All protein samples were tested in duplicates or triplicates, the number of independent experiments is indicated in the text below each figure.

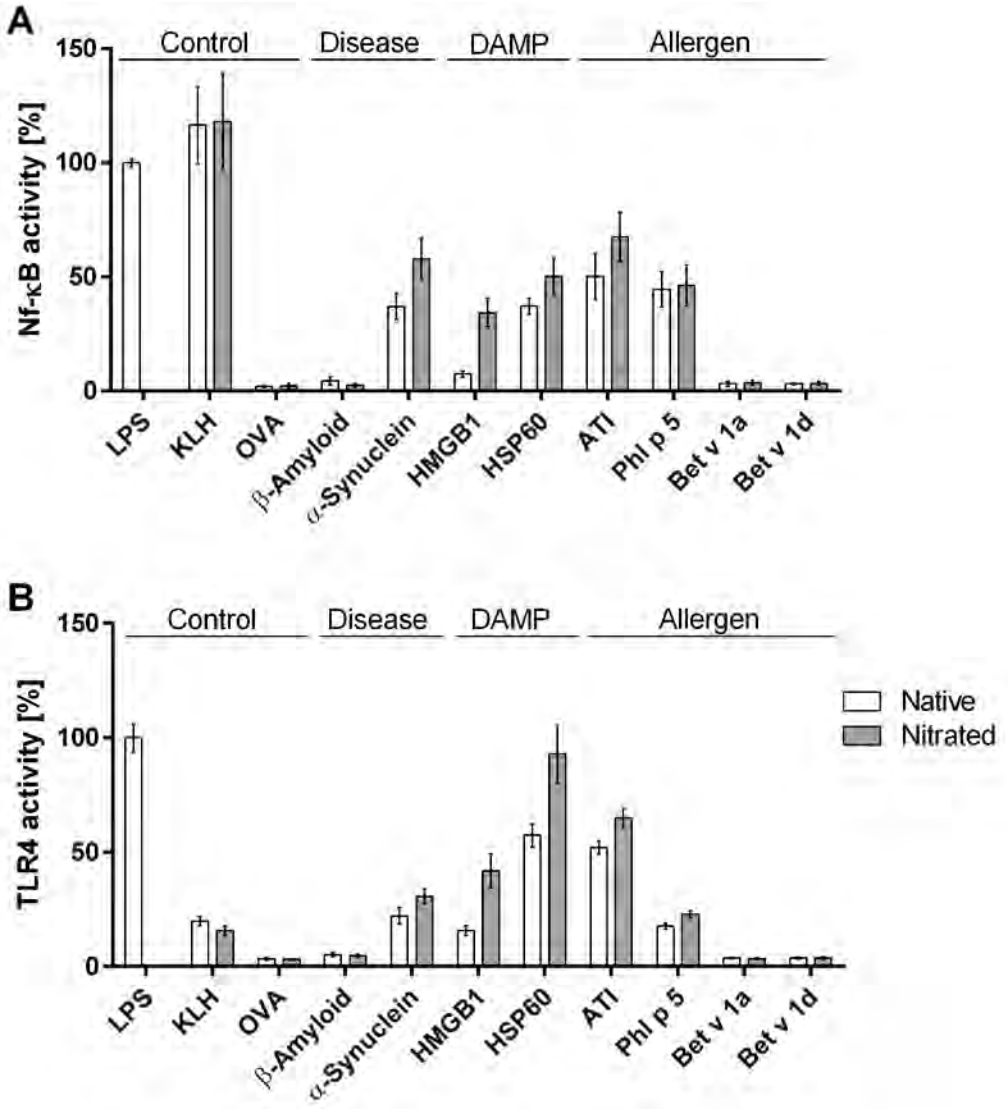

Figure 1: TLR4 and NF-κB related inflammatory reactions after peroxynitrite treatment. (A) NF-κB signaling of THP-1 NF-κB reporter cells after challenge with native and modified proteins; 25 ng/mL LPS EB UP served as reference; n ≥ 2. LPS and KLH served as positive control and OVA as negative control for NF-κB activation, whereas peroxynitrite treatment had no major effect. Under the condition of our experiments, neither native nor modified β-Amyloid peptide 1-42 induced activation of NF-κB. Strong differences in signaling are observed for the modified α-Synuclein, the modified DAMPs HMGB1 and HSP60 and the modified allergens ATI and Phl p 5. No differences were observed for the allergens Bet v 1a and Bet v 1d as well as their modified counterparts. (B) TLR4 response of HeLa TLR4 dual reporter cells after stimulation with native and modified proteins; 25 ng/mL LPS EB served as reference; n = 3. α-Synuclein, HMGB1, HSP60, ATI and Phl p 5 exhibit clearly stronger stimulation after modification with peroxynitrite than their native counterparts. Modified KLH shows slightly reduced TLR4 stimulation. The proteins OVA, β-Amyloid, Betv 1a and Betv 1d, did not alter in TLR4 stimulation potential after peroxynitrite treatment.

Protein groups		Controls	Disease	DAMP	Allergens	
		OVA	α-Synuclein	HMG-1	ATI	Phl p 5
Stimulation	NF-kB	ns	****	****	****	ns
	TLR4	ns	****	****	***	***
mRNA expression	TNF alpha	ns	***	***	*	**
	IL-1 beta	ns	**	**	*	*
	IL-6	ns	ns	*	ns	***
	IL-8	ns	*	***	ns	***
	IFN-gamma	ns	**	*	ns	*
	CCL-5	ns	**	**	ns	ns
	TGF beta	ns	ns	ns	ns	ns
Cytokine release	IL-6	ns	*	ns	ns	ns
	IL-8	ns	ns	**	ns	ns
	IL-1 beta	ns	**	*	*	ns

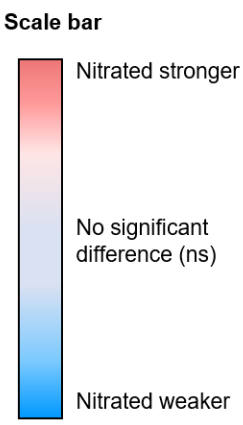

Figure 2: Modified proteins, which induced stronger TLR4 stimulation, also induce enhanced mRNA expression of inflammation relevant genes and cytokine secretion. The red color indicates a significant stronger response of cells to the modified protein, the grey color indicates no significant difference between native and modified protein and the blue color indicates a significant weaker response to the peroxynitrite modified protein. Native and modified proteins were compared by an unpaired t-test $p > 0.05$ *, $p > 0.01$ **, $p > 0.005$ ***, $p > 0.001$ ****; NF-κB $n \geq 2$; TLR4 $n = 3$, mRNA and cytokine release $n = 1$.

3. Results

3.1 Several pro-inflammatory proteins induce a stronger stimulation of NF-κB and TLR4 after peroxynitrite modification

All proteins were tested for their pro-inflammatory potential inducing TLR4 stimulation and activation NF-κB. Only if significant differences between native and medium control or modified protein and mock control were observed, the respective proteins where tested further (Suppl. Figure 1). No toxic effects were observed in the concentrations applied (see Table 1) for THP-1 monocytes (Suppl. Figure 2).

In the disease specific protein group, the Parkinson's disease relevant modified α-Synuclein induced a significant stronger TLR4 stimulation and NF-κB activation compared to native α-Synuclein. The Alzheimer's disease relevant ß-Amyloid was already described to be NF-κB and TLR4 active. But this activity depends strongly of entangling (Ryan *et al.*, 2013). Anyhow, in our experiments neither the native nor the synthetically nitrated ß-Amyloid peptide 1-42 induced significant TLR4 stimulation or NF-κB activation. Here we used synthetic nitro-Tyr comprising ß-Amyloid, with a nitration degree of 100%.

In the group of DAMPs HMGB1 and HSP60 induced a stronger NF-κB and TLR4 activity after modification compared to induction by their native form. Remarkable is the by factor four stronger (Suppl. Figure 3C + 3D & Suppl. Figure 4C + 4D).

In the allergen group, we could show that the native grass pollen allergen Phl p 5 is a strong TLR4 agonist. Further, modified Phl p 5 and ATI induced a stronger TLR4 stimulation then their native counterparts. For NF-κB activation, we found significant higher effects for modified ATI but only slightly enhancement for modified Phl p 5 (Figure 1 A+B). For modified Bet v 1a and Bet v 1d no differences in NF-κB or TLR4 stimulation were observed. Both native and modified Bet v 1 isoforms induced only a minor TLR4 stimulation and NF-κB activation.

3.2 Proteins, which induced after modification a stronger TLR4 activation, induce additionally enhanced mRNA expression and cytokine secretion of pro-inflammatory genes

The proteins, which were more pro-inflammatory in their modified form where further analyzed for mRNA expression and cytokine secretion of pro-inflammatory genes (Figure 2). Secretion of TNF-α and IL-1 β were enhanced for all of the tested modified proteins, compared to the native form. For modified HMGB1 moreover IL-8, IFN-γ and CCL-5 mRNA expression and IL-8 and IL-1 β secretion was significantly enhanced. For α-Synuclein IL-8, CCL-5 mRNA expression and IL-6 and IL-1 β secretion was significantly higher after modification. For the modified variant of the major grass pollen allergen Phl p 5 mRNA expression of IL-6 and IL-8

was enhanced. For modified ATI enhanced IL-1β secretion was found. The control, modified and native OVA, induced no significant differences in mRNA expression or cytokine secretion, all values were at background level. The positive, TLR4 agonistic control, native and modified KLH, stimulated TLR4 and activated NF-κB similarly strong.

Of note, the TLR4 specific inhibitor TAK242 substantially mitigate the NF-κB response to the modified and native forms of HMGB1, α-Synuclein, Phl p 5 and partially to ATI (Suppl. Figures 3 & 5). Inhibition of the RAGE receptor by FPS-ZM1 did only induce slightly reduction of NF-κB signaling for HMGB1 (Supp. Figures 3C & 5). Due to low availability of HSP60 no inhibitory testing, qPCR or ELISA were performed.

3.3 Modification by peroxynitrite induces nitrotyrosine and protein oligomers

After modification by peroxynitrite the proteins were analyzed for oligomerization degree by silver stain (Table 2 & Suppl. Figure 6) and for presence of nitrotyrosine (Table 3) by HPLC and for. All proteins analyzed were found to have a nitration degree between 8% to 70%, whereas the strongest nitration was observed for HSP60 and the weakest for HMGB1. In a close correlation to the nitration degree, the oligomerization was found to be the highest for HSP60 (45%) and the weakest for HMGB1 (4%). Anyhow, all peroxynitrite treated proteins were found to have an increased number of oligomers compared to their native counterparts. As KLH has a size of 391 kDa and beta-Amyloid of 4.5 kDa, both proteins were not detectable by this method.

4. Discussion

4.1 Summary

In the present study, we found that several TLR4 agonistic proteins exhibit enhanced TLR4 stimulation and NF-κB activation after peroxynitrite treatment. We conclude that these modification conditions can cause amplification of inflammatory reactions by generating nitrated and oligomerized proteins, which induce enhanced inflammation. Future experiments must clarify, whether this effect regards to nitrotyrosine formation, protein oligomerization, or both. The observed amplification effects seem to be related to TLR4, since the TLR4 specific antagonist almost completely abolished amplification, whereas the RAGE antagonist had no effect. The presence of nitrotyrosine in a protein per se seems unlikely to be TLR4 agonistic, since the modified OVA and the synthetic nitrotyrosine comprising β-Amyloid showed no TLR4 stimulation.

Alpha-Synuclein misfolding, aggregation and chronic inflammation are hallmarks of Parkinson's disease (PD) (Villar-Pique *et al.*, 2016), therefore, the significant enhanced pro-inflammatory effects induced by modified α-Synuclein may be another relevant factor in the progression of this disease. α-Synuclein is described as TLR4 agonist in Alpha-synucleinopathies (Fellner *et al.*, 2013) and oligomeric alpha-synuclein is sensed by TLR4, what is regarded as important for the development of PD (Hughes *et al.*, 2019). Oxidative and nitrating conditions of α-Synuclein modification are discussed as central mechanism of PD (Schildknecht *et al.*, 2013; Hodara *et al.*, 2004). Dimerization of Peroxynitrite treated α-Synuclein proteins seem to occur preferential via Tyrosine 125 (Takahashi *et al.*, 2002). Indeed a recent study listed the possible implications of nitrated α-Synuclein in Parkinsons Disease (He *et al.*, 2018). New here is a direct and enhanced positive feedback of peroxynitrite modified α-Synuclein via TLR4.

Moreover, Parkinson's disease affected patients show elevated levels in pro-inflammatory molecules such as TNF-alpha, iNOS and IL-1 beta (Herrero *et al.*, 2015). Thereby elevated iNOS levels may implicate enhanced production of nitric oxide, consequently enhanced presence of peroxynitrite and therefore protein nitration and oligomerization. However, for the pathology of PD also other factors such as the DAMP HMGB1 is of major relevance, since patients with PD were found to have an increased expression of TLR4 and HMGB1 (Yang *et al.*, 2018). Moreover, the DAMP HSP60 is discussed to play a role in Parkinson's disease, since it showed toxic effects to dopaminergic cells and was upregulated in a mouse model of PD (Noelker *et al.*, 2014). Moreover, a second study suggested that extracellular HSP60 released by damaged cells may activate microglia in models of PD (Feng *et al.*, 2013). Here we find at least a three-fold or higher induction of modified HMGB1 and HSP60 in NF-κB

activation and TLR4 stimulation, which implicates an additional serious stressor in Parkinson's disease. This drastic amplification may be also relevant for inflammation in many other acute and chronic diseases.

Previous studies showed that nitration of the major birch pollen allergen Bet v 1a leads to enhanced allergenicity and immune reactions (Karle *et al.*, 2012; Franze *et al.*, 2005; Ackaert *et al.*, 2014; Gruijthuijsen *et al.*, 2006). As no adjuvant was added, or samples of birch allergic patients were challenged, we observed for both modified Bet v 1a and Bet v 1d no NF-kB activation or TLR4 stimulation. Notably, we found that the grass pollen allergen Phl p 5 is a TLR4 agonist, which acts in a stronger manner after peroxynitrite treatment. It can be hypothesized that the pro-inflammatory function of Phl p 5 acts as an "on board adjuvant", which can be enhanced by nitrating conditions, modulating its allergenicity. Recently we could show an enhanced immune reacitivity for nitrated ATI (Ziegler *et al.*, 2019), which was manifested by enhanced T-cell proliferation, pro-inflammatory cytokine secretion and TLR4 stimulation. Additionally we could demonstrate by this study, that modified ATI activates NF-κB stronger. Altogether, we demonstrated for three different allergens stronger pathological properties after contact with nitrating conditions. Since nitration of proteins can occur also under summer smog conditions, nitration may generally contribute to the rising prevalence of allergies worldwide.

It is known, that the introduction of a nitro group on a tyrosine can affect the chemical and physiological properties of the protein. One consequence is a lowered pKa value (Hodara *et al.*, 2004; Turko and Murad, 2002), which may strengthen or lower binding abilities to certain receptors, thereby modulating downstream cascades. Moreover, conformational changes of the modified protein may create new epitopes or shield immunological relevant epitopes (Rouvinen *et al.*, 2010; Ackaert *et al.*, 2014; Gruijthuijsen *et al.*, 2006; Scholl *et al.*, 2005). Therefore, the nitrated or oligomerized protein may possess an increased stability and immune reactivity (Untersmayr *et al.*, 2010; Karle *et al.*, 2012; Ackaert *et al.*, 2014). Oligomerization of the major birch pollen allergen Bet v 1a resulted in slower degradation and enhanced surface representation in antigen presenting cells (Ackaert *et al.*, 2014; Karle *et al.*, 2012). Oligomers are discussed to cross link Fcε receptors and thereby mast cell degranulation, a major factor in type 1 hypersensitivities (Scholl *et al.*, 2005; Rouvinen *et al.*, 2010; Ackaert *et al.*, 2014; Gruijthuijsen *et al.*, 2006).

The vicious cycle of inflammation of TLR receptors, DAMPs, cytokines and reactive oxygen species (ROS) was previously introduced as the "TLR Radical Cycle" (Lucas and Maes, 2013). In the former study we mainly discussed secreted DAMPs such as HMGB1 and HSPs, and the mechanism of oxidation (ox), which induces the formation of oxDAMPs. With our new

findings that also peroxynitrite modified proteins can fuel this recursive inflammatory process, the model of the “TLR Radical Cycle” can be extended by a substantial contribution of protein modification by nitration and oligomerization. Moreover, during inflammation RS can be formed which induces further protein modifications (Reinmuth-Selzle *et al.*, 2017; Bernstein *et al.*, 2004). Therefore, the term “*TLR-Reactive Species Cycle”* might be more adequate, since peroxynitrite is not a radical*.* Additionally the positive feedback of the cytokines IL-1β and TNFα and their respective receptors are now taken into consideration in our model (Suppl. Figure 7).

Our findings on amplification of inflammation of five TLR4 stimulating proteins after modification by peroxynitrite may be only the peak of an iceberg. Future studies are necessary to find out, whether this phenomenon applies for more proteins and further receptors. Anyhow, therapeutically intervention to reduce protein nitration may help to reduce the burden of Parkinson’s disease and possibly in many other diseases such as sepsis, Alzheimer’s disease, stroke and many others, where high nitration conditions occur.

Inflammation induced oxidation is a well-known mechanism, frequently referred as ROS-induced ROS (Zorov *et al.*, 2014). Of note, reactive nitrogen species and resulting protein nitration are mainly considered as a consequence of inflammation but not as a cause. Here we suggest a nitration induced nitration mechanism by which the reactive species peroxynitrite, induces the formation of modified proteins amplifying inflammation, extending the current view on the pathomechanism of inflammation.

Since inflammation is part of many diseases and frequently associated with protein nitration, it might be worthwhile to examine, whether nitration scavenger and or the mitigation of RS production can improve the burden of disease. Peroxynitrite is the main causing agent for endogenous protein nitration. Peroxynitrite scavenger have been shown to reduce inflammation in several diseases (Pacher *et al.*, 2007) and specifically TLR4 mediated signaling (Das *et al.*, 2015). Therefore, a deeper understanding of the underlying molecular mechanism may pave the way for the development of new treatments.

5. Supplement:

Protein Groups		Control		DAMPs		Disease		Allergen			
		OVA	KLH	HMG-1	HSP60	α-Synuclein	β-Amyloid	Phl p 5	Bet v 1a	Bet v 1d	ATI
NF-kB activity	Native vs Medium	ns	****	****	****	****	*	****	*	***	****
	Nitrated vs Mock	ns	****	****	****	****	ns	****	**	**	****
TLR4 stimulation	Native vs Medium	ns	****	****	****	****	ns	****	ns	*	****
	Nitrated vs Mock	ns	****	****	****	****	ns	****	*	**	****

Supplement Figure 1: Initial test of pro-inflammatory potential of tested proteins. Native and nitrated proteins were tested for NF-κB activity and TLR4 stimulation to assess their pro-inflammatory potential. Native proteins were tested against medium control and nitrated proteins vs mock control by an unpaired t-test $p > 0.05$ *, $p > 0.01$ **, $p > 0.005$ ***, $p > 0.001$ ****.

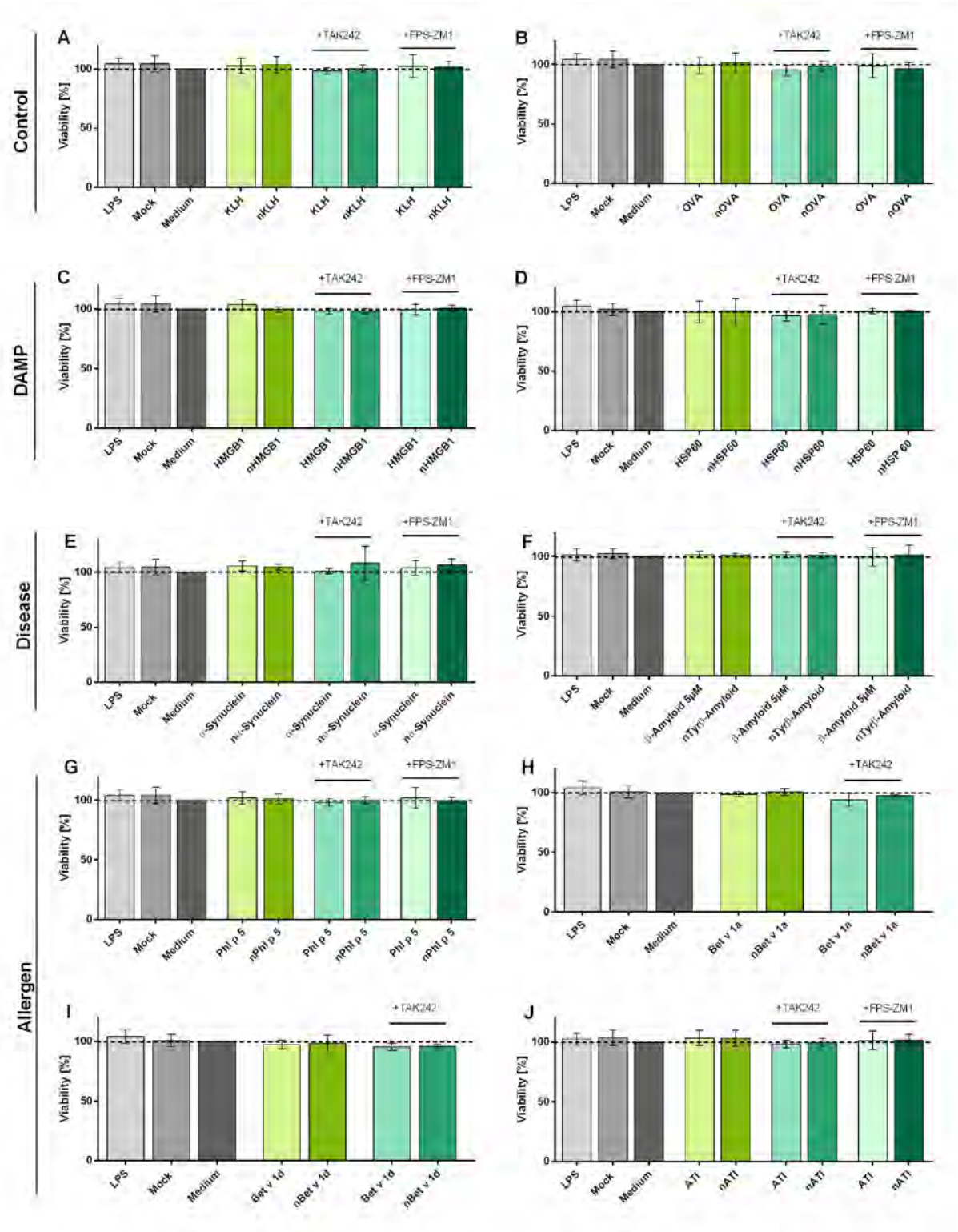

Supplement Figure 2: Viability of THP-1 NF-kB reporter cells treated with native and nitrated proteins with and without TLR4 or RAGE inhibitor. The cell viability was measured using the Alamar blue assay according to the manufacturer's instructions.

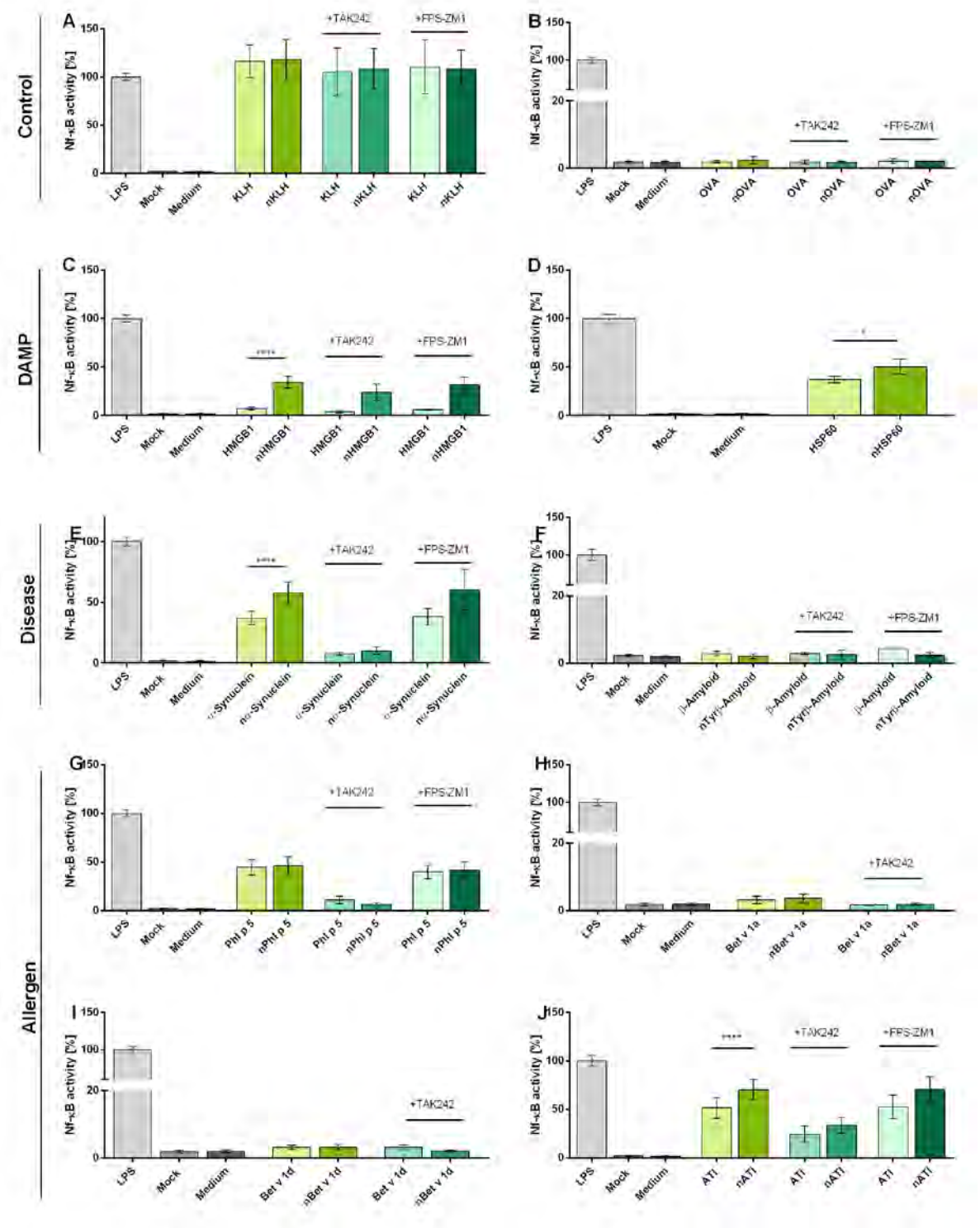

Supplement Figure 3: NF-κB activation by native and modified proteins and TLR4 or RAGE blocking. To determine if NF-κB activation was mainly TLR4 or RAGE dependent, cells were pre-incubated for two hours with the TLR4 antagonist (TAK242) or RAGE antagonist (FPS-ZM1). Shown are the means ± SD from two independent experiments. Unpaired T-tests were performed, comparing NF-κB induction by native to nitrated proteins p > 0.05 *,p > 0.01 **, p > 0.005 ***, p > 0.001 ****.

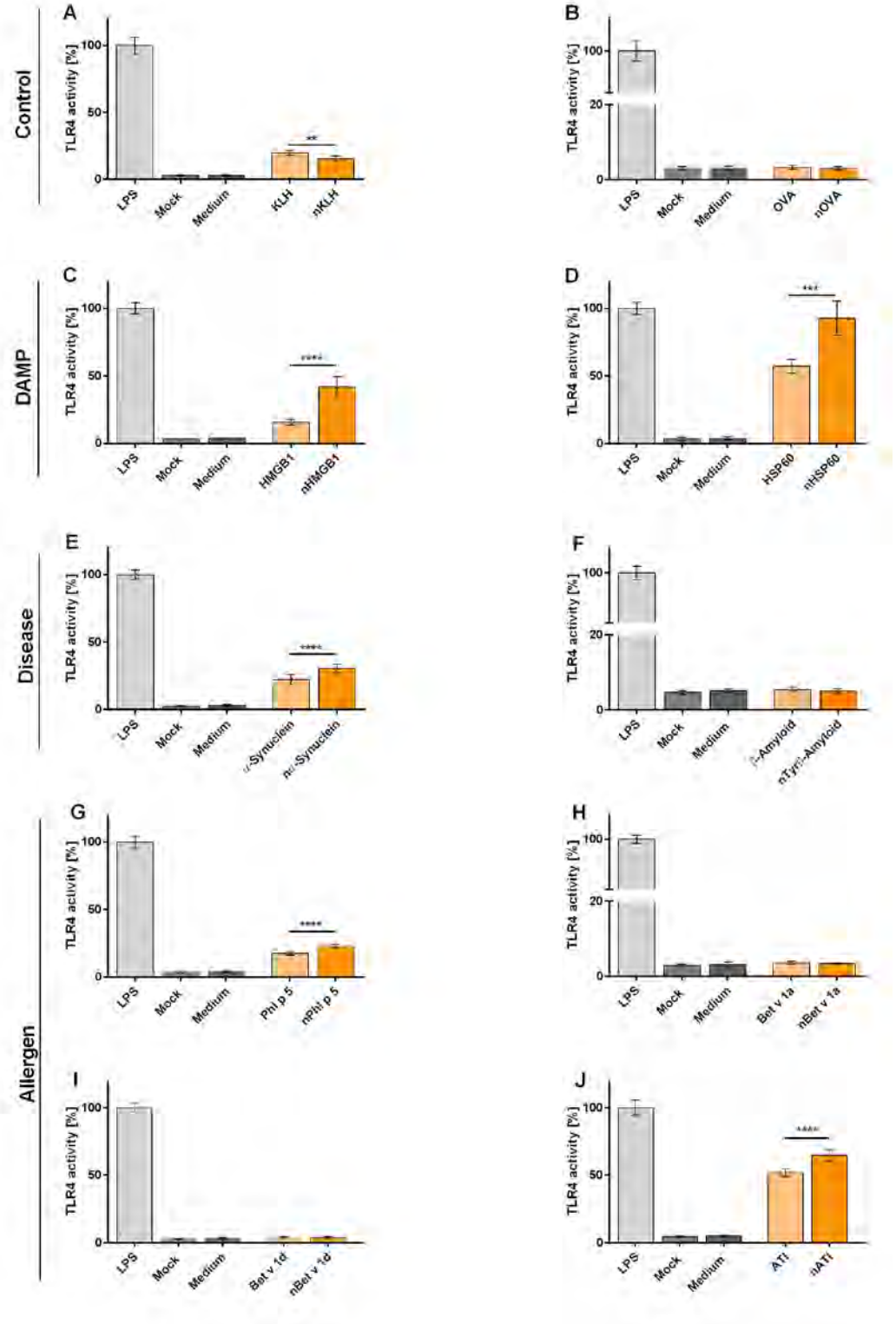

Supplement Figure 4: TLR4 stimulation by native and modified proteins. HeLa TLR4 dual reporter cells were incubated for 7 h with the respective proteins. TLR4 stimulation was measured by Renilla luciferase expression. Shown are the means ± SD from three independent experiments. Unpaired T-tests were performed, comparing TLR4 induction by native to nitrated proteins p > 0.05 *, p > 0.01 **, p > 0.005 ***, p > 0.001 ****.

Protein Groups		Control		DAMPs		Disease		Allergen			
		OVA	KLH	HMG-1	HSP60	α-Synuclein	β-Amyloid	Phl p 5	Bet v 1a	Bet v 1d	ATI
TLR4 dependent	Native vs Native + TAK242	ns	ns	***	****	****		****	*	ns	****
	Nitrated vs Nitrated + TAK242	ns	ns	*	***	****		****	*	ns	****
RAGE dependent	Native vs Native + FPS-ZM1	ns	ns	*		ns		ns			ns
	Nitrated vs Nitrated + FPS-ZM1	ns	ns	ns		ns		ns			ns

Supplement Figure 5: TLR4 and RAGE dependent NF-κB activation by native and nitrated proteins. To determine whether NF-κB activation was mainly TLR4 or RAGE dependent, THP-1 NF-κB reporter cells were pre-incubated with the TLR4 antagonist (TAK242) or RAGE antagonist (FPS-ZM1) for two hours, followed by 24 h stimulation with the respective proteins. Unpaired T-tests were performed, comparing NF-κB induction of cells treated with native proteins to cells pre-treated with TAK242 or FPS-ZM1 and the respective native protein $p > 0.05$ *, $p > 0.01$ **, $p > 0.005$ ***, $p > 0.001$ ****.

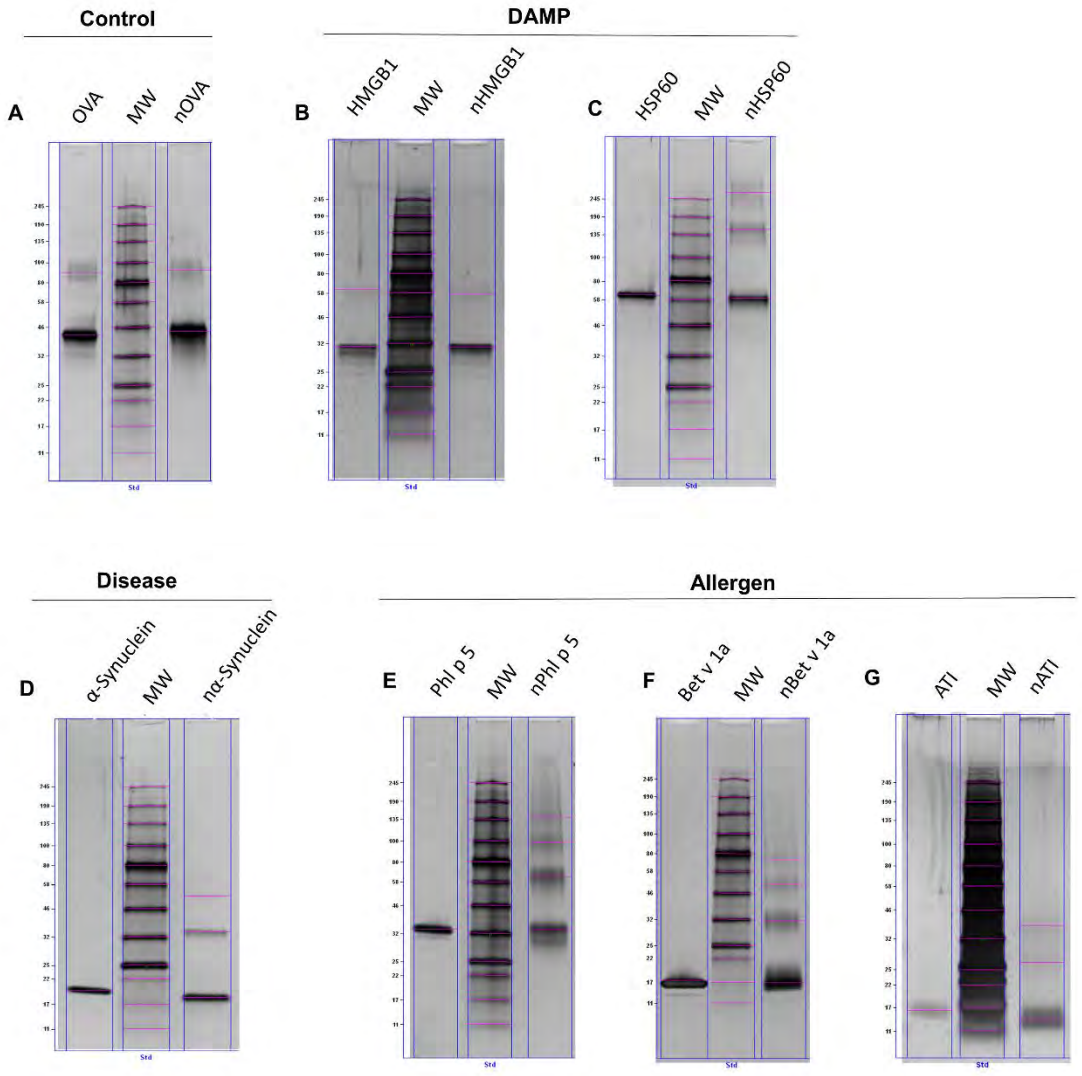

Supplement Figure 6: Quantification of oligomerized proteins by SDS PAGE and silver stain. To analyze the oligomerized fractions, 50 ng of each protein and its modified counterpart were loaded on a 4-20% mini-protean TGX gel (Biorad) and stained using silver stain (Thermo fisher Scientific) for quantification ImageLab software (Biorad) was used.

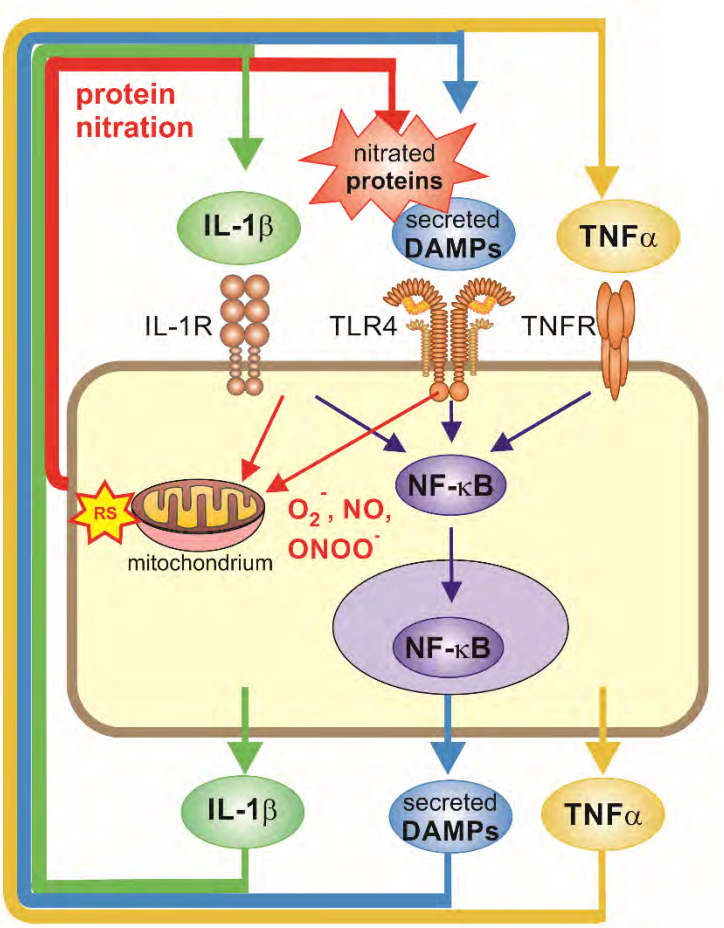

Supplement Figure 7: Schematic cycle of inflammatory-processes inducing protein nitration and oligomerization and enhanced inflammation. Nitrated DAMPs or proteins may stimulate enhanced TLR4 and thereby NF-κB translocation. Additionally, TLR4 stimulation triggers ROS and NO formation and in order protein nitration. Enhanced NF-κB translocation is followed by enhanced transcription and secretion of IL-1 β and TNF-α, which trigger again IL-1- and TNF-receptor.

6. Literature

Ackaert, C., Kofler, S., Horejs-Hoeck, J., Zulehner, N., Asam, C., von Grafenstein, S., Fuchs, J. E., Briza, P., Liedl, K. R., Bohle, B., Ferreira, F., Brandstetter, H., Oostingh, G. J., and Duschl, A.: The impact of nitration on the structure and immunogenicity of the major birch pollen allergen Bet v 1.0101, PloS one, 9, e104520, 10.1371/journal.pone.0104520, 2014.

Balducci, C., Frasca, A., Zotti, M., La Vitola, P., Mhillaj, E., Grigoli, E., Iacobellis, M., Grandi, F., Messa, M., Colombo, L., Molteni, M., Trabace, L., Rossetti, C., Salmona, M., and Forloni, G.: Toll-like receptor 4-dependent glial cell activation mediates the impairment in memory establishment induced by beta-amyloid oligomers in an acute mouse model of Alzheimer's disease, Brain, behavior, and immunity, 60, 188-197, 10.1016/j.bbi.2016.10.012, 2017.

Bastl, K., Kmenta, M., Pessi, A. M., Prank, M., Saarto, A., Sofiev, M., Bergmann, K. C., Buters, J. T. M., Thibaudon, M., Jager, S., and Berger, U.: First comparison of symptom data with allergen content (Bet v 1 and Phl p 5 measurements) and pollen data from four European regions during 2009-2011, The Science of the total environment, 548-549, 229-235, 10.1016/j.scitotenv.2016.01.014, 2016.

Bellinghausen, I., Weigmann, B., Zevallos, V., Maxeiner, J., Reissig, S., Waisman, A., Schuppan, D., and Saloga, J.: Wheat amylase-trypsin inhibitors exacerbate intestinal and airway allergic immune responses in humanized mice, The Journal of allergy and clinical immunology, 10.1016/j.jaci.2018.02.041, 2018.

Benner, E. J., Banerjee, R., Reynolds, A. D., Sherman, S., Pisarev, V. M., Tsiperson, V., Nemachek, C., Ciborowski, P., Przedborski, S., Mosley, R. L., and Gendelman, H. E.: Nitrated alpha-synuclein immunity accelerates degeneration of nigral dopaminergic neurons, PloS one, 3, e1376, 10.1371/journal.pone.0001376, 2008.

Bernstein, J. A., Alexis, N., Barnes, C., Bernstein, I. L., Bernstein, J. A., Nel, A., Peden, D., Diaz-Sanchez, D., Tarlo, S. M., and Williams, P. B.: Health effects of air pollution, The Journal of allergy and clinical immunology, 114, 1116-1123, 10.1016/j.jaci.2004.08.030, 2004.

Chandramouleeswaran, P. M., Shen, D., Lee, A. J., Benitez, A., Dods, K., Gambanga, F., Wilkins, B. J., Merves, J., Noah, Y., Toltzis, S., Yearley, J. H., Spergel, J. M., Nakagawa, H., Malefyt, R., Muir, A. B., and Wang, M. L.: Preferential Secretion of Thymic Stromal Lymphopoietin (TSLP) by Terminally Differentiated Esophageal Epithelial Cells: Relevance to Eosinophilic Esophagitis (EoE), PloS one, 11, e0150968, 10.1371/journal.pone.0150968, 2016.

Chandrashekaran, V., Seth, R. K., Dattaroy, D., Alhasson, F., Ziolenka, J., Carson, J., Berger, F. G., Kalyanaraman, B., Diehl, A. M., and Chatterjee, S.: HMGB1-RAGE pathway drives peroxynitrite signaling-induced IBD-like inflammation in murine nonalcoholic fatty liver disease, Redox biology, 13, 8-19, 10.1016/j.redox.2017.05.005, 2017.

Cohen-Sfady, M., Nussbaum, G., Pevsner-Fischer, M., Mor, F., Carmi, P., Zanin-Zhorov, A., Lider, O., and Cohen, I. R.: Heat shock protein 60 activates B cells via the TLR4-MyD88 pathway, Journal of immunology (Baltimore, Md. : 1950), 175, 3594-3602, 2005.

Das, S., Alhasson, F., Dattaroy, D., Pourhoseini, S., Seth, R. K., Nagarkatti, M., Nagarkatti, P. S., Michelotti, G. A., Diehl, A. M., Kalyanaraman, B., and Chatterjee, S.: NADPH Oxidase-Derived Peroxynitrite Drives Inflammation in Mice and Human Nonalcoholic Steatohepatitis via TLR4-Lipid Raft Recruitment, The American journal of pathology, 185, 1944-1957, 10.1016/j.ajpath.2015.03.024, 2015.

Fellner, L., Irschick, R., Schanda, K., Reindl, M., Klimaschewski, L., Poewe, W., Wenning, G. K., and Stefanova, N.: Toll-like receptor 4 is required for alpha-synuclein dependent activation of microglia and astroglia, Glia, 61, 349-360, 10.1002/glia.22437, 2013.

Feng, M., Zhang, L., Liu, Z., Zhou, P., and Lu, X.: The expression and release of Hsp60 in 6-OHDA induced in vivo and in vitro models of Parkinson's disease, Neurochemical research, 38, 2180-2189, 10.1007/s11064-013-1127-8, 2013.

Franze, T., Weller, M. G., Niessner, R., and Poschl, U.: Protein nitration by polluted air, Environmental science & technology, 39, 1673-1678, 2005.

Glenner, G. G., and Wong, C. W.: Alzheimer's disease: initial report of the purification and characterization of a novel cerebrovascular amyloid protein. 1984, Biochemical and biophysical research communications, 425, 534-539, 10.1016/j.bbrc.2012.08.020, 2012.

Gruijthuijsen, Y. K., Grieshuber, I., Stocklinger, A., Tischler, U., Fehrenbach, T., Weller, M. G., Vogel, L., Vieths, S., Poschl, U., and Duschl, A.: Nitration enhances the allergenic potential of proteins, Int Arch Allergy Immunol, 141, 265-275, 10.1159/000095296, 2006.

He, Y., Yu, Z., and Chen, S.: Alpha-Synuclein Nitration and Its Implications in Parkinson's Disease, ACS chemical neuroscience, 10.1021/acschemneuro.8b00288, 2018.

Herrero, M. T., Estrada, C., Maatouk, L., and Vyas, S.: Inflammation in Parkinson's disease: role of glucocorticoids, Frontiers in neuroanatomy, 9, 32, 10.3389/fnana.2015.00032, 2015.

Hodara, R., Norris, E. H., Giasson, B. I., Mishizen-Eberz, A. J., Lynch, D. R., Lee, V. M., and Ischiropoulos, H.: Functional consequences of alpha-synuclein tyrosine nitration: diminished binding to lipid vesicles and increased fibril formation, J Biol Chem, 279, 47746-47753, 10.1074/jbc.M408906200, 2004.

Hughes, C. D., Choi, M. L., Ryten, M., Hopkins, L., Drews, A., Botia, J. A., Iljina, M., Rodrigues, M., Gagliano, S. A., Gandhi, S., Bryant, C., and Klenerman, D.: Picomolar concentrations of oligomeric alpha-synuclein sensitizes TLR4 to play an initiating role in Parkinson's disease pathogenesis, Acta neuropathologica, 137, 103-120, 10.1007/s00401-018-1907-y, 2019.

Junker, Y., Zeissig, S., Kim, S. J., Barisani, D., Wieser, H., Leffler, D. A., Zevallos, V., Libermann, T. A., Dillon, S., Freitag, T. L., Kelly, C. P., and Schuppan, D.: Wheat amylase trypsin inhibitors drive intestinal inflammation via activation of toll-like receptor 4, J. Exp. Med, 209, 2395-2408, 2012.

Kampf, C. J., Liu, F., Reinmuth-Selzle, K., Berkemeier, T., Meusel, H., Shiraiwa, M., and Poschl, U.: Protein Cross-Linking and Oligomerization through Dityrosine Formation upon Exposure to Ozone, Environmental science & technology, 49, 10859-10866, 10.1021/acs.est.5b02902, 2015.

Kanwar, R., and Balasubramanian, D.: Structural studies on some dityrosine-cross-linked globular proteins: stability is weakened, but activity is not abolished, Biochemistry, 39, 14976-14983, 2000.

Karle, A. C., Oostingh, G. J., Mutschlechner, S., Ferreira, F., Lackner, P., Bohle, B., Fischer, G. F., Vogt, A. B., and Duschl, A.: Nitration of the pollen allergen bet v 1.0101 enhances the presentation of bet v 1-derived peptides by HLA-DR on human dendritic cells, PloS one, 7, e31483, 10.1371/journal.pone.0031483, 2012.

Kawasaki, T., and Kawai, T.: Toll-like receptor signaling pathways, Frontiers in immunology, 5, 461, 10.3389/fimmu.2014.00461, 2014.

Liu, F., Reinmuth-Selzle, K., Lai, S., Weller, M. G., Poschl, U., and Kampf, C. J.: Simultaneous determination of nitrated and oligomerized proteins by size exclusion high-performance

liquid chromatography coupled to photodiode array detection, J Chromatogr A, 1495, 76-82, 10.1016/j.chroma.2017.03.015, 2017.

Liu, L., Yang, M., Kang, R., Dai, Y., Yu, Y., Gao, F., Wang, H., Sun, X., Li, X., Li, J., Wang, H., Cao, L., and Tang, D.: HMGB1-DNA complex-induced autophagy limits AIM2 inflammasome activation through RAGE, Biochemical and biophysical research communications, 450, 851-856, 10.1016/j.bbrc.2014.06.074, 2014.

Lucas, K., and Maes, M.: Role of the Toll Like receptor (TLR) radical cycle in chronic inflammation: possible treatments targeting the TLR4 pathway, Molecular neurobiology, 48, 190-204, 2013.

Noelker, C., Morel, L., Osterloh, A., Alvarez-Fischer, D., Lescot, T., Breloer, M., Gold, M., Oertel, W. H., Henze, C., Michel, P. P., Dodel, R. C., Lu, L., Hirsch, E. C., Hunot, S., and Hartmann, A.: Heat shock protein 60: an endogenous inducer of dopaminergic cell death in Parkinson disease, Journal of neuroinflammation, 11, 86, 10.1186/1742-2094-11-86, 2014.

Pacher, P., Beckman, J. S., and Liaudet, L.: Nitric oxide and peroxynitrite in health and disease, Physiological reviews, 87, 315-424, 10.1152/physrev.00029.2006, 2007.

Park, H. S., Jung, H. Y., Park, E. Y., Kim, J., Lee, W. J., and Bae, Y. S.: Cutting edge: direct interaction of TLR4 with NAD(P)H oxidase 4 isozyme is essential for lipopolysaccharide-induced production of reactive oxygen species and activation of NF-kappa B, Journal of immunology (Baltimore, Md. : 1950), 173, 3589-3593, 2004.

Radi, R.: Protein tyrosine nitration: biochemical mechanisms and structural basis of functional effects, Acc Chem Res, 46, 550-559, 10.1021/ar300234c, 2013.

Reinmuth-Selzle, K., Ackaert, C., Kampf, C. J., Samonig, M., Shiraiwa, M., Kofler, S., Yang, H., Gadermaier, G., Brandstetter, H., Huber, C. G., Duschl, A., Oostingh, G. J., and Poschl, U.: Nitration of the birch pollen allergen Bet v 1.0101: efficiency and site-selectivity of liquid and gaseous nitrating agents, J Proteome Res, 13, 1570-1577, 10.1021/pr401078h, 2014.

Reinmuth-Selzle, K., Kampf, C. J., Lucas, K., Lang-Yona, N., Frohlich-Nowoisky, J., Shiraiwa, M., Lakey, P. S. J., Lai, S., Liu, F., Kunert, A. T., Ziegler, K., Shen, F., Sgarbanti, R., Weber, B., Bellinghausen, I., Saloga, J., Weller, M. G., Duschl, A., Schuppan, D., and Poschl, U.: Air Pollution and Climate Change Effects on Allergies in the Anthropocene: Abundance, Interaction, and Modification of Allergens and Adjuvants, Environmental science & technology, 51, 4119-4141, 10.1021/acs.est.6b04908, 2017.

Rouvinen, J., Janis, J., Laukkanen, M. L., Jylha, S., Niemi, M., Paivinen, T., Makinen-Kiljunen, S., Haahtela, T., Soderlund, H., and Takkinen, K.: Transient dimers of allergens, PloS one, 5, e9037, 10.1371/journal.pone.0009037, 2010.

Ryan, T. M., Caine, J., Mertens, H. D., Kirby, N., Nigro, J., Breheney, K., Waddington, L. J., Streltsov, V. A., Curtain, C., Masters, C. L., and Roberts, B. R.: Ammonium hydroxide treatment of Abeta produces an aggregate free solution suitable for biophysical and cell culture characterization, PeerJ, 1, e73, 10.7717/peerj.73, 2013.

Scheurer, S., Toda, M., and Vieths, S.: What makes an allergen?, Clinical and experimental allergy : journal of the British Society for Allergy and Clinical Immunology, 45, 1150-1161, 10.1111/cea.12571, 2015.

Schildknecht, S., Gerding, H. R., Karreman, C., Drescher, M., Lashuel, H. A., Outeiro, T. F., Di Monte, D. A., and Leist, M.: Oxidative and nitrative alpha-synuclein modifications and proteostatic stress: implications for disease mechanisms and interventions in synucleinopathies, Journal of neurochemistry, 125, 491-511, 10.1111/jnc.12226, 2013.

Scholl, I., Kalkura, N., Shedziankova, Y., Bergmann, A., Verdino, P., Knittelfelder, R., Kopp, T., Hantusch, B., Betzel, C., Dierks, K., Scheiner, O., Boltz-Nitulescu, G., Keller, W., and Jensen-Jarolim, E.: Dimerization of the major birch pollen allergen Bet v 1 is important for its in vivo IgE-cross-linking potential in mice, Journal of immunology (Baltimore, Md. : 1950), 175, 6645-6650, 2005.

Selzle, K., Ackaert, C., Kampf, C. J., Kunert, A. T., Duschl, A., Oostingh, G. J., and Poschl, U.: Determination of nitration degrees for the birch pollen allergen Bet v 1, Analytical and bioanalytical chemistry, 405, 8945-8949, 10.1007/s00216-013-7324-0, 2013.

Shiraiwa, M., Sosedova, Y., Rouviere, A., Yang, H., Zhang, Y., Abbatt, J. P., Ammann, M., and Poschl, U.: The role of long-lived reactive oxygen intermediates in the reaction of ozone with aerosol particles, Nature chemistry, 3, 291-295, 10.1038/nchem.988, 2011.

Shiraiwa, M., Selzle, K., Yang, H., Sosedova, Y., Ammann, M., and Poschl, U.: Multiphase chemical kinetics of the nitration of aerosolized protein by ozone and nitrogen dioxide, Environmental science & technology, 46, 6672-6680, 10.1021/es300871b, 2012.

Stefano, L., Racchetti, G., Bianco, F., Passini, N., Gupta, R. S., Panina Bordignon, P., and Meldolesi, J.: The surface-exposed chaperone, Hsp60, is an agonist of the microglial TREM2 receptor, Journal of neurochemistry, 110, 284-294, 10.1111/j.1471-4159.2009.06130.x, 2009.

Takahashi, T., Yamashita, H., Nakamura, T., Nagano, Y., and Nakamura, S.: Tyrosine 125 of alpha-synuclein plays a critical role for dimerization following nitrative stress, Brain research, 938, 73-80, 2002.

Tatham, A. S., and Shewry, P. R.: Allergens to wheat and related cereals, Clin. Exp. Allergy, 38, 1712-1726, 2008.

Turko, I. V., and Murad, F.: Protein nitration in cardiovascular diseases, Pharmacol Rev, 54, 619-634, 2002.

Untersmayr, E., Diesner, S. C., Oostingh, G. J., Selzle, K., Pfaller, T., Schultz, C., Zhang, Y., Krishnamurthy, D., Starkl, P., Knittelfelder, R., Forster-Waldl, E., Pollak, A., Scheiner, O., Poschl, U., Jensen-Jarolim, E., and Duschl, A.: Nitration of the egg-allergen ovalbumin enhances protein allergenicity but reduces the risk for oral sensitization in a murine model of food allergy, PloS one, 5, e14210, 10.1371/journal.pone.0014210, 2010.

Villar-Pique, A., Lopes da Fonseca, T., Sant'Anna, R., Szego, E. M., Fonseca-Ornelas, L., Pinho, R., Carija, A., Gerhardt, E., Masaracchia, C., Abad Gonzalez, E., Rossetti, G., Carloni, P., Fernandez, C. O., Foguel, D., Milosevic, I., Zweckstetter, M., Ventura, S., and Outeiro, T. F.: Environmental and genetic factors support the dissociation between alpha-synuclein aggregation and toxicity, Proceedings of the National Academy of Sciences of the United States of America, 113, E6506-e6515, 10.1073/pnas.1606791113, 2016.

Walusiak, J., Wiszniewska, M., Krawczyk-Adamus, P., and Palczynski, C.: Occupational allergy to wheat flour. Nasal response to specific inhalative challenge in asthma and rhinitis vs. isolated rhinitis: a comparative study, Int J Occup Med Environ Health, 17, 433-440, 2004.

Yang, Y., Han, C., Guo, L., and Guan, Q.: High expression of the HMGB1-TLR4 axis and its downstream signaling factors in patients with Parkinson's disease and the relationship of pathological staging, Brain and behavior, 8, e00948, 10.1002/brb3.948, 2018.

Yu, M., Wang, H., Ding, A., Golenbock, D. T., Latz, E., Czura, C. J., Fenton, M. J., Tracey, K. J., and Yang, H.: HMGB1 signals through toll-like receptor (TLR) 4 and TLR2, Shock (Augusta, Ga.), 26, 174-179, 10.1097/01.shk.0000225404.51320.82, 2006.

Zaborsky, N., Brunner, M., Wallner, M., Himly, M., Karl, T., Schwarzenbacher, R., Ferreira, F., and Achatz, G.: Antigen aggregation decides the fate of the allergic immune response, Journal of immunology (Baltimore, Md. : 1950), 184, 725-735, 10.4049/jimmunol.0902080, 2010.

Zanin-Zhorov, A., Cahalon, L., Tal, G., Margalit, R., Lider, O., and Cohen, I. R.: Heat shock protein 60 enhances CD4+CD25+ regulatory T cell function via innate TLR2 signaling, The Journal of clinical investigation, 128, 2651, 10.1172/jci121856, 2018.

Zevallos, V. F., Raker, V. K., Maxeiner, J., Scholtes, P., Steinbrink, K., and Schuppan, D.: Dietary wheat amylase trypsin inhibitors exacerbate murine allergic airway inflammation, Eur J Nutr, 10.1007/s00394-018-1681-6, 2018.

Ziegler, K., Neumann, J., Liu, F., Fröhlich-Nowoisky, J., Cremer, C., Saloga, J., Reinmuth-Selzle, K., Pöschl, U., Schuppan, D., Bellinghausen, I., and Lucas, K.: Nitration of Wheat Amylase Trypsin Inhibitors Increases Their Innate and Adaptive Immunostimulatory Potential in vitro, Frontiers in immunology, 9, 10.3389/fimmu.2018.03174, 2019.

Zorov, D. B., Juhaszova, M., and Sollott, S. J.: Mitochondrial reactive oxygen species (ROS) and ROS-induced ROS release, Physiological reviews, 94, 909-950, 10.1152/physrev.00026.2013, 2014.

B.4 Schink *et al.*, PLoS ONE, 2018

Screening of herbal extracts for TLR2- and TLR4-dependent anti-inflammatory effects

Schink A.[1], Neumann J.[1,2], Leifke A. L.[1], Ziegler K.[1], Fröhlich-Nowoisky J.[1], Cremer C.[2], Thines E.[3], Weber B.[1], Pöschl U.[1], Schuppan D.[5] and Lucas K.[1]

[1]Max Planck Institute for Chemistry, Multiphase Chemistry Department, 55128 Mainz, Germany

[2]Institute of Molecular Biology, 55128 Mainz, Germany

[3]Institut für Biotechnologie und Wirkstoff Forschung gGmbH, Kaiserslautern, Germany

[4]Institute of Molecular Physiology, Johannes Gutenberg University Mainz, 55128 Mainz, Germany

[5]Institute of Translational Immunology, University Medical Center of the Johannes Gutenberg University, 55131 Mainz, Germany

PLoS ONE, DOI: 10.1371/journal.pone.0203907 (2018).

Author contributions.

AS, ET, UP, DS and KL designed the experiments. AS, JN and ALL performed the experiments. AS, JN, ALL and KL
analyzed and interpreted the data. AS, JN BW, UP, DS and KL contributed materials/methods/analysis tools. AS and JN wrote the
manuscript. All authors were involved in the editing and proof reading of the manuscript.

PLOS ONE

RESEARCH ARTICLE

Screening of herbal extracts for TLR2- and TLR4-dependent anti-inflammatory effects

Anne Schink[1], Jan Neumann[1,2], Anna Lena Leifke[1], Kira Ziegler[1], Janine Fröhlich-Nowoisky[1], Christoph Cremer[1,2], Eckhard Thines[3,4], Bettina Weber[1], Ulrich Pöschl[1], Detlef Schuppan[5,6‡], Kurt Lucas[1‡]*

1 Multiphase Chemistry Department, Max Planck Institute for Chemistry, Mainz, Germany, **2** Institute of Molecular Biology, Mainz, Germany, **3** Institut für Biotechnologie und Wirkstoff-Forschung gGmbH, Kaiserslautern, Germany, **4** Institute of Molecular Physiology, Johannes Gutenberg University Mainz, Mainz, Germany, **5** Institute of Translational Immunology, University of Mainz Medical Center, Mainz, Germany, **6** Division of Gastroenterology, Beth Israel Deaconess Medical Center, Harvard Medical School, Boston, MA, United States of America
‡ These authors are joint senior authors on this work.
* k.lucas@mpic.de

Citation: Schink A, Neumann J, Leifke AL, Ziegler K, Fröhlich-Nowoisky J, Cremer C, et al. (2018) Screening of herbal extracts for TLR2- and TLR4-dependent anti-inflammatory effects. PLoS ONE 13 (10): e0203907. https://doi.org/10.1371/journal.pone.0203907

Editor: David M. Ojcius, University of the Pacific, UNITED STATES

Received: July 6, 2018

Accepted: August 29, 2018

Published: October 11, 2018

Data Availability Statement: All relevant data are within the paper and its Supporting Information files.

Funding: AS, JN, KZ received funding from Max Planck Graduate Center with the Johannes Gutenberg University Mainz (MPGC) (http://www.mpgc-mainz.de/). IMB Microscopy and Histology Core Facility received funding from German Research Foundation (DFG) (http://www.dfg.de/en/) for Opera Phenix High Content Spinning Disk Microscope (Project 402386039). The funders had

Abstract

Herbal extracts represent an ample source of natural compounds, with potential to be used in improving human health. There is a growing interest in using natural extracts as possible new treatment strategies for inflammatory diseases. We therefore aimed at identifying herbal extracts that affect inflammatory signaling pathways through toll-like receptors (TLRs), TLR2 and TLR4. Ninety-nine ethanolic extracts were screened in THP-1 monocytes and HeLa-TLR4 transfected reporter cells for their effects on stimulated TLR2 and TLR4 signaling pathways. The 28 identified anti-inflammatory extracts were tested in comparative assays of stimulated HEK-TLR2 and HEK-TLR4 transfected reporter cells to differentiate between direct TLR4 antagonistic effects and interference with downstream signaling cascades. Furthermore, the ten most effective anti-inflammatory extracts were tested on their ability to inhibit nuclear factor-κB (NF-κB) translocation in HeLa-TLR4 transfected reporter cell lines and for their ability to repolarize M1-type macrophages. Ethanolic extracts which showed the highest anti-inflammatory potential, up to a complete inhibition of pro-inflammatory cytokine production were *Castanea sativa* leaves, *Cinchona pubescens* bark, *Cinnamomum verum* bark, *Salix alba* bark, *Rheum palmatum* root, *Alchemilla vulgaris* plant, *Humulus lupulus* cones, *Vaccinium myrtillus* berries, *Curcuma longa* root and *Arctostaphylos uva-ursi* leaves. Moreover, all tested extracts mitigated not only TLR4, but also TLR2 signaling pathways. Seven of them additionally inhibited translocation of NF-κB into the nucleus. Two of the extracts showed impact on repolarization of pro-inflammatory M1-type to anti-inflammatory M2-type macrophages. Several promising anti-inflammatory herbal extracts were identified in this study, including extracts with previously unknown influence on key TLR signaling pathways and macrophage repolarization, serving as a basis for novel lead compound identification.

no role in study design, data collection and analysis, decision to publish, or preparation of the manuscript.

Competing interests: The authors have declared that no competing interests exist.

Introduction

Herbs, algae, fungi and cyanobacteria have been used in traditional medicine for centuries. During the last decades, plant extracts and natural compounds became a focal point of interest again as novel lead compounds for the treatment of inflammatory diseases are needed [1]. Several diseases progression and development are influenced by acute and chronic inflammation, such as: autoimmune diseases, allergies, obesity, diabetes, organ fibrosis and dysfunction. Plant extracts that contain largely orally available compounds which attenuate inflammatory processes may be highly attractive as potential therapies [2±8]. Regardless of the origin, inflammation is often associated with a self-enhancing, cyclic process, involving stimulation of innate immunity, prominently of TLRs, production of reactive oxygen and nitrogen species (ROS/RNS), pro-inflammatory cytokine/chemokine secretion, as well as the release of host-derived damage associated molecular patterns (DAMPs) [9,10]. In healthy individuals the initial immune response to an acute stimulus, e.g. a microbial infection, is mitigated over time by downregulation of TLR stimulation, leading to a diminished cytokine production and interruption of the vicious inflammatory circle. In diseases associated with chronic inflammation, the appropriate regulation of TLRs and their downstream signaling pathways is often absent [1, 11]. Antagonists for TLR signaling play an important role in counter-regulating such overwhelming reactions, especially for TLR4 which is a central danger-sensing innate immune receptor. Different from all other TLRs, stimulation of TLR4, leads to activation of two major pathways: 1) the myeloid differentiation 88-dependent (MyD88) or canonical pathway of NF-κB activation, and 2) the MyD88-independent or Toll/interleukin-1 receptor (TIR)-domain-containing adaptor molecule (TRAM) pathway. The canonical pathway can also be activated via TLR2 stimulation [12,13]. Some synthetic small molecules (e.g. Eritoran and TAK-242), but also natural compounds (e.g. epigallocatechin-3-gallate and 6-shogaol) inhibit TLR4 signaling [14±18]. Nevertheless, to date, no effective orally active TLR4 antagonist is available for experimental or clinical application.

Due to their easy oral application and minor adverse effects, herbal extracts compromising of TLR4 antagonistic activity would be highly interesting as new oral treatment strategies for inflammatory diseases. Nevertheless, identification of the active compounds and their targets are often complex. Furthermore, also metabolization products and not only the applied compounds themselves might interact with the TLR signaling pathways. This further complicates the identification of the responsible mechanism(s). Recently, numerous studies have focused on Chinese herbal medicines and their impact on several diseases [19±22], however, their anti-inflammatory effects remain largely unknown. Thus, in the current study we analyzed ethanolic extracts of medicinal plants, which may have anti-inflammatory properties (see S1 Table in the supplementary data).

Materials and methods

Ethanolic extracts

Most of the ethanolic extracts were purchased directly from Maros Arznei GmbH. All other samples listed in Table 1 were freshly prepared by grinding 10 g plants or algae in a mortar, if necessary under liquid nitrogen. Afterwards, the powder was resuspended in 50 ml of 70% ethanol (VWR International GmbH, Darmstadt, Germany). Subsequently, the samples were incubated for ten days in the dark at room temperature (RT), being inverted once a day. Then, the extracts were filtered through Rotilabo-folded filters (type 113P; Carl Roth, Karlsruhe, Germany) to remove unresolved residues.

Table 1. Sources of ethanolic herbal extracts.

Latin name	Common English name	Used part	Source
Achillea millefolium	Common yarrow	Whole plant	Maros Arznei, Fürth, Germany
Aconitum napellus	Monkshood	Whole plant	Maros Arznei, Fürth, Germany
Aesculus hippocastanum	Horse-chestnut	Fruit/berry/seed	Maros Arznei, Fürth, Germany
Alchemilla vulgaris	Common lady's mantle	Whole plant	Maros Arznei, Fürth, Germany
Allium sativum	Garlic	Root[2]	Farmer's market, Mainz, Germany
Allium ursinum	Wild garlic	Leaf[1]	Tee und Gewürze Lilianna Kamberg und Marianne Schmidt, Offenbach, Germany
Aloe ferox	Aloe	Whole plant	Maros Arznei, Fürth, Germany
Alpinia officinarum	Galangal	Root	Maros Arznei, Fürth, Germany
Althaea officinalis	Common marshmallow	Root	Maros Arznei, Fürth, Germany
Arctostaphylos uva-ursi	Bearberry	Leaf	Maros Arznei, Fürth, Germany
Armoracia rusticana	Horseradish	Root[2]	Farmer's market, Mainz, Germany
Arnica montana	Arnica	Whole plant	Maros Arznei, Fürth, Germany
Arnica montana	Arnica	Flower	Maros Arznei, Fürth, Germany
Artemisia absinthium	Wormwood	Whole plant	Maros Arznei, Fürth, Germany
Avena sativa	Oat	Whole plant	Maros Arznei, Fürth, Germany
Betula alba	Birch	Juice/resin	Maros Arznei, Fürth, Germany
Betula verrucosa	Weeping birch	Juice/resin	Maros Arznei, Fürth, Germany
Boswellia carterii	Frankincense	Whole plant[1]	Olibanum B.V., Kerkrade, Netherlands
Boswellia serrata	Frankincense	Juice/resin	Maros Arznei, Fürth, Germany
Calendula officinalis	Marigold	Flower	Maros Arznei, Fürth, Germany
Camellia sinensis (L.)	Green tea	Leaf[1]	Ostfriesische Tee Gesellschaft, Seevetal, Germany
Capsicum frutescens	Chili	Fruit/berry/seed[1]	Tee und Gewürze Lilianna Kamberg und Marianne Schmidt, Offenbach, Germany
Carum carvi	Caraway	Fruit/berry/seed	Maros Arznei, Fürth, Germany
Castanea sativa	Sweet chestnut	Leaf	Maros Arznei, Fürth, Germany
Chelidonium majus	Celandine	Root	Maros Arznei, Fürth, Germany
Chlorella pyrenoidosa	Chlorella	Whole green algae[1]	Naturya, Southstoke, United Kingdom
Cinchona pubescens	Cinchona	Bark	Maros Arznei, Fürth, Germany
Cinnamomum verum	Cinnamon	Bark	Maros Arznei, Fürth, Germany
Convallaria majalis	Lily of the valley	Whole plant	Maros Arznei, Fürth, Germany
Coriandrum sativum	Coriander	Fruit/berry/seed	Maros Arznei, Fürth, Germany
Crataegus species	Hawthorn	Fruit/berry/seed	Maros Arznei, Fürth, Germany
Curcuma longa	Turmeric	Root	Maros Arznei, Fürth, Germany
Cynara scolymus	Artichoke	Leaf	Maros Arznei, Fürth, Germany
Daucus carota subsp. *sativus*	Carrot	Root[2]	Aldi Süd, Mainz, Germany
Digitalis purpurea	Common foxglove	Leaf	Maros Arznei, Fürth, Germany
Dioscorea villosa	Yam	Root	Maros Arznei, Fürth, Germany
Echinacea purpurea	Purple coneflower	Whole plant	Maros Arznei, Fürth, Germany
Elettaria cardamomum	Cardamom	Fruit/berry/seed[1]	Tee und Gewürze Lilianna Kamberg und Marianne Schmidt, Offenbach, Germany
Equisetum arvense	Field horsetail	Whole plant	Maros Arznei, Fürth, Germany
Erythraea centaurium	Common centaury	Whole plant	Maros Arznei, Fürth, Germany
Euphrasia officinalis	Eyebright	Whole plant	Maros Arznei, Fürth, Germany
Filipendula ulmaria	Meadowsweet	Flower	Maros Arznei, Fürth, Germany
Foeniculum vulgare	Fennel	Fruit/berry/seed	Maros Arznei, Fürth, Germany
Fucus vesiculosus	Bladderwrack	Whole plant	Maros Arznei, Fürth, Germany

(*Continued*)

Table 1. (Continued)

Latin name	Common English name	Used part	Source
Gentiana lutea	Gentian	Root	Maros Arznei, Fürth, Germany
Geranium robertianum	Herb robert	Whole plant	Maros Arznei, Fürth, Germany
Ginkgo biloba	Ginkgo	Leaf	Maros Arznei, Fürth, Germany
Glycyrrhiza glabra	Liquorice	Root	Maros Arznei, Fürth, Germany
Hamamelis virginiana	Witch hazel	Leaf	Maros Arznei, Fürth, Germany
Harpagophytum procumbens	Devil's claw	Root	Maros Arznei, Fürth, Germany
Hedera helix	Common ivy	Leaf	Maros Arznei, Fürth, Germany
Hibiscus sabdariffa	Roselle	Leaf	Maros Arznei, Fürth, Germany
Humulus lupulus	Hops	Flower	Maros Arznei, Fürth, Germany
Hypericum perforatum	St John's wort	Whole plant	Maros Arznei, Fürth, Germany
Ilex paraguariensis	Yerba mate	Leaf	Maros Arznei, Fürth, Germany
Juniperus communis	Common juniper	Fruit/berry/seed	Maros Arznei, Fürth, Germany
Lavandula angustifolia	Lavender	Flower	Maros Arznei, Fürth, Germany
Marrubium vulgare	Common horehound	Whole plant	Maros Arznei, Fürth, Germany
Matricaria chamomilla	Chamomile	Whole plant	Maros Arznei, Fürth, Germany
Melilotus officinalis	Sweet clover	Whole plant	Maros Arznei, Fürth, Germany
Melissa officinalis	Lemon balm	Leaf	Maros Arznei, Fürth, Germany
Mentha piperita	Peppermint	Whole plant	Maros Arznei, Fürth, Germany
Nicotiana tabacum	Tobacco	Leaf[1]	British American Tobacco Nederland B.V., Amstelveen, Netherlands
Origanum majorana	Marjoram	Whole plant	Maros Arznei, Fürth, Germany
Panax ginseng	Ginseng	Root	Maros Arznei, Fürth, Germany
Petroselinum crispum	Parsley	Whole plant	Maros Arznei, Fürth, Germany
Pimpinella anisum	Anise	Fruit/berry/seed	Maros Arznei, Fürth, Germany
Plantago lanceolata	Ribwort	Whole plant	Maros Arznei, Fürth, Germany
Primula officinalis	Common cowslip	Root	Maros Arznei, Fürth, Germany
Primula vulgaris	Common primrose	Root	Maros Arznei, Fürth, Germany
Pulmonaria officinalis	Common lungwort	Flower	Maros Arznei, Fürth, Germany
Quercus robur	English oak	Bark[1]	Holger Senger Naturrohstoffe und Gartenbau, Dransfeld, Germany
Rheum palmatum	Rhubarb	Root	Maros Arznei, Fürth, Germany
Rosmarinus officinalis	Rosemary	Leaf	Maros Arznei, Fürth, Germany
Rubus fruticosus	Blackberry	Leaf	Maros Arznei, Fürth, Germany
Salix alba	White willow	Bark	Maros Arznei, Fürth, Germany
Salvia officinalis	Salvia	Leaf	Maros Arznei, Fürth, Germany
Sambucus nigra (L.)	Elderflowers	Flower[1]	Tee und Gewürze Lilianna Kamberg und Marianne Schmidt, Offenbach, Germany
Schinus terebinthifolius	Brazilian pepper tree	Fruit/berry/seed[1]	Tee und Gewürze Lilianna Kamberg und Marianne Schmidt, Offenbach, Germany
Scrophularia nodosa	Common figwort	Whole plant	Maros Arznei, Fürth, Germany
Spirulina	Spirulina	Whole cyanobacteria[1]	VegaVital UG, Berlin, Germany
Symphytum officinale	Comfrey	Root	Maros Arznei, Fürth, Germany
Syzygium aromaticum	Clove	Flower[1]	FUCHS Gewürze, Dissen, Germany
Tanacetum parthenium	Feverfew	Whole plant	Maros Arznei, Fürth, Germany
Taraxacum officinale	Dandelion	Whole plant	Maros Arznei, Fürth, Germany
Thymus vulgaris	Common thyme	Whole plant	Maros Arznei, Fürth, Germany
Tropaeolum majus	Nasturtium	Whole plant	Maros Arznei, Fürth, Germany
Uncaria tomentosa	Cat's claw	Whole plant[1]	Herbathek Naturheilmittel, Berlin, Germany

(*Continued*)

Table 1. (Continued)

Latin name	Common English name	Used part	Source
Urtica dioica	Stinging nettle	Root	Maros Arznei, Fürth, Germany
Usnea barbata	Barber's itch	Whole plant	Maros Arznei, Fürth, Germany
Vaccinium myrtillus	Bilberry	Fruit/berry/seed	Maros Arznei, Fürth, Germany
Valeriana officinalis (L.)	Common valerian	Root	Maros Arznei, Fürth, Germany
Vanilla planifolia	Vanilla	Fruit/berry/seed	Maros Arznei, Fürth, Germany
Verbena officinalis	Common vervain	Whole plant	Maros Arznei, Fürth, Germany
Vigna radiata	Mung bean (dried)	Fruit/berry/seed[1]	Thai World Import Export, Bangkok, Thailand
Vigna radiata	Mung bean (cooked in boiling water for 20 min)	Fruit/berry/seed[2]	Thai World Import Export, Bangkok, Thailand
Viscum album	European mistletoe	Whole plant	Maros Arznei, Fürth, Germany
Xanthoria parietina	Common orange lichen	Whole lichen[1]	AG Weber, Max Planck Institute for Chemistry, Mainz, Germany
Zingiber officinale	Ginger	Root	Maros Arznei, Fürth, Germany

[1]10 g dry sample used for extract preparation

[2]10 g wet sample used for extract preparation

https://doi.org/10.1371/journal.pone.0203907.t001

Cell cultures and treatments

HeLa-TLR4 cell line. The HeLa-TLR4 transfected reporter cell line (Novusbio, Wiesbaden Nordenstadt, Germany) was cultured in Dulbecco's Modified Eagle Medium (DMEM, Thermo Fisher Scientific, Darmstadt, Germany) supplemented with 10% fetal bovine serum (FBS, Biochrom, Berlin, Germany), 1% penicillin-streptomycin (Thermo Fisher Scientific), 5 μg/ml blasticidine (Sigma-Aldrich, Darmstadt, Germany), 1 μg/ml puromycin (Sigma-Aldrich), and 1 mg/ml geneticin (G418, Sigma-Aldrich) at 37ÊCin humidified atmospheric air supplemented with 5% CO_2. In black 96-well microplates with clear bottom (Greiner Bio-One, Solingen, Germany), 2×10^5 cells/ml were seeded in 100 μl medium and allowed to settle overnight. Experiments were conducted with different concentrations of the extracts or the same amount of vehicle (70% ethanol). Concentrations ranging from 0.01% to 3% in cell culture medium were used to receive a dose-response curve and to cover a broad spectrum of concentrations. Due to toxic effects, higher concentrations than 3% were not used in the performed assay systems. Cells were pre-incubated with extracts or vehicle (70% ethanol) for 2 h at 37ÊC. Afterwards, lipopolysaccharide (LPS-EB, from *E. coli* O111:B4, Invivogen, Toulouse, France) in a final concentration of 25 ng/ml was added to stimulate TLR4 (incubation for 8 h at 37ÊC). Alamar Blue assay was used to determine cell viability and TLR4 stimulation was measured using luciferase assay (Novusbio).

NF-κB translocation experiments were conducted on a monoclonal HeLa-TLR4 cell line (Novusbio) stably transfected with a plasmid expressing constitutive active firefly luciferase, as a reporter for cell viability (HeLa-TLR4 dual reporter cell line). Cells were cultured as described for HeLa-TLR4 reporter cell line, but selective antibiotics were replaced by 140 μg/ml Hygromycin B Gold (Invivogen). HeLa-TLR4 dual reporter cells were seeded on 12-well glass bottom plates (Cellvis, Mountain View, USA) at a concentration of 2.0×10^5 cells/ml in 1 ml complete medium per well and incubated for 48 h at 37ÊC.Cells were pre-incubated with 0.6% extracts in final cell culture medium or with the same amount of vehicle control for 2 h at 37ÊC.After pre-incubation, LPS-EB in a final concentration of 50 ng/ml was added for 1 h at 37ÊC.Next, cells were washed 1x with phosphate buffered saline (PBS) and fixed with 4% formaldehyde in PBS buffer (Thermo Fisher Scientific) for 10 min at 37ÊC.Subsequently, cells were washed 3x with PBS before proceeding with immunostaining for NF-κB.

THP-1 cell line. The myeloid THP-1 cell line TIB-202 (ATCC; LGC Standards, Wesel, Germany) was cultured in Roswell Park Memorial Institute (RPMI) 1640 medium (Thermo Fisher Scientific) supplemented with 10% FBS (heat-inactivated), 1% penicillin/streptomycin and 0.05 mM β-mercaptoethanol (Sigma-Aldrich) at 37ÊCin humidified atmospheric air supplemented with 5% CO_2. In a 96-well microplate (Greiner Bio-One), 4×10^5 cells/ml were seeded in 80 μl complete medium and were allowed to settle for 1 h. Experiments were conducted at the same extract concentration range used for HeLa-TLR4 cells. Cells were incubated with extracts or vehicle for 2 h at 37ÊC.Afterwards, LPS-EB in a final concentration of 50 ng/ml was added to stimulate TLR4 (4 h incubation at 37ÊC).Alamar Blue assay was used to determine cell viability. TLR4 stimulation was measured using enzyme-linked immunosorbent assay (ELISA, BD Biosciences, Heidelberg, Germany).

Polarization experiments were conducted with THP-1 monocytes differentiated to macrophages. In a 96-well microplate (Greiner Bio-One), $1.5x10^5$ cells/ml were seeded in 200 μl complete growth medium containing 10 ng/ml phorbol 12-myristate 13-acetate (PMA, Sigma-Aldrich). Cells were incubated for three days at 37ÊCto differentiate to M0 macrophages. Afterwards, the medium was exchanged to 200 μl complete growth medium without PMA and cells were incubated overnight at 37ÊC.Cells were polarized to M1-type macrophages with 20 ng/ml interferon-gamma (IFNγ, Thermo Fisher Scientific) for 24 h. All further steps were performed as described for THP-1 monocytes.

HEK-TLR2 and HEK-TLR4 cell lines. The HEK-Blue hTLR2 (HEK-TLR2) and HEK--Blue hTLR4 cell lines (HEK-TLR4) (both Invivogen) were cultured in DMEM high glucose medium supplemented with 10% FBS (heat-inactivated), 1% penicillin/streptomycin and 1x HEK-Blue Selection (Invivogen) at 37ÊCin humidified atmospheric air supplemented with 5% CO_2. In experiments examining cell viability, medium without HEK-Blue Selection was used. In experiments analyzing TLR2 and TLR4 stimulation, cells were cultured in HEK-Blue detection medium (Invivogen). Extracts with concentrations between 0.01% and 3% in final cell culture medium or vehicle (70% ethanol) were added in empty 96-well microplates. Directly afterwards, cells were seeded with 2.8×10^5 cells/ml in 100 μl complete growth medium and were incubated with the extracts for 2 h at 37ÊC.Subsequently, receptor activity was stimulated by adding 1 ng/ml S-(2,3-bis(palmitoyloxy)-(2RS)-propyl)-(R)-cysteinyl-(S)-seryl-(S)-lysyl-(S)-lysyl-(S)-lysyl-(S)-lysine (Pam2CSK4, HEK-TLR2 cell line, Invivogen) or 100 ng/ml LPS-EB Ultrapure (HEK-TLR4 cell line, LPS from *E. coli* O111:B4, Invivogen). Cells were incubated overnight at 37ÊC.Alamar Blue assay was used to determine cell viability and TLR2/TLR4 stimulation was measured using HEK-Blue detection assay (Invivogen).

Determination of cell viability

Cell viability was measured by the Alamar Blue assay (Thermo Fisher Scientific) according to the manufacturer's protocol (10% final concentration of Alamar Blue solution in cell culture medium). Cells were incubated with Alamar Blue solution at 37ÊCfor 4 h (HeLa-TLR4 cell line) or overnight (all other cell lines). Fluorescence intensity was measured with microplate reader Synergy Neo (Biotek, Bad Friedrichshall, Germany) at an excitation wavelength of 560 nm and an emission wavelength of 590 nm.

IL-8 transcriptional activity in HeLa-TLR4 cells

LightSwitch Luciferase assay (Novusbio) was used to determine production of renilla luciferase under transcriptional control of interleukin-8 (IL-8) promoter. HeLa-TLR4 cells were washed with PBS (Thermo Fisher Scientific) after performing the cell viability assay to remove the Alamar Blue staining and were frozen overnight at -80ÊCfor better cell lysis. After thawing the

cells, LightSwitch Luciferase assay was performed according to manufacturer's protocol and luminescence was measured with microplate reader Synergy Neo (Biotek).

IL-8, IL-10 and TNF-α secretion

Supernatants of pre-treated THP-1 monocytes and macrophages were examined for concentration of IL-8, IL-10 or tumor necrosis factor alpha (TNF-α) using ELISAs (BD Biosciences). Sandwich ELISA was carried out according to manufacturer's protocol with optimized washing buffer volume. Supernatant was diluted up to 6-fold (total used volume: 100 μl/well). Absorbance was measured using a Synergy Neo plate reader at a wavelength of 450 nm and a reference wavelength of 570 nm. Based on pipetted standard values, a four-parameter logarithmic standard curve was determined with the Gen5 software on SynergyNeo (Biotek). Cytokine production of THP-1 monocytes and macrophages were calculated according to standard curves and dilution factors.

Determination of transcription activity in HEK-Blue cells

HEK-Blue Detection assay (Invivogen) was used to determine production of inducible secreted embryonic alkaline phosphatase (SEAP), based on activation of NF-κB and activator protein 1 (AP-1). HEK-Blue cells were cultured in HEK-Blue Detection medium during incubation with extracts and stimulation of receptor activity. Afterwards, stimulation of TLR2 (HEK-TLR2 cell line) and TLR4 (HEK-TLR4 cell line) were determined using a Synergy Neo plate reader (Biotek) at a wavelength of 640 nm.

Determination of NF-κB p65 translocation by fluorescence microscopy

For immunostaining of NF-κB, HeLa-TLR4 dual reporter cells were incubated in blocking solution consisting of 5% bovine serum albumin (BSA, Cell Signaling Technology, Cambridge, UK) and 0.3% Triton X-100 (Merck, Darmstadt, Germany) in PBS for 1 h at RT. Next, cells were incubated with primary anti-NF-κB p65 antibody (D14E12, Cell Signaling Technology) overnight at 4ÊC. After washing, secondary anti-rabbit Alexa Fluor 568 antibody was applied (Thermo Fisher Scientific) for 1 h at RT. Both antibodies were diluted 1:400 in PBS containing 1% BSA and 0.3% Triton X-100. Cell nuclei were counterstained using 4',6-diamidino-2-phenylindole (DAPI, Thermo Fisher Scientific).

Stained cells were imaged using the Opera Phenix High-Content Screening System (PerkinElmer, Waltham, USA) with laser lines for Alexa Fluor 568 at 568 nm excitation and 570 nmÐ630 nm emission and laser lines for DAPI at 405 nm excitation and 435 nmÐ480 nm emission. Image processing was done using Harmony software (PerkinElmer). Nuclear masks (DAPI stained cell nuclei) and surrounding ring-like masks (cytoplasm) were identified and the mean fluorescence intensity ratio of nuclear to cytoplasmic NF-κB was determined.

Statistical analyses

Statistical analyses were accomplished in GraphPad Prism 5.01 (GraphPad Software, San Diego, California, USA, www.graphpad.com) conducting one-way ANOVA followed by Dunnett's post hoc test. Values of $p<0.05$ were considered as significant. For statistical analyses of data from macrophage polarization, ANOVA was accomplished, followed by an unpaired t-test. Values of $p<0.05$ were considered significant.

Results

Screening of ethanolic herbal extracts for TLR-dependent anti-inflammatory effects

During initial screening, 99 ethanolic extracts (96 herbal extracts, one cyanobacterial, one green algae and one lichen extract) were tested for their anti-inflammatory activity. Ten extracts displayed major anti-inflammatory activity combined with a high cell viability (Fig 1, Fig 2 and Fig 3). The results for the other 89 extracts are graphically displayed in the supplementary data (S1 Fig). Comparing the effects in both cell lines used for efficacy and toxicity readout, HeLa-TLR4 transfected reporter cells were more susceptible to toxic effects of most extracts. THP-1 monocytes showed a viability above 85% after treatment with the ten most effective anti-inflammatory extracts in concentrations up to 1%, except for *Humulus lupulus* and *Arctostaphylos uva-ursi* (Fig 1, Fig 2 and Fig 3). Some extracts such as *Castanea sativa*, *Cinnamomum verum*, *Humulus lupulus* and *Curcuma longa* revealed comparable anti-inflammatory efficacy in both cell lines, whereas other extracts (e.g. *Cinchona pubescens* and *Rheum palmatum*) were more effective in THP-1 monocytes than in HeLa-TLR4 cells. *Castanea sativa* was the only extract with a dose-dependent anti-inflammatory activity already at low concentrations, whereas most of the other extracts possessed an inhibition threshold (e.g. between 0.3% and 0.6% for cinnamon extract). Ethanolic extracts with the highest anti-inflammatory potential were sweet chestnut (*Castanea sativa*), cinchona (*Cinchona pubescens*), cinnamon (*Cinnamomum verum*), white willow (*Salix alba*), rhubarb (*Rheum palmatum*), common lady's mantle (*Alchemilla vulgaris*), hops (*Humulus lupulus*), bilberries (*Vaccinium myrtillus*), turmeric (*Curcuma longa*) and bearberry (*Arctostaphylos uva-ursi*) (Fig 1, Fig 2 and Fig 3). Three bark extracts were within the top five anti-inflammatory extracts (number 2: *Cinchona pubescens*, number 3: *Cinnamomum verum* and number 4: *Salix alba*). Fig 4 shows the 25 most effective anti-inflammatory extracts and S2 Fig displays all 99 extracts with a ranking according to their anti-inflammatory potential. For visualization, heat maps display TLR4 stimulation normalized to viability shown in green for anti-inflammatory and in red for pro-inflammatory effects. THP-1 monocytes naturally express TLR4 and several other innate immune receptors, in contrast to HeLa-TLR4 cells, which were transfected with TLR4. THP-1 monocytes more reflect the physiological mechanisms in the human body, therefore effects on THP-1 monocytes vs. HeLa-TLR4 cells were weighted in a ratio of 2:1 for ranking of the extracts. In addition, TLR4 inhibition was calculated with a higher impact than toxic effects. Extracts resulting in anti-inflammatory activity but with a viability below 75% should be viewed critically, since the anti-inflammatory effects have to be rather attributed to toxicity. In the heat maps these values are displayed in grey.

Screening for exclusive TLR4 antagonistic effects

Besides the identification of anti-inflammatory extracts, we were also interested in specific antagonists for TLR4. Twenty-eight ethanolic extracts with strong anti-inflammatory effects were additionally tested in a comparative assay with Pam2CSK4-stimulated HEK-TLR2 and LPS-EB Ultrapure-stimulated HEK-TLR4 cells to discriminate a direct TLR4 antagonistic effect from interference with downstream signaling pathways shared by TLR2 and TLR4 signaling. All tested extracts exhibited mitigation of TLR2- and TLR4-dependent responses (see Figs 5 and 6 for the five most effective anti-inflammatory extracts and S3 Fig for all other extracts). For most of the extracts, especially the most effective anti-inflammatory extracts, HEK-TLR2 and HEK-TLR4 cell lines showed comparable dose-dependent anti-inflammatory effects. Interestingly, *Castanea sativa* leaves inhibited TLR2- and TLR4-dependent

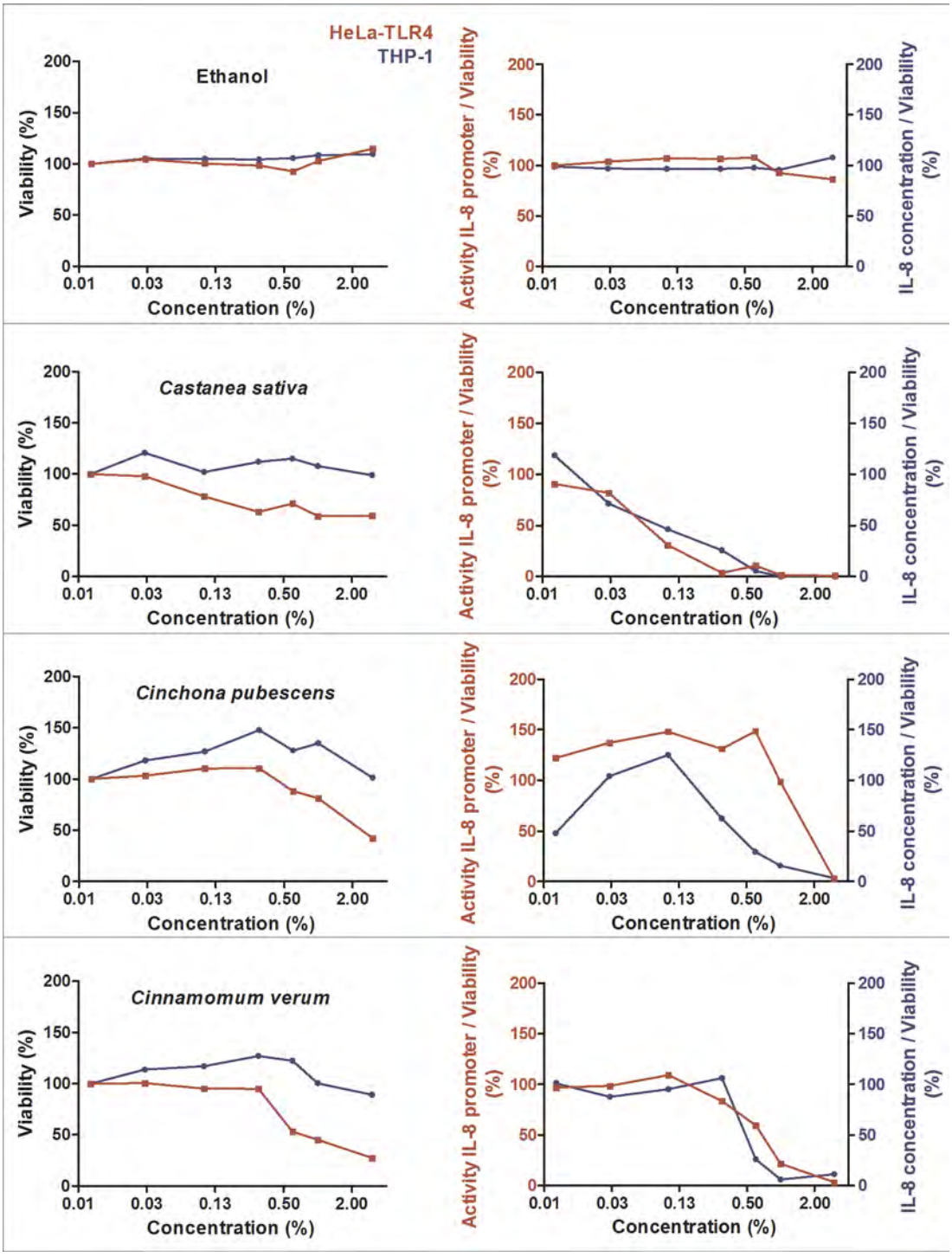

Fig 1. Cell viability and concentration-dependent anti-inflammatory effects of selected herbal extracts (part 1). HeLa-TLR4 cells (red) and THP-1 monocytes (blue) were incubated with extracts in different concentrations or vehicle (70% ethanol), followed by stimulation with LPS-EB. Viability was measured using the Alamar Blue Assay and was normalized to the negative control (untreated cells). TLR4 receptor stimulation was measured using Renilla luciferase expression for the HeLa-TLR4 cell line and IL-8 ELISA (pg/ml) for the THP-1 monocytes and was normalized to ethanol-treated cells. Data are displayed as viability (%) in the left graphs and TLR4 stimulation divided by normalized viability (%) in the right graphs. Data represents means ($n \geq 2$). For graphical display of further extracts, see Fig 2, Fig 3 and supplementary data S1 Fig.

https://doi.org/10.1371/journal.pone.0203907.g001

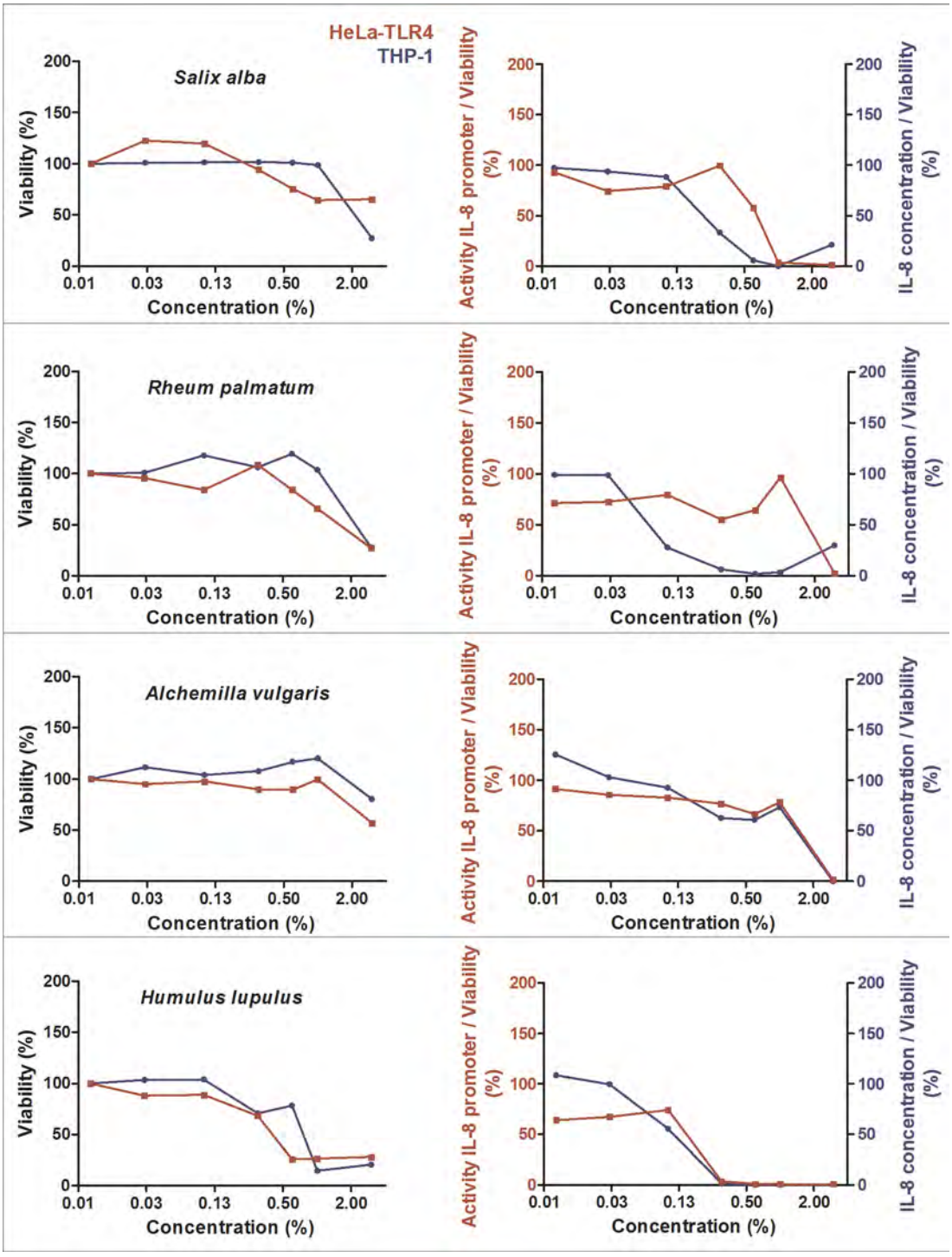

Fig 2. Cell viability and concentration-dependent anti-inflammatory effects of selected herbal extracts (part 2). HeLa-TLR4 cells (red) and THP-1 monocytes (blue) were incubated with extracts in different concentrations or vehicle (70% ethanol), followed by stimulation with LPS-EB. Viability was measured using the Alamar Blue Assay and was normalized to the negative control (untreated cells). TLR4 receptor stimulation was measured using Renilla luciferase expression for the HeLa-TLR4 cell line and IL-8 ELISA (pg/ml) for the THP-1 monocytes and was normalized to ethanol-treated cells. Data are displayed as viability (%) in the left graphs and TLR4 stimulation divided by normalized viability (%) in the right graphs. Data represents means ($n \geq 2$). For graphical display of further extracts, see Fig 1, Fig 3 and supplementary data S1 Fig.

https://doi.org/10.1371/journal.pone.0203907.g002

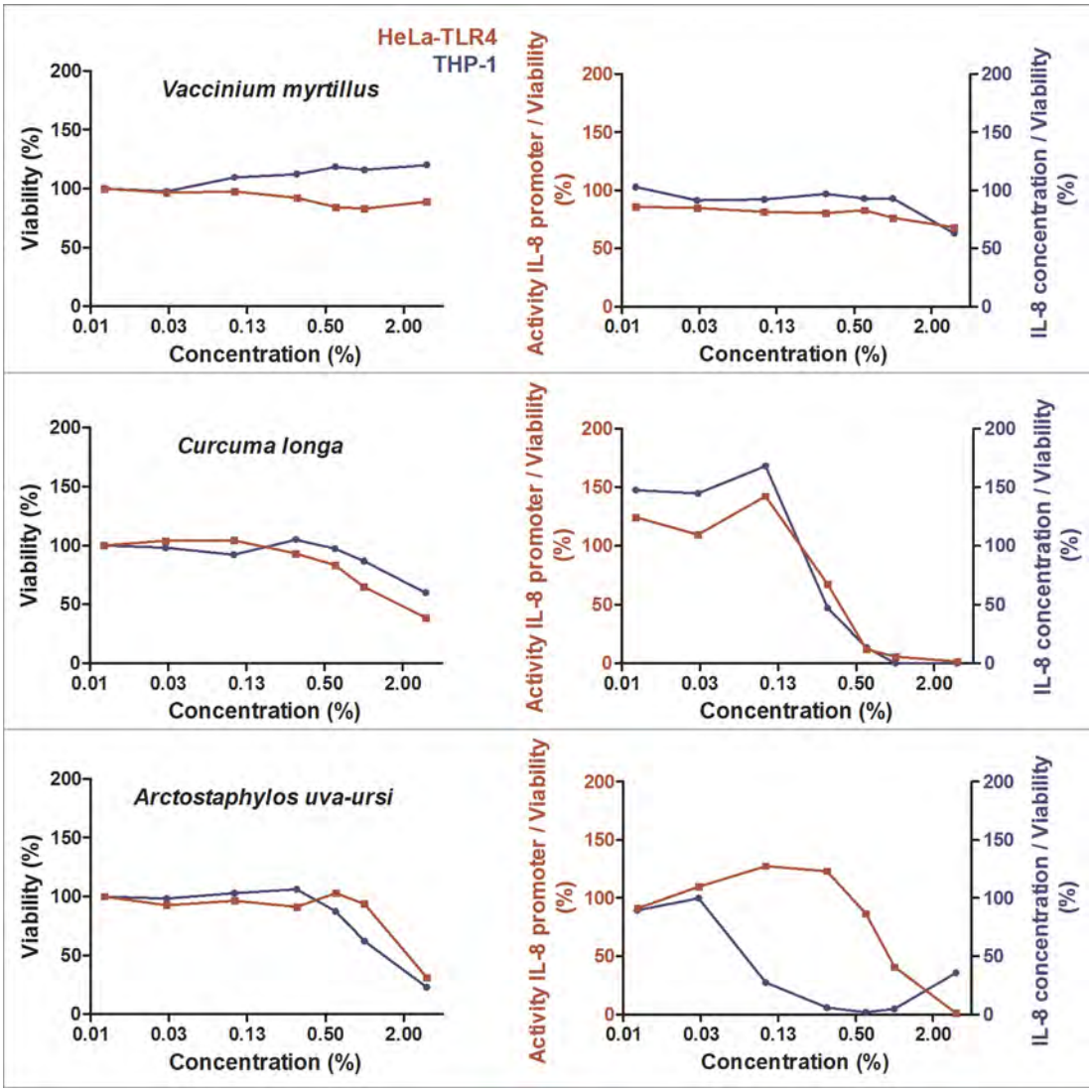

Fig 3. Cell viability and concentration-dependent anti-inflammatory effects of selected herbal extracts (part 3). HeLa-TLR4 cells (red) and THP-1 monocytes (blue) were incubated with extracts in different concentrations or vehicle (70% ethanol), followed by stimulation with LPS-EB. Viability was measured using the Alamar Blue Assay and was normalized to the negative control (untreated cells). TLR4 receptor stimulation was measured using Renilla luciferase expression for the HeLa-TLR4 cell line and IL-8 ELISA (pg/ml) for the THP-1 monocytes and was normalized to ethanol-treated cells. Data are displayed as viability (%) in the left graphs and TLR4 stimulation divided by normalized viability (%) in the right graphs. Data represents means ($n \geq 2$). For graphical display of further extracts, see Fig 1, Fig 2 and supplementary data S1 Fig.

https://doi.org/10.1371/journal.pone.0203907.g003

inflammatory responses already at 0.01% extract dilution, accompanied by a cell viability of 98%. An increase of inflammatory activity was observed for most of the extracts with concentrations between 1% and 3% in cell culture medium. This may be due to toxic effects and should therefore be viewed critically. Heat maps displaying the TLR2- and TLR4 stimulation are shown in Fig 7 (the five most promising extracts) and S4 Fig (all 28 extracts), with anti-inflammatory activity shown in green to pro-inflammatory activity shown in red. The ranking of the extracts was taken from the THP-1 and HeLa-TLR4 screening shown in Fig 4 and S2 Fig. Values with viability below 75% are marked in grey.

Inflammatory scale: anti-inflammatory — pro-inflammatory

Toxicity scale: viability < 75%

Latin name	Common English name	Used part	HeLa-TLR4 reporter cell line							THP-1 monocytes						
			0.01%	0.03%	0.1%	0.3%	0.6%	1%	3%	0.01%	0.03%	0.1%	0.3%	0.6%	1%	3%
Ethanol control			100,00	101,30	103,67	102,01	93,23	85,77	90,26	98,88	97,04	96,54	96,59	97,67	95,66	107,91
Castanea sativa	Sweet chestnut	Leaf	90,53	82,03	30,91	3,53	10,59	1,34	0,79	118,69	71,34	46,42	25,73	5,65	0,00	0,00
Cinchona pubescens	Cinchona	Bark	122,15	137,25	148,02	131,28	148,76	98,71	2,77	47,68	104,26	125,10	62,37	29,49	15,68	3,49
Cinnamomum verum	Cinnamon	Bark	96,77	98,57	109,17	83,50	59,41	21,59	3,24	101,16	87,70	95,31	106,02	26,08	6,08	11,36
Salix alba	White willow	Bark	93,03	74,48	79,05	99,83	58,02	3,79	1,45	97,50	93,93	88,45	33,44	5,95	0,00	21,34
Rheum palmatum	Rhubarb	Root	71,38	72,58	79,60	55,28	64,48	96,37	2,34	99,17	98,60	27,86	6,42	1,94	3,57	29,89
Alchemilla vulgaris	Common lady's mantle	Whole plant	91,35	85,79	82,86	76,83	66,53	78,18	1,63	125,37	102,96	92,63	62,93	60,89	73,46	0,00
Humulus lupulus	Hops	Flower	64,31	67,38	74,08	3,57	1,10	0,92	0,96	108,76	99,78	55,66	1,46	0,00	0,00	0,73
Vaccinium myrtillus	Bilberries	Fruit/berry/ seed	86,00	84,71	81,50	80,48	83,01	76,30	68,10	102,84	91,37	92,22	96,85	92,91	92,95	63,02
Curcuma longa	Turmeric	Root	124,40	109,62	142,43	67,28	11,92	5,54	1,83	127,14	110,90	115,73	45,39	8,99	0,00	15,80
Arctostaphylos uva-ursi	Bearberry	Leaf	91,28	109,88	127,59	123,26	86,52	40,81	1,18	89,45	99,97	27,43	5,97	1,72	4,71	35,80
Allium ursinum	Wild garlic	Leaf	115,74	118,86	97,71	91,94	81,27	78,25	42,93	105,80	109,20	77,64	38,94	24,16	5,90	11,21
Hypericum perforatum	St John's wort	Whole plant	120,77	104,44	85,91	83,69	71,41	53,35	14,06	91,44	85,40	90,32	71,54	51,19	32,03	1,14
Arnicae montana	Arnica	Flower	114,17	96,34	2,78	2,14	2,61	2,55	1,28	144,96	146,96	11,90	0,70	0,69	1,67	0,53
Aloe ferox	Aloe	Whole plant	105,30	105,90	82,53	58,19	27,69	5,15	1,30	123,82	117,87	88,51	38,22	9,71	7,37	0,13
Cynara scolymus	Artichoke	Leaf	109,98	112,42	117,52	100,14	90,16	31,21	1,99	47,40	53,68	127,22	228,92	16,56	6,13	2,86
Salvia officinalis	Salvia	Leaf	94,88	96,95	107,50	89,57	73,14	17,55	2,65	94,87	87,05	79,10	72,53	97,48	42,03	0,00
Ginkgo biloba	Ginkgo	Leaf	107,04	120,25	119,37	90,15	44,17	4,77	2,22	124,31	101,09	22,26	7,98	16,68	9,27	0,00
Tanacetum parthenium	Feverfew	Whole plant	127,34	111,53	120,04	114,28	99,98	68,82	2,22	129,88	139,58	123,43	124,51	72,56	21,24	6,12
Vigna radiata	Mung bean (dried)	Fruit/berry/ seed	83,31	85,02	87,84	85,99	69,53	52,04	25,33	121,14	141,32	120,83	62,61	38,87	23,18	11,00
Betula verrucosa	Weeping birch	Juice/resin	144,10	148,90	136,35	139,46	143,77	154,99	88,24	120,90	131,27	106,29	88,92	93,49	94,35	93,18
Filipendula ulmaria	Meadowsweet	Flower	120,04	113,11	130,06	117,06	106,72	131,55	52,01	132,40	135,84	124,42	75,12	23,05	8,87	1,88
Matricaria chamomilla	Chamomile	Whole plant	100,35	104,50	90,84	78,36	84,92	5,43	1,26	107,39	110,30	81,01	78,37	109,61	0,00	0,00
Spirulina	Spirulina	Whole cyanobacteria	93,17	100,77	107,05	92,24	76,80	50,64	3,57	142,68	138,71	169,61	74,85	20,59	2,70	36,20
Gentiana lutea	Gentian	Root	120,08	105,07	118,69	89,81	89,96	82,85	39,06	80,63	60,91	89,51	140,23	62,51	43,53	2,92
Quercus robur	English oak	Bark	143,68	142,56	127,88	124,88	134,53	106,17	8,76	106,31	116,82	88,62	57,00	35,67	16,07	16,81

Fig 4. Ethanolic extracts with highest anti-inflammatory activity. HeLa-TLR4 cells or THP-1 monocytes were incubated with extracts in different concentrations or vehicle (70% ethanol), followed by stimulation with LPS-EB. Viability was measured using the Alamar Blue Assay and was normalized to the negative control (untreated cells) (*Viability (%)*). TLR4 receptor activity was measured using Renilla luciferase expression for the HeLa-TLR4 cell line or IL-8 ELISA for the THP-1 monocytes and was normalized to ethanol-treated cells (*TLR4-Activity*). Data are displayed as TLR4 stimulation divided by viability and ranked ascending by the following formula: (150Ð *Viability (%)*) * (2 * *TLR4-Activity* + 100) weighted in a ratio of 2:1 for THP-1 monocytes vs. HeLa-TLR4 cells. The 25 extracts with the highest mitigation of LPS-induced inflammatory signal are displayed here (for comparison of all extracts see S2 Fig). Data represents means ($n \geq 2$).

https://doi.org/10.1371/journal.pone.0203907.g004

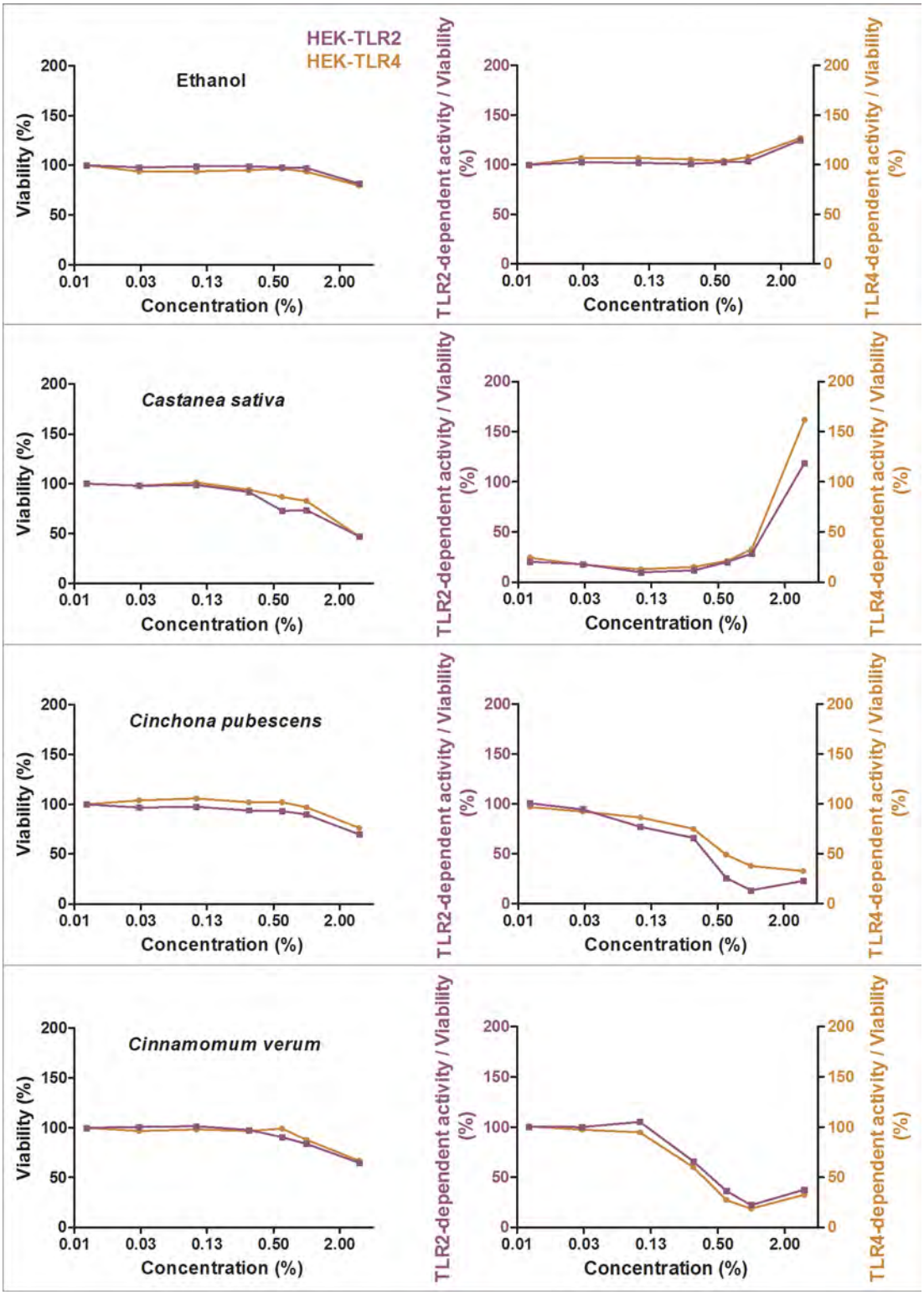

Fig 5. Extracts with TLR2 and TLR4 antagonistic effects (part 1). HEK-TLR2 cells (purple) and HEK-TLR4 cells (orange) were incubated with extracts in different concentrations or vehicle (70% ethanol), followed by stimulation of HEK-TLR2 cells with Pam2CSK4 or HEK-TLR4 cells with LPS-EB Ultrapure. Viability was measured using the Alamar Blue Assay and was normalized to the negative control (untreated cells). TLR2 and TLR4 receptor stimulation were measured using SEAP production and were normalized to ethanol-treated cells. Data are displayed as viability (%) in the left graphs and TLR4 stimulation divided by viability

(%) in the right graphs. Data represents means ($n \geq 4$). For graphical display of further extracts, see Fig 6 and supplementary data S3 Fig.

https://doi.org/10.1371/journal.pone.0203907.g005

Inhibition of NF-κB p65 translocation by select extracts

Several pro-inflammatory signaling pathways cumulate in the nuclear translocation of the transcription factor NF-κB. Therefore, the ten extracts with the highest anti-inflammatory activity, combined with no or low toxicity in THP-1 and HeLa-TLR4 cells (Fig 1, Fig 2 and Fig 3) were tested regarding their influence on NF-κB p65 translocation in LPS-stimulated HeLa-TLR4 dual reporter cells. Here *Castanea sativa*, *Cinnamomum verum*, *Salix alba*, *Rheum palmatum*, *Humulus lupulus*, *Curcuma longa* as well as *Arctostaphylos uva-ursi* significantly inhibited NF-κB translocation, compared to the LPS-stimulated vehicle control (Fig 8). Interestingly, *Cinchona pubescens*, *Alchemilla vulgaris* and *Vaccinium myrtillus*, which demonstrated strong anti-inflammatory activity in the THP-1 and HeLa-TLR4 as well as in the comparative HEK-TLR2/HEK-TLR4 assays, did not prevent the LPS-induced NF-κB translocation into the nucleus, indicating interference with another, alternative pro-inflammatory mechanism.

Repolarization of THP-1 macrophages by select extracts

The same ten extracts were additionally tested for their influence on repolarization of pro-inflammatory M1-type to anti-inflammatory M2-type macrophages. Here, enhanced secretion

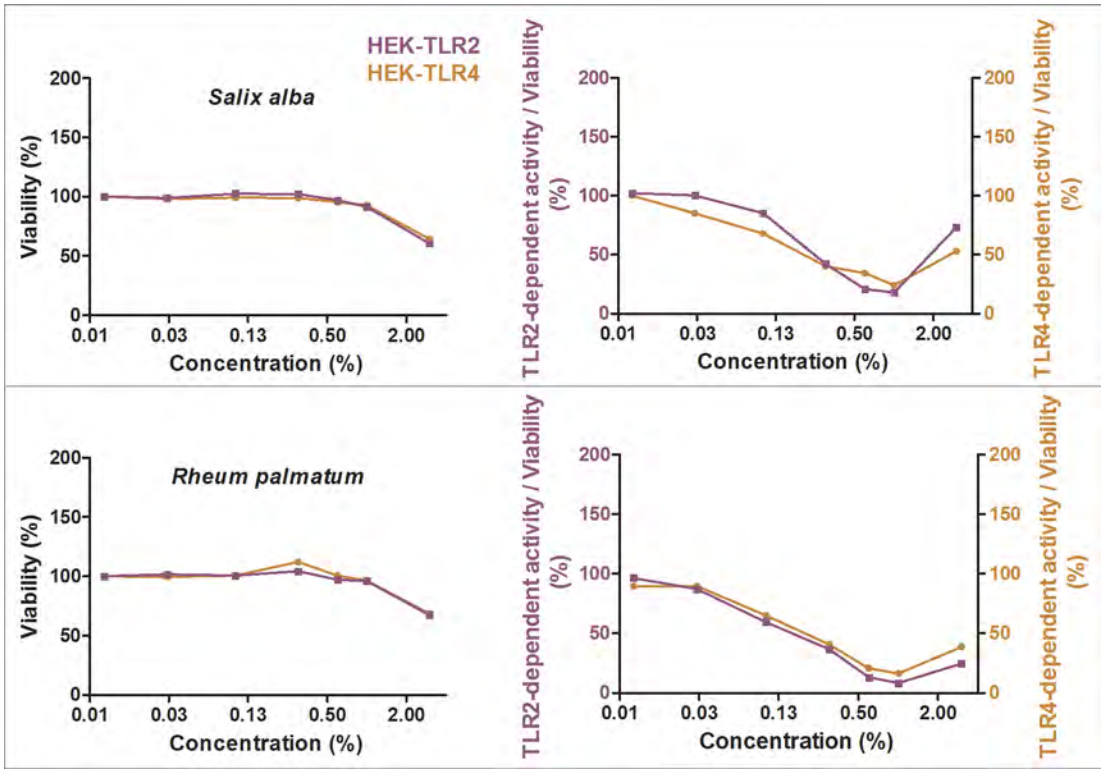

Fig 6. Extracts with TLR2 and TLR4 antagonistic effects (part 2). HEK-TLR2 cells (purple) and HEK-TLR4 cells (orange) were incubated with extracts in different concentrations or vehicle (70% ethanol), followed by stimulation of HEK-TLR2 cells with Pam2CSK4 or HEK-TLR4 cells with LPS-EB Ultrapure. Viability was measured using the Alamar Blue Assay and was normalized to the negative control (untreated cells). TLR2 and TLR4 receptor stimulation were measured using SEAP production and were normalized to ethanol-treated cells. Data are displayed as viability (%) in the left graphs and TLR4 stimulation divided by viability (%) in the right graphs. Data represents means (n≥4). For graphical display of further extracts, see Fig 5 and supplementary data S3 Fig.

https://doi.org/10.1371/journal.pone.0203907.g006

Inflammatory scale

anti-inflammatory — pro-inflammatory

Toxicity scale

viability < 75%

			HEK-TLR2 reporter cell line							HEK-TLR4 reporter cell line						
Latin name	Common English name	Used part	0.01%	0.03%	0.1%	0.3%	0.6%	1%	3%	0.01%	0.03%	0.1%	0.3%	0.6%	1%	3%
Ethanol control			100,00	102,45	101,84	101,03	102,55	103,43	124,76	100,00	106,70	106,82	105,37	103,93	107,97	127,11
Castanea sativa	Sweet chestnut	Leaf	20,06	17,83	9,78	11,82	19,94	28,56	118,82	24,28	17,36	12,78	15,09	20,87	32,77	161,75
Cinchona pubescens	Cinchona	Bark	100,53	94,50	77,03	65,89	25,61	13,17	22,78	96,97	92,46	86,34	75,11	48,95	37,82	32,81
Cinnamomum verum	Cinnamon	Bark	100,40	100,11	105,47	65,88	36,23	22,34	37,65	100,75	97,62	94,69	59,98	27,50	18,82	32,43
Salix alba	White willow	Bark	102,12	100,18	85,03	42,14	20,67	17,65	73,17	100,01	85,03	67,85	40,08	34,16	24,12	52,75
Rheum palmatum	Rhubarb	Root	96,48	87,24	59,40	36,53	13,11	8,17	24,68	89,65	89,52	64,85	40,62	20,74	16,27	38,65

Fig 7. Ethanolic extracts with TLR2 and TLR4 antagonistic activities in HEK-TLR2 and HEK-TLR4 cell lines. HEK-TLR2 or HEK-TLR4 cells were incubated with extracts in different concentrations or vehicle (70% ethanol), followed by stimulation of HEK-TLR2 cells with Pam2CSK4 or HEK-TLR4 cells with LPS-EB Ultrapure. Viability was measured using the Alamar Blue Assay and was normalized to the negative control (untreated cells). TLR2 and TLR4 receptor activity were measured using SEAP production and were normalized to ethanol-treated cells. Data are displayed as receptor stimulation divided by normalized viability. The five extracts with the highest mitigation of LPS-induced inflammatory signal from Fig 4 are displayed here (for comparison of further extracts, see S4 Fig). Data represents means ($n \geq 4$).

https://doi.org/10.1371/journal.pone.0203907.g007

of TNF-α is an indicator for M1-type polarization, whereas IL-10 secretion suggests M2-type polarization. All tested M1-polarized, LPS and extract treated THP-1 macrophages showed a viability above 85%, except for *Humulus lupulus* extract, which resulted in 64% viability compared to the vehicle control (Fig 9A). A significant mitigation of TNF-α secretion was observed after incubation with all extracts, except for *Salix alba* and *Vaccinium myrtillus* (Fig 9B). Furthermore, IL-10 production was significantly induced by several extracts, especially *Rheum palmatum* and *Arctostaphylos uva-ursi* (Fig 9C).

Discussion

Potent anti-inflammatory effects were observed in THP-1 monocytes and HeLa-TLR4 cells after treatment with various ethanolic extracts (Fig 1, Fig 2 and Fig 3). In addition, the most effective extracts were tested in a comparative assay of HEK-TLR2 and HEK-TLR4 cells (Figs 5 and 6). Comparable dose-dependent anti-inflammatory activities in both transfected HEK cell lines suggested that all tested extracts interfere with the NF-κB/AP-1 signaling pathways of TLR2 and TLR4 (and some other innate immune receptors). Thus, it is reasonable that no exclusive TLR4 antagonist was found among the tested extracts. Furthermore, the ten most effective extracts were tested for their ability to inhibit translocation of NF-κB p65 into the cell nucleus (Fig 8). Seven extracts mitigated NF-κB p65 translocation. Despite being anti-inflammatory in THP-1 and HeLa-TLR4 screening as well as in the comparative HEK-TLR2/HEK-TLR4 assay, three extracts (*Cinchona pubescens*, *Alchemilla vulgaris* and *Vaccinium myrtillus*) showed no effect on NF-κB p65 translocation. This is remarkable, since nuclear translocation of NF-κB is an essential step in inflammation. Thus, other signaling pathways, such as those triggered by TNF-α receptor (TNFαR) and interleukin-1 receptor (IL-1R) lead to the observed translocation of NF-κB, however, without IL-8 cytokine release. Those three extracts that lack inhibition of NF-κB translocation may inhibit other molecules downstream of NF-κB. Ethanolic and organic extracts were shown to mainly comprise of anti-inflammatory compounds, whereas water extracts primarily comprise of compounds stimulating the immune system [23, 24]. A mixture of anti-inflammatory and pro-inflammatory compounds within our tested 70% ethanolic extracts might therefore serve as a partial explanation for the

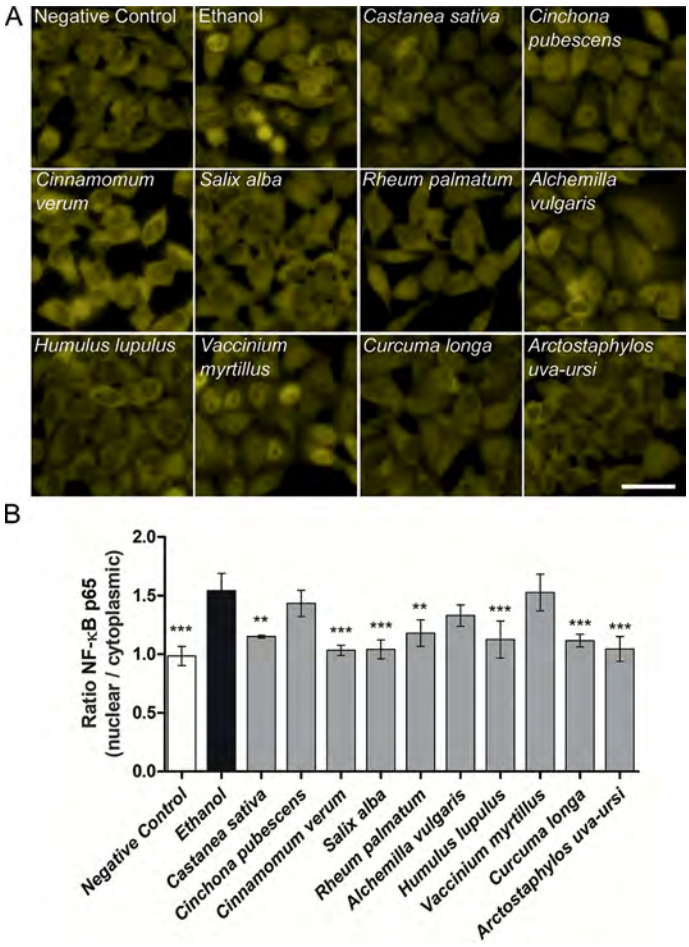

Fig 8. NF-κB translocation of select anti-inflammatory extracts. A: Fluorescence microscopy images of NF-κB stained HeLa-TLR4 dual reporter cells incubated with extracts or vehicle (70% ethanol), followed by stimulation with LPS-EB. For better visibility, images were cropped and adjusted in brightness and contrast. Scale bar = 50 μm. **B**: Quantitative evaluation of NF-κB p65 translocation. Mean fluorescence ratios of nuclear to cytoplasmic NF-κB p65 were calculated and compared to ethanol control. Data represents means ± SD (n = 3, 72 images (fields) per experiment and per treatment condition). Dunnett's post hoc test with $^{**}p<0.01$; $^{***}p<0.001$ compared to ethanol control.

https://doi.org/10.1371/journal.pone.0203907.g008

contradictory results between the anti-inflammatory effects in HeLa-TLR4 and THP-1 screening vs. the lack of inhibition of LPS-induced NF-κB translocation observed after incubation with *Cinchona pubescens*, *Alchemilla vulgaris* and *Vaccinium myrtillus*. Furthermore, incubation with two out of the ten most effective extracts (*Rheum palmatum* and *Arctostaphylos uva-ursi*, Fig 9) suggest an activity to repolarize pro-inflammatory and tissue destructive M1-type towards M2-type macrophages, which are involved in tissue repair and angiogenesis [25]. Comparing both cell lines, THP-1 monocytes were more susceptible to TLR4-dependent anti-inflammatory effects than HeLa-TLR4 cells. Since HeLa-TLR4 cells were co-transfected with the functional human TLR4, MD-2 and CD-14 complex they do exhibit high TLR4 canonical pathway specificity compared to other TLR4-related pathways. Extracts with stronger anti-inflammatory effects in THP-1 monocytes could possibly influence molecular mechanisms absent in HeLa-TLR4 cells. Therefore, the results observed in THP-1 monocytes may be better suited to reflect physiological TLR4 signaling.

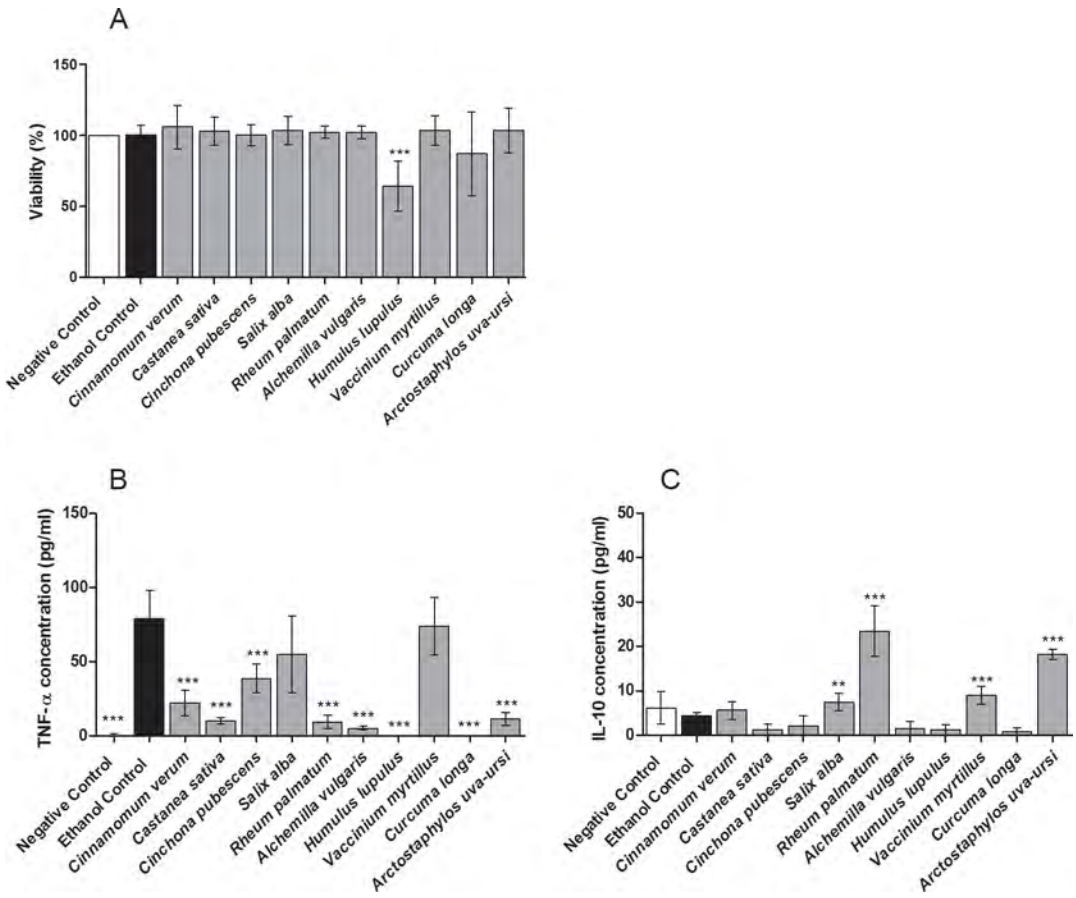

Fig 9. Effect of ten most effective anti-inflammatory extracts on macrophage repolarization. THP-1 M1 macrophages were incubated with extracts or vehicle (70% ethanol) control, followed by stimulation with LPS-EB. Negative control: untreated M1-type macrophages. **A**: Viability (Alamar Blue assay) was normalized to viability of untreated cells. **B**: TNF-α secretion (pg/ml) measured by ELISA. **C**: IL-10 secretion (pg/ml) measured by ELISA. Data represents means ± SD of 2 independent experiments (each with $n = 3$); unpaired t-test with $^{***}p<0.001$, $^{**}p<0.005$ compared to respective ethanol control.

https://doi.org/10.1371/journal.pone.0203907.g009

In the NF-κB translocation experiments, the incubation time differs from those in THP-1 and HeLa-TLR4 based screening assays (1 h vs. 4±8 h incubation with LPS), which might also explain the differing results. These LPS incubation times were chosen, as influences of the extracts on THP-1 and HeLa TLR4 screening were best seen after 4 h and 8 h, whereas NF-κB showed highest translocation into the nucleus at 1-2 h.

Due to the high number of extracts tested, we focused on the ten most effective anti-inflammatory extracts identified on screening. These included *Castanea sativa* leaves, *Cinchona pubescens* bark, *Cinnamomum verum* bark, *Salix alba* bark, *Rheum palmatum* root, *Alchemilla vulgaris* plant, *Humulus lupulus* cones, *Vaccinium myrtillus* berries, *Curcuma longa* root and *Arctostaphylos uva-ursi* leaves. To the best of our knowledge, *Castanea sativa* leaves and *Alchemilla vulgaris* plant extracts had not been reported to modulate the NF-κB, TLR2 or TLR4 signaling pathways, thus representing new promising candidates for further investigations. However, spiny burrs of sweet chestnuts inhibited NF-κB activation *in vivo* [26] and ellagitannins present in *Alchemilla vulgaris* were shown to possess NF-κB dependent anti-inflammatory effects [27].

Sweet chestnut (*Castanea sativa*)ÐLeaves

Strong dose-dependent anti-inflammatory effects, represented by decreased IL-8 concentrations, were observed after sweet chestnut extract incubation. In addition, high anti-inflammatory activity in the comparative HEK-Blue assay, even at low extract concentrations, were found. Apparently, sweet chestnut leaf extracts affect the signaling pathway of both TLR2 and TLR4. Sweet chestnut extract is used in traditional medicines for treatment of skin and soft tissue infections [28]. In modern studies several medicinal properties have been reported, e.g. anti-oxidant and anti-microbial effects [28±30]. Spiny burrs of sweet chestnuts applied for hepatorenal injury in diabetic rats inhibit NF-κB activation [27]. The carotenoid content in fruit and leaves has been suggested to possess direct anti-oxidant effects as well as to influence redox-sensitive and vitamin A signaling pathways [29,31]. Nevertheless, for sweet chestnut leaves only limited information has been available concerning its anti-inflammatory potential, including its ability to suppress TLR2 or TLR4 signaling pathways.

Common lady's mantle (*Alchemilla vulgaris)*–whole plant

In our experiments, common lady's mantle plant extract led to a decrease of LPS-induced IL-8 release and showed inhibitory effects on stimulated signaling pathways of both TLR2 and TLR4, but it displayed no inhibitory effects on nuclear NF-κB translocation. Thus, these results offer a promising starting point for identification of novel pro-inflammatory pathways and anti-inflammatory lead compounds. Common lady's mantle has been used traditionally in Europe to treat several disorders like urogenital diseases, eczema, inflammation, diarrhea and sepsis [32, 33]. But also, in modern science, beneficial health effects like anti-viral, anti-oxidant and wound-healing properties have been reported [32±35]. Again, its properties to mitigate TLR2 or TLR4 stimulation and to influence NF-κB signaling has not yet been described. However, ellagitannins, which are known to be present in *Alchemilla vulgaris*, were reported to mitigate inflammatory effects via the NF-κB pathway [27].

Besides these two extracts, with newly TLR2 and TLR4 dependent anti-inflammatory effects, the anti-inflammatory activities of our remaining herbal extracts are supported by existing descriptions in the literature. For several of these extracts, anti-inflammatory effects or the influence on TLR2 and TLR4 signaling pathways were solely described for single compounds but not for the complex mixtures present within the whole extract. Therefore, it is possible that further compounds, not investigated so far, contribute to their beneficial health effects.

Bearberry (*Arctostaphylos uva-ursi*)±leaves

In our assays, bearberry leaves showed strong dose-dependent anti-inflammatory activities in several cell lines and inhibition of LPS-induced NF-κB translocation. In addition, this extract mitigated the secretion of TNF-α accompanied with an increased secretion of IL-10 in macrophages, indicating a switch from pro-inflammatory M1-type to anti-inflammatory M2-type macrophages [26]. Bearberry leaves are traditionally used to treat symptoms of lower urinary tract infections and have been proven in modern medicine to possess anti-septic and anti-adhesion properties [36]. The most representative constituent of bearberry, the phenolic glycoside arbutin, is an anti-oxidant and anti-inflammatory agent [37]. Among others, arbutin significantly reduced production of pro-inflammatory cytokines including IL-1β and TNF-α, and other inflammation-related genes such as monocyte chemoattractant protein-1 (MCP-1) and IL-6. Furthermore, it inhibits the nuclear translocation of NF-κB [37]. These data support our data. Although arbutin is the major active ingredient, whole bearberry extracts are necessary to reveal the complete pharmaceutical activity [38]. The complex mixture of bearberry extract

has not yet been reported to influence TLR2/TLR4 signaling pathways or to induce macrophage repolarization, making it a suitable candidate for further investigations.

Cinchona (*Cinchona pubescens)*–bark

Cinchona bark extract diminished LPS-induced inflammatory signals, especially in THP-1 monocytes and the comparative HEK-TLR2/TLR4 assay system, whereas LPS-induced NF-κB translocation was not affected. *In vivo* inhibition of TLR2- and TLR4-mediated signaling cascades by cinchonine from cinchona bark are demonstrated in literature, supporting our observed inhibition of pro-inflammatory cytokine production in stimulated TLR2 and TLR4 signaling pathways [39]. Besides cinchonine, further quinine derivatives in cinchona bark, e.g. chloroquine inhibited different TLR signaling pathways [40,41]. However, whole cinchona bark extract has, based on our present knowledge, not yet been described to influence TLR2 and/or TLR4 signaling pathways. Further analyses need to be performed to explore the underlying active constituents, besides cinchonine, especially those that affect TLR2 and TLR4 signaling.

Hops (*Humulus lupulus)*–cones

A strong decrease of pro-inflammatory cytokine production and a mitigation of LPS-induced NF-κB translocation were observed after hops extract treatment in our cell culture-based assays. Flavonoids from hops cones possess pharmaceutically important properties, e.g. antioxidant, anti-microbial, anti-carcinogenic, anti-inflammatory and estrogenic effects [42]. In particular, flavonoids like xanthohumol are effective inhibitors of arachidonic acid metabolism through inhibition of cyclooxygenase 1 and 2 (COX-1, COX-2) [43]. Furthermore, LPS-induced production of nitric oxide (NO), IL-1β, and TNF-α, and the activation of NF-κB signaling were inhibited by xanthohumol isolated from hops [44,45]. Again, it is likely that further compounds present in hops extract contribute to its strong anti-inflammatory effects demonstrated in our experiments.

White willow (*Salix alba)*–bark

Strong dose-dependent anti-inflammatory effects, as shown by decreased IL-8 production, were observed in TLR2- and TLR4-stimulated cell lines, coupled with a significant decrease in LPS-induced NF-κB translocation. White willow extract is commonly known for its beneficial health effects. Its active compound, the alcoholic β-glucoside salicin, was the basis for the discovery of Aspirin, a COX inhibitor, which still is one of the most widely used medicines in the world [46]. During absorption, salicin is metabolized into several salicylate derivatives resulting in pharmaceutical activities based on various components. This leads to a different mode of action compared to Aspirin and its pure compound acetylsalicylic acid, with less severe side effects [47]. In numerous *in vitro* and *in vivo* studies, anti-inflammatory effects have been shown for white willow extract, e.g. downregulation of several pro-inflammatory cytokines like TNF-α and inhibition of NF-κB translocation, which supports the data obtained by us [48±50]. The anti-inflammatory effects have been credited to salicin [48]. However, salicin alone cannot satisfactorily explain the anti-inflammatory effects, and other compounds within the complex mixture, especially polyphenols such as flavonoids and proanthocyanidins, are suggested to contribute to its overall activity and thereby broaden the mechanisms of action [51].

Turmeric (*Curcuma longa*)±root

Our results suggest that TLR2/TLR4 signaling pathways are molecular targets of turmeric extract. This is supported by reports that show that turmeric and some of its compounds, especially curcumin and aromatic-turmerone, inhibit LPS-induced NF-κB activation, and expression of TLR4 and the downstream genes IL-1 receptor-associated kinase 1 (IRAK-1) and tumor necrosis factor receptor-associated factor 6 (TRAF-6) [52]. Treatment with curcumin inhibits both MyD88- and TRAM/TRIF-dependent pathways in LPS-induced TLR4 signaling. Production of TNF-α, IL-6 and ROS as well as levels of TLR4, MyD88 and the downstream effectors including NF-κB, interferon regulatory factor 3 (IRF3), MyD88, and TIRF were attenuated [53±55]. Incubation with aromatic-turmerone, another compound of turmeric extract, blocked TLR4-mediated downstream signaling and the release of pro-inflammatory mediators [56]. Furthermore, *Curcuma longa* induced a shift from M1-type to M2-type macrophages in the murine RAW 264.7 macrophage cell line [57], which is in line with our data showing a decreased TNF-α secretion.

Rhubarb (*Rheum palmatum)*–root

Rhubarb root extract led to a decrease of LPS-induced cytokine production, inhibited both TLR2 and TLR4 signaling, nuclear NF-κB translocation, and induced M1-type to M2-type macrophage polarization. Treatment of inflammatory diseases with rhubarb roots has been described to significantly decrease TLR2, TLR4 and NF-κB mRNA, and protein expression *in vivo* [58,59], which is in line with our results. Emodin, which has been isolated from rhizomes of *Rheum palmatum*, inhibits several target molecules in inflammation and cancer, such as NF-κB and the serine/threonine kinase Akt, both important molecules in TLR2 and TLR4 signaling pathways [60]. Furthermore, emodin suppressed LPS-induced pro-inflammatory cytokines and chemokines as well as NF-κB inhibitor alpha (IκBα) degradation and thus NF-κB activation by disruption of lipid rafts [61]. Further research has to be conducted on whether the inhibition of TLR2- and TLR4 mediated signaling is only related to the reported effects of emodin or if further compounds present in the complex mixture of rhubarb root extract play a role in the observed anti-inflammatory effects.

Cinnamon (*Cinnamomum verum)*–bark

Cinnamon bark extract strongly mitigated pro-inflammatory cytokine production in stimulated TLR2 and TLR4 signaling pathways, and in LPS-induced nuclear NF-κB translocation. For cinnamon extract, several beneficial health effects are reported in literature, e.g. anti-inflammatory effects on murine alcohol-induced steatosis and colitis [62±64]. Ethanolic cinnamon bark extracts have been shown to suppress release of TNF-α, IL-1β and IL-6 and NF-κB activation, in line with our data [65,66]. The major constituent present in cinnamon bark extract, *trans*-cinnamaldehyde, showed several anti-inflammatory effects [67±70]. Still, more active compounds may be present in cinnamon extract.

Bilberries (*Vaccinium myrtillus)*–berries

Bilberry extract mitigated LPS-induced inflammatory signals, whereas LPS-induced NF-κB translocation was not affected. Bilberry extract, which is rich in antioxidant anthocyanins, showed anti-inflammatory effects *in vivo*, e.g. suppression of LPS-induced inducible nitric oxide synthase (iNOS), TNF-α, IL-1β and IL-6 transcripts, and iNOS, TNF-α and NF-κB protein levels in liver inflammation [71], compatible with our results. In a randomized, controlled dietary intervention for patients with the metabolic syndrome, bilberry supplementation

reduced serum high-sensitivity C-reactive protein (CRP), IL-6, IL-12 and LPS levels, and downregulated genes associated with the TLR pathway [72]. Consumption of bilberry juice by patients with an increased risk for cardiovascular disease led to decreased plasma concentrations of CRP, IL-6 and IL-15 [73]. Overall, bilberry consumption may reduce low-grade metabolic inflammation, decreasing the risk of cardiometabolic diseases [72]. In our study, bilberries showed no inhibitory effects on nuclear translocation of NF-κB. In contrast, quercetin, resveratrol and epicatechin, all polyphenols present in bilberry, were shown to inhibit LPS-induced NF-κB activation *in vitro*, which suggests that conflicting effects of compounds in whole bilberry extract may play a significant role [73]. Taken together, both clinical studies demonstrate not only the anti-inflammatory potential of bilberries, but also their oral effectiveness in humans.

In conclusion, we showed that numerous ethanolic herbal extracts mitigate TLR2- and TLR4-dependent signaling and downstream inflammation. Several of them are known as officinal plants, but the underlying molecular mechanisms of their anti-inflammatory effects are often ill-defined or unknown. TLR pathways are of fundamental relevance in diverse inflammatory diseases. With the identification of orally active TLR-and/or NF-κB antagonizing herbal extracts and their active compounds, new promising treatment strategies might be developed. Moreover, a previously unknown attenuation of TLR-induced inflammatory responses by *Castanea sativa* leaves and *Alchemilla vulgaris* plants could be shown in our study. Interestingly, three out of the ten most effective anti-inflammatory extracts showed no inhibition of NF-κB translocation. Further identification of the active compounds of different extracts, investigations concerning their anti-inflammatory activity and their molecular targets within the signaling cascades are necessary. Furthermore, the anti-inflammatory activity demonstrated with our *in vitro* assays might differ in animals and humans due to alterations by digestion, absorption and metabolism of different compounds, as well as excretion of the extracts. Often, the overall efficacy in complex herbal mixtures is not only based on single compound activity, but on the combination of several different compounds. Hereby, not only additive but also synergistic effects were observed [74±76]. Therefore, experiments with combinations of defined compounds can help to elucidate these interactions.

Supporting information

S1 Table. Overview of herbal extracts. Scientific and common names, taxonomic information, active compounds and classification and reported beneficial health effects. ↓: downregulation, ↑: upregulation, AChE: acetylcholinesterase, ALP: alkaline phosphatase, ALT: alanine transaminase, AP-1: activator protein 1, AST: aspartate transaminase, CRP: C-reactive protein, CXCL1: chemokine (C-X-C motif) ligand 1, EGCG: epigallocatechin-3-gallate, ERK: extracellular signal-regulated kinase, Fg: Fibrinogen, GSH: glutathione, Hmox1: heme oxygenase (decycling) 1, IBD: inflammatory bowel disease, IFN: interferon, IL: interleukin, iNOS: inducible nitric oxide synthase, IRAK1: IL-1 receptor-associated kinase, IRF: interferon regulatory factor, IκBα: NF-κB inhibitor alpha, JNK: c-Jun N-terminal kinase, LDH: lactate dehydrogenase, LOX: lipoxygenase, MCP-1: monocyte chemoattractant protein-1, MDA: malondialdehyde, MPO: myeloperoxidase, MyD88: myeloid differentiation primary response 88, NF-κB: Nuclear factor-κB, NLRP3: NOD-like receptor family pyrin domain-containing 3, NO: nitric oxide, Nrf2: nuclear factor erythroid 2-related factor 2, PGE2: prostaglandin E2, RAGE: receptor for advanced glycation end products, RANKL: receptor activator of nuclear factor kappa-B ligand, ROS: reactive oxygen species, SOD: superoxide dismutase, TLR4: Toll-like receptor 4, TGFβ1: Transforming growth factor beta 1, TRAF6: TNF receptor-associated factor 6.
(PDF)

S1 Fig. Cell viability and anti-inflammatory effects of ethanolic herbal extracts. HeLa-TLR4 cells (red) and THP-1 monocytes (blue) were incubated with extracts (the ten extracts with highest anti-inflammatory potential are displayed in Fig 1, Fig 2 and Fig 3) or vehicle (70% ethanol), followed by stimulation with LPS-EB. Viability was measured using the Alamar Blue Assay was normalized to the negative control (untreated cells). TLR4 receptor activity was measured using Renilla luciferase expression for the HeLa-TLR4 cell line or IL-8 ELISA (pg/ml) for the THP-1 monocytes and was normalized to ethanol-treated cells. Data are displayed as viability (%) in the left graphs and TLR4 activity divided by normalized viability (%) in the right graphs. Data represents means ($n \geq 2$).
(PDF)

S2 Fig. Anti- and pro-inflammatory effect of ethanolic extracts in HeLa-TLR4 reporter cells and THP-1 monocytes. HeLa-TLR4 reporter cells or THP-1 monocytes were incubated with extracts in different concentrations or vehicle (70% ethanol), followed by stimulation with LPS-EB. Viability was measured using Alamar Blue Assay and was normalized to the negative control (*Viability (%)*). TLR4 receptor activity was measured using Renilla luciferase expression for the HeLa-TLR4 cell line or IL-8 ELISA (pg/ml) for THP-1 monocytes and was normalized to ethanol-treated cells (*TLR4-Activity*). Data are displayed as TLR4 stimulation divided by viability and sorted ascending by the following formula: (150Ð *Viability (%)*) * (2 * *TLR4-Activity* + 100) weighted in a ratio of 2:1 for THP-1 monocytes vs. HeLa-TLR4 cells. Data represents means ($n \geq 2$).
(PDF)

S3 Fig. TLR2 and TLR4 antagonistic effects of ethanolic herbal extracts. HEK-TLR2 cells (purple) and HEK-TLR4 cells (orange) were incubated with extracts (the five extracts with highest anti-inflammatory potential are displayed in Figs 5 and 6) or vehicle (70% ethanol), followed by stimulation of HEK-TLR2 cells with Pam2CSK4 or HEK-TLR4 cells with LPS-EB Ultrapure. Viability was measured using the Alamar Blue Assay was normalized to the respective negative control. TLR2 and TLR4 receptor activity were measured using SEAP production was normalized to ethanol-treated cells. Data are displayed as viability (%) in the left graphs and receptor activity divided by viability (%) in the right graphs. Data represents means ($n \geq 2$).
(PDF)

S4 Fig. TLR2 and TLR4 antagonistic effects of select ethanolic extracts in HEK-TLR2 and HEK-TLR4 cell lines. HEK-TLR2 or HEK-TLR4 cells were incubated with extracts in different concentrations or vehicle (70% ethanol), followed by stimulation of HEK-TLR2 cells with Pam2CSK4 or HEK-TLR4 cells with LPS-EB Ultrapure. Viability was measured using Alamar Blue Assay was normalized to the negative control. TLR2 and TLR4 receptor activity were measured using SEAP production and were normalized to ethanol-treated cells. Data are displayed as receptor activity divided by normalized viability. Data represents means ($n \geq 2$).
(PDF)

Acknowledgments

The authors thank Fangxia Shen for providing samples from mung beans. The authors acknowledge the financial support by the Max Planck Graduate Center with the Johannes Gutenberg University Mainz (MPGC). They also acknowledge the stimulating exchange and discussions with the members of the Mainz Program for Chemical Allergology (MPCA), and numerous colleagues in the scientific communities in life sciences, pharmaceutics and medicine. Support by the IMB Microscopy and Histology Core Facility is gratefully acknowledged,

as well as the German Research Foundation (DFG) for funding the Opera Phenix High Content Spinning Disk Microscope (Project 402386039).

Author Contributions

Conceptualization: Anne Schink, Eckhard Thines, Ulrich Pöschl, Detlef Schuppan, Kurt Lucas.

Formal analysis: Anne Schink, Jan Neumann.

Investigation: Anne Schink, Jan Neumann, Anna Lena Leifke.

Methodology: Anne Schink, Jan Neumann, Ulrich Pöschl, Detlef Schuppan, Kurt Lucas.

Project administration: Ulrich Pöschl, Detlef Schuppan, Kurt Lucas.

Resources: Bettina Weber, Ulrich Pöschl, Detlef Schuppan, Kurt Lucas.

Supervision: Ulrich Pöschl, Detlef Schuppan, Kurt Lucas.

Validation: Anne Schink, Jan Neumann, Kurt Lucas.

Visualization: Anne Schink, Jan Neumann, Bettina Weber, Ulrich Pöschl, Kurt Lucas.

Writing ± original draft: Anne Schink, Jan Neumann.

Writing ± review & editing: Anne Schink, Jan Neumann, Anna Lena Leifke, Kira Ziegler, Janine Fröhlich-Nowoisky, Christoph Cremer, Eckhard Thines, Bettina Weber, Ulrich Pöschl, Detlef Schuppan, Kurt Lucas.

References

1. Chahal DS, Sivamani RK, Isseroff RR, Dasu MR. Plant-based modulation of Toll-like receptors: an emerging therapeutic model. Phytother Res. 2013; 27(10):1423–38. https://doi.org/10.1002/ptr.4886 PMID: 23147906
2. Liu X, Wu WY, Jiang BH, Yang M, Guo DA. Pharmacological tools for the development of traditional Chinese medicine. *Trends Pharmacol Sci*. 2013; 34(11):620–8. https://doi.org/10.1016/j.tips.2013.09.004 PMID: 24139610
3. Buenz EJ, Verpoorte R, Bauer BA. The Ethnopharmacologic Contribution to Bioprospecting Natural Products. *Annu Rev Pharmacol Toxicol*. 2018;6; 58:509–530. https://doi.org/10.1146/annurev-pharmtox-010617-052703 PMID: 29077533
4. McGrath KW, Icitovic N, Boushey HA, Lazarus SC, Sutherland ER, Chinchilli VM et al. A large subgroup of mild-to-moderate asthma is persistently noneosinophilic. Am J Respir Crit Care Med. 2012; 185 (6):612–9. https://doi.org/10.1164/rccm.201109-1640OC PMID: 22268133
5. Schuppan D, Kim YO. Evolving therapies for liver fibrosis. J Clin Invest. 2013; 123(5):1887–901. https://doi.org/10.1172/JCI66028 PMID: 23635787
6. Holmdahl R, Malmström V, Burkhardt H. Autoimmune priming, tissue attack and chronic inflammation—the three stages of rheumatoid arthritis. Eur J Immunol. 2014; 44(6):1593–9. https://doi.org/10.1002/eji.201444486 PMID: 24737176
7. McAlees JW, Whitehead GS, Harley IT, Cappelletti M, Rewerts CL, Holdcroft AM et al. Distinct Tlr4-expressing cell compartments control neutrophilic and eosinophilic airway inflammation. Mucosal Immunol. 2015; 8(4):863–73. https://doi.org/10.1038/mi.2014.117 PMID: 25465099
8. Martel J, Ojcius DM, Chang CJ, Lin CS, Lu CC, Ko YF et al. Anti-obesogenic and antidiabetic effects of plants and mushrooms. *Nat Rev Endocrinol*. 2017; 13(3):149–160. https://doi.org/10.1038/nrendo.2016.142 PMID: 27636731
9. Lucas K, Maes M. Role of the Toll Like receptor (TLR) radical cycle in chronic inflammation: possible treatments targeting the TLR4 pathway. Mol Neurobiol., 2013; 48(1):190–204. https://doi.org/10.1007/s12035-013-8425-7 PMID: 23436141
10. Walsh D, McCarthy J, O'Driscoll C, Melgar S. Pattern recognition receptors—molecular orchestrators of inflammation in inflammatory bowel disease. Cytokine Growth Factor Rev. 2013; 24(2):91–104. https://doi.org/10.1016/j.cytogfr.2012.09.003 PMID: 23102645

11. Kramer CD, Genco CA. Microbiota, Immune Subversion, and Chronic Inflammation. Front Immunol. 2017; 8:255. https://doi.org/10.3389/fimmu.2017.00255 PMID: 28348558

12. Takeuchi O, Akira S. Toll-like receptors; their physiological role and signal transduction system. Int Immunopharmacol. 2001; 1(4):625–35. PMID: 11357875

13. Ghosh S, Dass JF. Study of pathway cross-talk interactions with NF-κB leading to its activation via ubiquitination or phosphorylation: A brief review. Gene. 2016; 584(1):97–109. https://doi.org/10.1016/j.gene.2016.03.008 PMID: 26968890

14. Yamada M, Ichikawa T, Ii M, Sunamoto M, Itoh K, Tamura N et al. Discovery of novel and potent small-molecule inhibitors of NO and cytokine production as antisepsis agents: synthesis and biological activity of alkyl 6-(N-substituted sulfamoyl)cyclohex-1-ene-1-carboxylate. J Med Chem. 2005; 48(23):7457–67. https://doi.org/10.1021/jm050623t PMID: 16279805

15. Youn HS, Lee JY, Saitoh SI, Miyake K, Kang KW, Choi YJ et al. Suppression of MyD88- and TRIF-dependent signaling pathways of Toll-like receptor by (-)-epigallocatechin-3-gallate, a polyphenol component of green tea. Biochem Pharmacol. 2006; 72(7):850–9. https://doi.org/10.1016/j.bcp.2006.06.021 PMID: 16890209

16. Park SJ, Lee MY, Son BS, Youn HS. TBK1-targeted suppression of TRIF-dependent signaling pathway of Toll-like receptors by 6-shogaol, an active component of ginger. Biosci Biotechnol Biochem. 2009; 73(7):1474–1478. https://doi.org/10.1271/bbb.80738 PMID: 19584560

17. Tidswell M, Tillis W, Larosa SP, Lynn M, Wittek AE, Kao R et al. Phase 2 trial of eritoran tetrasodium (E5564), a toll-like receptor 4 antagonist, in patients with severe sepsis. Crit Care Med. 2010; 38(1):72–83. https://doi.org/10.1097/CCM.0b013e3181b07b78 PMID: 19661804

18. Peri F, Calabrese V. Toll-like receptor 4 (TLR4) modulation by synthetic and natural compounds: an update. J Med Chem. 2014; 57(9):3612–3622. https://doi.org/10.1021/jm401006s PMID: 24188011

19. Tian J, Zhao Y, Liu Y, Liu Y, Chen K, Lyu S. Roles and Mechanisms of Herbal Medicine for Diabetic Cardiomyopathy: Current Status and Perspective. Oxid Med Cell Longev. 2017; 2017:8214541. https://doi.org/10.1155/2017/8214541 PMID: 29204251

20. Zhao Y, Liu Y. A mechanistic overview of herbal medicine and botanical compounds to target transcriptional factors in Breast cancer. Pharmacol Res. 2017;pii: S1043-6618(17)30838-1. https://doi.org/10.1016/j.phrs.2017.12.027

21. Jiao L, Bi L, Lu Y, Wang Q, Gong Y, Shi J et al. Cancer chemoprevention and therapy using chinese herbal medicine. Biol Proced Online. 2018; 20:1. https://doi.org/10.1186/s12575-017-0066-1 PMID: 29321719

22. Pan Y, Kong LD. High fructose diet-induced metabolic syndrome: pathophysiological mechanism and treatment by traditional Chinese medicine. *Pharmacol Res*. 2018;pii: S1043-6618(17)31549-9. https://doi.org/10.1016/j.phrs.2018.02.020

23. Lu CC, Hsu YJ, Chang CJ, Lin CS, Martel J, Ojcius DM et al. Immunomodulatory properties of medicinal mushrooms: differential effects of water and ethanol extracts on NK cell-mediated cytotoxicity. *Innate Immun*. 2016; 22(7):522–33. https://doi.org/10.1177/1753425916661402 PMID: 27469258

24. Martel J, Ko YF, Ojcius DM, Lu CC, Chang CJ, Lin CS et al. Immunomodulatory Properties of Plants and Mushrooms. *Trends Pharmacol Sci*. 2017; 38(11):967–981. https://doi.org/10.1016/j.tips.2017.07.006 PMID: 28863984

25. Fraternale A, Brundu S, Magnani M. Polarization and Repolarization of Macrophages. J Clin Cell Immunol. 2015; 6: 319. https://doi.org/10.4172/2155-9899.1000319

26. Jovanović JA, Mihailović M, Uskoković AS, Grdović N, Dinić S, Poznanović G et al. Evaluation of the Antioxidant and Antiglycation Effects of Lactarius deterrimus and Castanea sativa Extracts on Hepatorenal Injury in Streptozotocin-Induced Diabetic Rats. Front Pharmacol. 2017; 8:793. https://doi.org/10.3389/fphar.2017.00793 PMID: 29163175

27. Landete JM. Ellagitannins, ellagic acid and their derived metabolites: a review about source, metabolism, functions and health. *Food Research International*. 2011; 44(5):1150–1160.

28. Quave CL, Lyles JT, Kavanaugh JS, Nelson K, Parlet CP, Crosby HA et al. Castanea sativa (European Chestnut) Leaf Extracts Rich in Ursene and Oleanene Derivatives Block Staphylococcus aureus Virulence and Pathogenesis without Detectable Resistance. PLoS One. 2015; 10(8):e0136486. https://doi.org/10.1371/journal.pone.0136486 PMID: 26295163

29. De Vasconcelos MC, Bennett RN, Rosa EA, Ferreira-Cardoso JV. Composition of European chestnut (Castanea sativa Mill.) and association with health effects: fresh and processed products. J Sci Food Agric. 2010; 90(10):1578–89. https://doi.org/10.1002/jsfa.4016 PMID: 20564434

30. Pinto D, Rodrigues F, Braga N, Santos J, Pimentel FB, Palmeira-de-Oliveira A et al. The Castanea sativa bur as a new potential ingredient for nutraceutical and cosmetic outcomes: preliminary studies. Food Funct. 2017; 8(1):201–208. https://doi.org/10.1039/c6fo01469k PMID: 27990543

31. Elliott R. Mechanisms of genomic and non-genomic actions of carotenoids. Biochim Biophys Acta. 2005; 1740(2):147–54. https://doi.org/10.1016/j.bbadis.2004.12.009 PMID: 15949681

32. Kiselova Y, Ivanova D, Chervenkov T, Gerova D, Galunska B, Yankova T. Correlation between the in vitro antioxidant activity and polyphenol content of aqueous extracts from Bulgarian herbs. Phytother Res. 2006; 20(11):961–5. https://doi.org/10.1002/ptr.1985 PMID: 16906640

33. Takır S, Altun IH, Sezgi B, Süzgeç-Selçuk S, Mat A, Uydeş-Doğan BS. Vasorelaxant and blood pressure lowering effects of alchemilla vulgaris: A comparative study of methanol and aqueous extracts. Pharmacogn Mag. 2015; 11(41):163–9. https://doi.org/10.4103/0973-1296.149733 PMID: 25709228

34. Shrivastava R, Cucuat N, John GW. Effects of Alchemilla vulgaris and glycerine on epithelial and myofibroblast cell growth and cutaneous lesion healing in rats. Phytother Res. 2007; 21(4):369–73. https://doi.org/10.1002/ptr.2060 PMID: 17236169

35. Filippova EI. Antiviral Activity of Lady's Mantle (Alchemilla vulgaris L.) Extracts against Orthopoxviruses. Bull Exp Biol Med. 2017; 163(3):374–377. https://doi.org/10.1007/s10517-017-3807-x PMID: 28744637

36. Yarnell E. Botanical medicines for the urinary tract. World J Urol. 2002; 20(5):285–93. https://doi.org/10.1007/s00345-002-0293-0 PMID: 12522584

37. Lee HJ, Kim KW. Anti-inflammatory effects of arbutin in lipopolysaccharide-stimulated BV2 microglial cells. Inflamm Res. 2012; 61(8):817–25. https://doi.org/10.1007/s00011-012-0474-2 PMID: 22487852

38. de Arriba SG, Naser B, Nolte KU. Risk assessment of free hydroquinone derived from Arctostaphylos Uva-ursi folium herbal preparations. Int J Toxicol. 2013; 32(6):442–53. https://doi.org/10.1177/1091581813507721 PMID: 24296864

39. Jung SA, Choi M, Kim S, Yu R, Park T. Cinchonine Prevents High-Fat-Diet-Induced Obesity through Downregulation of Adipogenesis and Adipose Inflammation. PPAR Res. 2012; 2012:541204. https://doi.org/10.1155/2012/541204 PMID: 22675336

40. Kuznik A, Bencina M, Svajger U, Jeras M, Rozman B, Jerala R. Mechanism of endosomal TLR inhibition by antimalarial drugs and imidazoquinolines. *J Immunol*. 2011; 186(8):4794–804. https://doi.org/10.4049/jimmunol.1000702 PMID: 21398612

41. Kalia S, Dutz JP. New concepts in antimalarial use and mode of action in dermatology. Dermatol Ther. 2007; 20(4):160–74. https://doi.org/10.1111/j.1529-8019.2007.00131.x PMID: 17970883

42. Karabin M, Hudcova T, Jelinek L, Dostalek P. Biotransformations and biological activities of hop flavonoids. Biotechnol Adv. 2015; 33(6 Pt 2):1063–90. https://doi.org/10.1016/j.biotechadv.2015.02.009

43. Gerhäuser C Beer constituents as potential cancer chemopreventive agents. Eur J Cancer. 2005; 41(13):1941–54. https://doi.org/10.1016/j.ejca.2005.04.012 PMID: 15953717

44. Albini A, Dell'Eva R, Vené R, Ferrari N, Buhler DR, Noonan DM et al. Mechanisms of the antiangiogenic activity by the hop flavonoid xanthohumol: NF-kappaB and Akt as targets. FASEB J. 2006; 20(3):527–9. https://doi.org/10.1096/fj.05-5128fje PMID: 16403733

45. Lee IS, Lim J, Gal J, Kang JC, Kim HJ, Kang BY et al. Anti-inflammatory activity of xanthohumol involves heme oxygenase-1 induction via NRF2-ARE signaling in microglial BV2 cells. Neurochem Int. 2011; 58(2):153–60. https://doi.org/10.1016/j.neuint.2010.11.008 PMID: 21093515

46. Desborough MJR, Keeling DM. The aspirin story—from willow to wonder drug. Br J Haematol. 2017; 177(5):674–683. https://doi.org/10.1111/bjh.14520 PMID: 28106908

47. Vlachojannis J, Magora F, Chrubasik S. Willow species and aspirin: different mechanism of actions. Phytother Res. 2011; 25(7):1102–4. https://doi.org/10.1002/ptr.3386 PMID: 21226125

48. Bonaterra GA, Heinrich EU, Kelber O, Weiser D, Metz J, Kinscherf R. Anti-inflammatory effects of the willow bark extract STW 33-I (Proaktiv) in LPS-activated human monocytes and differentiated macrophages. Phytomedicine. 2010; 17(14):1106–13. https://doi.org/10.1016/j.phymed.2010.03.022 PMID: 20570123

49. Shakibaei M, Allaway D, Nebrich S, Mobasheri A. Botanical Extracts from Rosehip (*Rosa canina*), Willow Bark (*Salix alba*), and Nettle Leaf (*Urtica dioica*) Suppress IL-1β-Induced NF-κB Activation in Canine Articular Chondrocytes. Evid Based Complement Alternat Med. 2012; 2012:509383. https://doi.org/10.1155/2012/509383 PMID: 22474508

50. Shara M, Stohs SJ. Efficacy and Safety of White Willow Bark (Salix alba) Extracts. Phytother Res. 2015; 29(8):1112–6. https://doi.org/10.1002/ptr.5377 PMID: 25997859

51. Nahrstedt A, Schmidt M, Jäggi R, Metz J, Khayyal MT. Willow bark extract: the contribution of polyphenols to the overall effect. Wien Med Wochenschr. 2007; 157(13–14):348–51. https://doi.org/10.1007/s10354-007-0437-3 PMID: 17704985

52. Angel-Morales G, Noratto G, Mertens-Talcott SU. Standardized curcuminoid extract (Curcuma longa l.) decreases gene expression related to inflammation and interacts with associated microRNAs in human

umbilical vein endothelial cells (HUVEC). Food Funct. 2012; 3(12):1286–93. https://doi.org/10.1039/c2fo30023k PMID: 22972459

53. Youn HS, Saitoh SI, Miyake K, Hwang DH. Inhibition of homodimerization of Toll-like receptor 4 by curcumin. Biochem Pharmacol. 2006; 72(1):62–9. https://doi.org/10.1016/j.bcp.2006.03.022 PMID: 16678799

54. Zhu HT, Bian C, Yuan JC, Chu WH, Xiang X, Chen F et al. Curcumin attenuates acute inflammatory injury by inhibiting the TLR4/MyD88/NF-κB signaling pathway in experimental traumatic brain injury. J Neuroinflammation. 2014; 11:59. https://doi.org/10.1186/1742-2094-11-59 PMID: 24669820

55. Yu S, Wang X, He X, Wang Y, Gao S, Ren L et al. Curcumin exerts anti-inflammatory and antioxidative properties in 1-methyl-4-phenylpyridinium ion (MPP(+))-stimulated mesencephalic astrocytes by interference with TLR4 and downstream signaling pathway. Cell Stress Chaperones. 2016; 21(4):697–705. https://doi.org/10.1007/s12192-016-0695-3 PMID: 27164829

56. Chen M, Chang YY, Huang S, Xiao LH, Zhou W, Zhang LY et al. Aromatic-turmerone Attenuates LPS-Induced Neuroinflammation and Consequent Memory Impairment by Targeting TLR4-Dependent Signaling Pathway. Mol Nutr Food Res. 2018; 62(2). https://doi.org/10.1002/mnfr.201700281

57. Li B, Hu Y, Zhao Y, Cheng M, Qin H, Cheng T et al. Curcumin Attenuates Titanium Particle-Induced Inflammation by Regulating Macrophage Polarization In Vitro and In Vivo. Front Immunol. 2017; 8:55. https://doi.org/10.3389/fimmu.2017.00055 PMID: 28197150

58. Liu Y, Yan F, Liu Y, Zhang C, Yu H, Zhang Y et al. Aqueous extract of rhubarb stabilizes vulnerable atherosclerotic plaques due to depression of inflammation and lipid accumulation. Phytother Res. 2008; 22 (7):935–42. https://doi.org/10.1002/ptr.2429 PMID: 18384190

59. Yao P, Cui M, Li Y, Deng Y, Wu H. Effects of rhubarb on intestinal flora and toll-like receptors of intestinal mucosa in rats with severe acute pancreatitis. Pancreas. 2015; 44(5):799–804. https://doi.org/10.1097/MPA.0000000000000339 PMID: 25931256

60. Shrimali D, Shanmugam MK, Kumar AP, Zhang J, Tan BK, Ahn KS et al. Targeted abrogation of diverse signal transduction cascades by emodin for the treatment of inflammatory disorders and cancer. Cancer Lett. 2013; 341(2):139–49. https://doi.org/10.1016/j.canlet.2013.08.023 PMID: 23962559

61. Meng G, Liu Y, Lou C, Yang H. Emodin suppresses lipopolysaccharide-induced pro-inflammatory responses and NF-κB activation by disrupting lipid rafts in CD14-negative endothelial cells. Br J Pharmacol. 2010; 161(7):1628–44. https://doi.org/10.1111/j.1476-5381.2010.00993.x PMID: 20726986

62. Kanuri G, Weber S, Volynets V, Spruss A, Bischoff SC, Bergheim I. Cinnamon extract protects against acute alcohol-induced liver steatosis in mice. J Nutr. 2009; 139(3):482–7. https://doi.org/10.3945/jn.108.100495 PMID: 19126670

63. Hagenlocher Y, Hösel A, Bischoff SC, Lorentz A. Cinnamon extract reduces symptoms, inflammatory mediators and mast cell markers in murine IL-10(-/-) colitis. 2016;J Nutr Biochem. 30:85–92. https://doi.org/10.1016/j.jnutbio.2015.11.015 PMID: 27012624

64. Hagenlocher Y, Satzinger S, Civelek M, Feilhauer K, Köninger J, Bischoff SC et al. Cinnamon reduces inflammatory response in intestinal fibroblasts in vitro and in colitis in vivo leading to decreased fibrosis. Mol Nutr Food Res. 2017; 61(9). https://doi.org/10.1002/mnfr.201601085

65. Ho SC, Chang KS, Chang PW. Inhibition of neuroinflammation by cinnamon and its main components. Food Chem. 2013; 138(4):2275–82. https://doi.org/10.1016/j.foodchem.2012.12.020 PMID: 23497886

66. Gunawardena D, Govindaraghavan S, Münch G. Anti-inflammatory properties of cinnamon polyphenols and their monomeric precursors. In: Watson RR, Preedy VR, Zibadi S, editors. Polyphenols in Human Health and Disease, volume 1. Elsevier, Amsterdam, Boston, Heidelberg, London, New York, Oxford, Paris, San Diego, San Francisco, Singapore, Sydney, Tokyo, 2014. pp 30:409–425.

67. Chao LK, Hua KF, Hsu HY, Cheng SS, Lin IF, Chen CJ et al. Cinnamaldehyde inhibits pro-inflammatory cytokines secretion from monocytes/macrophages through suppression of intracellular signaling. Food Chem Toxicol. 2008; 46(1):220–231. https://doi.org/10.1016/j.fct.2007.07.016 PMID: 17868967

68. Youn HS, Lee JK, Choi YJ, Saitoh SI, Miyake K, Hwang DH et al. Cinnamaldehyde suppresses toll-like receptor 4 activation mediated through the inhibition of receptor oligomerization. Biochem Pharmacol. 2008; 75(2):494–502. https://doi.org/10.1016/j.bcp.2007.08.033 PMID: 17920563

69. Gunawardena D, Karunaweera N, Lee S, van Der Kooy F, Harman DG, Raju R et al. Anti-inflammatory activity of cinnamon (C. zeylanicum and C. cassia) extracts–identification of E-cinnamaldehyde and o-methoxy cinnamaldehyde as the most potent bioactive compounds. Food Funct. 2015; 6(3):910–9. https://doi.org/10.1039/c4fo00680a PMID: 25629927

70. Hagenlocher Y, Kiessling K, Schäffer M, Bischoff SC, Lorentz A. Cinnamaldehyde is the main mediator of cinnamon extract in mast cell inhibition. Eur J Nutr. 2015; 54(8):1297–309. https://doi.org/10.1007/s00394-014-0810-0 PMID: 25504111

71. Luo H, Lv XD, Wang GE, Li YF, Kurihara H, He RR. Anti-inflammatory effects of anthocyanins-rich extract from bilberry (Vaccinium myrtillus L.) on croton oil-induced ear edema and Propionibacterium acnes plus LPS-induced liver damage in mice. Int J Food Sci Nutr. 2014; 65(5):594–601. https://doi.org/10.3109/09637486.2014.886184 PMID: 24548119

72. Kolehmainen M, Mykkänen O, Kirjavainen PV, Leppänen T, Moilanen E, Adriaens M et al. Bilberries reduce low-grade inflammation in individuals with features of metabolic syndrome. Mol Nutr Food Res. 2012; 56(10):1501–10. https://doi.org/10.1002/mnfr.201200195 PMID: 22961907

73. Karlsen A, Paur I, Bøhn SK, Sakhi AK, Borge GI, Serafini M et al. Bilberry juice modulates plasma concentration of NF-kappaB related inflammatory markers in subjects at increased risk of CVD. Eur J Nutr. 2010; 49(6):345–55. https://doi.org/10.1007/s00394-010-0092-0 PMID: 20119859

74. Stickel F, Schuppan D. Herbal medicine in the treatment of liver diseases. Dig Liver Dis. 2007; 39:293–304. https://doi.org/10.1016/j.dld.2006.11.004 PMID: 17331820

75. Wink M. Evolutionary advantage and molecular modes of action of multi-component mixtures used in phytomedicine. Curr. Drug Metab. 2008; 9(10):996–1009. PMID: 19075616

76. Wink. Modes of Action of Herbal Medicines and Plant Secondary Metabolites. Medicines. 2015; 2 (3):251–286. https://doi.org/10.3390/medicines2030251 PMID: 28930211

Latin name	Common English name	Common German name	Family	Active compound	Compound classification	Influence on (inflammatory) marker	Beneficial human health effect	Reference
Achillea millefolium	Common yarrow	Gemeine Schafgarbe	*Asteraceae*	Kaempferol, luteolin, apigenin	Flavonoids	↓ ALT, ↓ AST, ↑ GSH, ↓ MPO, ↑ SOD	Ameliorating several neuro-degenerative disorders	Potrich et al., 2010; Yaeesh et al., 2006; Ayoobi et al., 2017
Aesculus hippocastanum	Horse-chestnut	Gewöhnliche Rosskastanie	*Sapindaceae*	Escin	Saponin	↓ IκBα, ↓ NF-κB, ↑ ROS	Prolongation of survival in thyroid cancer patients	Cheong et al., 2018
Alchemilla vulgaris	Common lady's mantle	Spitzlappiger Frauenmantel	*Rosaceae*				Weight loss (when combined with other plants)	Said et al., 2011
Allium sativum	Garlic	Knoblauch	*Amaryllidaceae*	Diallyl sulfide	Sulfide	↓ ALT, ↓ AST, ↓ COX-2, ↓ IL-1β, ↓ iNOS, ↑ insulin, ↓ NF-κB, ↓ TNF-α	Reduction of body fat mass and body weight	Eidi et al., 2006; Soleimani et al., 2016; Suman and Shukla, 2016
Aloe ferox	Aloe	Aloen	*Xanthorrhoeaceae*	Aloeresin I	Glucoside	↓ caspase-1, ↓ COX-1, ↓ ERK, ↓ IL-1β, ↓ IL-6, ↓ IL-8, ↓ JNK, ↓ NF-κB, ↓ NLRP3, ↓ p38, ↓ TNF-α	Wound healing	Speranza et al., 2005; Fawole et al., 2010; Budai et al., 2013; Radha and Laxmipriya, 2014
Alpinia officinarum	Galangal	Galgant	*Zingiberaceae*	Galangin	Flavonoid	↓ IL-6, ↑ IL-10, ↓ NO, ↓ ROS, ↓ TNF-α		Choi et al., 2017
Althaea officinalis	Common marshmallow	Eibisch	*Malvaceae*				Treatment of Old World cutaneous leishmaniasis; Cough reduction	Cravotto et al., 2010

Latin name	Common English name	Common German name	Family	Active compound	Compound classification	Influence on (inflammatory) marker	Beneficial human health effect	Reference
Arctostaphylos uva-ursi	Bearberry	Bärentrauben	*Ericaceae*	Arbutin	Glucoside	↓ COX-2, ↓ IL-1β, ↓ iNOS, ↓ NF-κB, ↓ NO, ↓ TNF-α		Lee and Kim, 2012
Armoracia rusticana	Horseradish	Meerrettich	*Brassicaceae*			↓ c-Jun, ↓ COX-2, ↓ ERK1/2, ↓ IL-6, ↓ NO, ↓ PGE_2, ↓ TNF-α		Marzocco et al., 2015; Herz et al., 2017
Arnica montana	Arnica	Arnika	*Asteraceae*	Helenalin	Sesquiterpene	↓ IL-1β, ↓ IL-6, ↓ IL-12, ↓ NF-κB, ↓ NO, ↓ TNF-α	Osteoarthritis	Lass et al., 2008; Chahal et al., 2013; Dragos et al., 2017
Artemisia absinthium	Wormwood	Wermutkraut	*Asteraceae*		Flavonoids	↓ COX-2, ↓ iNOS, ↓ NF-κB, ↓ NO, ↓ PGE_2, ↓ TNF-α	Crohn's disease	Lee et al., 2004; Omer et al., 2007; Krebs et al., 2010
Avena sativa	Oat	Saat-Hafer	*Poaceae*	β-Glucan	Glucan	↓ COX-2, ↓ NO, ↑ TGFβ1, ↓ TNF-α	Anti-diabetic, prevention of cardiovascular diseases, protection against breast cancer	Singh et al., 2013
Boswellia carterii	Frankincense	Afrikanischer Weihrauch	*Burseraceae*	Boswellic acid	Triterpene	↓ 5-LOX, ↓ AChE, ↑ GSH, ↓ MDA		Safayhi et al., 2000; Ebrahimpour et al., 2017
Boswellia serrata	Frankincense	Weihrauch	*Burseraceae*	Boswellic acid	Triterpene	↓ 5-LOX, ↓ IFNγ, ↓ IL-1β, ↓ IL-2, ↑ IL-4, ↓ IL-6, ↑ IL-10, ↓ IL-12, ↓ NO, ↓ TNF-α	Osteoarthritis	Safayhi et al., 2000; Gayathri et al., 2007; Dragos et al., 2017
Calendula officinalis	Marigold	Ringelblume	*Asteraceae*		Several triterpenes and flavonoids	↓ COX-2, ↓ IL-1(β), ↓ TNF-α	Wound healing; Prevention of acute dermatitis	Ukiya et al., 2006; Cravotto et al., 2010; Kirichenko et al., 2016; Alexandre et al., 2017

Latin name	Common English name	Common German name	Family	Active compound	Compound classification	Influence on (inflammatory) marker	Beneficial human health effect	Reference
Camellia sinensis (L.)	Green tea	Grüner Tee	*Theaceae*	EGCG	Flavonoid	↓ COX-2, ↓ IFNγ, ↓ NF-κB, ↑ ROS, ↓ TNF-α	Metabolism, cardiovascular system, neuro-degenerative diseases and cancer	Cooper et al., 2005; Arab et al., 2009; Shirakami et al., 2016
Capsicum frutescens	Chili	Chili	*Solanaceae*	Capsaicin	Polyunsaturated alkamide	↓ AP-1, ↓ IκBα, ↓ NF-κB	Pain reduction	Han et al., 2001; Bortolotti and Porta, 2011; Gagnier et al., 2016
Carum carvi	Caraway	Echter Kümmel	*Apiaceae*			↓ cholesterol, ↓ triglycerides	Anti-obesity	Lemhadri et al., 2006; Kazemipoor et al., 2013
Castanea sativa	Sweet chestnut	Edelkastanie	*Fagaceae*		Phenols	↓ NF-κB, ↓ RAGE, ↓ $O_2^{\cdot-}$, ↓ ·OH		Calliste et al., 2005; Jovanović et al., 2017
Chelidonium majus	Celandine	Schöllkraut	*Papaveraceae*	Berberine, norchelidonine, chelidonine, 8-hydroxydihydro-sanguinarine	Alkaloids	↓ COX-2, ↓ iNOS, ↓ NO, ↓ PGE_2	Anticancer drug (Ukrain) based on plant extract	Kuo et al., 2004; Ernst and Schmidt, 2005; Park et al., 2011
Chlorella pyrenoidosa	Chlorella	Chlorella	*Chlorellaceae*	Rhamnose, glucose, galactose, mannose, xylose	Mono-saccharides	↑ IL-1β	Pregnant and breastfeeding women	Nakano et al., 2007; Nakano et al., 2010; Chahal et al., 2013
Cinchona pubescens	Cinchona	Chinarinde	*Rubiaceae*	Quinine	Quinoline	↓ NF-κB	Malaria treatment	An et al., 2017
Cinnamomum verum	Cinnamon	Zimt	*Lauraceae*	Cinnamaldehyde	Flavonoid	↓ IκB, ↓ iNOS, ↓ MyD88, ↓ NF-κB, ↓ TNF-α	Anti-hyperlipidaemic and blood pressure lowering, stimulation of glycogen synthesis and insulin secretion	Khan et al., 2003; Kanuri et al., 2009; Hariri and Ghiasvand, 2016; Ranasinghe et al., 2017

Latin name	Common English name	Common German name	Family	Active compound	Compound classification	Influence on (inflammatory) marker	Beneficial human health effect	Reference
Coriandrum sativum	Coriander	Echter Koriander	*Apiaceae*			↓ COX-2, ↓ IL-1β, ↓ iNOS, ↓ NO, ↓ PGE_2	Reduction of UV-induced erythema	Reuter et al., 2008; Wu et al., 2010
Crataegus species	Hawthorn	Weißdorn	*Rosaceae*	Vitexin	Flavonoid	↓ IL-1(β), ↑ IL-10, ↓ NO, ↓ p-ERK1/2, ↓ PGE_2, ↓ p-JNK, ↓ p-p38, ↓ TNF-α	Adjunctive treatment for chronic heart failure; Hypotensive and hypolipidemic effects	Pittler et al., 2003; Walker et al., 2006; Dalli et al., 2011; Kirichenko et al., 2016; Rosa et al., 2016
Curcuma longa	Turmeric	Kurkuma	*Zingiberaceae*	Curcumin	Catechol	↓ AP-1, ↓ COX-2, ↓ IFNγ, ↓ IL-1, ↓ IL-6, ↓ IL-8, ↓ IL-12, ↓ iNOS, ↓ JNK, ↓ NF-κB, ↓ RANKL, ↓ TNF-α	Suppression of IBD symptoms; Osteoarthritis	Joe et al., 2004; Goel et al., 2008; Pari et al., 2008; Baliga et al., 2012; Dragos et al., 2017
Cynara scolymus	Artichoke	Artischocken	*Asteraceae*			↓ CRP, ↓ Fg, ↓ MDA	Decreased cholesterol level	Bundy et al., 2008; Ben Salem et al., 2017
Daucus carota subsp. *sativus*	Carrot	Karotte	*Apiaceae*	*trans*-Asarone	Anisole	↓ COX-2		Momin et al., 2003
				2,4,5-Trimethoxybenz-aldehyde	Benzaldehyde			
Digitalis purpurea	Common foxglove	Roter Fingerhut	*Plantaginaceae*	Digoxin	Digitalis glycoside		Cardiac disorders	Hauptman and Kelly, 1999
Dioscorea villosa	Yam	Yams	*Dioscoreaceae*	Diosgenin	Cholestane	↓ p-AKT, ↓ p-ERK, ↓ p-JNK, ↓ p-p38, ↓ ROS, ↓ TNF-α		Choi et al., 2010
Echinacea purpurea	Purple coneflower	Purpur-Sonnenhut	*Asteraceae*		Alkamides	↓ COX-1, ↓ COX-2, ↓ IL-1β, ↓ IL-6, ↓ IL-8, ↓ NO, ↓ TNF-α		Senchina et al., 2006; Woelkart and Bauer, 2007; Sharma et al., 2009

Latin name	Common English name	Common German name	Family	Active compound	Compound classification	Influence on (inflammatory) marker	Beneficial human health effect	Reference
Elettaria cardamomum	Cardamom	Kardamom	*Zingiberaceae*	Cardamonin	Flavonoid	↓ COX-2, ↓ IL-1β, ↓ IL-6, ↓ iNOS, ↓ NF-κB, ↓ NO, ↓ PGE_2, ↓ TNF-α		Prasad and Aggarwal, 2014
Equisetum arvense	Field horsetail	Acker-Schachtelhalm	*Equisetaceae*	Kynurenic acid	Quinoline	↓ IFNγ, ↓ TNF-α	Rheumatoid arthritis	Gründemann et al., 2014; Dragos et al., 2017
Erythraea centaurium	Common centaury	Echtes Tausendgülden-kraut	*Gentianaceae*			↓ ALT, ↓ AST, ↓ LDH		Mroueh et al., 2004
Euphrasia officinalis	Eyebright	Gemeiner Augentrost	*Orobanchaceae*			↓ IL-1β, ↓ IL-6, ↓ TNF-α		Paduch et al., 2014
Filipendula ulmaria	Meadowsweet	Mädesüß	*Rosaceae*	Quercetin	Flavonoid	↓ COX-1, ↓ COX-2, ↓ IL-1β, ↓ IL-6, ↓ TNF-α		Drummond et al., 2013; Katanić et al., 2016
Foeniculum vulgare	Fennel	Fenchel	*Apiaceae*	Limonene *trans*-Anethole	Cyclohexene Anisole	↓ IL-6, ↓ LDH, ↓ NO, ↓ p-ERK, ↓ TNF-α		Lee et al., 2015
Fucus vesiculosus	Bladderwrack	Blasentang	*Fucaceae*	Fucoidan	Polysaccharide	↓ COX-2, ↓ NO		Lim et al., 2015
Gentiana lutea	Gentian	Enzian	*Gentianaceae*	Gentiopicroside	Glucoside	↓ ERK 1/2, ↓ iNOS, ↓ MPO, ↓ NO		Nastasijević et al., 2012; Kesavan et al., 2013
Geranium robertianum	Herb robert	Ruprechtskraut	*Geraniaceae*			↓ NO		Catarino et al., 2017
Ginkgo biloba	Ginkgo	Ginkgo	*Ginkgoaceae*	Bilobalide	Ginkgolide	↓ ERK1/2	Enhancing certain neuro-psychological / memory processes	Mix and Crews, 2002; Dodge et al., 2008; Weinmann et al., 2010; Chahal et al., 2013
Glycyrrhiza glabra	Liquorice	Süßholz	*Fabaceae*	Isoliquiritigenin	Flavonoid	↓ COX-2, ↓ iNOS, ↓ IRF3, ↓ NF-κB	Decrease of mucositis and oral mucosal irritation	Park and Youn, 2010; Najafi et al., 2017

Latin name	Common English name	Common German name	Family	Active compound	Compound classification	Influence on (inflammatory) marker	Beneficial human health effect	Reference
Hamamelis virginiana	Witch hazel	Hamamelis	*Hamamelidaceae*	Hamamelitannin	Benzoate	↓ TNF-α	Erythema suppression	Hughes-Formella et al., 1998; Habtemariam, 2002
Harpagophytum procumbens	Devil's claw	Afrikanische Teufelskralle	*Pedaliaceae*	Harpagoside, harpagide, procumbide	Iridoid glycosides	↓ c-FOS, ↓ COX-2, ↓ IL-1β, ↓ iNOS, ↓ NF-κB, ↓ TNF-α	Osteoarthritis and low back pain	Gagnier et al., 2004; Rodriguez Villanueva et al., 2016; Dragos et al., 2017
Hedera helix	Common ivy	Efeu	*Araliaceae*	α-Hederin	Saponin	↓ IL-17		Ebrahimi et al., 2016
Hibiscus sabdariffa	Roselle	Roselle	*Malvaceae*		Polyphenols	↓ COX-2, ↓ ERK1/2, ↓ IFNγ, ↓ IL-6, ↑ IL-10, ↓ JNK, ↓ NF-κB, ↓ NO, ↓ p38, ↓ PGE_2, ↓ ROS, ↓ TNF-α		Da-Costa-Rocha et al., 2014; Herranz-López et al., 2017
Humulus lupulus	Hops	Hopfen	*Cannabaceae*	Xanthohumol	Flavonoid	↓ IL-1β, ↓ MCP-1, ↓ NF-κB, ↓ NO, ↓ TNF-α		Lupinacci et al., 2009; Lee et al., 2011
Hypericum perforatum	St John's wort	Echtes Johanniskraut	*Hypericaceae*	Pseudohypericin	Benz(a)-anthracene	↓ COX-2, ↓ IL-1, ↓ IL-6, ↓ NO, ↓ PGE_2, ↓ TNF-α	Depression	Schulz, 2006; Kasper et al., 2010; Huang et al., 2012; Kirichenko et al., 2016; Bonaterra et al., 2018
					Flavonoids			
				Amentoflavone, quercetin				
				Chlorogenic acid	Cyclohexane			
Ilex paraguariensis	Yerba mate	Mate-Strauch	*Aquifoliaceae*	Quercetin	Flavonoid	↓ COX-2, ↑ IκBα, ↓ iNOS, ↓ NF-κB, ↓ TNF-α		Arçari et al., 2011; Bracesco et al., 2011; Pimentel et al., 2013
Juniperus communis	Common juniper	Gemeiner Wacholder	*Cupressaceae*	Amentoflavone	Flavonoid	↓ ALT, ↓ ALP, ↓ AST, ↓ TNF-α		Bais et al., 2017
Marrubium vulgare	Common horehound	Andornkraut	*Lamiaceae*	Marrubiin	Diterpene	↓ COX-2		Sahpaz et al., 2002; Meyre-Silva et al., 2005

Latin name	Common English name	Common German name	Family	Active compound	Compound classification	Influence on (inflammatory) marker	Beneficial human health effect	Reference
Matricaria chamomilla	Chamomile	Kamille	*Asteraceae*	Apigenin	Flavonoid	↓ IL-1β, ↓ IL-6, ↓ TNF-α		Drummond et al., 2013
Melilotus officinalis	Sweet clover	Steinkleekraut	*Fabaceae*	Caffeic acid	Cinnamate	↓ COX-2, ↓ IL-6, ↓ iNOS, ↓ NF-κB, ↓ NO, ↓ PGE_2, ↓ TNF-α		Bazazzadegan et al., 2017; Liu et al., 2018
Melissa officinalis	Lemon balm	Zitronenmelisse	*Lamiaceae*	Rosmarinic acid	Benzoate	↓ IL-1β, ↓ IL-6, ↓ IRAK1, ↓ MyD88, ↓ TLR4, ↓ TNF-α, ↓ TRAF6		Jiang et al., 2017; Chizzola et al., 2018
Mentha piperita	Peppermint	Pfefferminze	*Lamiaceae*			↓ PGE_2, ↓ NO		Sun et al., 2014
Origanum majorana	Marjoram	Majoran	*Lamiaceae*	Rosmarinic acid	Benzoate	↓ IL-1β, ↓ IL-6, ↓ TNF-α		Villalva et al., 2018
Panax ginseng	Ginseng	Ginseng	*Araliaceae*	Ginsan	Polysaccharide Saponins	↓ COX-2, ↓ IFNγ, ↓ IL-1β, ↓ IL-6, ↓ IL-12, ↓ IL-18, ↓ iNOS, ↓ MyD88, ↓ TLR4, ↓ TNF-α	Osteoarthritis; Improvement of glucose metabolism and modulating of immune response	Kang and Min, 2012; Chahal et al., 2013; Shergis et al., 2013; Dragos et al., 2017
Petroselinum crispum	Parsley	Petersilie	*Apiaceae*	Apigenin	Flavonoid	↓ NO	Increase in anti-oxidant enzymes	Nielsen et al., 1999; Farzaei et al., 2013
Pimpinella anisum	Anise	Anis	*Apiaceae*	Anethole	Anisole	↓ AP-1, ↑ IL-10, ↓ NF-κB, ↓ p38, ↓ TNF-α		Aprotosoaie et al., 2016
Plantago lanceolata	Ribwort	Spitzwegerich	*Plantaginaceae*	Acteoside	Phenol glycoside	(↓ COX-1), (↓ COX-2), ↓ IL-8, ↓ iNOS, ↓ MCP-1, ↓ NO		Murai et al., 1995; Vigo et al., 2005; Fakhrudin et al., 2017
Rheum palmatum	Rhubarb	Rhabarber	*Polygonaceae*	Rhein, emodin	Anthraquinones	↓ TNF-α		Chahal et al., 2013
Rosmarinus officinalis	Rosemary	Rosmarin	*Lamiaceae*	Rosmarinic acid	Benzoate	↓ IL-1β, ↓ IL-6, ↑ NF-κB, ↓ TNF-α		Rocha et al., 2015

Latin name	Common English name	Common German name	Family	Active compound	Compound classification	Influence on (inflammatory) marker	Beneficial human health effect	Reference
Rubus fruticosus	Blackberry	Brombeere	*Rosaceae*	Cyanidin-3-O-glucoside	Anthocyanin	↓ iNOS, ↓ NF-κB, ↓ NO		Pergola et al., 2006; Zia-Ul-Haq et al., 2014
Salix alba	White willow	Silber-Weide	*Salicaceae*	Salicin	Glucoside	↓ COX-2, ↓ IL-6, ↓ NF-κB, ↓ TNF-α	Pain relief	Drummond et al., 2013; Shara and Stohs, 2015; Dragos et al., 2017
Salvia officinalis	Salvia	Salbei	*Lamiaceae*		Different flavonoids and terpenes	↓ MDA, ↓ NF-κB, ↓ NO, ↓ TNF-α		Ghorbani and Esmaeilizadeh, 2017; Kolac et al., 2017
Sambucus nigra (L.)	Elderflowers	Holunder	*Adoxaceae*		Anthocyanins	↓ IFNγ, ↓ IL-1, ↓ TNF-α		Badescu et al., 2015; Kirichenko et al., 2016
Schinus terebinthifolius	Brazilian pepper tree	Brasilianischer Pfefferbaum	*Anacardiaceae*			↓ CXCL1, ↓ IL-1β, ↓ IL-6, ↓ TNF-α	Reduction of gingival inflammation	Freires et al., 2013; Rosas et al., 2015
Spirulina	Spirulina	Spirulina	*Spirulinaceae*	Phycocyanin	Phycobiliprotein	↓ IL-6, ↑ Nrf2, ↓ TNF-α		Khafaga and El-Sayed, 2018; Kim et al., 2018
Symphytum officinale	Comfrey	Echter Beinwell	*Boraginaceae*	Rosmarinic acid Salvianolic acid	Benzoate Cinnamate	↓ IL-1β, ↓ IL-6, ↓ NF-κB, ↓ NO, ↓ TNF-α	Reduction of pain, inflammation and swelling	Koll et al., 2004; Giannetti et al., 2010; Staiger, 2013; Dragos et al., 2017; Trifan et al., 2018
Syzygium aromaticum	Clove	Nelken	*Myrtaceae*	Eugenol	Cinnamate	↓ COX-2, ↓ NF-κB	Local anti-inflammatory, antiseptic, and anesthetic effects on dental pulp	Fujisawa and Murakami, 2016
Tanacetum parthenium	Feverfew	Mutterkraut	*Asteraceae*	Tanetin Parthenolide	Flavonoid Sesquiterpene	↓ 5-LOX, ↓ COX-2, ↓ IL-6, ↓ IL-8, ↓ iNOS, ↓ NF-κB, ↓ NO, ↓ TNF-α		Williams et al., 1995; Mazor et al., 2000; Aviram et al., 2012; Magni et al., 2012
Taraxacum officinale	Dandelion	Löwenzahn	*Asteraceae*	Taraxinic acid β-d-glucopyranosyl	Sesquiterpene	↑ Hmox1, ↓ iNOS,		Liu et al., 2014; Esatbeyoglu et al.,

Latin name	Common English name	Common German name	Family	Active compound	Compound classification	Influence on (inflammatory) marker	Beneficial human health effect	Reference
				ester		↓ NF-κB, ↑ Nrf2		2017
Thymus vulgaris	Common thyme	Thymian	*Lamiaceae*	Thymol	Monoterpene	↓ IL-1β, ↓ TNF-α		Amirghofran et al., 2011; Oliveira et al., 2017
Tropaeolum majus	Nasturtium	Kapuzinerkresse	*Tropaeolaceae*	Benzyl glucosinolate	Isothiocyanate	↓ COX-2, ↓ ERK1/2, ↓ JNK, ↓ PGE_2		Rodriguez Villanueva et al., 2016
Uncaria tomentosa	Cat's claw	Katzenkralle	*Rubiaceae*	Mitraphylline	Indole alkaloid	↓ c-Fos, ↓ c-Jun, ↓ IL-1α, ↓ IL-1β, ↓ IL-4, ↓ IL-17, ↓ Jun-B, ↓ Jun-D, ↓ TNF-α	Adjuvant treatment for reducing adverse chemotherapy effects	Sandoval et al., 2000; Allen-Hall et al., 2010; Rojas-Duran et al., 2012; Santos Araújo et al., 2012
Urtica dioica	Stinging nettle	Große Brennnessel	*Urticaceae*	Hydroxycinnamic acid, chlorogenic acid	Cinnamate	↓ 12-LOX, ↓ COX-1, ↓ COX-2, ↓ MCP-1, ↓ NO		Carvalho et al., 2017; Franciškovic et al., 2017
Usnea barbata	Barber's itch	Bartflechte	*Parmeliaceae*	Usnic acid	Benzofuran	↓ PGE_2		Engel et al., 2007; Ranković et al., 2012
Vaccinium myrtillus	Bilberry	Heidelbeere	*Ericaceae*		Anthocyanins	↓ COX-2, ↓ IL-6, ↓ IL-12, ↓ iNOS	Different inflammatory processes	Sautebin et al., 2004; Karlsen et al., 2010; Kolehmainen et al., 2012
Valeriana officinalis (L.)	Common valerian	Echter Baldrian	*Caprifoliaceae*	Valerenic acid	Sesquiterpene	↓ MDA		Nam et al., 2013
Vanilla planifolia	Vanilla	Gewürzvanille	*Orchidaceae*	Vanillin	Benzaldehyde	↑ GSH, ↓ MDA, ↓ NF-κB, ↓ TNF-α		Elseweidy et al., 2017
Verbena officinalis	Common vervain	Echtes Eisenkraut	*Verbenaceae*					
Vigna radiata	Mung bean (dried)	Mungbohnen (getrocknet)	*Fabaceae*	Gallic acid Vitexin, isovitexin	Benzoate Flavonoids	↓ IL-1β, ↓ IL-6, ↓ IL-12β, ↓ iNOS, ↓ TNF-α		Tang et al., 2014
Vigna radiata	Mung bean (cooked in boiling water for	Mungbohnen (gekocht)	*Fabaceae*	Gallic acid Vitexin, isovitexin	Benzoate Flavonoids	↓ IL-1β, ↓ IL-6, ↓ IL-12β,		Tang et al., 2014

Latin name	Common English name	Common German name	Family	Active compound	Compound classification	Influence on (inflammatory) marker	Beneficial human health effect	Reference
	20 min)					↓ iNOS, ↓ TNF-α		
Viscum album	European mistletoe	Weißbeerige Mistel	*Santalaceae*		Diarylheptanoids	↓ IL-6, ↓ IL-12, ↓ TNF-α	Quality of life and reduction of side effects in cancer	Kienle and Kiene, 2010; Büssing et al., 2012; Nhiem et al., 2013
Zingiber officinale	Ginger	Ingwer	*Zingiberaceae*	6-Gingerol, 6-shogaol	Catechols	↓ AP-1, ↓ COX-1, ↓ COX-2, ↓ IL-1β, ↓ IL-12, ↓ IκBα, ↓ LOX, ↓ NF-κB, ↓ TNF-α	Antiemetic and inhibition of nausea and vomiting in pregnancy; Beneficial effects in osteoarthritis	Prasad and Aggarwal, 2014; Mohd Yusof, 2016; Dragos et al., 2017

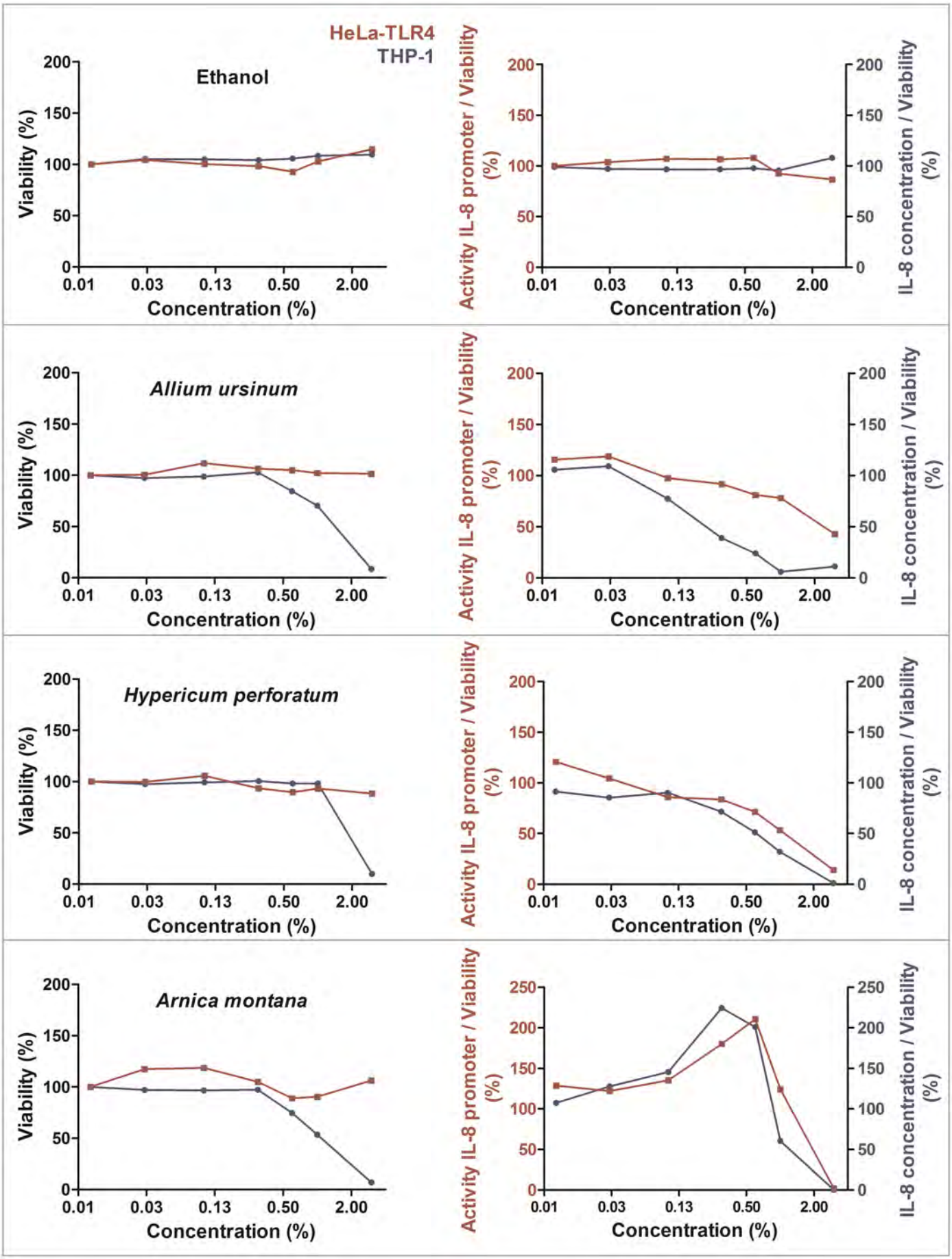
HeLa-TLR4
THP-1
Ethanol
Viability (%)
Activity IL-8 promoter / Viability (%)
IL-8 concentration / Viability (%)
Concentration (%)
0.01
0.03
0.13
0.50
2.00
Allium ursinum
Hypericum perforatum
Arnica montana

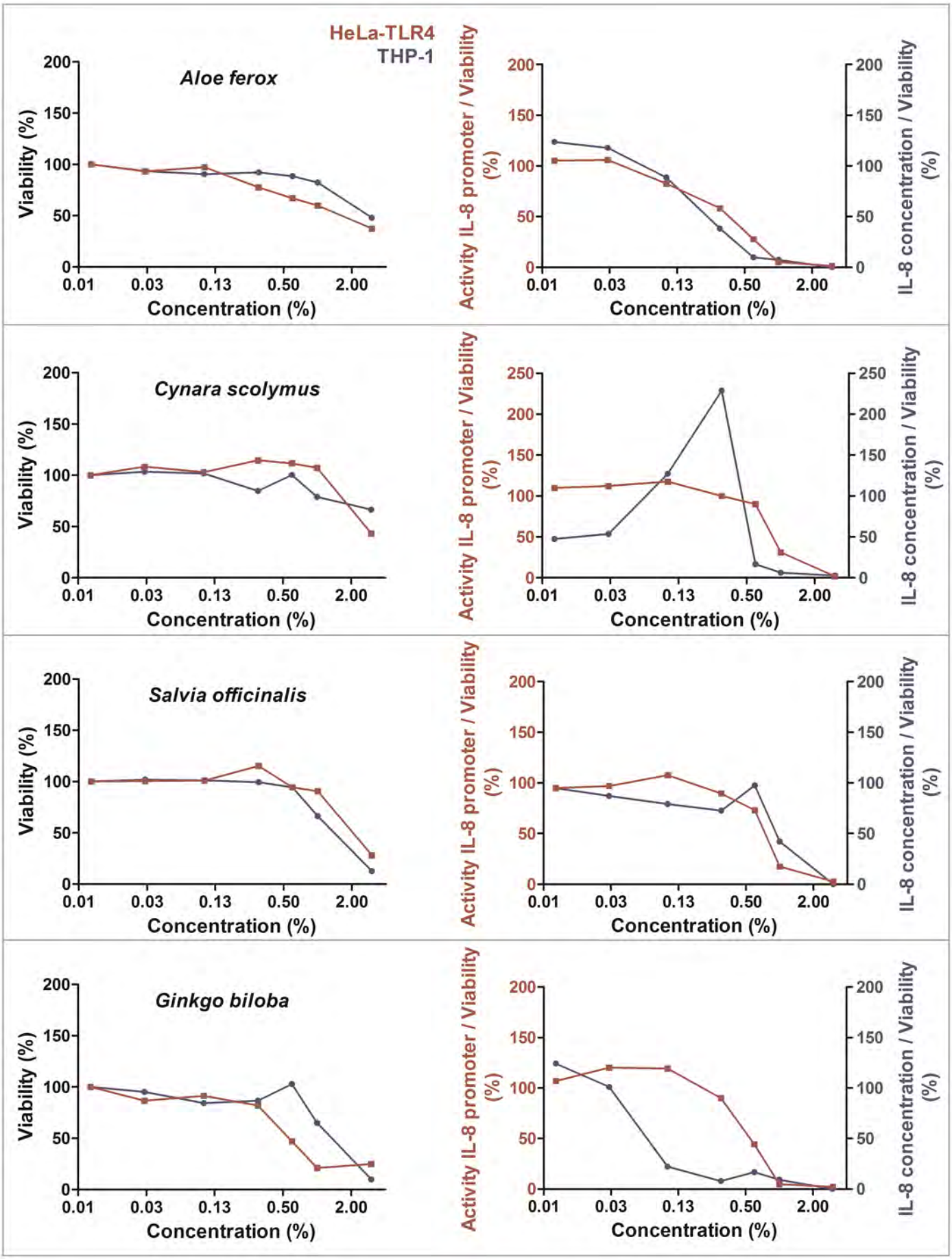
HeLa-TLR4
THP-1
Aloe ferox
Cynara scolymus
Salvia officinalis
Ginkgo biloba
Viability (%)
Activity IL-8 promoter / Viability (%)
IL-8 concentration / Viability (%)
Concentration (%)
0.01
0.03
0.13
0.50
2.00

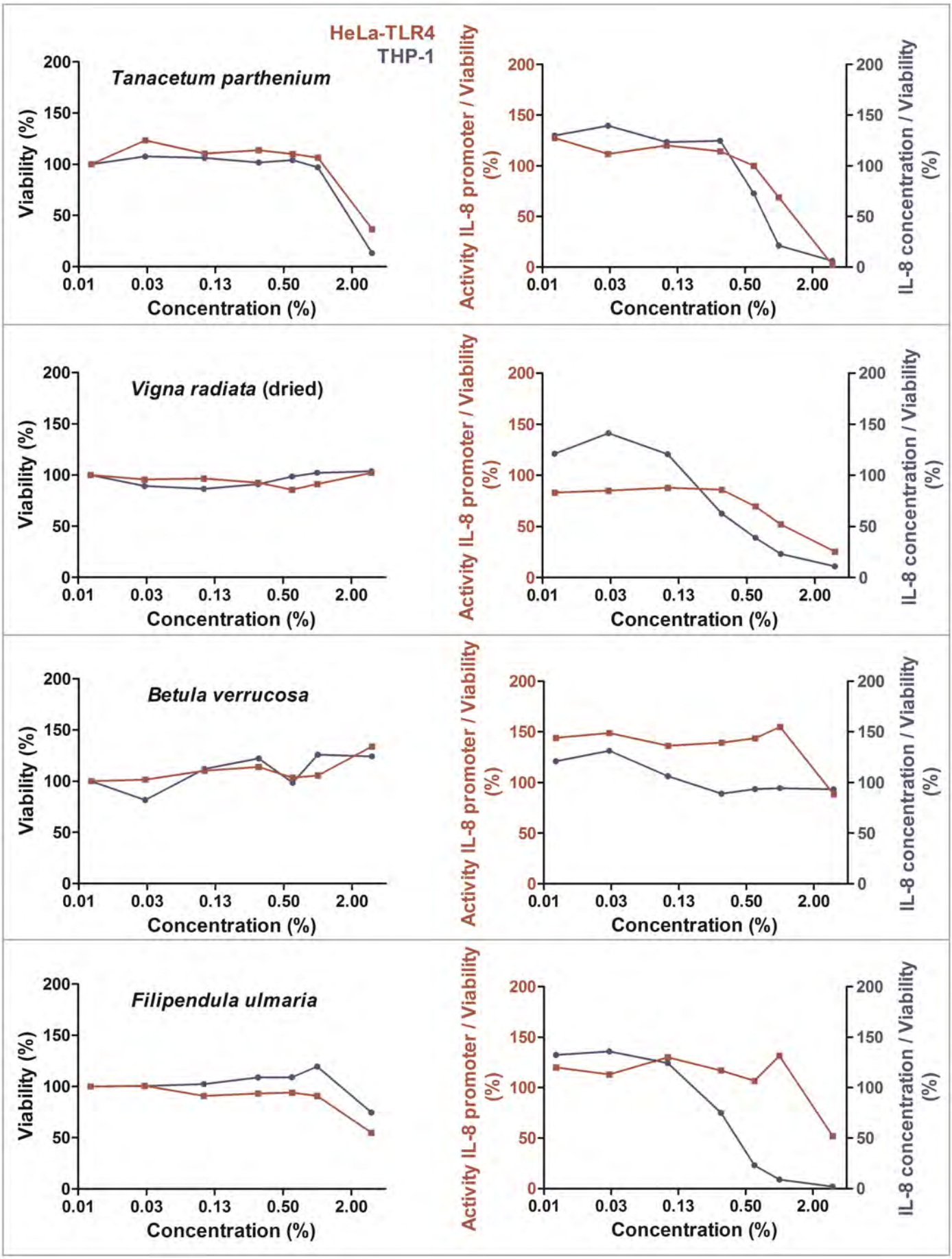
HeLa-TLR4
THP-1
Tanacetum parthenium
Vigna radiata (dried)
Betula verrucosa
Filipendula ulmaria
Viability (%)
Activity IL-8 promoter / Viability (%)
IL-8 concentration / Viability (%)
Concentration (%)
0.01
0.03
0.13
0.50
2.00
0
50
100
150
200

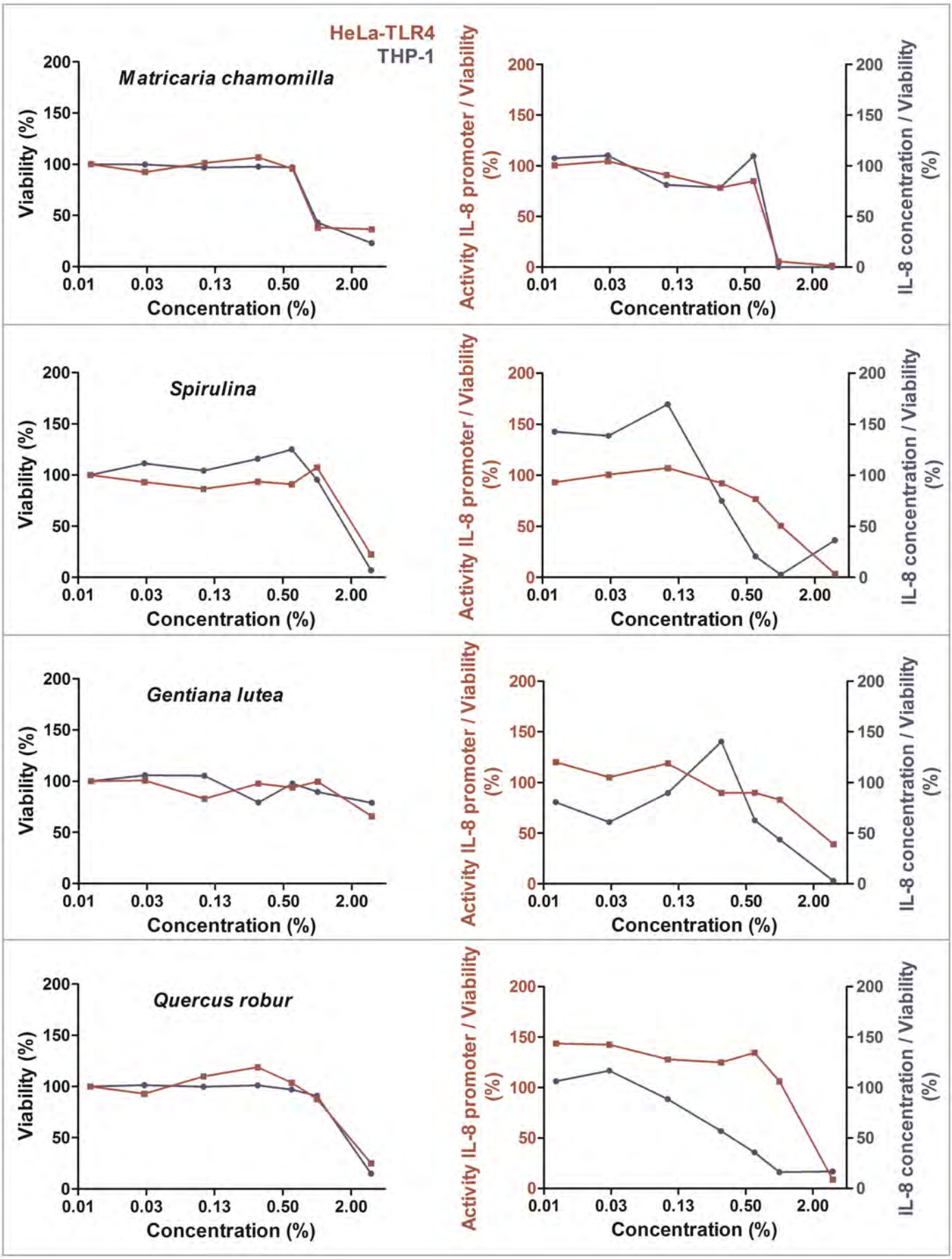
HeLa-TLR4
THP-1
Matricaria chamomilla
Spirulina
Gentiana lutea
Quercus robur
Viability (%)
Activity IL-8 promoter / Viability (%)
IL-8 concentration / Viability (%)
Concentration (%)
0.01
0.03
0.13
0.50
2.00
0
50
100
150
200

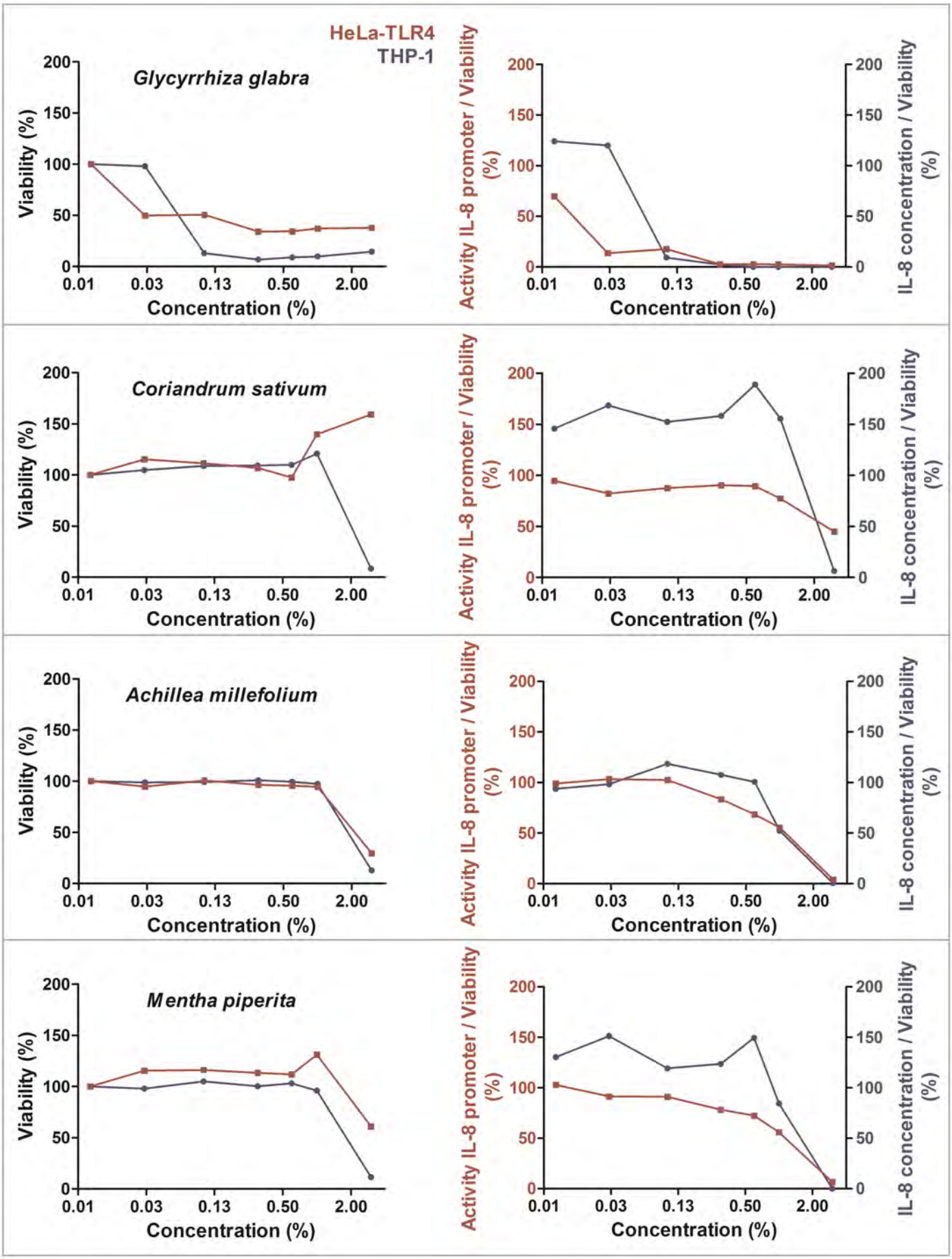
HeLa-TLR4
THP-1
Glycyrrhiza glabra
Coriandrum sativum
Achillea millefolium
Mentha piperita
Viability (%)
Activity IL-8 promoter / Viability (%)
IL-8 concentration / Viability (%)
Concentration (%)
0.01
0.03
0.13
0.50
2.00
0
50
100
150
200

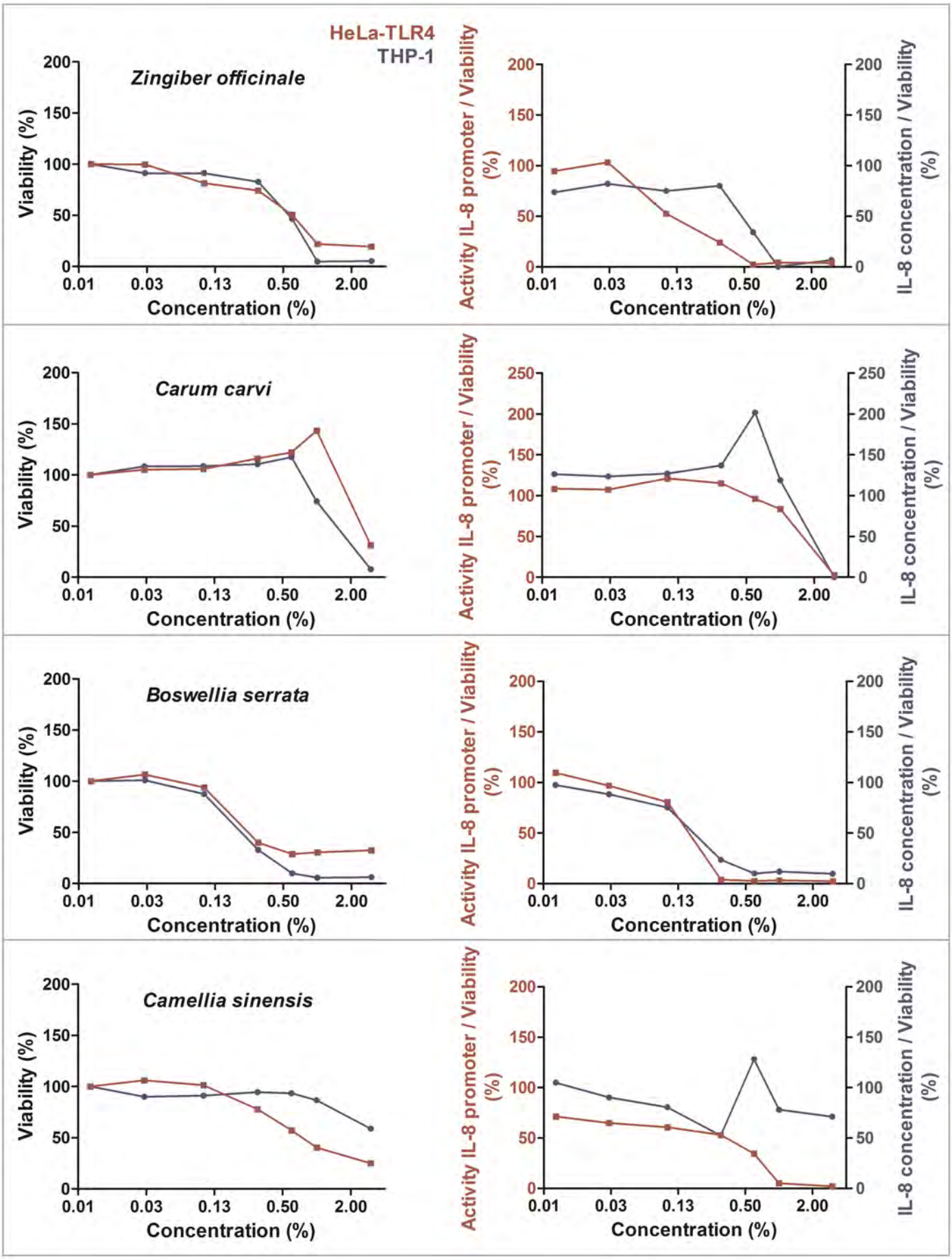
HeLa-TLR4
THP-1
Zingiber officinale
Carum carvi
Boswellia serrata
Camellia sinensis
Viability (%)
Activity IL-8 promoter / Viability (%)
IL-8 concentration / Viability (%)
Concentration (%)
0.01
0.03
0.13
0.50
2.00

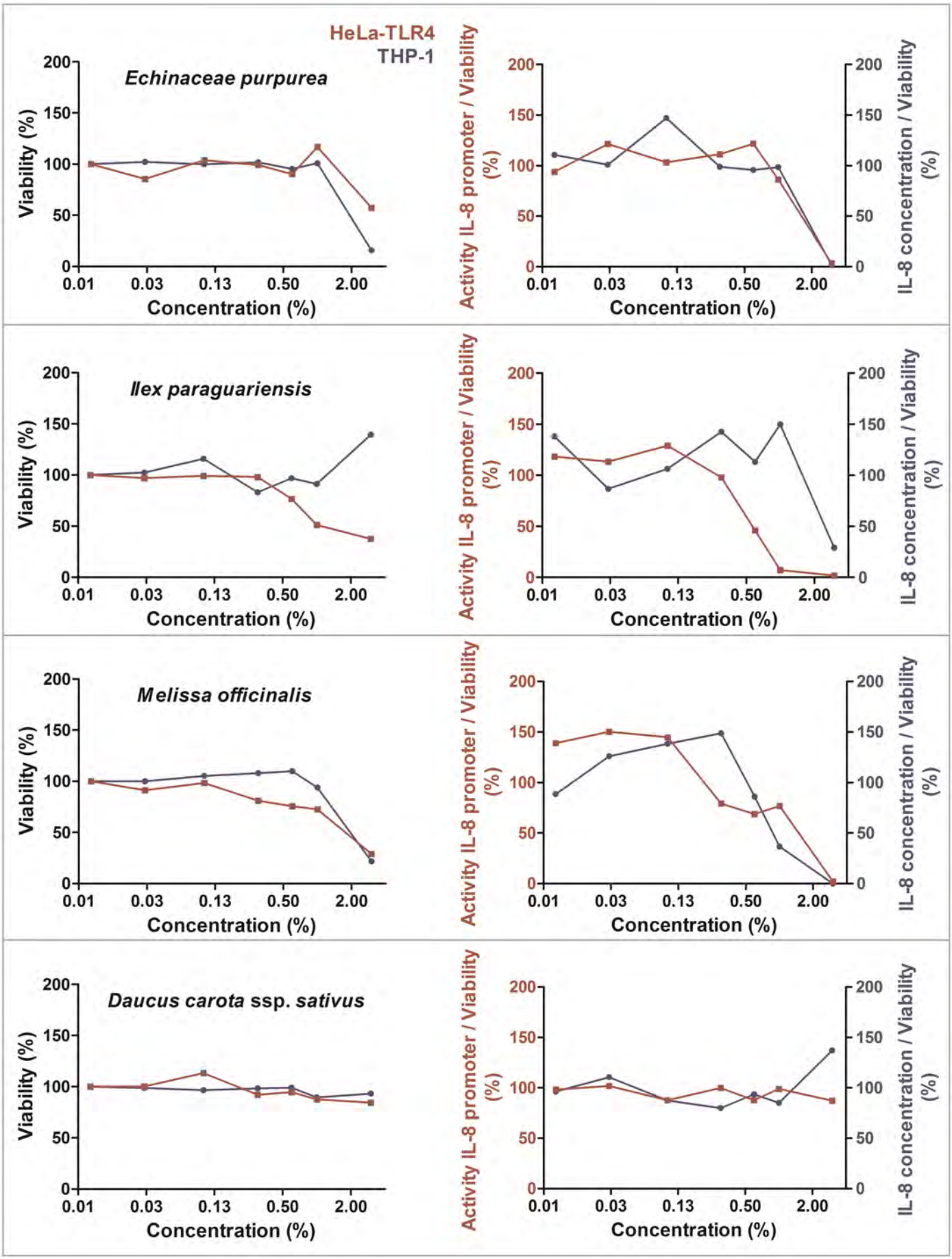
HeLa-TLR4
THP-1
Echinaceae purpurea
Ilex paraguariensis
Melissa officinalis
Daucus carota ssp. sativus
Viability (%)
Activity IL-8 promoter / Viability (%)
IL-8 concentration / Viability (%)
Concentration (%)
0.01
0.03
0.13
0.50
2.00
0
50
100
150
200

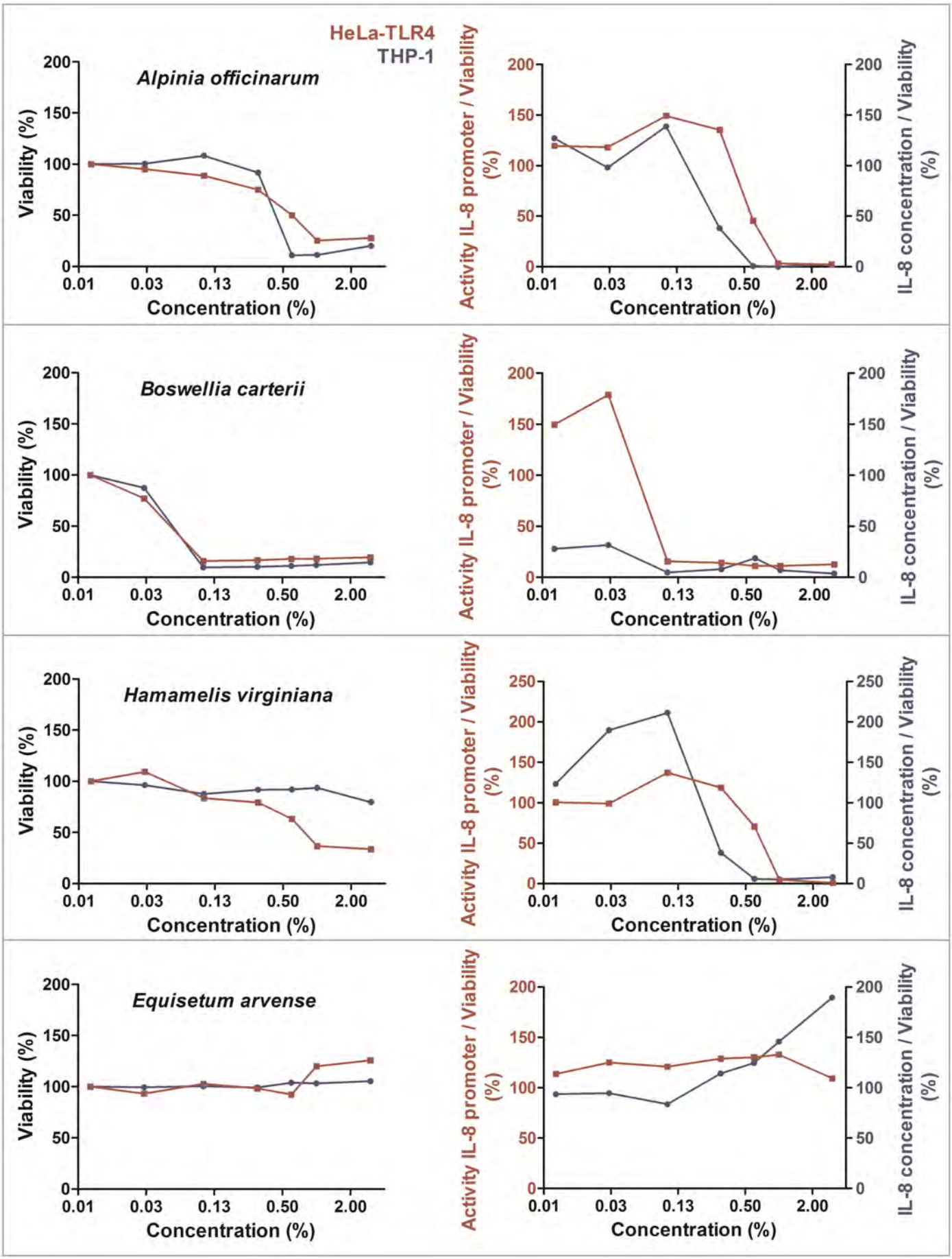
HeLa-TLR4
THP-1
Alpinia officinarum
Boswellia carterii
Hamamelis virginiana
Equisetum arvense
Viability (%)
Activity IL-8 promoter / Viability (%)
IL-8 concentration / Viability (%)
Concentration (%)
0.01
0.03
0.13
0.50
2.00

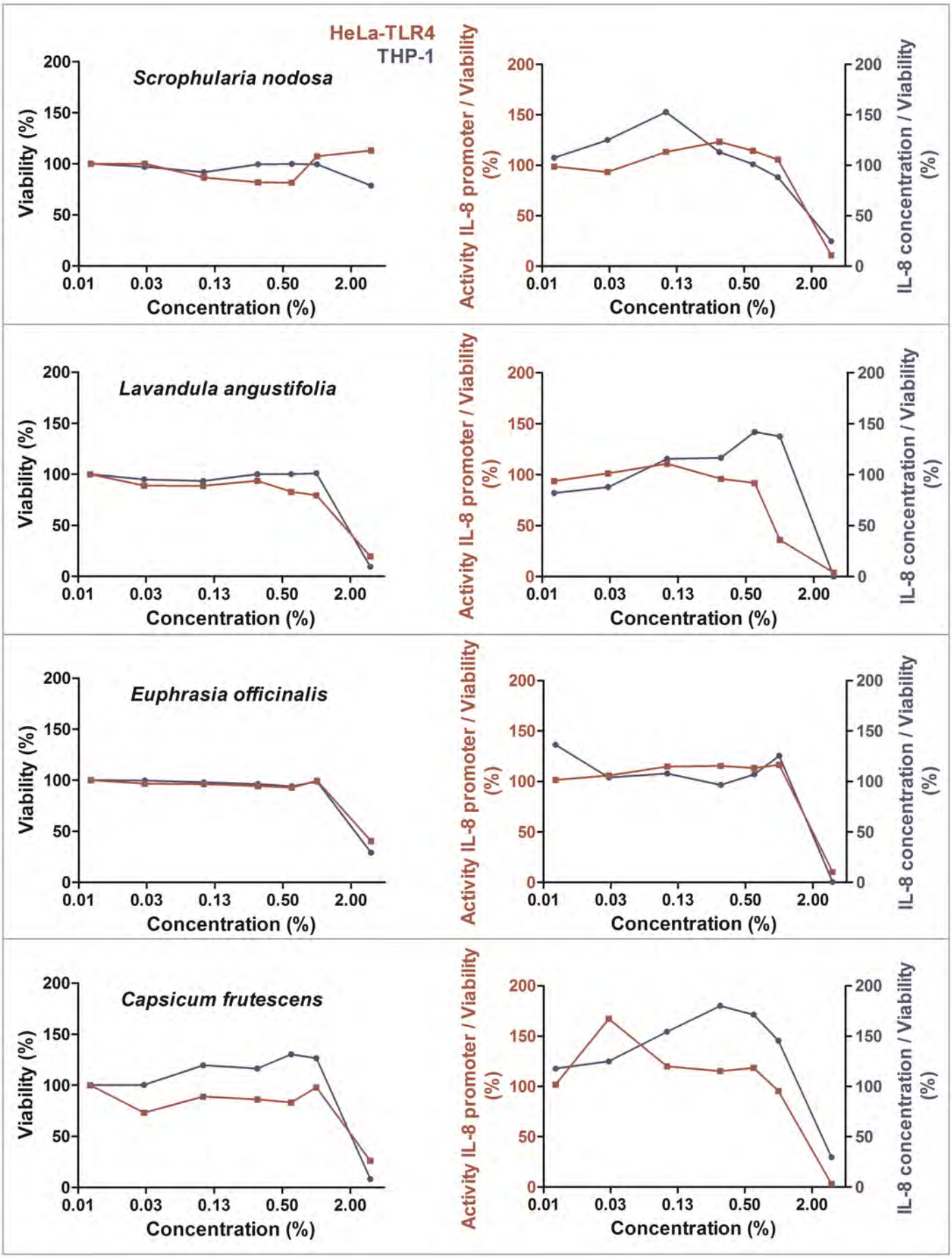
HeLa-TLR4
THP-1
Scrophularia nodosa
Lavandula angustifolia
Euphrasia officinalis
Capsicum frutescens
Viability (%)
Activity IL-8 promoter / Viability (%)
IL-8 concentration / Viability (%)
Concentration (%)
0.01
0.03
0.13
0.50
2.00
0
50
100
150
200

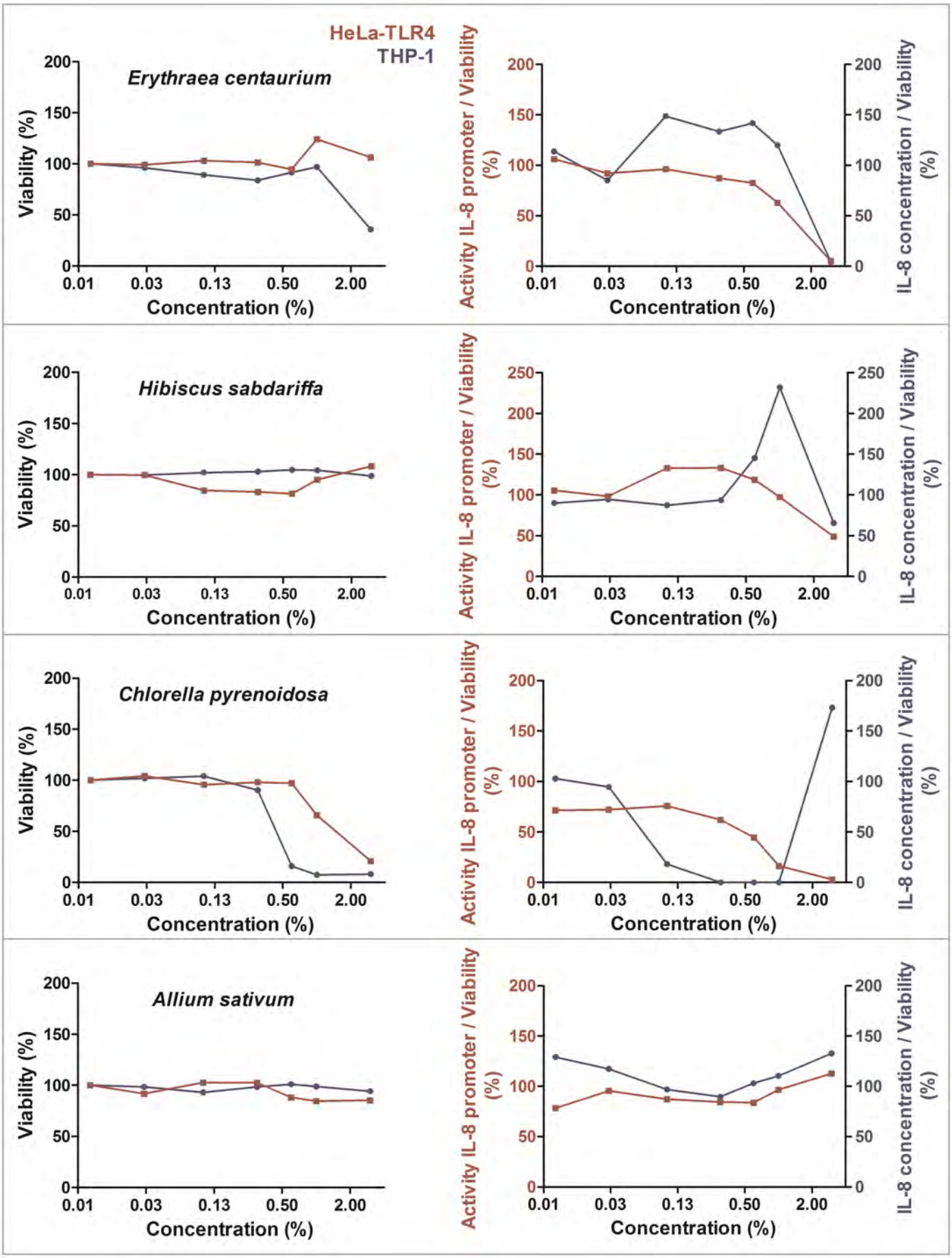
HeLa-TLR4
THP-1
Erythraea centaurium
Hibiscus sabdariffa
Chlorella pyrenoidosa
Allium sativum
Viability (%)
Activity IL-8 promoter / Viability (%)
IL-8 concentration / Viability (%)
Concentration (%)
0.01
0.03
0.13
0.50
2.00

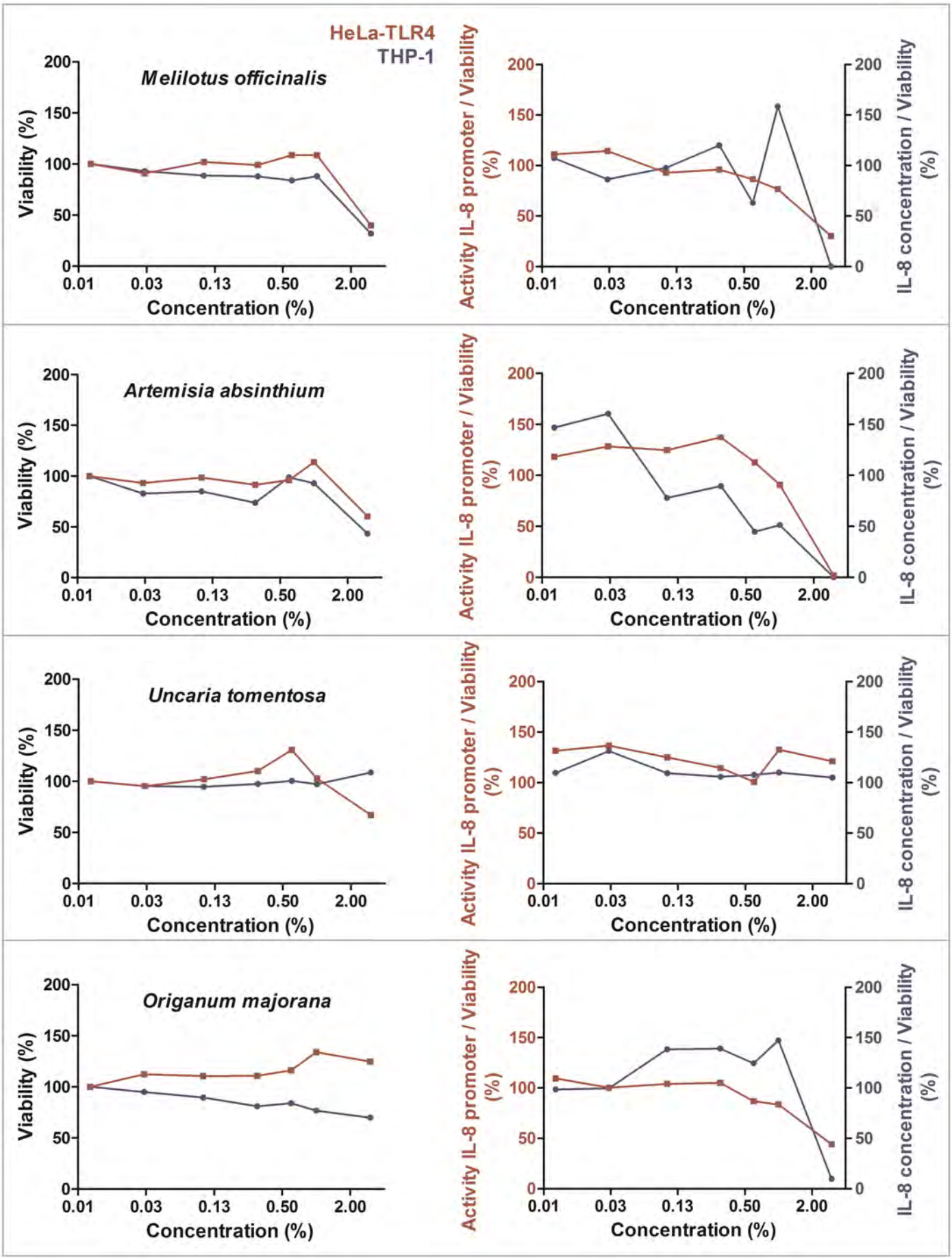
HeLa-TLR4
THP-1
Melilotus officinalis
Artemisia absinthium
Uncaria tomentosa
Origanum majorana
Viability (%)
Activity IL-8 promoter / Viability (%)
IL-8 concentration / Viability (%)
Concentration (%)
0.01
0.03
0.13
0.50
2.00
0
50
100
150
200

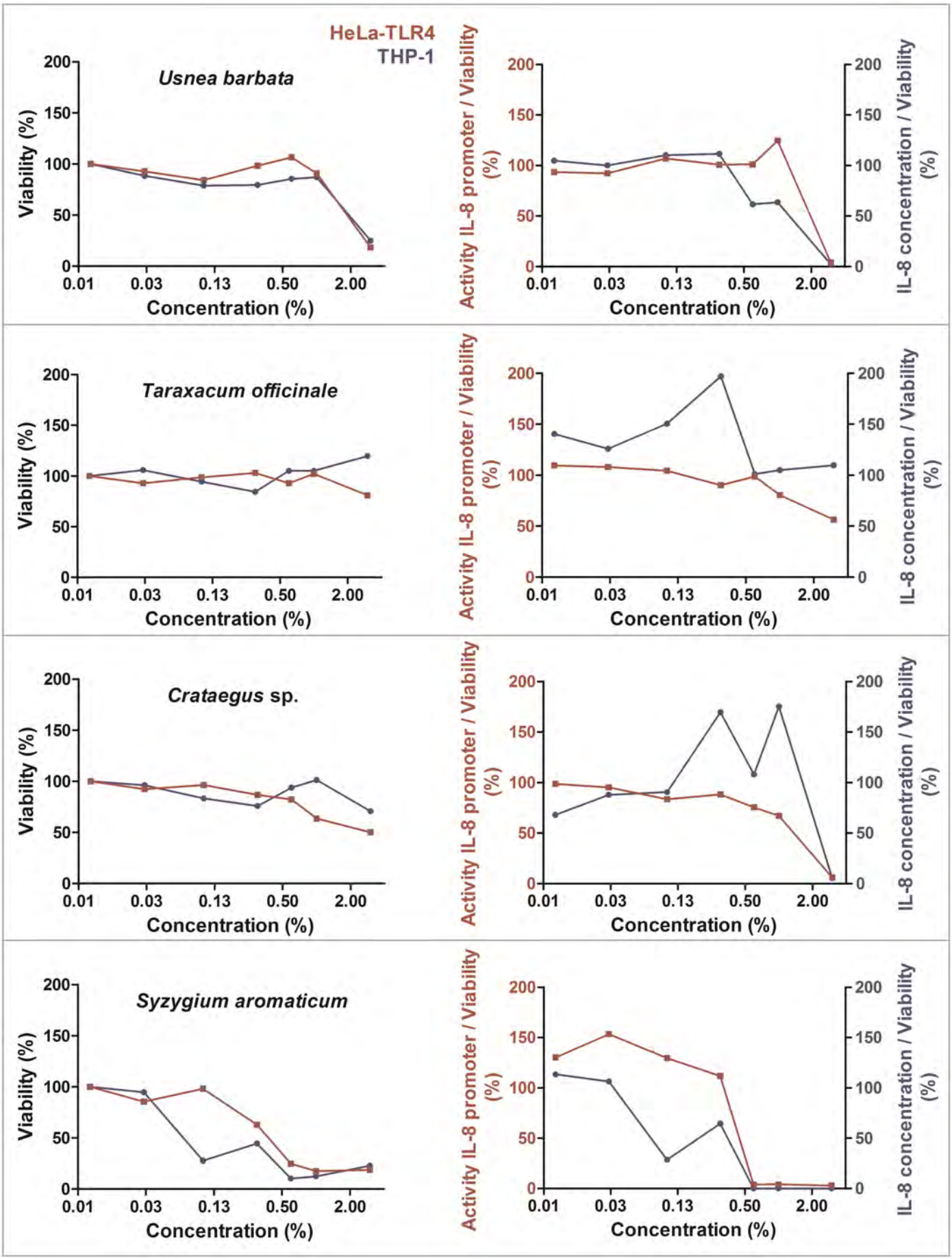
HeLa-TLR4
THP-1
Usnea barbata
Taraxacum officinale
Crataegus sp.
Syzygium aromaticum
Viability (%)
Activity IL-8 promoter / Viability (%)
IL-8 concentration / Viability (%)
Concentration (%)
0.01
0.03
0.13
0.50
2.00
0
50
100
150
200

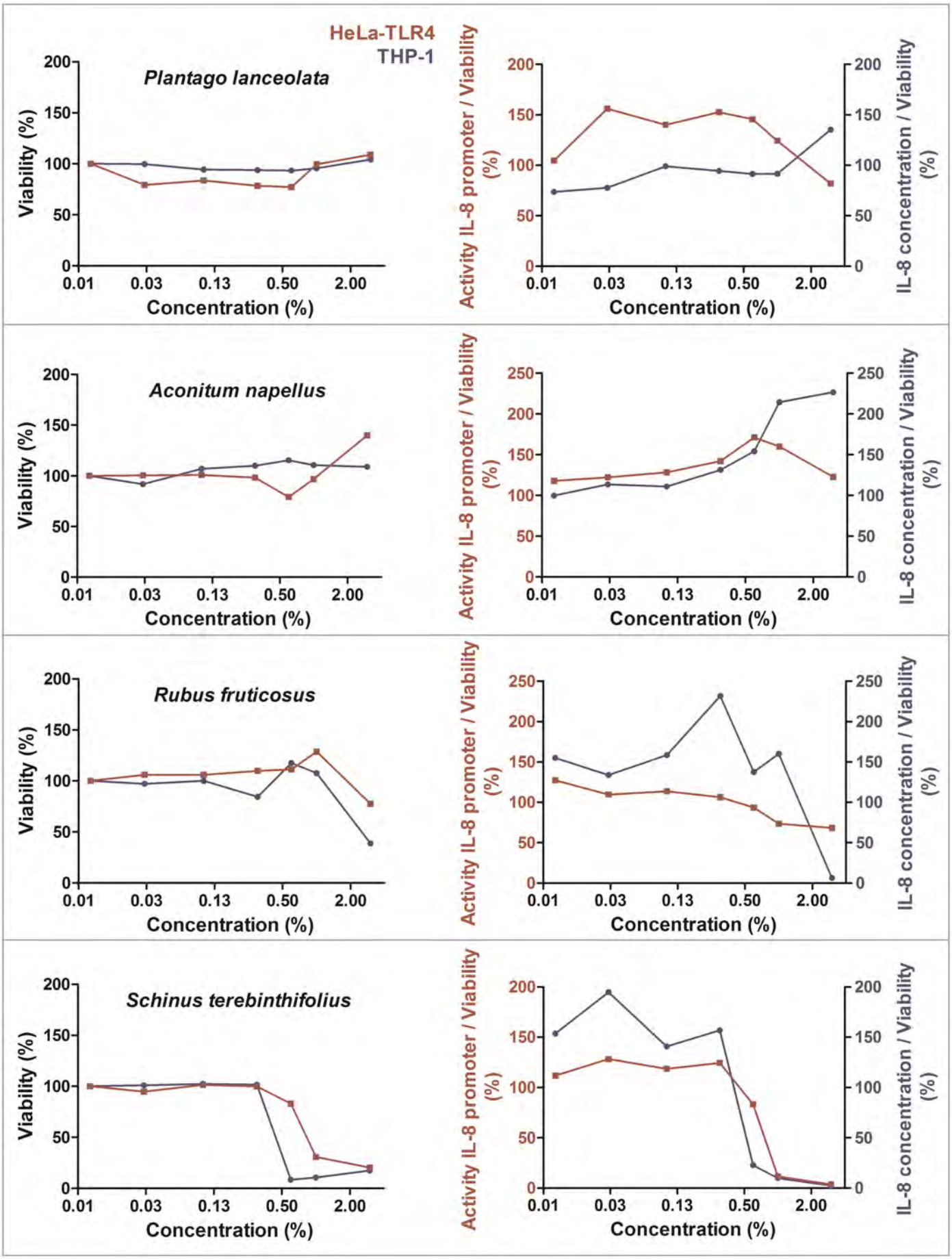
HeLa-TLR4
THP-1
Plantago lanceolata
Viability (%)
Activity IL-8 promoter / Viability (%)
IL-8 concentration / Viability (%)
Concentration (%)
0.01
0.03
0.13
0.50
2.00
Aconitum napellus
Rubus fruticosus
Schinus terebinthifolius

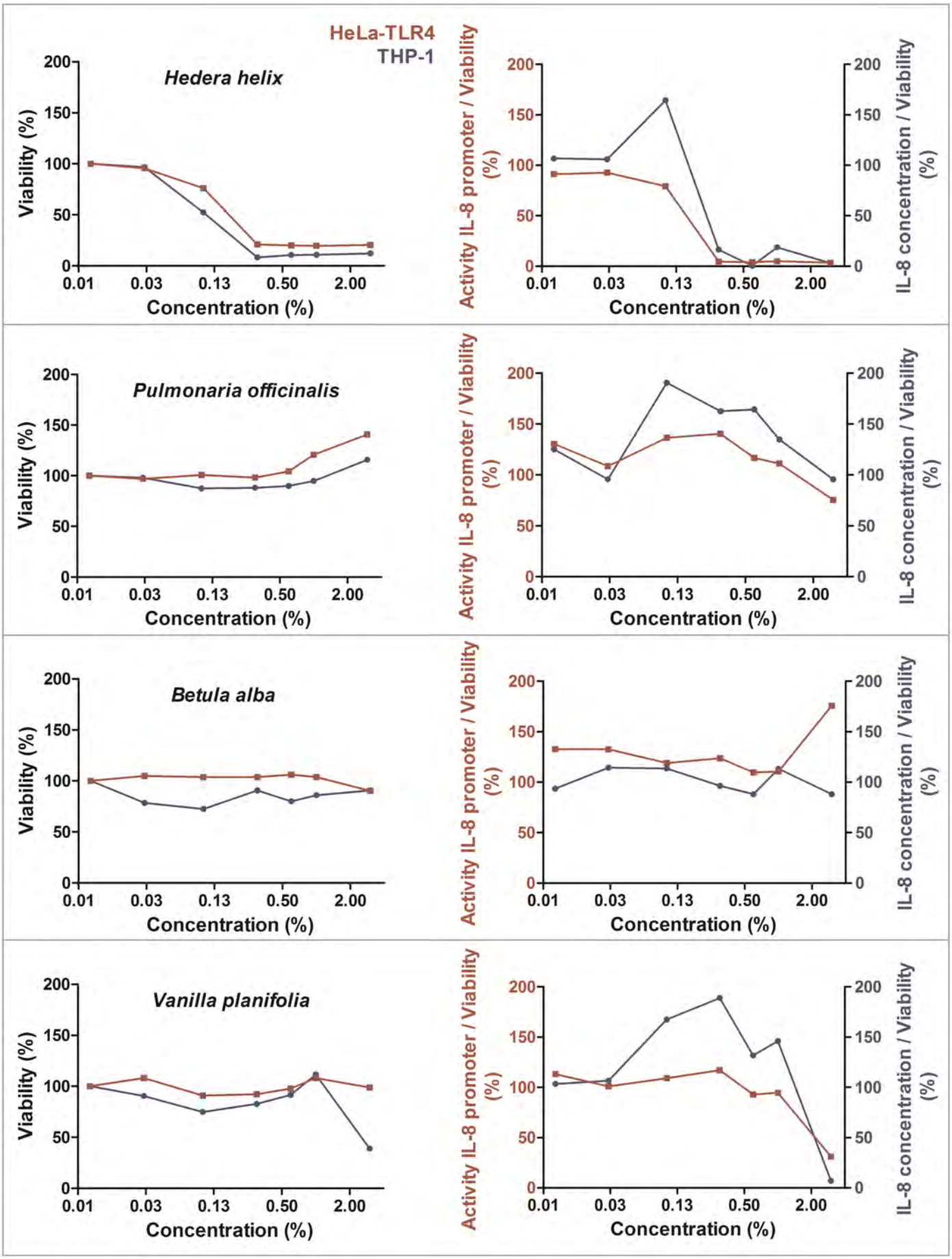
HeLa-TLR4
THP-1
Hedera helix
Pulmonaria officinalis
Betula alba
Vanilla planifolia
Viability (%)
Activity IL-8 promoter / Viability (%)
IL-8 concentration / Viability (%)
Concentration (%)
0.01
0.03
0.13
0.50
2.00
0
50
100
150
200

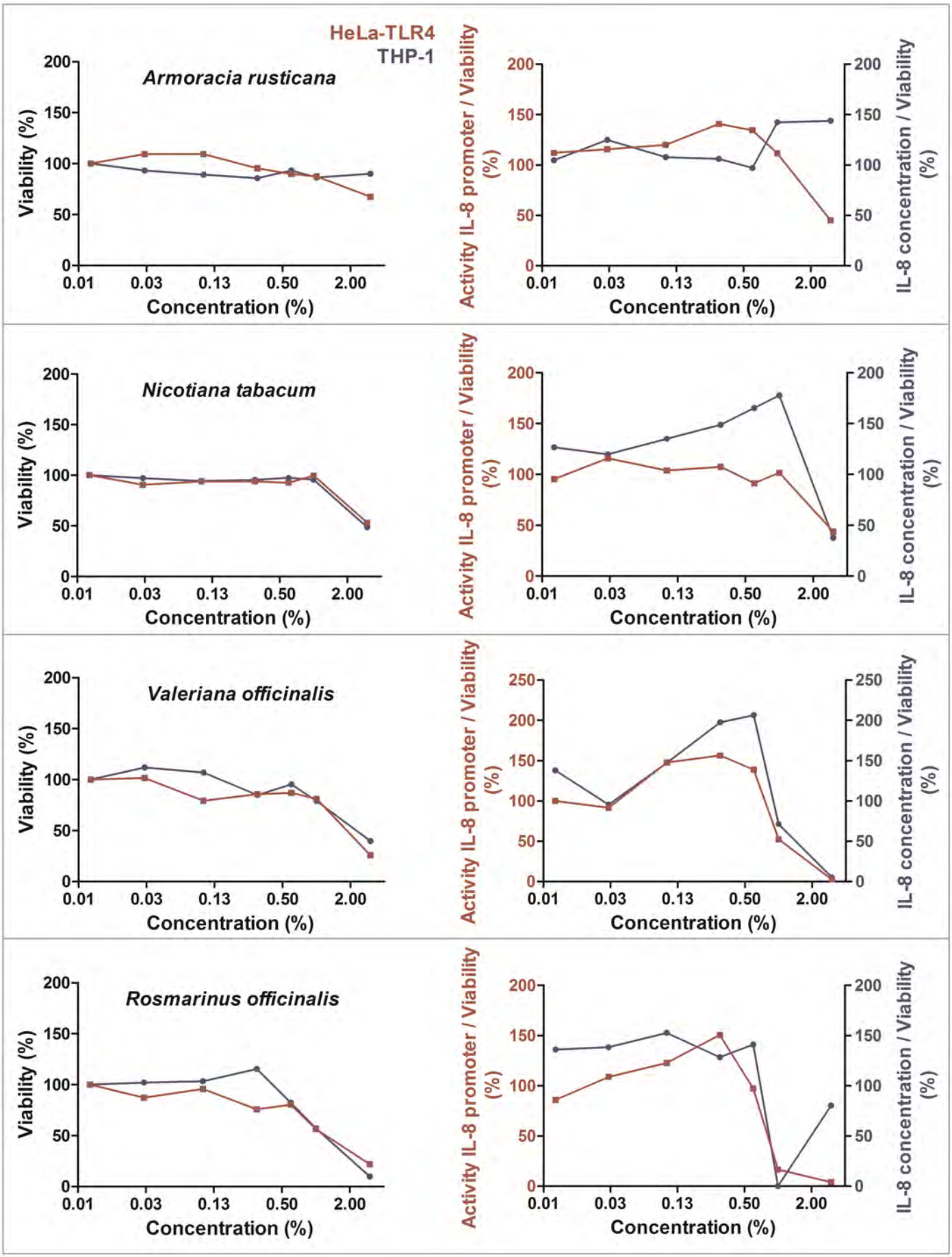
HeLa-TLR4
THP-1
Armoracia rusticana
Nicotiana tabacum
Valeriana officinalis
Rosmarinus officinalis
Viability (%)
Activity IL-8 promoter / Viability (%)
IL-8 concentration / Viability (%)
Concentration (%)
0.01
0.03
0.13
0.50
2.00

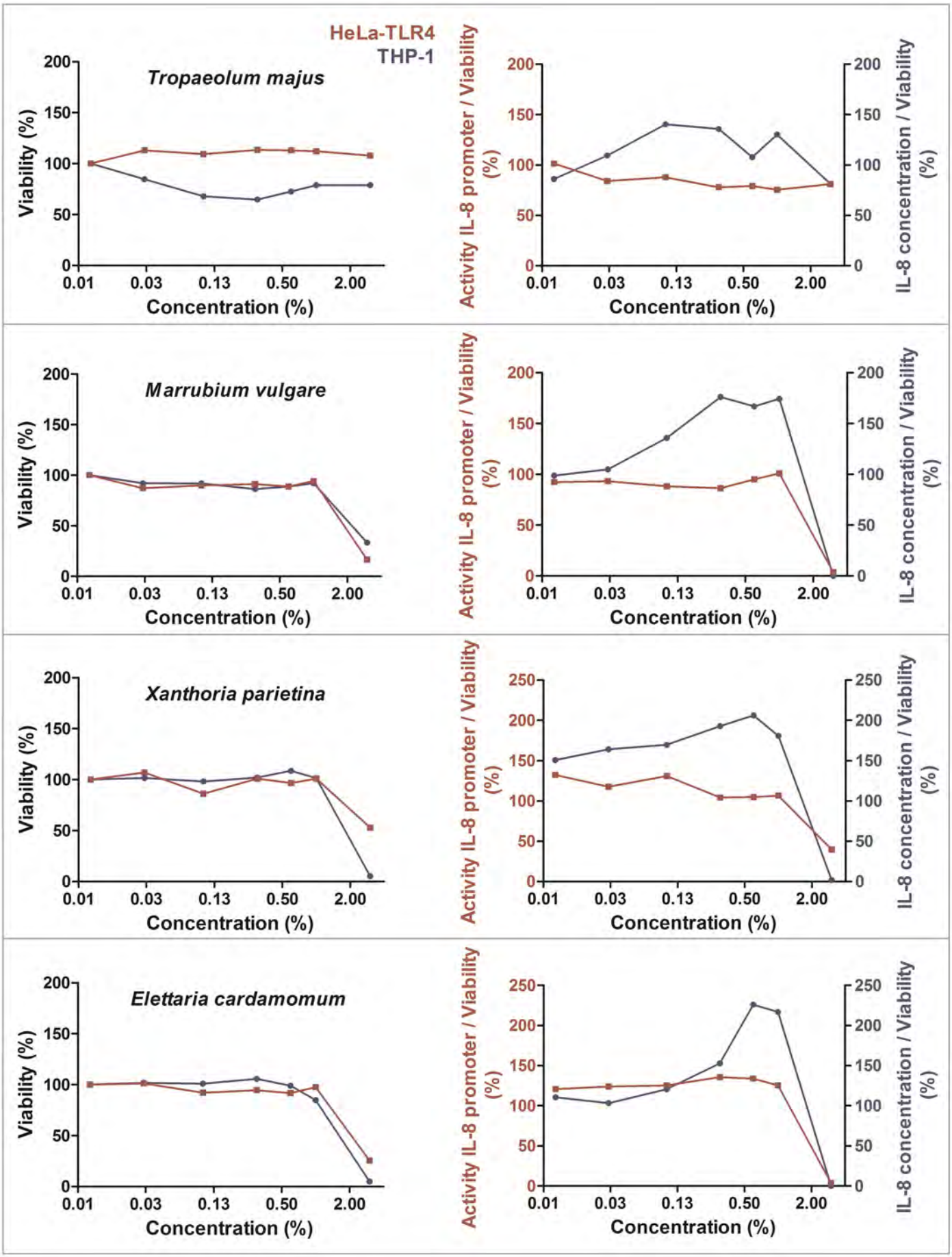
HeLa-TLR4
THP-1
Tropaeolum majus
Viability (%)
Activity IL-8 promoter / Viability (%)
IL-8 concentration / Viability (%)
Concentration (%)
0.01
0.03
0.13
0.50
2.00
Marrubium vulgare
Xanthoria parietina
Elettaria cardamomum

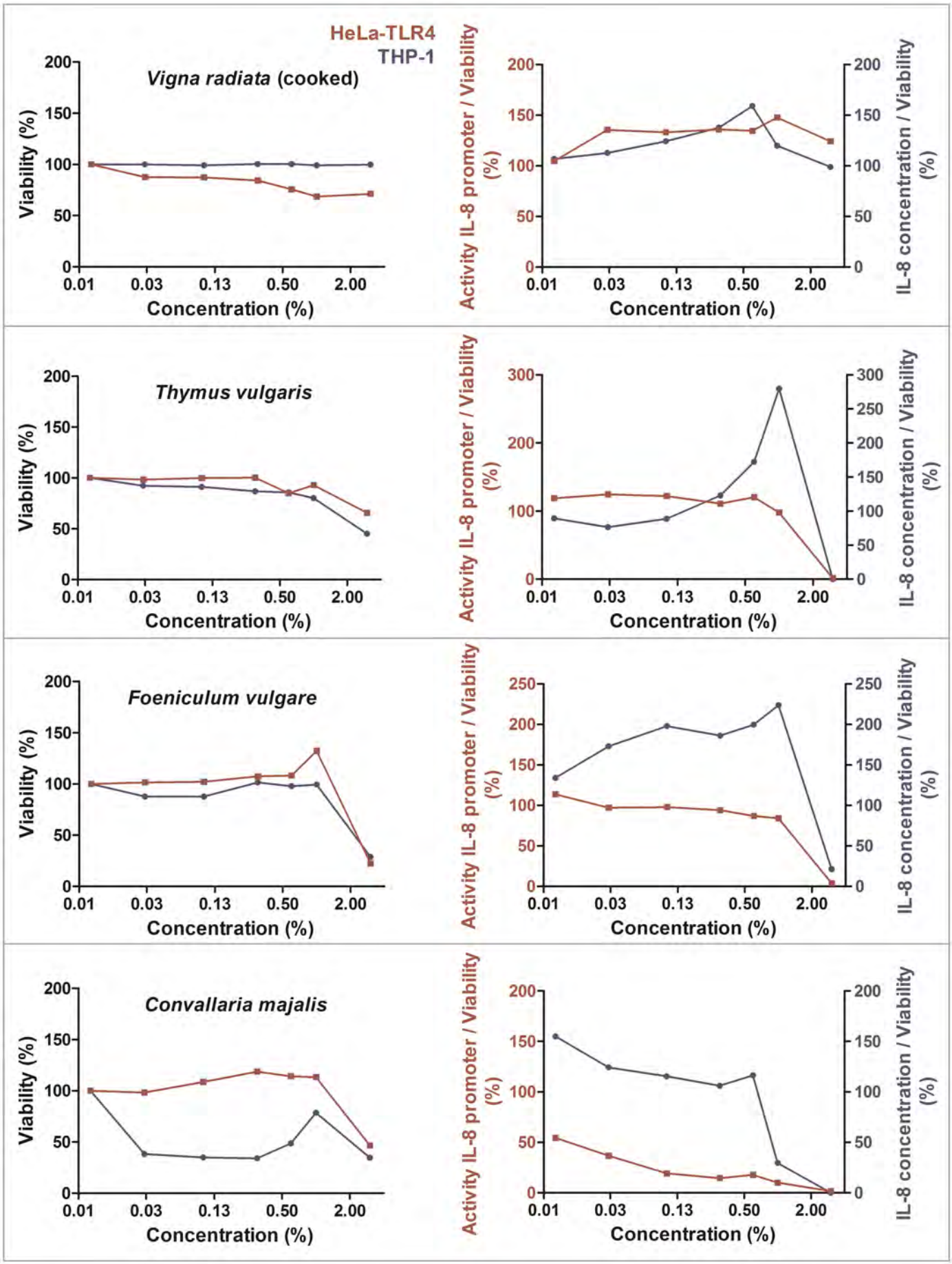
HeLa-TLR4
THP-1
Vigna radiata (cooked)
Viability (%)
Activity IL-8 promoter / Viability (%)
IL-8 concentration / Viability (%)
Concentration (%)
0.01
0.03
0.13
0.50
2.00
Thymus vulgaris
Foeniculum vulgare
Convallaria majalis

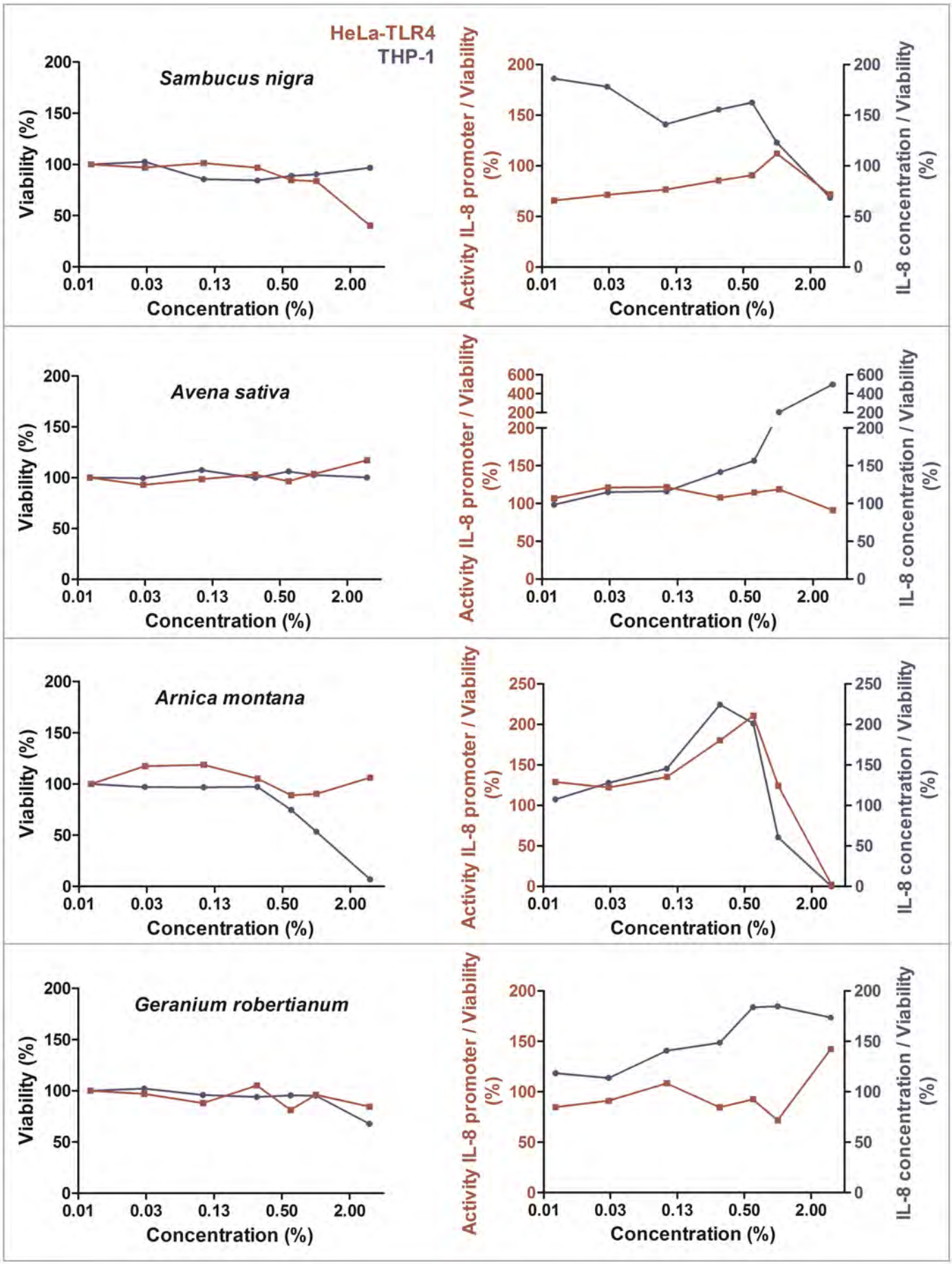
HeLa-TLR4
THP-1
Sambucus nigra
Viability (%)
Concentration (%)
Activity IL-8 promoter / Viability (%)
IL-8 concentration / Viability (%)
Avena sativa
Arnica montana
Geranium robertianum
0.01
0.03
0.13
0.50
2.00

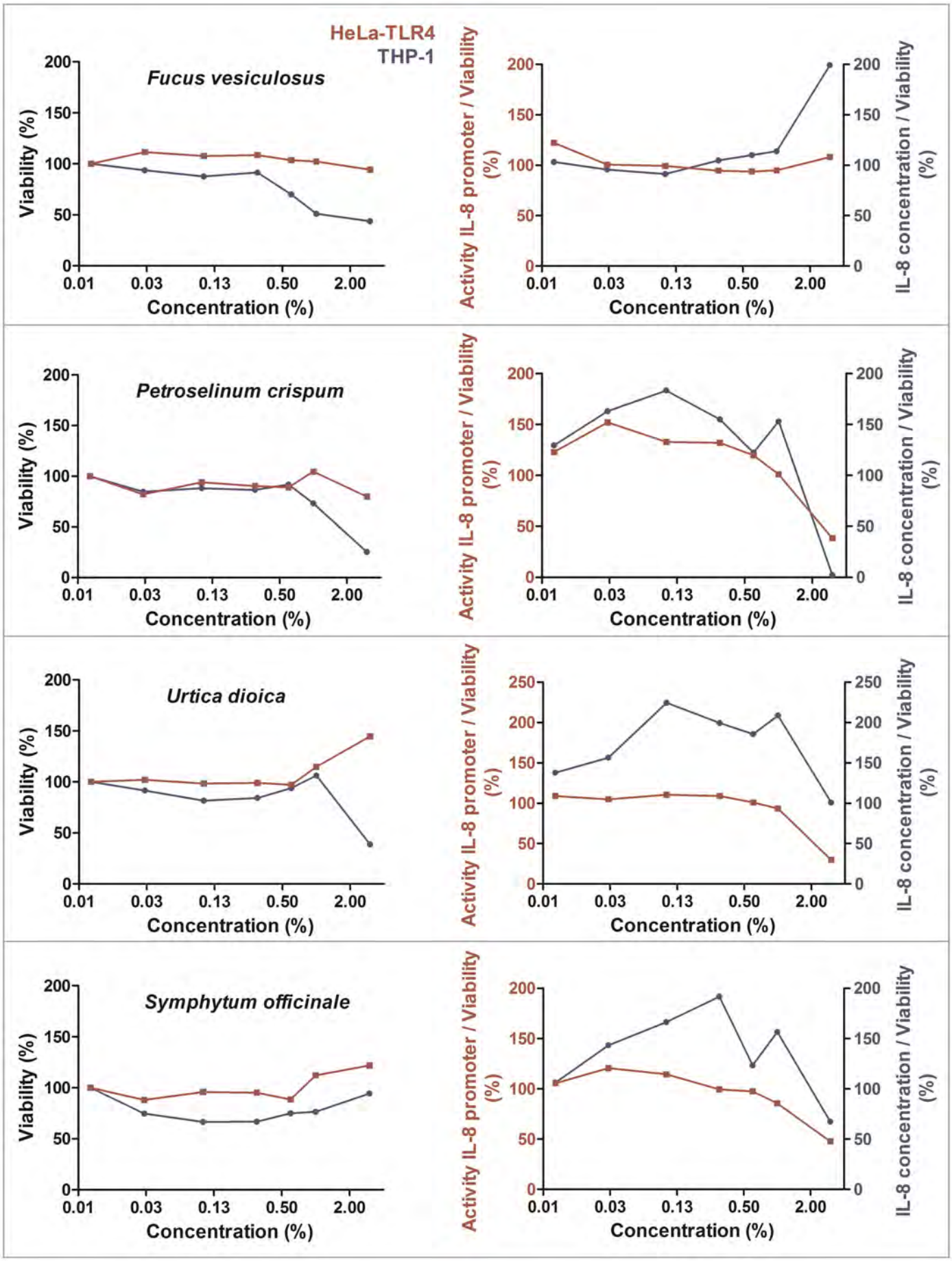
HeLa-TLR4
THP-1
Fucus vesiculosus
Petroselinum crispum
Urtica dioica
Symphytum officinale
Viability (%)
Activity IL-8 promoter / Viability (%)
IL-8 concentration / Viability (%)
Concentration (%)
0.01
0.03
0.13
0.50
2.00

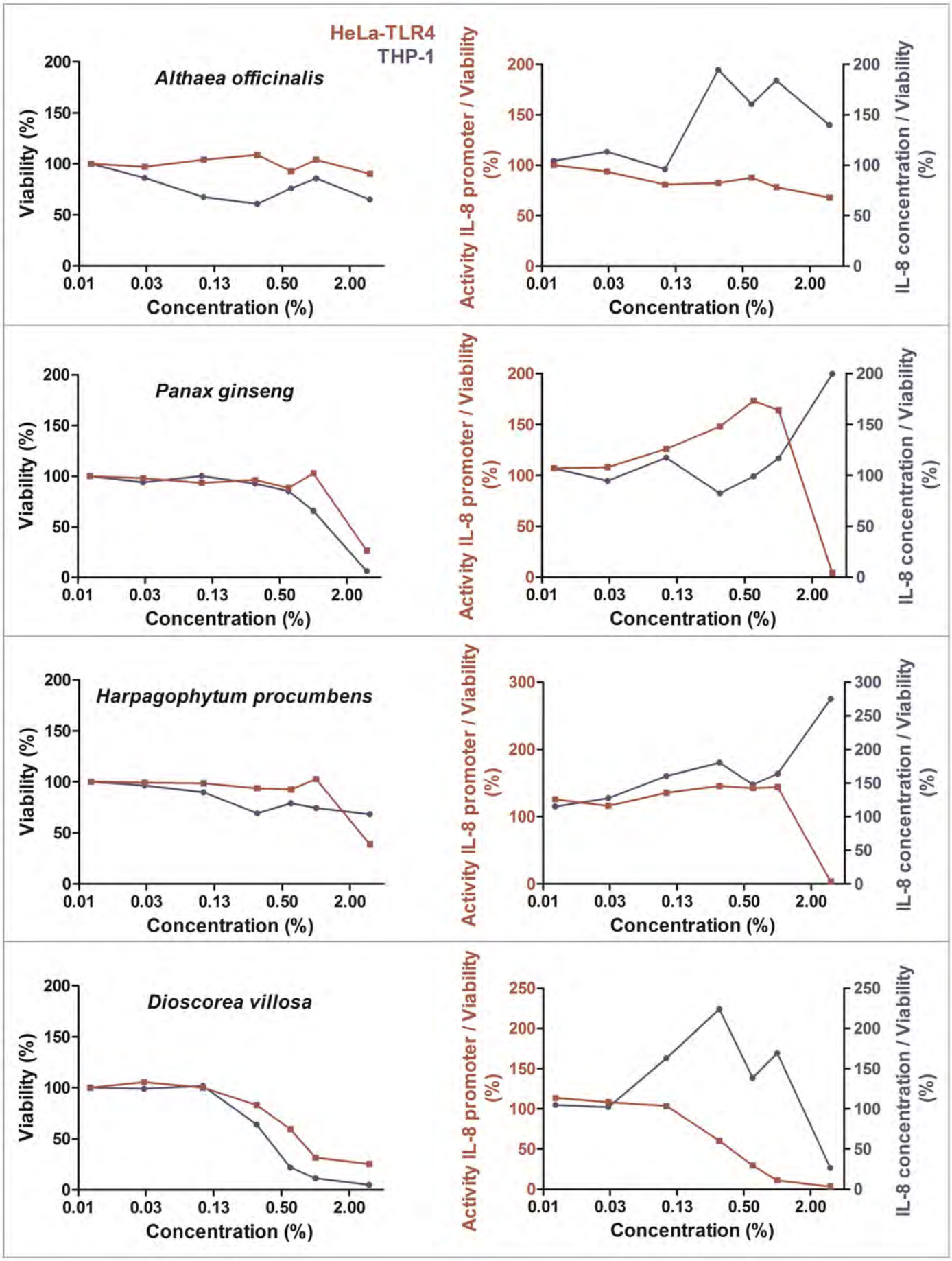
HeLa-TLR4
THP-1
Althaea officinalis
Panax ginseng
Harpagophytum procumbens
Dioscorea villosa
Viability (%)
Activity IL-8 promoter / Viability (%)
IL-8 concentration / Viability (%)
Concentration (%)
0.01
0.03
0.13
0.50
2.00

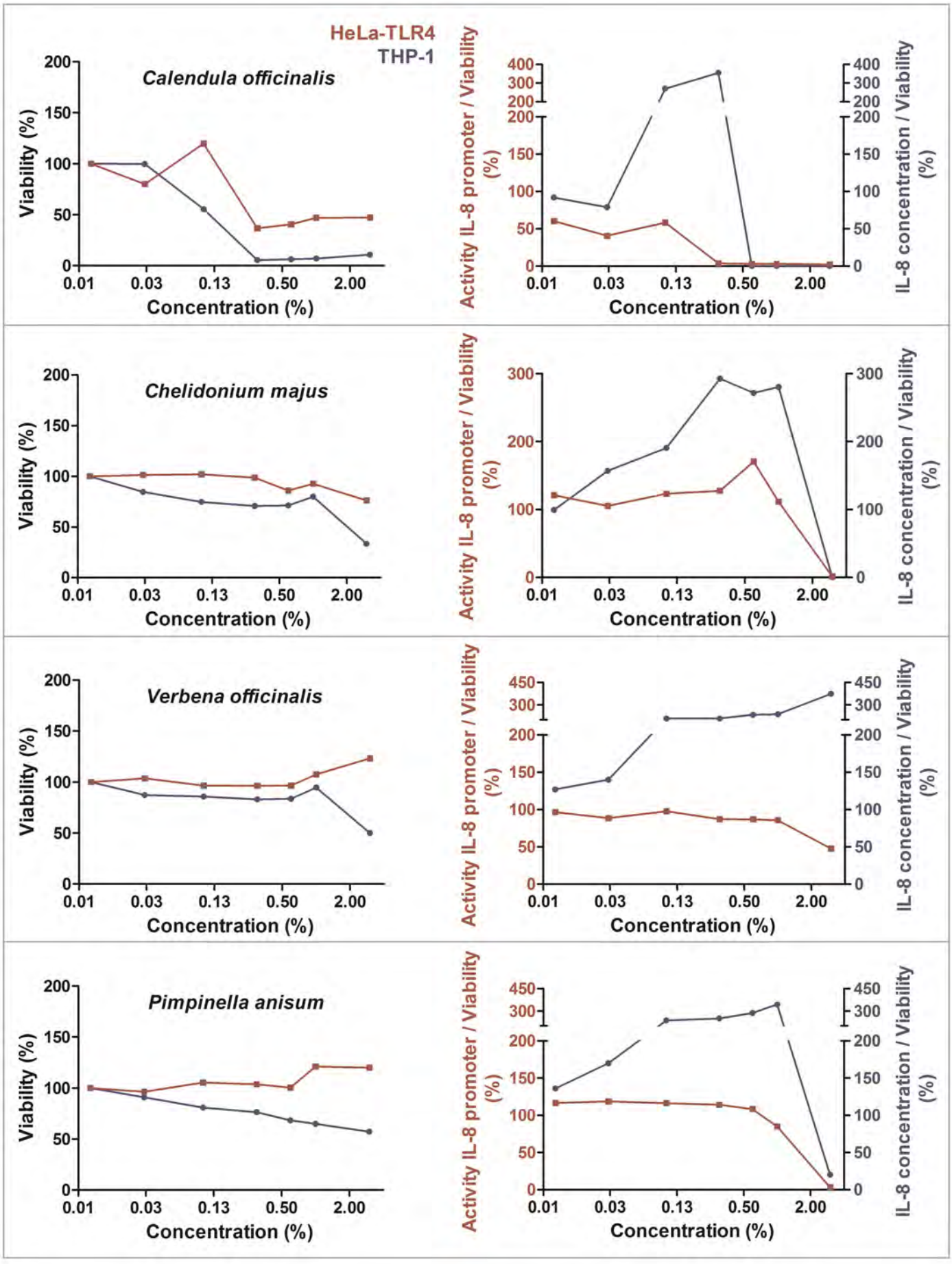
HeLa-TLR4
THP-1
Calendula officinalis
Chelidonium majus
Verbena officinalis
Pimpinella anisum
Viability (%)
Activity IL-8 promoter / Viability (%)
IL-8 concentration / Viability (%)
Concentration (%)
0.01
0.03
0.13
0.50
2.00

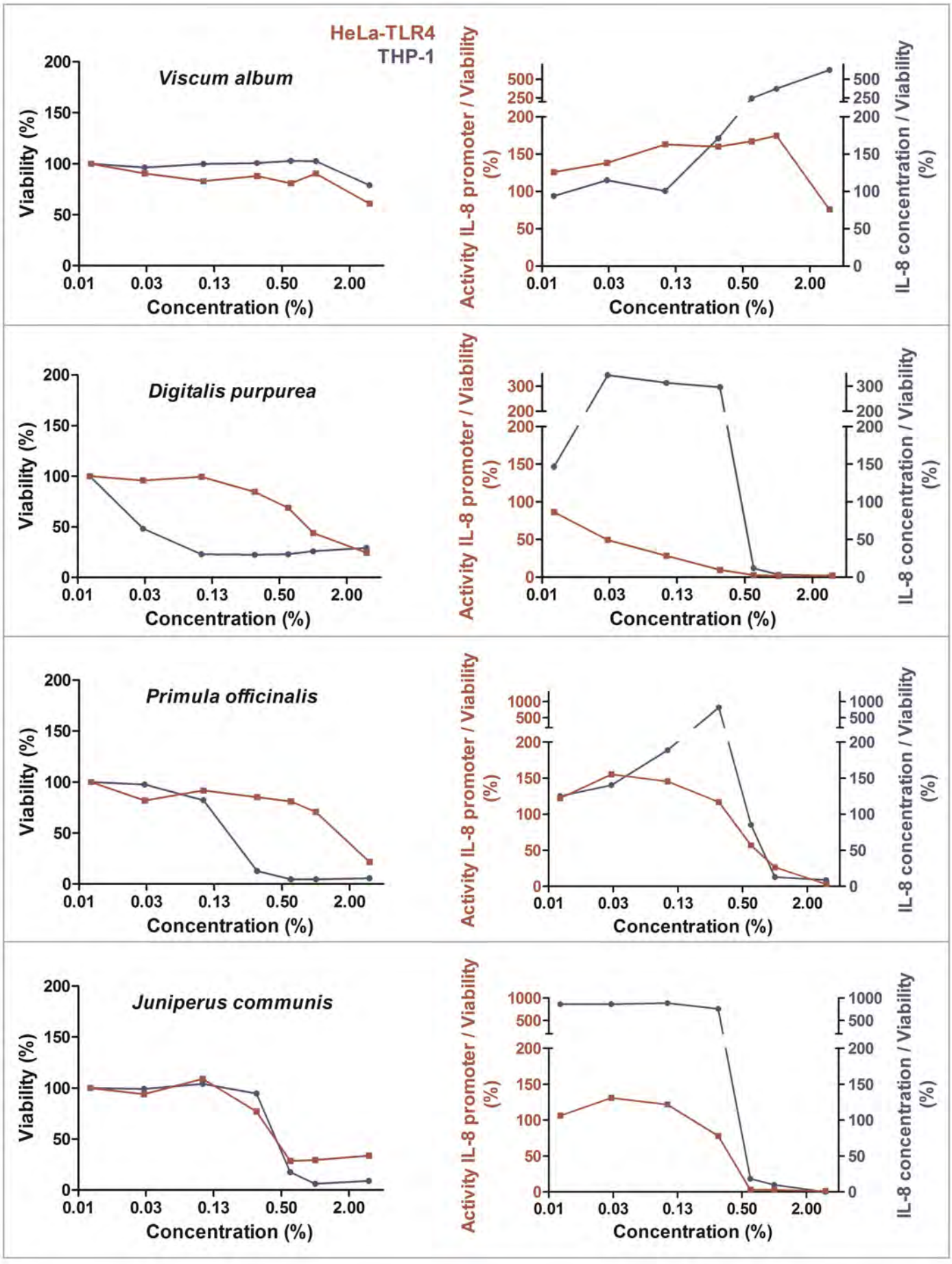
HeLa-TLR4
THP-1
Viscum album
Digitalis purpurea
Primula officinalis
Juniperus communis
Viability (%)
Activity IL-8 promoter / Viability (%)
IL-8 concentration / Viability (%)
Concentration (%)
0.01
0.03
0.13
0.50
2.00

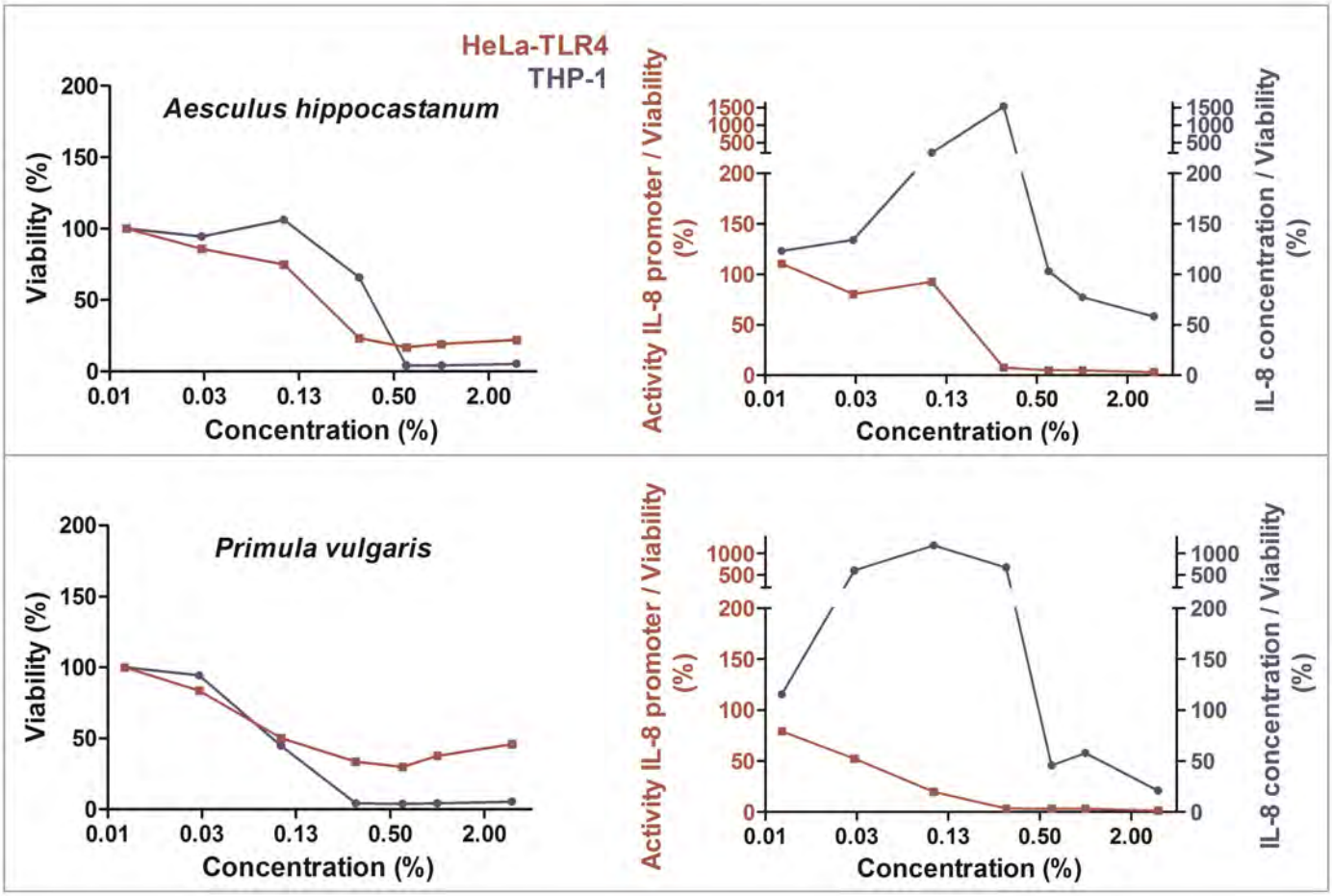
HeLa-TLR4
THP-1
Aesculus hippocastanum
Viability (%)
Concentration (%)
0.01
0.03
0.13
0.50
2.00
Activity IL-8 promoter / Viability (%)
IL-8 concentration / Viability (%)
Primula vulgaris

Inflammatory scale — anti-inflammatory ... pro-inflammatory

Toxicity scale — viability < 75%

			HeLa-TLR4 reporter cell line							THP-1 monocytes						
Latin name	**Common English name**	**Used part**	**0.01%**	**0.03%**	**0.1%**	**0.3%**	**0.6%**	**1%**	**3%**	**0.01%**	**0.03%**	**0.1%**	**0.3%**	**0.6%**	**1%**	**3%**
Ethanol control			100,00	101,30	103,67	102,01	93,23	85,77	90,26	98,88	97,04	96,54	96,59	97,67	95,66	107,91
Castanea sativa	Sweet chestnut	Leaf	90,53	82,03	30,91	3,53	10,59	1,34	0,79	118,69	71,34	46,42	25,73	5,65	0,00	0,00
Cinchona pubescens	Cinchona	Bark	122,15	137,25	148,02	131,28	148,76	98,71	2,77	47,68	104,26	125,10	62,37	29,49	15,68	3,49
Cinnamomum verum	Cinnamon	Bark	96,77	98,57	109,17	83,50	59,41	21,59	3,24	101,16	87,70	95,31	106,02	26,08	6,08	11,36
Salix alba	White willow	Bark	93,03	74,48	79,05	99,83	58,02	3,79	1,45	97,50	93,93	88,45	33,44	5,95	0,00	21,34
Rheum palmatum	Rhubarb	Root	71,38	72,58	79,60	55,28	64,48	96,37	2,34	99,17	98,60	27,86	6,42	1,94	3,57	29,89
Alchemilla vulgaris	Common lady's mantle	Whole plant	91,35	85,79	82,86	76,83	66,53	78,18	1,63	125,37	102,96	92,63	62,93	60,89	73,46	0,00
Humulus lupulus	Hops	Flower	64,31	67,38	74,08	3,57	1,10	0,92	0,96	108,76	99,78	55,66	1,46	0,00	0,00	0,73
Vaccinium myrtillus	Bilberries	Fruit/berry/ seed	86,00	84,71	81,50	80,48	83,01	76,30	68,10	102,84	91,37	92,22	96,85	92,91	92,95	63,02
Curcuma longa	Turmeric	Root	124,40	109,62	142,43	67,28	11,92	5,54	1,83	127,14	110,90	115,73	45,39	8,99	0,00	15,80
Arctostaphylos uva-ursi	Bearberry	Leaf	91,28	109,88	127,59	123,26	86,52	40,81	1,18	89,45	99,97	27,43	5,97	1,72	4,71	35,80
Allium ursinum	Wild garlic	Leaf	115,74	118,86	97,71	91,94	81,27	78,25	42,93	105,80	109,20	77,64	38,94	24,16	5,90	11,21
Hypericum perforatum	St John's wort	Whole plant	120,77	104,44	85,91	83,69	71,41	53,35	14,06	91,44	85,40	90,32	71,54	51,19	32,03	1,14
Arnicae montana	Arnica	Flower	114,17	96,34	2,78	2,14	2,61	2,55	1,28	144,96	146,96	11,90	0,70	0,69	1,67	0,53
Aloe ferox	Aloe	Whole plant	105,30	105,90	82,53	58,19	27,69	5,15	1,30	123,82	117,87	88,51	38,22	9,71	7,37	0,13
Cynara scolymus	Artichoke	Leaf	109,98	112,42	117,52	100,14	90,16	31,21	1,99	47,40	53,68	127,22	228,92	16,56	6,13	2,86
Salvia officinalis	Salvia	Leaf	94,88	96,95	107,50	89,57	73,14	17,55	2,65	94,87	87,05	79,10	72,53	97,48	42,03	0,00
Ginkgo biloba	Ginkgo	Leaf	107,04	120,25	119,37	90,15	44,17	4,77	2,22	124,31	101,09	22,26	7,98	16,68	9,27	0,00
Tanacetum parthenium	Feverfew	Whole plant	127,34	111,53	120,04	114,28	99,98	68,82	2,22	129,88	139,58	123,43	124,51	72,56	21,24	6,12
Vigna radiata	Mung bean (dried)	Fruit/berry/ seed	83,31	85,02	87,84	85,99	69,53	52,04	25,33	121,14	141,32	120,83	62,61	38,87	23,18	11,00
Betula verrucosa	Weeping birch	Juice/resin	144,10	148,90	136,35	139,46	143,77	154,99	88,24	120,90	131,27	106,29	88,92	93,49	94,35	93,18
Filipendula ulmaria	Meadowsweet	Flower	120,04	113,11	130,06	117,06	106,72	131,55	52,01	132,40	135,84	124,42	75,12	23,05	8,87	1,88
Matricaria chamomilla	Chamomile	Whole plant	100,35	104,50	90,84	78,36	84,92	5,43	1,26	107,39	110,30	81,01	78,37	109,61	0,00	0,00
Spirulina	Spirulina	Whole cyanobacteria	93,17	100,77	107,05	92,24	76,80	50,64	3,57	142,68	138,71	169,61	74,85	20,59	2,70	36,20
Gentiana lutea	Gentian	Root	120,08	105,07	118,69	89,81	89,96	82,85	39,06	80,63	60,91	89,51	140,23	62,51	43,53	2,92
Quercus robur	English oak	Bark	143,68	142,56	127,88	124,88	134,53	106,17	8,76	106,31	116,82	88,62	57,00	35,67	16,07	16,81
Glycyrrhiza glabra	Liquorice	Root	69,76	13,55	17,52	2,60	2,55	2,39	1,41	124,15	119,86	9,19	2,26	0,00	0,00	0,00
Coriandrum sativum	Coriander	Fruit/berry/ seed	94,70	82,24	87,66	90,37	89,65	77,49	44,98	145,74	168,38	152,38	158,20	188,96	155,51	6,45
Achillea millefolium	Common yarrow	Whole plant	99,04	103,48	102,37	83,36	68,35	55,50	4,09	93,70	98,28	118,44	107,59	100,57	52,47	0,54
Mentha piperita	Peppermint	Whole plant	102,97	91,41	91,14	78,20	72,36	55,95	6,57	130,45	151,24	119,30	123,66	149,47	84,49	0,00
Zingiber officinale	Ginger	Root	94,65	103,21	52,82	24,16	2,18	4,32	3,92	73,81	82,12	75,13	80,11	34,29	0,19	6,73
Carum carvi	Caraway	Fruit/berry/ seed	108,52	107,56	121,15	115,23	96,15	83,63	2,63	126,27	123,61	127,15	136,91	201,67	118,87	0,00
Boswellia serrata	Frankincense	Juice/resin	109,56	96,96	80,61	3,87	2,80	3,49	2,35	97,42	88,36	75,32	23,64	10,16	11,86	9,76
Camellia sinensis (L.)	Green tea	Leaf	71,42	64,90	60,73	53,03	34,40	5,10	2,05	104,85	90,19	80,66	52,63	128,30	78,12	71,24
Echinacea purpurea	Purple coneflower	Whole plant	93,87	121,50	103,17	111,27	121,75	86,28	3,42	110,63	100,92	147,05	98,88	95,70	98,35	1,71
Ilex paraguariensis	Yerba mate	Leaf	118,38	113,40	129,00	98,03	46,11	7,19	1,87	138,05	86,82	106,45	142,70	113,19	149,98	29,15
Melissa officinalis	Lemon balm	Leaf	139,03	150,28	144,79	79,25	68,78	76,74	2,31	88,63	126,13	138,48	148,82	86,05	36,73	0,00
Daucus carota ssp. sativus	Carrot	Root	98,38	101,96	87,71	99,88	87,68	98,85	87,26	96,35	110,50	87,33	79,92	93,51	85,16	137,06
Alpinia officinarum	Galangal	Root	119,58	118,04	149,25	135,19	45,52	3,29	2,27	127,08	98,10	138,77	38,12	0,70	0,00	2,44
Boswellia carterii	Frankincense	Whole plant	149,54	178,92	15,63	14,15	11,16	11,09	12,66	27,95	31,63	4,81	7,98	18,51	6,92	3,63
Hamamelis virginiana	Witch hazel	Leaf	100,46	99,15	137,19	118,74	70,76	4,96	1,01	123,19	189,63	211,05	38,28	5,85	5,40	7,92
Equisetum arvense	Field horsetail	Whole plant	113,79	125,14	120,99	128,87	130,20	133,00	109,17	93,55	94,65	83,58	114,07	124,64	145,69	189,41

Scrophularia nodosa	Common figwort	Whole plant	98,78	93,42	113,41	123,22	114,38	105,67	10,92	107,47	125,14	152,78	113,07	101,17	88,26	24,69
Lavandula angustifolia	Lavender	Flower	93,68	101,24	110,76	95,94	91,92	36,15	3,80	81,97	87,67	115,57	116,55	141,91	137,61	0,00
Euphrasia officinalis	Eyebright	Whole plant	101,53	105,92	114,90	115,55	113,31	116,53	10,37	136,41	103,87	107,91	96,64	107,09	125,33	0,38
Capsicum frutescens	Chili	Fruit/berry/ seed	101,94	167,29	120,07	115,20	118,62	95,65	3,07	117,80	124,86	154,50	180,15	171,38	145,55	29,51
Erythraea centaurium	Common centaury	Whole plant	106,04	92,14	96,31	87,33	82,62	62,99	5,13	113,71	85,01	148,74	133,41	141,78	119,84	4,22
Hibiscus sabdariffa	Roselle	Leaf	105,58	98,26	132,94	133,23	118,60	97,39	48,78	90,10	94,55	87,49	93,64	145,26	231,97	65,51
Chlorella pyrenoidosa	Chlorella	Whole green algae	71,44	72,14	75,70	62,00	44,51	16,46	2,86	102,98	94,60	18,27	0,00	0,00	0,00	173,01
Allium sativum	Garlic	Root	78,39	95,63	87,21	84,35	83,82	96,56	112,72	129,06	117,29	96,92	89,62	103,10	110,42	132,77
Melilotus officinalis	Sweet clover	Whole plant	111,02	114,31	92,87	95,90	86,37	76,52	30,05	107,23	86,20	97,54	119,85	62,88	158,37	0,00
Artemisia absinthium	Wormwood	Whole plant	118,20	128,44	124,74	137,46	112,64	90,75	1,69	146,74	160,40	77,99	89,46	44,77	51,21	0,00
Uncaria tomenosa	Cat's claw	Whole plant	131,44	136,66	124,86	114,39	100,57	132,50	121,12	109,66	131,32	109,33	105,76	107,51	109,99	104,97
Origanum majorana	Marjoram	Whole plant	109,40	100,22	104,08	105,12	87,00	83,56	44,13	98,64	99,81	138,44	139,16	124,52	147,26	9,77
Usnea barbata	Barber's itch	Whole plant	93,46	92,28	106,88	100,70	101,15	124,63	3,85	104,78	100,16	110,27	111,35	61,61	63,62	2,27
Taraxacum officinale	Dandelion	Whole plant	109,52	108,09	104,38	90,20	98,79	80,62	56,45	140,46	125,98	150,64	197,11	101,07	104,89	109,75
Crataegus sp.	Hawthorn	Fruit/berry/ seed	98,69	95,22	83,59	88,20	75,56	67,10	6,03	68,02	87,86	90,53	169,63	108,10	175,25	5,53
Syzygium aromaticum	Clove	Flower	130,27	153,49	129,52	111,74	3,84	4,04	2,97	113,40	106,43	28,55	64,60	0,00	0,00	0,00
Plantago lanceolata	Ribwort	Whole plant	104,81	156,04	140,16	152,61	145,60	124,31	81,91	73,59	77,75	99,03	94,45	91,42	91,59	135,20
Aconitum napellus	Monkshood	Whole plant	117,73	122,26	128,16	141,94	171,12	159,82	122,60	99,75	113,53	110,99	131,43	154,05	214,24	226,55
Rubus fruticosus	Blackberry	Leaf	127,50	109,58	113,80	106,40	93,56	73,60	68,53	155,10	133,75	158,55	231,87	137,62	160,15	6,26
Schinus terebinthifolius	Brazilian peppertree	Fruit/berry/ seed	111,76	128,25	118,65	124,42	83,27	11,51	3,58	153,65	194,72	140,78	156,82	22,67	9,93	2,35
Hedera helix	Common ivy	Leaf	91,23	92,82	79,19	4,54	3,93	4,92	3,35	106,81	105,99	164,47	16,45	0,48	18,81	3,05
Pulmonaria officinalis	Common lungwort	Flower	130,49	108,61	136,54	140,36	116,71	111,27	75,45	125,06	95,78	190,61	162,64	164,20	134,71	95,52
Betula alba	Birch	Juice/resin	132,70	132,59	119,10	123,74	109,52	110,59	175,69	93,66	114,38	113,57	96,37	88,04	113,21	88,16
Vanilla planifolia	Vanilla	Fruit/berry/ seed	113,32	101,03	109,01	117,05	92,96	94,61	31,02	103,36	106,83	167,48	188,94	131,81	146,05	6,91
Armoracia rusticana	Horseradish	Root	112,02	115,66	120,07	140,73	134,50	111,66	45,08	104,74	124,98	107,81	106,12	97,03	142,36	143,87
Nicotiana tabacum	Tobacco	Leaf	95,45	115,94	103,93	107,47	91,20	101,64	43,82	126,54	119,78	135,07	148,77	165,43	177,65	37,75
Valeriana officinalis (L.)	Common valerian	Root	100,20	91,61	147,82	156,35	138,95	52,36	2,58	138,12	95,56	147,35	197,61	206,61	71,26	5,16
Rosmarinus officinalis	Rosemary	Leaf	85,92	108,99	122,78	150,67	97,28	16,54	4,02	136,08	138,36	152,73	128,42	141,11	0,15	80,17
Tropaeolum majus	Nasturtium	Whole plant	101,46	84,01	87,90	77,92	79,16	75,39	81,14	86,16	109,46	140,46	135,69	107,73	130,22	81,44
Marrubium vulgare	Common horehound	Whole plant	92,34	93,29	88,32	86,32	95,10	100,87	3,75	98,80	104,74	135,83	176,09	166,83	174,18	0,00
Xanthoria parietina	Common orange lichen	Whole lichen	132,43	117,59	130,84	104,27	104,89	106,46	39,67	150,70	163,97	169,59	192,87	206,05	180,74	1,76
Elettaria cardamomum	Cardamom	Fruit/berry/ seed	120,81	123,83	125,38	135,62	133,76	125,41	3,62	110,45	103,25	120,45	152,87	225,96	216,74	0,00
Vigna radiata	Mung bean (cooked)	Fruit/berry/ seed	104,69	135,60	133,28	135,94	134,61	147,80	124,20	106,85	112,74	124,20	137,77	159,06	119,88	98,96
Thymus vulgaris	Common thyme	Whole plant	118,89	124,53	122,18	110,86	120,29	97,87	1,59	89,27	76,48	88,74	122,81	172,45	279,61	0,00
Foeniculum vulgare	Fennel	Fruit/berry/ seed	113,92	97,22	97,97	94,07	87,06	84,14	3,97	134,14	173,01	197,93	186,12	199,79	223,76	21,35
Convallaria majalis	Lily of the valley	Whole plant	54,48	36,78	19,24	14,57	17,70	10,11	1,72	154,97	124,30	115,50	106,13	116,39	29,53	0,00
Sambucus nigra (L.)	Elderflower	Flower	65,76	71,40	76,66	85,55	90,78	112,07	71,97	186,27	178,06	140,90	155,66	162,33	122,89	68,63
Avena sativa	Oat	Whole plant	106,83	121,15	121,84	107,76	114,50	118,79	91,19	98,22	114,88	116,09	141,54	156,55	204,12	498,22
Arnica montana	Arnica	Whole plant	128,77	122,08	135,39	180,41	210,78	124,21	2,17	107,35	127,87	145,42	224,38	201,18	60,44	0,00
Geranium robertianum	Herb Robert	Whole plant	84,73	91,07	108,37	84,64	92,55	71,75	142,28	118,42	113,83	140,82	148,56	183,75	184,72	173,60
Fucus vesiculosus	Bladderwrack	Whole plant	122,31	100,62	99,24	94,51	93,75	94,92	108,01	103,21	95,74	91,21	104,75	110,16	113,90	199,19
Petroselinum crispum	Parsley	Whole plant	122,97	152,03	133,00	132,12	119,74	101,03	38,49	129,60	163,16	183,36	155,06	122,44	153,04	2,18
Urtica dioica	Stinging nettle	Root	109,01	104,90	110,43	109,07	100,86	93,37	29,81	137,84	156,50	224,44	199,41	185,63	208,82	100,88
Symphytum officinale	Comfrey	Root	105,62	120,61	114,45	99,46	97,54	85,58	47,79	106,24	143,47	166,37	191,76	123,39	156,54	67,34
Althaea officinalis	Marshmallow	Root	100,22	93,79	80,71	82,49	87,56	78,29	67,86	104,25	113,39	96,02	194,59	160,52	183,97	139,71
Panax ginseng	Ginseng	Root	107,05	107,98	125,88	147,96	173,19	164,01	4,13	106,76	94,66	117,42	82,44	99,07	116,80	199,71
Harpagophytum procumbens	Devil's claw	Root	125,75	116,09	135,75	145,66	142,70	144,23	3,68	115,10	127,64	160,49	180,30	147,55	163,53	275,03

Dioscorea villosa	Yam	Root	113,51	108,51	103,64	60,24	29,52	11,04	3,27	104,81	102,20	163,08	224,08	138,65	169,18	26,64
Calendula officinalis	Marigold	Flower	60,30	40,34	58,30	3,49	2,91	2,77	2,19	91,73	78,85	269,59	354,55	0,00	0,00	0,00
Chelidonium majus	Celandine	Root	120,88	105,15	123,10	127,73	170,41	111,32	1,42	99,40	157,00	190,57	292,73	271,52	280,41	0,00
Verbena officinalis	Common vervain	Whole plant	96,47	88,48	97,54	86,98	86,77	85,59	47,65	127,02	140,00	208,28	208,79	233,55	236,51	374,51
Pimpinella anisum	Anise	Fruit/berry/ seed	116,49	118,67	116,39	114,10	108,54	84,98	3,36	136,25	169,95	236,67	250,31	286,11	344,07	20,08
Viscum album	European mistletoe	Whole plant	125,75	138,13	162,97	160,01	166,89	174,64	76,09	93,86	114,91	100,53	170,99	242,81	373,37	625,53
Digitalis purpurea	Common foxglove	Leaf	86,35	49,52	28,50	9,67	2,50	1,49	2,18	146,70	344,09	313,09	296,48	11,91	3,20	1,60
Primula officinalis	Common cowslip	Root	122,30	155,54	145,79	116,90	57,14	26,43	3,07	125,37	140,65	188,90	819,19	85,17	12,98	8,91
Juniperus communis	Common juniper	Fruit/berry/ seed	106,49	131,13	121,88	77,99	3,10	2,84	1,55	859,81	863,37	888,08	759,89	18,31	9,85	0,00
Aesculus hippocastanum	Horse-chestnut	Fruit/berry/ seed	110,81	80,80	92,60	7,84	5,11	5,00	3,20	123,23	134,19	212,88	1537,04	102,98	77,65	58,38
Primula vulgaris	Common primrose	Root	48,96	26,97	24,47	13,49	12,19	8,12	1,52	115,35	604,33	1193,00	674,91	45,73	58,06	21,03

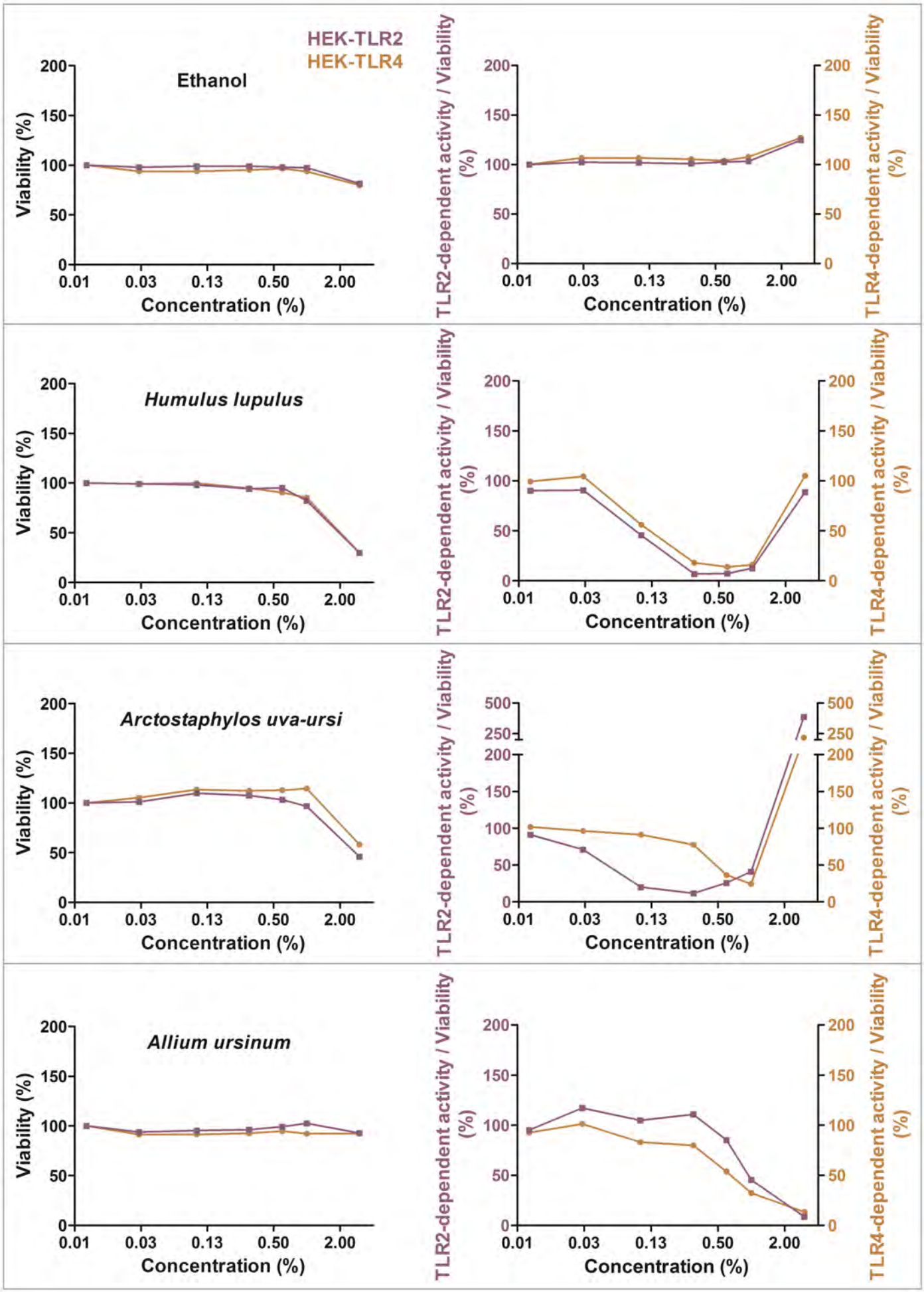
HEK-TLR2
HEK-TLR4
Ethanol
Humulus lupulus
Arctostaphylos uva-ursi
Allium ursinum
Viability (%)
Concentration (%)
0.01
0.03
0.13
0.50
2.00
TLR2-dependent activity / Viability (%)
TLR4-dependent activity / Viability (%)

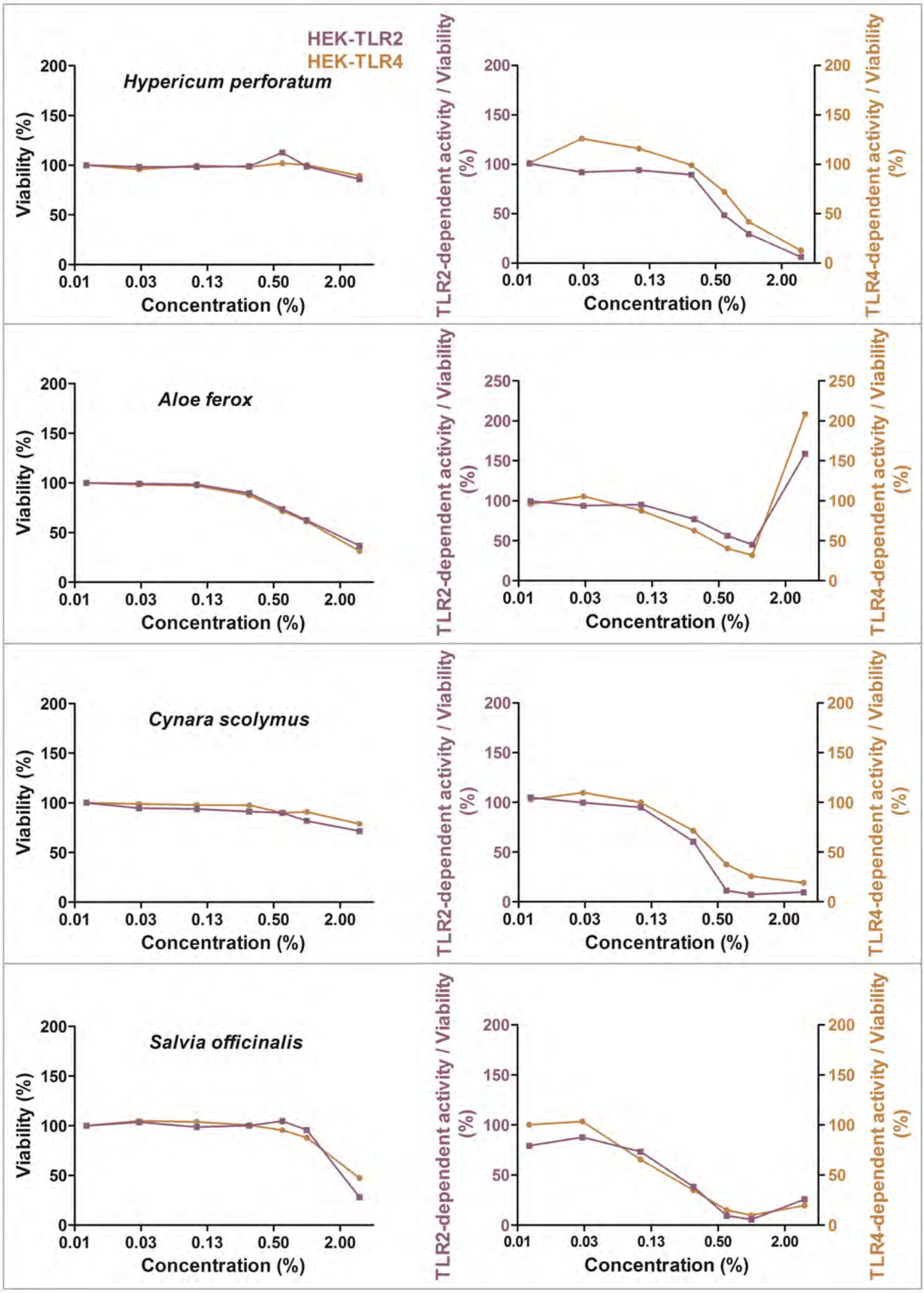
HEK-TLR2
HEK-TLR4
Hypericum perforatum
Aloe ferox
Cynara scolymus
Salvia officinalis
Viability (%)
TLR2-dependent activity / Viability (%)
TLR4-dependent activity / Viability (%)
Concentration (%)
0.01
0.03
0.13
0.50
2.00

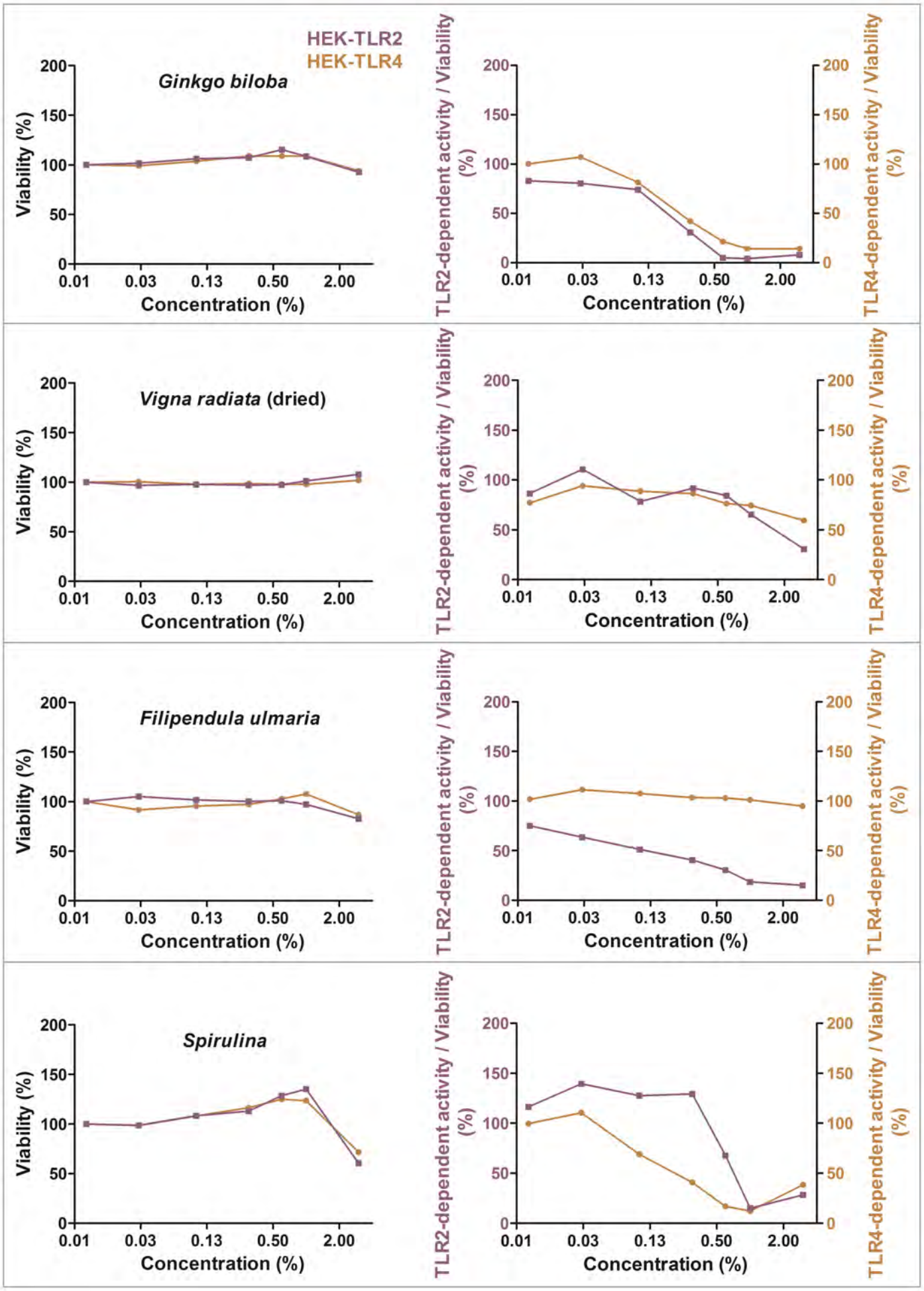
HEK-TLR2
HEK-TLR4
Ginkgo biloba
Viability (%)
Concentration (%)
TLR2-dependent activity / Viability (%)
TLR4-dependent activity / Viability (%)
Vigna radiata (dried)
Filipendula ulmaria
Spirulina
0.01
0.03
0.13
0.50
2.00
0
50
100
150
200

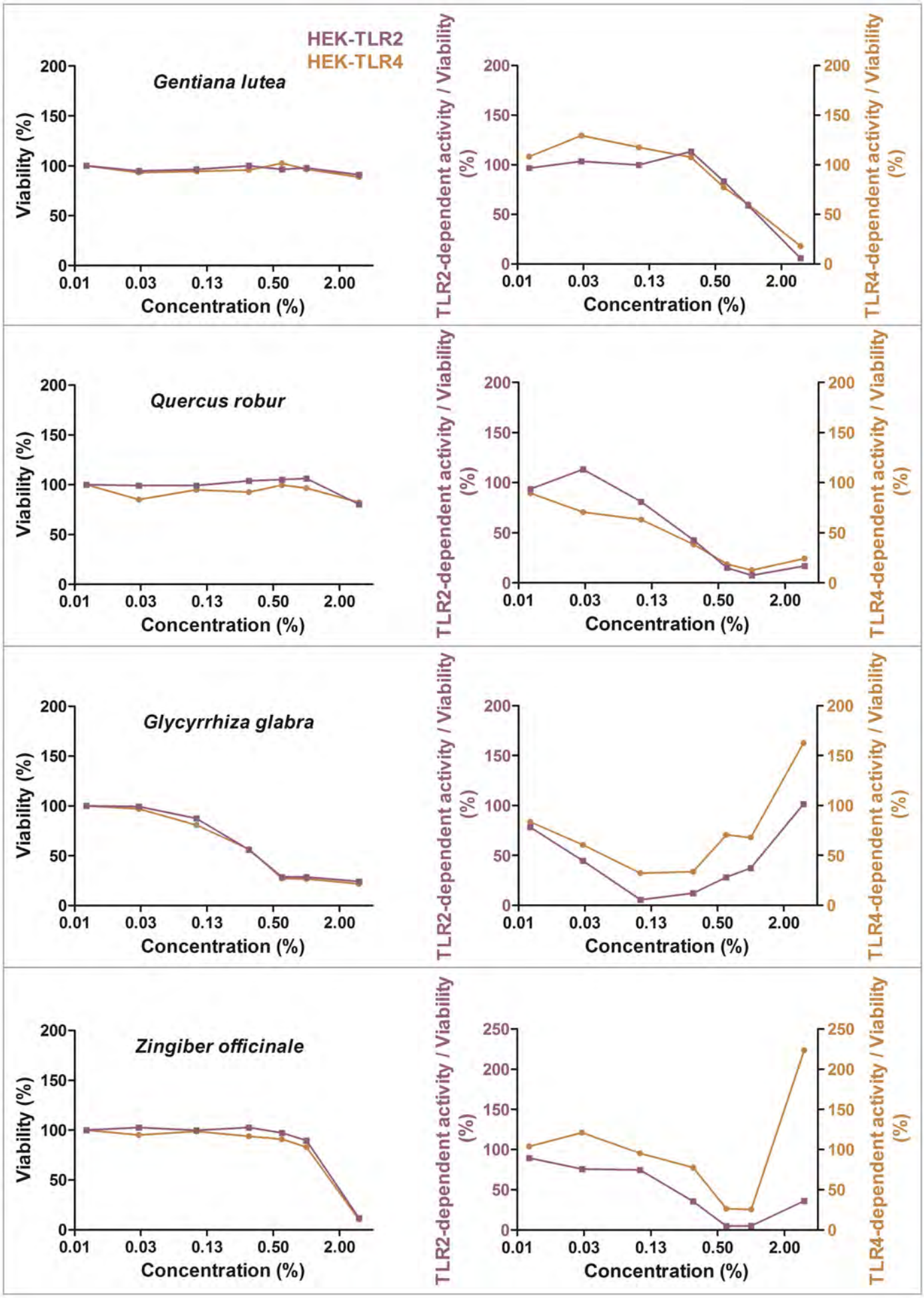
HEK-TLR2
HEK-TLR4
Gentiana lutea
Quercus robur
Glycyrrhiza glabra
Zingiber officinale
Viability (%)
TLR2-dependent activity / Viability (%)
TLR4-dependent activity / Viability (%)
Concentration (%)
0.01
0.03
0.13
0.50
2.00

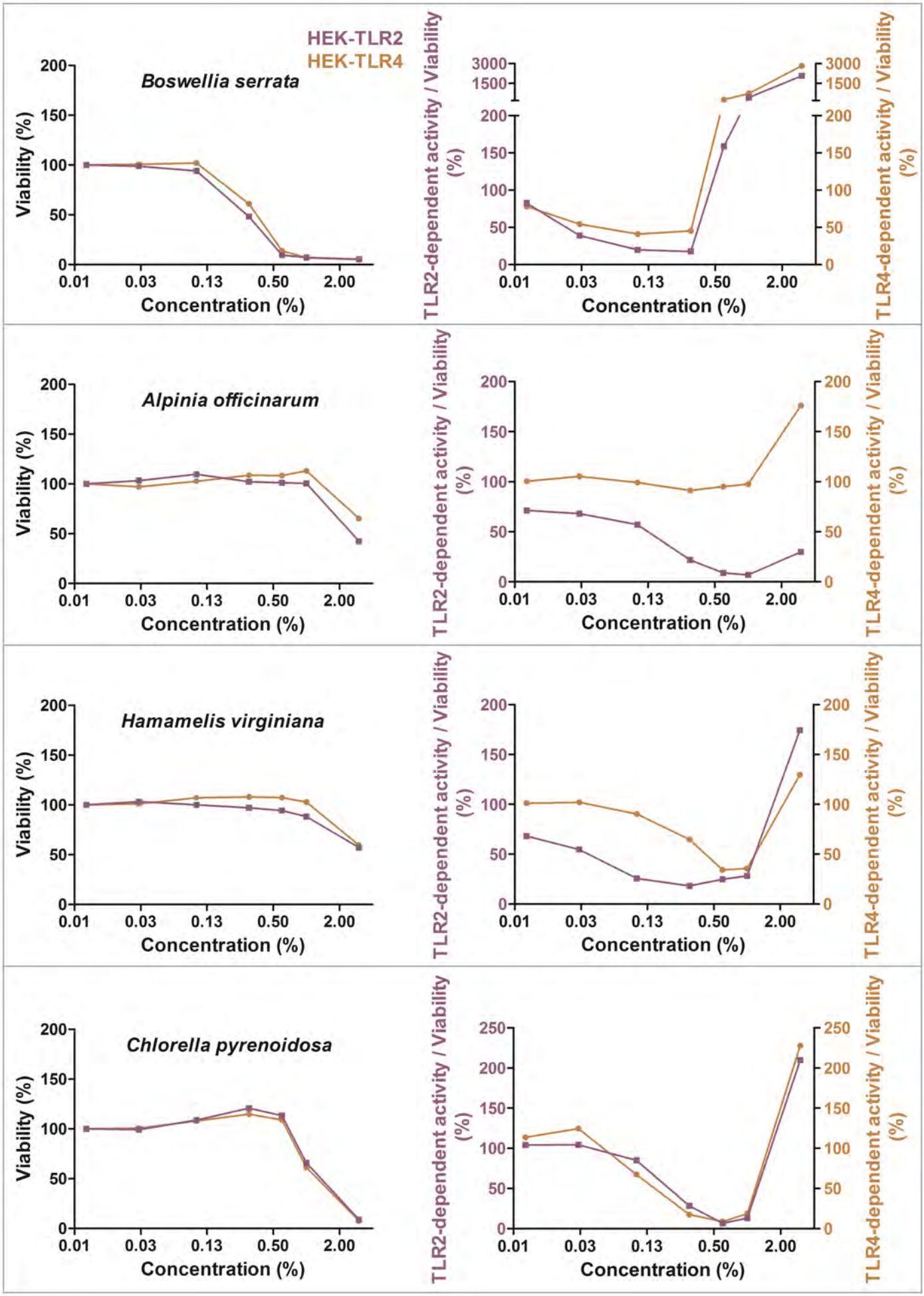
HEK-TLR2
HEK-TLR4
Boswellia serrata
Viability (%)
Concentration (%)
TLR2-dependent activity / Viability (%)
TLR4-dependent activity / Viability (%)
Alpinia officinarum
Hamamelis virginiana
Chlorella pyrenoidosa
0.01
0.03
0.13
0.50
2.00

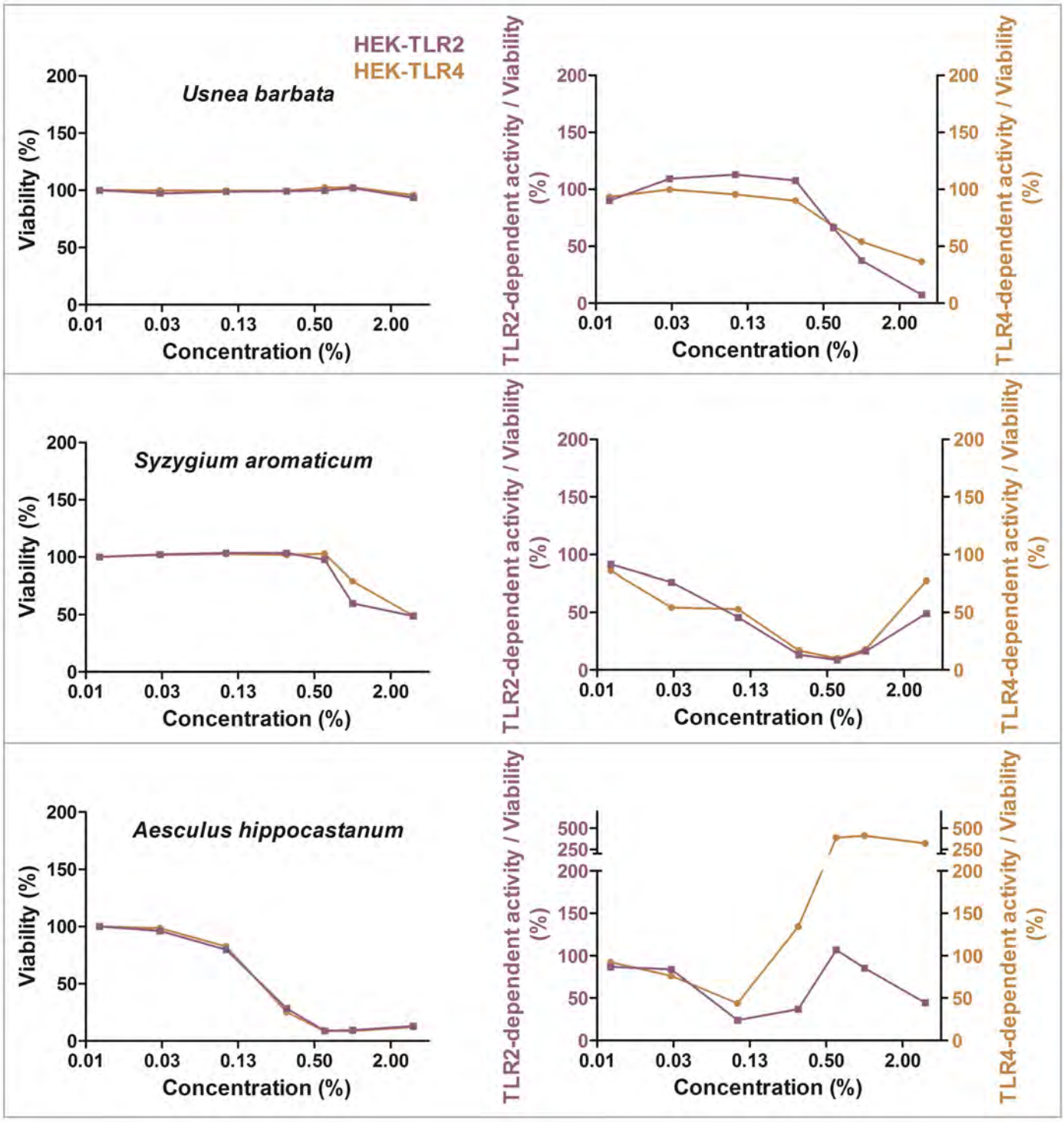
HEK-TLR2
HEK-TLR4
Usnea barbata
Viability (%)
Concentration (%)
TLR2-dependent activity / Viability (%)
TLR4-dependent activity / Viability (%)
Syzygium aromaticum
Aesculus hippocastanum
0.01
0.03
0.13
0.50
2.00

			HEK-TLR2 reporter cell line							HEK-TLR4 reporter cell line						
Latin name	**Common English name**	**Used part**	**0.01%**	**0.03%**	**0.1%**	**0.3%**	**0.6%**	**1%**	**3%**	**0.01%**	**0.03%**	**0.1%**	**0.3%**	**0.6%**	**1%**	**3%**
Ethanol control			100,00	102,45	101,84	101,03	102,55	103,43	124,76	100,00	106,70	106,82	105,37	103,93	107,97	127,11
Castanea sativa	Sweet chestnut	Leaf	20,06	17,83	9,78	11,82	19,94	28,56	118,82	24,28	17,36	12,78	15,09	20,87	32,77	161,75
Cinchona pubescens	Cinchona	Bark	100,53	94,50	77,03	65,89	25,61	13,17	22,78	96,97	92,46	86,34	75,11	48,95	37,82	32,81
Cinnamomum verum	Cinnamon	Bark	100,40	100,11	105,47	65,88	36,23	22,34	37,65	100,75	97,62	94,69	59,98	27,50	18,82	32,43
Salix alba	White willow	Bark	102,12	100,18	85,03	42,14	20,67	17,65	73,17	100,01	85,03	67,85	40,08	34,16	24,12	52,75
Rheum palmatum	Rhubarb	Root	96,48	87,24	59,40	36,53	13,11	8,17	24,68	89,65	89,52	64,85	40,62	20,74	16,27	38,65
Humulus lupulus	Hops	Flower	90,21	90,80	45,52	6,84	7,25	12,55	88,75	99,42	104,49	56,15	18,10	13,97	15,99	105,06
Arctostaphylos uva-ursi	Bearberry	Leaf	91,42	71,09	20,16	11,86	25,75	41,19	385,83	101,93	96,18	91,06	77,63	36,71	24,40	217,02
Allium ursinum	Wild garlic	Leaf	95,05	117,18	104,97	110,95	85,31	45,41	8,55	92,64	101,32	83,11	79,90	53,77	32,22	13,36
Hypericum perforatum	St John's wort	Whole plant	100,82	92,09	94,08	89,60	48,53	29,53	6,00	101,20	125,93	115,86	99,00	72,14	41,77	12,66
Aloe ferox	Aloe	Whole plant	99,50	94,02	95,36	76,96	56,33	45,12	158,90	95,70	105,77	87,57	62,60	40,30	32,00	208,70
Cynara scolymus	Artichoke	Leaf	104,96	99,81	95,14	60,38	11,43	7,45	9,75	102,92	109,70	99,86	71,37	37,63	25,76	19,01
Salvia officinalis	Salvia	Leaf	79,45	87,83	73,41	38,26	9,48	5,77	25,80	100,28	103,61	65,58	34,90	14,99	9,98	19,63
Ginkgo biloba	Ginkgo	Leaf	83,06	80,39	74,11	30,88	4,92	4,06	7,87	100,24	107,01	81,26	42,13	21,39	14,24	14,18
Vigna radiata	Mung bean (dried)	Fruit/berry/ seed	86,58	110,71	78,43	91,74	84,41	65,29	30,75	77,04	94,29	88,78	86,30	76,44	74,46	59,49
Filipendula ulmaria	Meadowsweet	Flower	75,12	63,58	51,28	40,60	30,35	18,59	15,08	101,71	111,43	107,58	103,43	102,99	101,11	94,91
Spirulina	Spirulina	Whole cyanobacteria	116,49	139,54	127,71	129,36	67,85	15,01	28,28	99,69	110,62	69,12	40,91	16,95	12,20	38,50
Gentiana lutea	Gentian	Root	96,77	103,65	99,90	113,40	83,38	59,14	5,82	108,21	129,60	117,81	107,54	77,28	60,19	18,10
Quercus robur	English oak	Bark	93,72	113,22	81,11	42,60	15,04	7,52	16,84	89,53	70,65	63,23	38,30	18,82	12,82	24,23
Glycyrrhiza glabra	Liquorice	Root	78,30	44,63	5,56	12,09	28,06	37,27	101,27	83,64	60,59	32,18	33,77	70,66	67,87	162,46
Zingiber officinale	Ginger	Root	89,51	75,69	74,77	35,53	4,69	5,18	35,84	103,89	120,85	95,36	77,68	26,45	25,34	223,46
Boswellia serrata	Frankincense	Juice/resin	82,46	38,96	19,81	17,73	159,07	432,24	2076,63	78,29	54,43	40,86	45,48	288,07	744,11	2813,02
Alpinia officinarum	Galangal	Root	71,36	68,16	57,03	21,85	8,95	6,85	29,83	100,45	105,34	99,27	91,33	95,04	97,57	176,07
Hamamelis virginiana	Witch hazel	Leaf	68,01	54,73	25,63	18,14	24,82	28,25	174,32	101,02	102,08	90,19	64,82	34,21	35,64	129,53
Chlorella pyrenoidosa	Chlorella	Whole algae	103,97	104,34	84,84	28,14	6,63	12,96	209,74	113,66	124,42	67,31	17,39	8,74	18,75	227,74
Usnea barbata	Barber's itch	Whole plant	90,08	109,48	113,03	107,82	66,29	37,56	7,49	93,50	99,92	95,64	90,15	67,63	54,02	36,36
Syzygium aromaticum	Clove	Flower	91,40	76,21	45,89	13,37	8,91	16,47	49,18	86,11	54,39	52,82	16,99	10,06	18,12	77,65
Aesculus hippocastanum	Horse-chestnut	Fruit/berry/ seed	86,76	83,98	24,02	36,87	106,93	85,46	44,41	92,43	76,26	43,91	134,14	388,13	413,57	323,76

B.5 Lang-Yona *et al.*, Sci Total Environ., 2018

Fresh water, marine and terrestrial cyanobacteria display distinct allergen characteristics

Lang-Yona N.[1], Kunert A. T.[1], Vogel L.[2], Kampf C. J.[3], Bellinghausen I.[4], Saloga J.[4], Schink A.[1], Ziegler K.[1], Lucas K.[1], Schuppan D.[5,6], Pöschl U.[1], Weber B.[1] and Fröhlich-Nowoisky J.[1]

[1] Max Planck Institute for Chemistry, Multiphase Chemistry Department, 55128 Mainz, Germany.

[2] Paul Ehrlich Institute, Department of Allergology, 63225 Langen, Germany.

[3] Johannes Gutenberg University, Institute of Organic Chemistry, 55128 Mainz, Germany.

[4] University Medical Center of the Johannes Gutenberg University, Department of Dermatology, 55131 Mainz, Germany.

[5]Institute of Translational Immunology, University Medical Center of the Johannes Gutenberg University, 55131 Mainz, Germany

[6] Division of Gastroenterology, Beth Israel Deaconess Medical Center and Harvard Medical School, Boston, MA, 02215, USA

Science of The Total Environment 612, 767-774,
DOI: 10.1016/j.scitotenv.2017.08.069., (2018).

Science of the Total Environment 612 (2018) 767–774

Contents lists available at ScienceDirect

Science of the Total Environment

journal homepage: www.elsevier.com/locate/scitotenv

Fresh water, marine and terrestrial cyanobacteria display distinct allergen characteristics

Naama Lang-Yona [a,*], Anna Theresa Kunert [a], Lothar Vogel [b], Christopher Johannes Kampf [c,a], Iris Bellinghausen [d], Joachim Saloga [d], Anne Schink [a], Kira Ziegler [a], Kurt Lucas [a], Detlef Schuppan [e,f], Ulrich Pöschl [a], Bettina Weber [a], Janine Fröhlich-Nowoisky [a,*]

[a] Max Planck Institute for Chemistry, Multiphase Chemistry Department, Mainz, Germany
[b] Paul-Ehrlich-Institut, Department of Allergology, Langen, Germany
[c] Johannes Gutenberg University, Institute of Organic Chemistry, Mainz, Germany
[d] University Medical Center of the Johannes Gutenberg University, Department of Dermatology, Mainz, Germany
[e] University Medical Center of the Johannes Gutenberg University, Institute of Translational Immunology and Research Center for Immunotherapy
[f] Beth Israel Deaconess Medical Center, Harvard Medical School, Boston, MA, USA

HIGHLIGHTS

- Cyanobacteria increase in abundance and usage, yet the allergenicity remained elusive.
- Allergenic potential of different taxa is demonstrated through three immunoassays.
- Similarities are observed between freshwater cyanobacteria and C-phycocyanin.
- *Nostoc* sp. shows anti-inflammatory and unique immune-reactive characteristics.
- Increase in public awareness would enable mitigation of the potential health risk.

GRAPHICAL ABSTRACT

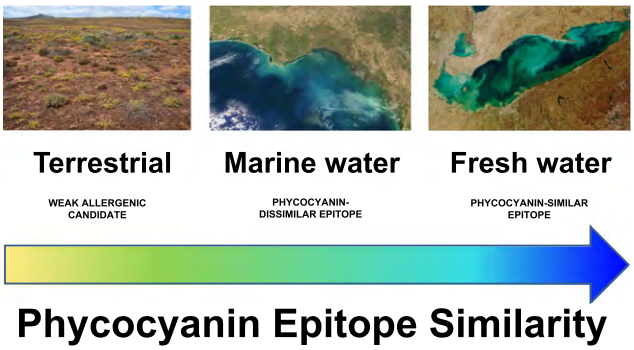

ARTICLE INFO

Article history:
Received 31 May 2017
Received in revised form 7 August 2017
Accepted 8 August 2017
Available online 1 September 2017

Editor: D. Barcelo

Keywords:
Phycocyanin
Protein mass spectrometry
Nostoc

ABSTRACT

During the last decades, global cyanobacteria biomass increased due to climate change as well as industrial usage for production of biofuels and food supplements. Thus, there is a need for thorough characterization of their potential health risks, including allergenicity. We therefore aimed to identify and characterize similarities in allergenic potential of cyanobacteria originating from the major ecological environments. Different cyanobacterial taxa were tested for immunoreactivity with IgE from allergic donors and non-allergic controls using immunoblot and ELISA. Moreover, mediator release from human FcεR1-transfected rat basophilic leukemia (RBL) cells was measured, allowing in situ examination of the allergenic reaction. Phycocyanin content and IgE-binding potential were determined and inhibition assays performed to evaluate similarities in IgE-binding epitopes. Mass spectrometry analysis identified IgE-reactive bands ranging between 10 and 160 kDa as phycobiliprotein compounds. Levels of cyanobacterial antigen-specific IgE in plasma of allergic donors and mediator release from sensitized RBL cells were significantly higher compared to non-allergic controls ($p < 0.01$). Inhibition studies indicated

Abbreviation list: BSA, bovine serum albumin; C-PC, C-phycocyanin; DC, dendritic cell; HRP, horseradish peroxidase; FcεR1, human high-affinity receptor for IgE; KLH, keyhole limpet hemocyanin; LCM, linker core-membrane; LPS, lipopolysaccharides; PBS, phosphate buffered saline; PL, plasma; RBL, rat basophilic leukemia; SDS-PAGE, sodium dodecyl sulfate polyacrylamide gel electrophoresis; TBS-T, Tris-buffered saline + 0.05% Tween 20.

* Corresponding authors.
E-mail addresses: naamalan@gmail.com (N. Lang-Yona), j.frohlich@mpic.de (J. Fröhlich-Nowoisky).

http://dx.doi.org/10.1016/j.scitotenv.2017.08.069

Immunoassay
Inhibition assay

cross-reactivity between IgE-binding proteins from fresh water cyanobacteria and phycocyanin standard. We further addressed IgE-binding characteristics of marine water and soil-originated cyanobacteria. Altogether, our data suggest that the intensive use and the strong increase in cyanobacterial abundance due to climate change call for increasing awareness and further monitoring of their potential health hazards.

1. Introduction

Cyanobacteria are considered to be the most ancient photosynthetically-active life form, having played a key role in Earth history and the evolution of life on Earth (Knoll, 2008; Lenton and Daines, 2016). Thus they are found in all illuminated environments on this planet, including salty lakes, ice fields, hot springs, soils, fresh and marine waters (Whitton, 2012).

Various cyanobacteria serve as main biocatalysts in the nitrogen cycle (Issa et al., 2014), and they may be responsible for about 50% of global nitrogen fixation (Elbert et al., 2012). Some species are used for biofuel production, e.g., *Synechococcus* spp. (Nozzi et al., 2013), and others serve as food additives, e.g., *Arthrospira platensis* (*Spirulina*), *Nostoc* spp., *Synechocystis* spp. due to their high nutrient value (Borowitzka, 2013) and anti-inflammatory properties (Ku et al., 2013). Increased and expended marine cyanobacterial blooms have been reported due to environmental change, e.g., increase in temperature and CO_2 (Gobler et al., 2017), which may lead to an extended aerosolization of such species, carried toward the coastal areas (Lang-Yona et al., 2014).

Human exposure to cyanobacteria can occur through skin contact, consumption of food or food supplements, contaminated water, or inhalation of aerosolized cyanobacteria (Genitsaris et al., 2011; Bernstein and Safferman, 1970; Mittal et al., 1979; Schlichting, 1974; Sharma and Rai, 2008). Numerous cyanobacterial species can produce dermatotoxic, neurotoxic or hepatotoxic agents (van Apeldoorn et al., 2007), which may cause animal and, rarely, human deaths (Osborne et al., 2001). In addition to toxins, lipopolysaccharides (LPS) present in the outer membrane of cyanobacteria, have been reported to induce influenza-like illnesses (Annadotter et al., 2005) and were detected in air samples (Lang-Yona et al., 2014).

First reports on allergic reactions to cyanobacteria have appeared around 1950 (Heise, 1951), and since then, several studies demonstrated a correlation between cyanobacteria crude extracts and cutaneous hypersensitivities (Sharma and Rai, 2008; Bernstein et al., 2011; Stewart et al., 2006b; Torokne et al., 2001; Stewart et al., 2006a). Few case studies have reported severe allergic reactions upon exposure to cyanobacteria, i.e. anaphylactic shocks after food supplement consumption (Le et al., 2014; Petrus et al., 2010) and after swimming in a lake during cyanobacterial bloom (Geh et al., 2016).

Phycocyanin, a blue pigment protein complex, is commonly found in cyanobacteria and serves as light-absorbing compound in their photosynthetic apparatus (Schirmer et al., 1985). This pigment is widely used in the industry as a natural fluorescent dye, in food and beverages as a natural coloring agent, or in pharmaceutical applications (Kuddus et al., 2013). Recent studies have identified this compound as a potential allergen in two cyanobacteria species, i.e., *A. platensis* (Petrus et al., 2010) and *Microcystis aeruginosa* (Geh et al., 2015). However, a wider characterization of cyanobacterial allergens is still needed to comprehensively understand their allergenic potential, as well as similarities or differences of the allergens present in the different species.

We therefore aimed to analyze and characterize the allergic reactivity of seven cyanobacterial taxa originating from terrestrial, fresh and marine water environments. We compared the allergenic behavior of these species to the previously characterized allergenic cyanobacterium *M. aeruginosa* (Geh et al., 2015), and searched for similarities through protein identification and IgE-binding inhibition patterns.

2. Materials and methods

2.1. Cultures of cyanobacteria

Eight cyanobacterial taxa as listed in Table 1 were obtained from the Culture Collection of Algae at the Göttingen University (international acronym: SAG; Göttingen, Germany). Five species originating from fresh water (*Microcystis aeruginosa*, *Cylindrospermum siamensis*, *Anabaena ambigua*, *Lyngbya lagerheimii*, *Planktothrix agardhii*), two from marine (*Synechocystis* sp. and *Phormidium* sp.), and one was from a terrestrial environment (*Nostoc* sp.). Cultures were grown in different media as detailed in Table 1 at 20 °C, 120 rpm, and a 16 h/8 h light/dark cycle (76 μmoles m^{-2} s^{-1} daylight lamps; Heraeus BK 6160 low temperature incubator, Thermo Fisher Scientific, Darmstadt, Germany). Growing cultures were screened by light microscopy (Axio Imager A2, Zeiss, Göttingen, Germany) for purity of the cultures and morphological validation.

2.2. Human plasma samples

Six plasma samples (PL 1–6) were obtained from PlasmaLab Ltd. (Everett, WA, USA) and four (PL 7, PL N1–N3) from the Department of Dermatology (University Medical Center of the Johannes Gutenberg University, Mainz, Germany). Donors of plasma PL 1–7 were sensitized to a variety of aeroallergens and food allergens as summarized in Table 2, (the complete list is detailed in Table S1). Plasma N1–N3 were from non-allergic donors with no sensitization against aeroallergens or food allergens, with low levels of total IgE. All plasma samples were aliquoted and stored at −80 °C until use. The study was approved by the local ethics committee (Landesaerztekammer Rheinland-Pfalz, no. 837.055.16 (10374)), and written consent was obtained from all subjects in advance.

2.3. Protein extraction and quantification

Crude extraction of total proteins from cyanobacteria was performed as previously described (Ivleva and Golden, 2007) with some modifications (Lang-Yona et al., 2016). In brief, cultures of cyanobacteria in the late exponential growth phase were transferred into 50 mL tubes and centrifuged at 10,000 × *g* for 10 min. The pellets were washed with sterile phosphate buffered saline (PBS; Sigma-Aldrich, Munich, Germany), and resuspended in 200 μL PBS buffer before overnight storage at −80 °C. After thawing at 37 °C, the samples were placed on ice and a protease inhibitor cocktail (Sigma-Aldrich) together with 0.5 mm acid washed glass beads (Sigma-Aldrich) were added to the samples. They were then homogenized for 30 s using the Fastprep 24 homogenizer (MP Biomedicals, Heidelberg, Germany), and additional 100 μL PBS were added. After 10 min centrifugation at 4 °C and 10,000 × *g*, the supernatant was collected. This step was repeated twice followed by filtration through sterile 5 and 0.45 μm syringe filters (Pall Corporations, Bad Kreuznach, Germany). *Phleum pratense* and *Betula pendula* pollen (Allergon AB, Ängelholm, Sweden) were used as positive controls for the allergic reaction assays, and the extraction of proteins followed the same procedure as described above.

Protein concentrations were determined with Pierce bicinchoninic acid assay (BCA, Thermo Fisher Scientific) according to the

Table 1
Species tested for allergenic reaction.

Tested organism	Strain	Origin	Growth environment	Growth medium	Special characteristics	Reference
Microcystis aeruginosa	SAG 1450-1	Wisconsin, USA	Fresh water	ES[b]	Produce microcystin and cyanopeptolin	(Dittmann et al., 1997)
Cylindrospermum siamensis (Antarikanonda)	SAG 11.82	Thailand	Fresh water, damp soil	BG-11[a]	Grow under a wide range of environmental conditions	(Johansen et al., 2014)
Anabaena ambigua (C.B. Rao)	SAG 1403-7	India	Fresh water	ES[b]	Nitrogen fixing abilities; neurotoxin production	(Komárek, 2005)
Lyngbya lagerheimii (Gomont ex Gomont)	SAG 24.99	Hungary	Fresh water	BG-11[a]	Grow in mats; natural compounds used for pharmaceutics	(Komárek and Komárková-Legnerová, 1992)
Planktothrix agardhii (Gomont) Anagnostidis & Komárek	SAG 3.82	Norway	Fresh water	ES[b]	High abundance in shallow and eutrophic lakes; microcystin production	(Rücker et al., 1997)
Synechocystis sp. (C. Sauvageau)	SAG 37.92	California, USA	Marine water	1/2 SWES[b]	Used for biofuel production	(Lang et al., 2011)
Phormidium sp. (Kützing ex Gomont)	SAG 9.92	Spain	Marine water	SWES[b]	Red-pigmented cyanobacteria	(Komarek et al., 2014)
Nostoc sp. (Vaucher ex Bornet & Flahault)	SAG 70.79	France	Soil	ES[b]	Grow under a wide range of environmental conditions; characteristic morphology of colonies comprising filaments in a gelatinous sheaths	(Potts, 1997)
Phleum pratense	011312102	–	–	–		
Betula pendula	11101	–	–	–		

[a] Recipe from by Sammlung von Algenkulturen Göttingen (SAG) culture collection of algae.
[b] Recipes from SAG culture collection of algae.

manufacturer's protocol, and absorbance was measured with a microplate photometer (Multiskan GO, Thermo Fisher Scientific). The extracts were stored at −80 °C until further analysis.

2.4. SDS-PAGE and immunoblot

The extracted proteins were separated by sodium dodecyl sulfate polyacrylamide gel electrophoresis (SDS-PAGE) using 4–20% Precast Protein Gels (Mini-PROTEAN TGX, Bio-Rad, Munich, Germany) and detected with an imaging system (ChemiDoc XRS+, Bio-Rad). For Western blots, proteins were transferred onto PVDF membranes (PVDF Transfer Packs, Bio-Rad) using the Trans Blot Turbo semi-dry transfer system (Bio-Rad) according to the manufacturer's protocol. The membranes were washed with Tris-buffered saline containing 0.05% Tween 20 (TBS-T; Sigma-Aldrich), and blocked for 1 h with 5% bovine serum albumin (BSA; Sigma-Aldrich) in TBS-T buffer (5% BSA-TBS-T).

To detect human IgE-binding proteins, membranes were incubated overnight with 10% human plasma diluted in 5% BSA-TBS-T, followed by an overnight incubation with goat anti-human IgE antibody conjugated with horseradish peroxidase (HRP; Thermo Fisher Scientific) diluted in 5% BSA-TBS-T. To verify general reactivity of C-PC standard, detection was conducted with pooled plasma, containing PL 1, 3, 4 and 5. For the detection of phycocyanin compounds, blocked membranes were incubated overnight with a polyclonal rabbit anti-phycocyanin antibody conjugated to HRP (raised against C-phycocyanin whole protein from *Spirulina*, Biorbyt, Cambridge, UK) diluted in 5% BSA-TBS-T. Bound antibodies were developed with the enhanced chemiluminescence (ECL) Western Blotting Substrate kit according to the manufacturer's protocol (Pierce/Thermo Fisher Scientific). The resulting chemiluminescence was detected with the ChemiDoc XRS+ imaging system. Membranes were washed with TBS-T between all incubation steps and each assay was repeated 3 times.

2.5. IgE measurement and inhibition ELISA

The total and specific IgE concentrations were evaluated in human plasma as previously described (Bashir et al., 2013), with some modifications. Clear flat-bottom MaxiSorp 96-well plates (Nunc, Thermo Fisher Scientific) were coated with cyanobacteria/pollen extracts or C-phycocyanin from *Spirulina* sp. (C-PC; Sigma-Aldrich) at a protein concentration of 10 μg mL^{-1} in carbonate buffer. Wells reserved for standards and for the total IgE content were coated with anti-human IgE (A80-108A-15, Bethyl Laboratories, Inc., Montgomery, TX, US) at a concentration of 10 μg mL^{-1} in carbonate buffer. Plates were incubated at 4 °C overnight, washed three times with PBS-0.05% Tween 20 (PBS-T),

Table 2
Characterization of plasma samples for different allergens and total IgE levels.

Sample ID	IgE levels (kU L^{-1})										
	Phleum pratense	Other grass pollens	*Betula pendula*	Other tree pollen	Food	Weeds	Animals	Molds	Insects	Mites	Total[a]
PL 1	>100	>100	>100	>100	>100	33	40	37	24	81	5058
PL 2	90	90	37	43	29	10	92	61	12	32	5468
PL 3	>100	>100	12	32	32	38	3	21	26	2	5192
PL 4	78	[b]	>100	>100	>100	15	>100	65	[b]	>100	6036
PL 5	43	[b]	5	3	9	2	>100	10	1	>100	7085
PL 6	21	[b]	83	[b]	1	0.7	3	[c]	[d]	22	2391
PL 7	23.7	[d]	>100	[d]	68.1	[d]	[d]	[d]	[d]	[d]	2944
PL N1	[c]	[c]	[c]	[c]	[c]	[c]	[c]	[c]	[d]	[c]	19
PL N2	[c]	[c]	[c]	[c]	[c]	[c]	[c]	[c]	[d]	[c]	37.5
PL N3	[c]	[c]	[c]	[c]	[c]	[c]	[c]	[c]	[d]	[c]	27

[a] Tested in the current study.
[b] Not detected.
[c] <0.35 kU L^{-1}.
[d] No information available.

and blocked with 1% BSA in PBS-T (1% BSA-PBS-T; Sigma-Aldrich) at room temperature for 1 h. Standard serial dilutions (0.975 to 250 ng mL^{-1}) of the human IgE calibrator (RC80-108-6, Bethyl Laboratories) in 1% BSA-PBS-T, as well as buffer blanks, were dispensed to the corresponding wells. Plasma samples and controls (diluted with 1% BSA-PBS-T) were added to the remaining wells and incubated at room temperature for 2 h. Bound IgE was detected with HRP conjugated goat anti-human IgE antibody (A80-108P-35, Bethyl Laboratories, Inc.; diluted 1:100,000 in 1% BSA-PBS-T) incubated at room temperature for 2 h. Color development was achieved in the dark by addition of 1-Step Ultra TMB-ELISA reagent (Thermo Fisher Scientific) and terminated with 2 mM sulfuric acid (Sigma-Aldrich) after sufficient color development. Absorbance was detected at 450 nm using a microplate photometer (Multiskan GO, Thermo Fisher Scientific). The amount of bound IgE antibody was calculated from the standard curves. Plates were washed with PBS-T between all steps and each assay was repeated 3 times.

ELISA inhibition assays were performed as described previously (de Leon et al., 2003) with some modifications. Briefly, 96-well polystyrene plates were coated with protein extracts (10 μg mL^{-1}) and blocked as described above. In order to obtain a better assessment of similarities in IgE-binding epitopes, pooled plasma (containing PL 1, 3, 4 and 5) and controls (diluted with 1% BSA-PBS-T) were pre-incubated with serial dilutions of the cyanobacterial extracts or, as a control, keyhole limpet hemocyanin (KLH; Sigma-Aldrich) in sterile 96-well conically shaped polypropylene plates (Nunc, Thermo Fisher Scientific) at room temperature for 2 h. One hundred microliters of the inhibition mixtures (including plasma with no inhibitor as positive control) were then dispensed into coated wells and incubated at room temperature for 2 h. The incubation with secondary antibody and color development was performed as described above. After correction for non-specific binding (control wells containing no antigen), percentage of inhibition was calculated using the following formula:

$$\%\text{inhibition} = 100 - \frac{OD_{405}\ \text{serum with inhibitor}}{OD_{405}\ \text{serum without inhibitor}} \times 100$$

2.6. Mediator release assay

The mediator release assay followed an established protocol (Ladics et al., 2008). In short, HuFcεRI-transfected rat basophilic leukemia (RBL) cells expressing the α-chain of human FcεRI were sensitized overnight with patients' plasma diluted in minimum essential medium containing 5% fetal calf serum (Biochrom, Berlin, Germany). After washing, cells were stimulated with serial dilutions of protein extracts in Tyrode's buffer containing 0.1% BSA and 50% D_2O. Degranulation was quantified by measuring the β-hexosaminidase activity in the culture supernatants by a substrate reaction with 4-Nitrophenyl *N*-acetyl-β-D-glucosaminide (Sigma-Aldrich). The absorbance was measured in a microplate reader at 405/620 nm, and the release was expressed as percent of the total cellular β-hexosaminidase content obtained by lysing the cells with Triton X-100 (Sigma-Aldrich) after correction for spontaneous release (cells incubated with plasma alone). Vitality of cells was evaluated before each step using light microscopy observation.

2.7. Statistical analysis

Data are reported as the mean ± SD. Significant differences between samples and controls were calculated using unpaired, two-sided Student's *t*-test, after normal distribution and homogeneity of variance were verified. Significance of inhibition levels between samples and negative control was evaluated using One Way ANOVA followed by Tukey post-hoc analysis for means comparison (Origin Pro 9). Levene's test for homogeneity of variance and normal distribution were verified prior to the analysis. Significant differences were assumed for $p < 0.05$.

3. Results

3.1. Immunoblot and protein analysis of cyanobacterial extracts

Cyanobacterial proteins were probed for IgE-binding using seven plasma samples from allergic patients (PL 1–7) and three samples from IgE-negative, non-allergic controls (PL N1–N3). Fig. 1A and B present protein bands and immunoblot results, respectively, for all eight cyanobacterial taxa, after reaction with PL 4 as a representative plasma. Cyanobacterial IgE-binding proteins were found in all species (Table S3), and the frequency of immunoblot bands varied for different plasma samples (Fig. S1). Strong bands were observed for *M. aeruginosa*, *C. siamensis*, *A. ambigua*, *L. lagerheimii*, *P. agardhii* and *Synechocystis* sp. (Fig. 1B, lanes 1–6 respectively). All fresh water cyanobacteria showed bands at ~100–110 kDa, whereas the marine taxa *Synechocystis* sp. and *Phormidium* sp. (Fig. 1B, lane 6 and 7) showed different IgE-binding protein patterns, with a common band detected at ~10 kDa. *Nostoc* sp. bands were relatively weak (Fig. 1B, lane 8) and resembled the fresh water band patterns. The control allergen, *P. pratense* grass pollen (Fig. 1B, lane 9), presented typical IgE-reactive bands of about 10, 13, 28, 34 and 50 kDa (Dolecek et al., 1993; Rajashankar et al., 2002; Suck et al., 2000). Mass spectrometry analysis (Table S2) revealed phycobilisome-related proteins in ~100 kDa bands, e.g., the phycobilisome rod-core linker and phycobilisome linker (both in the range of 30 kDa), phycobilisome linker core-membrane (LCM, 101.06 kDa) as well as phycocyanin β chain and phycobiliprotein core-membrane linker, ApcE (100.9 kDa), with the highest identification score. These bands were previously identified as IgE-binding proteins from *M. aeruginosa* and *Spirulina* (i.e., LCM protein and phycocyanin β subunit) (Petrus et al., 2010; Geh et al., 2015). Other high-score proteins varied between the different species and included ATPase, ATP synthase subunits, and Photosystem I and II proteins, with the latter being bound to the phycobilisome complex at the inner part of the chloroplast membrane (Sidler, 1995).

Fig. 1C shows the C-PC protein bands on SDS-PAGE (lane 1) compared to IgE-binding bands in immunoblot (line 2) from pooled plasma samples (PL 1, 3, 4 and 5). Prominent IgE-binding bands were detected at ~50 and 60 kDa. The four additional species presenting IgE-binding bands in the size range of C-PC (Fig. 1B) were *C. siamensis*, *L. lagerheimii*, *Nostoc* sp. and *Phormidium* sp. Proteins within the 50 kDa band belong to the phycobilisome complex as identified by mass spectrometry (Table S2, in bold), and the highest identification score for these proteins was given to *Phormidium* sp., in concordance with the observed bands in Fig. 1B.

Further characterization and quantification of the phycocyanin protein in the different cyanobacteria is presented in Fig. 1D. The phycocyanin-related bands in immunoblot can be divided into five groups: group I (160–250 kDa) includes phycocyanin hexamers (Morschel et al., 1980), group II (90–120 kDa) comprises the core-membrane linker polypeptides as well as phycocyanin trimers (Sidler, 1995; Morschel et al., 1980), group III (45–60 kDa) contains C-PC monomers (Morschel et al., 1980), group IV (30–40 kDa) represents the rod and rod-core linker polypeptides (Sidler, 1995), and group V (10–20 kDa) contains the monomeric form of phycocyanin (Bloomfield and Jennings, 1969), phycobiliprotein subunits and small linker proteins (Sidler, 1995). The bands expressed by each species are summarized and compared to the IgE-binding bands in Table S3. An overlap between phycocyanin and IgE-binding proteins occurred for one or more bands of each cyanobacterial taxon, as well as for the C-PC standard, where both bands detected by the phycocyanin antibody reacted with allergic donor IgE as well. The monomeric form of α- (~21 kDa) and β-phycocyanin-subunits (~18 kDa) did not react with the IgE-antibodies (Fig. 1C, lane 2). As expected, no phycocyanin-binding band was observed for the grass pollen control.

Phycocyanin bands of 100–110 kDa, indicating core-membrane linker polypeptides or the trimer form of C-PC (Fig. 1D, group II), and

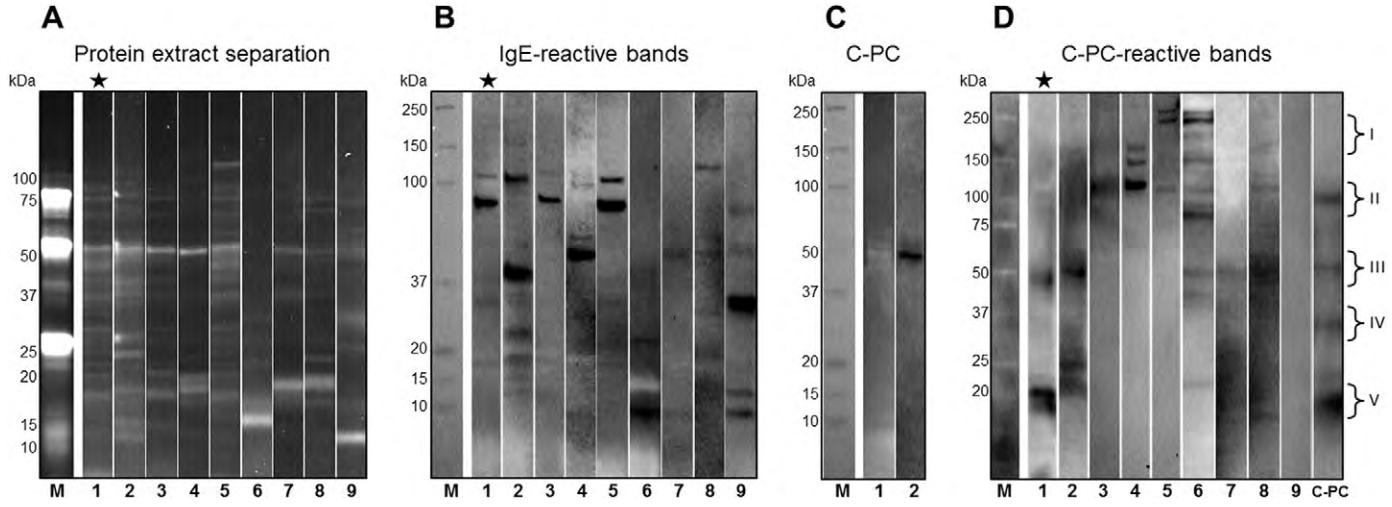

Fig. 1. Immunoblot analysis of cyanobacterial protein extracts. (A) SDS-PAGE separation of cyanobacterial protein extracts. (B) IgE-reactive bands from separated proteins blotted and probed with patient plasma. Results show species-extracts interacting with PL 4. (C) Immunoblot of C-PC standard with pooled patients' plasma (PL 1, 3, 4 and 5). Lanes: M, molecular weight standard; 1, C-PC protein bands; 2, IgE-binding protein bands. (D) C-PC-reactive bands from separated proteins blotted and probed with anti-phycocyanin antibody. Brackets I–V represent the five phycocyanin-related groups (Sidler, 1995; Morschel et al., 1980). Lanes in panel A, B and D: M, molecular weight standard; 1, *Microcystis aeruginosa*; 2, *Cylindrospermum siamensis*; 3, *Anabaena ambigua*; 4, *Lyngbya lagerheimii*; 5, *Planktothrix agardhii*; 6, *Synechocystis* sp.; 7, *Phormidium* sp.; 8, *Nostoc* sp.; 9, *Phleum pratense* and (D only) C-PC standard, respectively. Data are representative for ≥2 independent experimental repeats. The previously reported allergenic species *M. aeruginosa* is denoted (★).

corresponded with IgE-binding in fresh water cyanobacteria, and the *Nostoc* sp. (which presented weak phycocyanin-containing bands, superimposable to its IgE-binding bands, Fig. 1B, lane 9). Both *Synechocystis* sp. and *Phormidium* sp. showed distinct similarities between phycocyanin (Fig. 1D, lanes 6 and 7) and IgE-binding proteins, with multiple dual-reactive phycocyanin bands at higher molecular mass fractions for *Synechocystis* sp.

3.2. Higher cyanobacterial-specific IgE levels in plasma samples from allergic compared to non-allergic donors

To determine the amount of cyanobacteria specific IgE in the plasma samples, a quantitative ELISA was performed (Fig. 2). *Phleum pratense*-specific IgE levels are presented in comparison (Fig. 2, upper right). The different plasmas from the allergen-sensitized donors expressed varying amounts of IgE upon exposure to different cyanobacterial extracts. These IgE concentrations were approximately one order of magnitude lower than those obtained upon exposure to the *P. pratense* grass pollen extract (with levels over 100 kU L^{-1} in most plasmas), and in the same range as the phycocyanin-specific IgE. All examined donor plasmas presented significantly higher IgE levels compared to the negative control plasma, PL N1.

3.3. Induction of IgE-dependent and IgE-independent basophilic degranulation by cyanobacterial extracts

The presence of specific IgE levels in patients' plasma does not necessarily lead to IgE cross-linking and the initiation of an allergic response. Therefore, we further performed a mediator release assay with RBL cells expressing the human high-affinity receptor for IgE (FcεR1) on their surface (Vogel et al., 2005). In this assay, human IgE is bound by FcεR1, and functional cross-linking by allergens will lead to the release of mediators including β-hexosaminidase, which can easily be measured by a substrate reaction. Fig. 3 shows the results of a representative mediator release assay for cells sensitized with PL 4 and cross linked by exposure to serial dilutions of the different cyanobacterial extracts. High release levels were observed for *Nostoc* sp. (56 ± 3%), but similar levels were also detected after stimulation of the RBL cells sensitized with negative control plasma and treated with this cyanobacterial extract, and even without plasma sensitization.

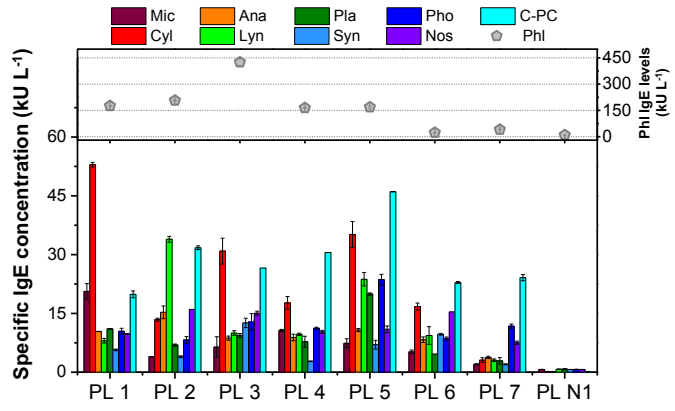

Fig. 2. Cyanobacteria-specific IgE concentration in examined plasmas. ELISA evaluation of specific IgE concentration against cyanobacteria and C-PC standard in plasma samples from allergic patients (PL 1–7) and a negative control plasma (PL N1). *Phleum pratense* grass pollen extract is shown for comparison. Data are representative of 3 independent experimental repeats.

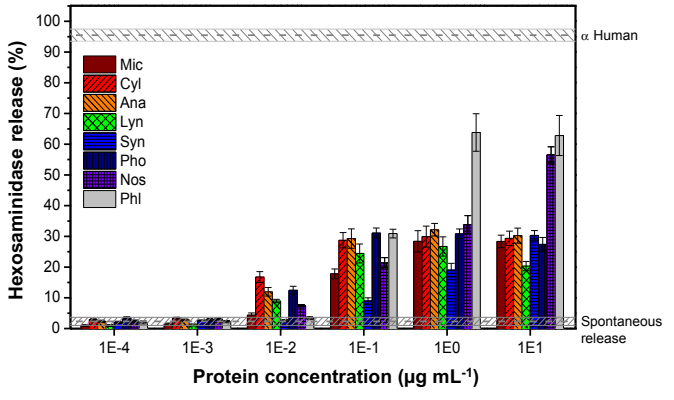

Fig. 3. In vitro characterization of cyanobacterial extracts. Mediator release from FcεRI-humanized RBL cells sensitized with human plasma (PL 4) was determined for serial dilutions of the cyanobacterial proteins. Anti-human IgE was used as positive control (upper dashed line), and cells without cyanobacterial extracts as negative control (lower dashed line). Mean values of triplicates are shown, with $p < 0.01$ compared with control plasma for all samples.

This indicates an IgE-independent degranulation response to antigens from this cyanobacterial species. The maximal release values of the other cyanobacteria did not differ much, and ranged from 26 to 31%. The species *C. siamensis* (30 ± 3%), *A. ambigua* (32 ± 2%), *L. lagerheimii* (27 ± 3%), and *M. aeruginosa* (28 ± 3%) showed their highest release levels at a protein concentration of 1 μg mL^{-1}. Mediator release induced by *Synechocystis* sp. (30 ± 2%) was highest at 10 μg mL^{-1} protein concentration, while *Phormidium* sp.-induced release was 31 ± 2% at 0.1 μg mL^{-1}. As a positive control, cells were sensitized with 0.3 μg mL^{-1} polyclonal human IgE and then cross-linked with goat anti-human IgE (1:500), or with PL 4 and timothy grass pollen extract, which resulted in maximal β-hexosaminidase release of 94 ± 5% and 64 ± 6% (at 1 μg mL^{-1}), respectively. No release was observed with the extracts for the control plasmas.

The unique behavior of *Nostoc* sp. was also noted in its anti-inflammatory properties (Fig. S1, A and B). This species was the only one showing a reduction of LPS-induced inflammation by 50% and 87% in the THP-1 cell line at 1 μg mL^{-1} and 10 μg mL^{-1}, respectively, compared to cells treated with LPS alone. Cyanobacteria-exposed THP-1 were tested for toxicity, as assessed by THP-1 viability demonstrating insignificant difference between THP-1 exposed to cyanobacterial extracts at both concentrations and the controls (see Supporting Information for more details).

3.4. Cross-reactivity between cyanobacterial species, pollen allergens and C-PC

To understand similarities in IgE-binding epitopes, we performed dose-dependent ELISA inhibition assays with cyanobacterial proteins as well as grass and birch pollen extracts (Fig. 4). The maximum inhibition values are presented in Fig. S2 as a heat map. Generally, *Nostoc* sp. and both the grass (*P. pratense*) and the birch pollen extract (*B. pendula*) were less efficient inhibitors for the tested cyanobacteria (compared to the average values), and pollen extracts were never exceeding an inhibition of 20% (Fig. 4, charts 1–8). Inhibition of *P. pratense* by cyanobacterial protein extracts was also relatively low (below 25% in all cases), whereas inhibition of *B. pendula* by cyanobacteria was higher, with highest rates observed by *Synechocystis* sp. (42.2 ± 4%), *A. ambigua* (38 ± 1%) and *P. agardhii* (34 ± 2%). Insignificant or no inhibition of IgE-binding was observed for the negative control (KLH). Self-inhibition in all samples was in the range of 70–80%.

Fresh water cyanobacterial extracts (Fig. 4, chart 1–5) showed cross-reactivity with *Spirulina*-extracted C-PC, which was significantly higher compared to species originating from other growth environments (Fig. 4, chart 6–8). Although low C-PC inhibited, marine species strongly inhibited fresh water cyanobacterial extracts, whereas fresh water species did not inhibit *Synechocystis* sp. or *Phormidium* sp.

4. Discussion

In recent years, cyanobacteria have been in the spotlight due to their beneficial effects, among which are their high nutrition levels and their ability to produce biofuel and assimilate carbon and nitrogen. As their global biomass also increases due to climate change, there is a need to properly characterize potential hazards associated with this phylum. In this study, we investigated the allergenic properties of cyanobacteria, thriving within different habitats and ecological niches.

We observed distinct IgE-binding patterns for the examined fresh water cyanobacteria. Analysis of the corresponding bands revealed phycobilisome-related proteins, previously identified as IgE-binding proteins from *M. aeruginosa* and *Spirulina* (i.e., LCM protein and phycocyanin β subunit) (Petrus et al., 2010; Geh et al., 2015). IgE binding was also found for the standard C-PC proteins, in contrast to the study by Geh et al. (Geh et al., 2015), where no IgE-reactive bands had been

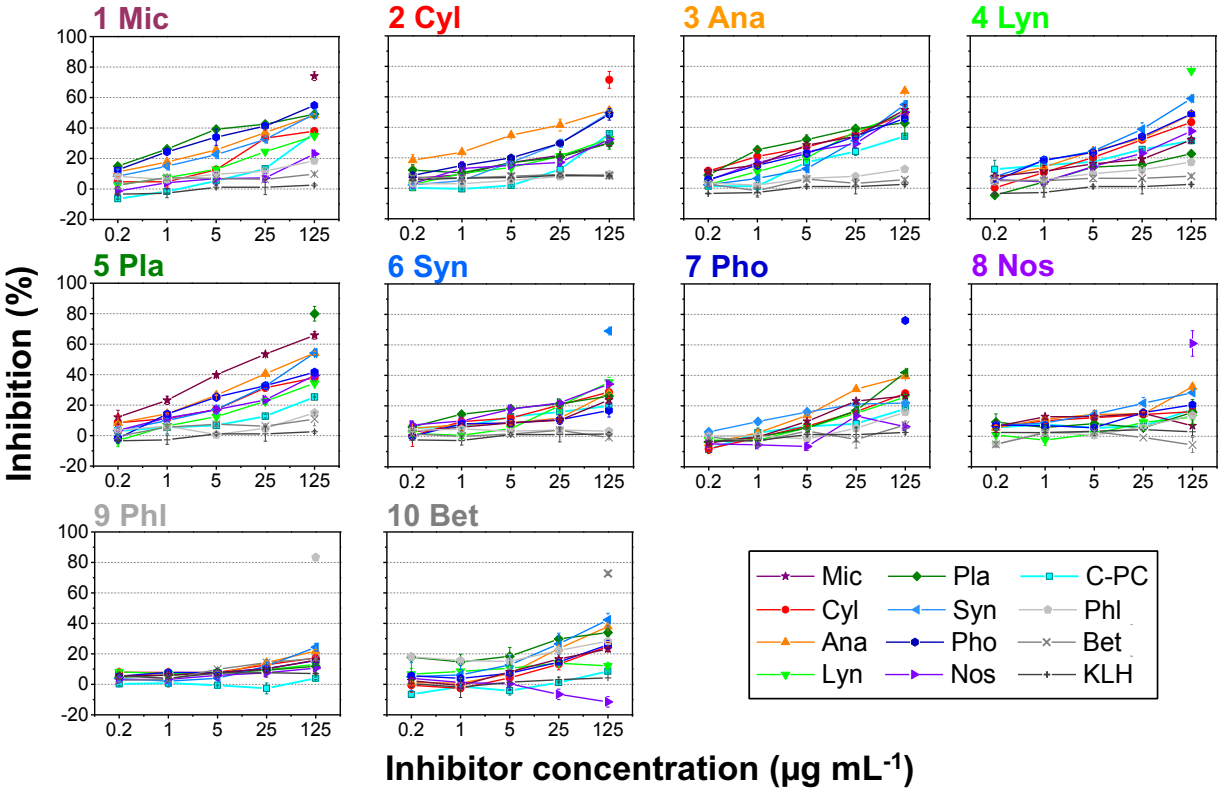

Fig. 4. Cross-reactivity of cyanobacterial proteins analyzed by inhibition ELISA. Cyanobacterial protein extracts (charts 1–8), *P. pratense* extract (chart 9), and *B. pendula* extract (chart 10) were tested for IgE-binding inhibition. Pooled plasma (including PL 1, 3, 4 and 5) were pre-incubated with cyanobacterial or pollen extracts and C-PC standard prior to their addition to plates, coated with extracts of the different cyanobacteria species as well as *P. pratense* and *B. pendula*, respectively. Bound IgE was quantified with an HRP-labeled anti-human IgE antibody. Data are representative of two independent experimental repeats. The same pooled plasma was used for all experiments.

detected for this standard. We attribute this difference to variations in specific IgE content in the tested plasmas/sera used in both studies. The absent IgE-binding signal of the monomer form of α- and β-phycocyanin subunits may indicate that the dimer form (~50 and 60 kDa) exposes IgE-binding epitopes different from the monomers.

The terrestrial *Nostoc* sp. presented weak IgE-binding bands, which might either result from low levels of IgE-binding proteins, lower exposure of the allergic individual to this subgroup or binding interferences by other substances. *Nostoc* spp. are known for their thick mucilaginous carbohydrate sheaths (Oren, 2014; Jordan, 2004), which might cause difficulties in isolation of different compounds from cells. They may also interact with specific compounds (e.g., proteins), as was previously shown for *Nostoc commune* DRH1 (Jordan, 2004), reducing their availability for IgE-binding. Nevertheless, the IgE-binding proteins shared common bands with phycocyanin in fresh water-derived cyanobacteria as well as *Nostoc* sp., suggesting the core-membrane linker polypeptides (indirectly binding the phycocyanin) or the trimer form of C-PC as IgE-binding candidates.

On the other hand, different IgE-binding bands were observed for *Synechocystis* sp. and *Phormidium* sp. (originating from marine environments), as well as distinct correlation patterns between phycocyanin and IgE-binding proteins. It might be that proteins other than phycocyanin are involved, or, alternatively, this may reflect differences in phycocyanin structure in these species. This conclusion is supported by previous publications that reported a unique phycocyanin structure of marine cyanobacteria (Sidler, 1995; Sonani et al., 2015). The differences in structure of the phycobiliprotein pigments compared to fresh water species are attributed to adaptation and modification for optimal light absorption in sea-water. However, conserved regions are yet present, allowing protein recognition by polyclonal antibody. The higher number of phycocyanin components as detected by western blotting using the anti-phycocyanin antibody compared to IgE-binding bands indicates a limited number of primarily allergenic proteins of the phycocyanin-complex.

In preliminary experiments C-PC was found to induce an upregulation of dendritic cell (DC) activation markers (data not shown), which was not due to LPS contamination. This implies that C-PC has intrinsic DC-activation properties that may contribute to its allergenicity, but this requires further investigation.

The different reactivity patterns of specific IgE against cyanobacterial strains indicate diverse epitope recognitions by IgE of the different plasma samples. This strengthens our statement that in addition to phycocyanin, other IgE-binding proteins/epitopes are present in cyanobacteria. The latter statement is further supported by the comparison of phycocyanin protein bands with the bands detected by patients' IgE, where some IgE-bound proteins were not identified as phycocyanin.

The false-positive behavior of the *Nostoc* sp. observed in the mediator release assay is most probably due to a substance that is able to activate the RBL cells independently from IgE, and not by an allergenic component. In a preliminary study, a slight degranulation could be observed for RBL cells, sensitized with various plasmas, cross-linked with C-PC standard. As the signal is not sufficient for the tested plasmas, to determine the C-PC allergenicity further, a larger cohort would be needed where the prior sensitization to cyanobacteria had been verified by skin tests.

The observed cross-reactivity of fresh water cyanobacteria with *Spirulina*-extracted C-PC may be explained by the origin of the *Spirulina*, which is mostly grown in fresh water (Vonshak, 1997). Thus, the structures of the phycocyanins probably share similarities in IgE-binding epitopes. Marine species strongly inhibited fresh water cyanobacterial extracts, however, a mild inhibition for the marine species was observed by C-PC. These results emphasize structural differences in phycocyanin molecules between species (Sidler, 1995), which apparently affect their IgE-binding efficiencies. Moreover, other molecules may participate in IgE-binding and in the potential induction of allergies by cyanobacteria.

The moderate to high inhibition of *B. pendula* by cyanobacterial strains implies a potential similarity between the cyanobacterial IgE-binding proteins and a selected *B. pendula* protein, requiring further investigation. The insignificant inhibition of *B. pendula* by phycocyanin suggests an alternative cyanobacterial IgE-binding protein for the observed similarity.

The low IgE-binding abilities observed for the *Nostoc* sp. throughout all assays, together with the false-positive stimulation of IgE cross-linking lead to the conclusion that this taxon is an unsuitable candidate for allergy induction. Self-inhibition of cyanobacteria is most probably influenced by other compounds in the crude protein extracts which interfere with IgE-binding, reducing binding efficiency to epitopes (Chlipala et al., 2009).

In conclusion, we observed distinguished allergenic activity of the examined fresh water cyanobacteria compared to marine- and soil-derived taxa. The standard C-PC from *Spirulina* demonstrated similarities in all immunoassays for fresh water cyanobacteria, supporting its role as a prime allergenic protein candidate in these species. Differences in IgE-binding proteins compared to the phycocyanin protein patterns observed in immunoblot and inhibition assays, indicate the presence of additional allergenic proteins, which should be investigated in further detail. Differences in inhibition patterns and in immunoassays between fresh water species and cyanobacteria from other environments suggest different allergenic protein types or structures. Low allergenic potential was determined by combined analyses for the terrestrial *Nostoc* sp., and the involvement of its mucilaginous layer in inhibition of the protein activity and availability should be examined. Further studies are needed to identify and fully characterize these allergens, including the abundance of such allergies in the general population, the suspected additional allergenic proteins observed in this study and the similarities with other allergens.

Acknowledgments

The authors would like to acknowledge stimulating discussions with the members of the Mainz Project for Chemical Allergology (MPCA) and of the Mainz Bioaerosol Laboratory (MBAL), Yoav Barak, Jan Neumann, Jan Frederik Scheel and Fobang Liu as well as numerous colleagues in the scientific communities of the Earth, environmental, and life sciences. Support by the IMB (Institute of Molecular Biology, Mainz) Proteomic Core Facility and technical assistance from Petya Yordanova, Gila Kopper and Isabel Maurus is gratefully acknowledged. N.L.-Y acknowledges support from the Weizmann Institute of Science - National Postdoctoral Award Program for Advancing Women in Science. C.J.K acknowledges support from the German Research Foundation (DFG, grant no. KA4008/1-2) and the Max Planck Graduate Center with Johannes Gutenberg University Mainz. B.W gratefully acknowledges support by the Max Planck Society (Nobel Laureate Fellowship).

All authors declare no financial or commercial conflicts of interests.

Appendix A. Supplementary data

Supplementary data to this article can be found online at http://dx.doi.org/10.1016/j.scitotenv.2017.08.069.

References

Annadotter, H., Cronberg, G., Nystrand, R., Rylander, R., 2005. Endotoxins from cyanobacteria and gram-negative bacteria as the cause of an acute influenza-like reaction after inhalation of aerosols. EcoHealth 2 (3), 209–221.

van Apeldoorn, M.E., van Egmond, H.P., Speijers, G.J., Bakker, G.J., 2007. Toxins of cyanobacteria. Mol. Nutr. Food Res. 51 (1), 7–60.

Bashir, M.E., Ward, J.M., Cummings, M., Karrar, E.E., Root, M., Mohamed, A.B., et al., 2013. Dual function of novel pollen coat (surface) proteins: IgE-binding capacity and proteolytic activity disrupting the airway epithelial barrier. PLoS One 8 (1), e53337.

Bernstein, I.L., Safferman, R.S., 1970. Viable algae in house dust. Nature 227 (5260), 851–852.

Bernstein, J.A., Ghosh, D., Levin, L.S., Zheng, S., Carmichael, W., Lummus, Z., et al., 2011. Cyanobacteria: an unrecognized ubiquitous sensitizing allergen? Allergy Asthma Proc. 32 (2), 106–110.
Bloomfield, V.A., Jennings, B.R., 1969. Molecular weight and shape of phycocyanin monomer and aggregates. Biopolymers 8 (2), 297–299.
Borowitzka, M.A., 2013. High-value products from microalgae—their development and commercialisation. J. Appl. Phycol. 25 (3), 743–756.
Chlipala, G., Mo, S., Carcache de Blanco, E.J., Ito, A., Bazarek, S., Orjala, J., 2009. Investigation of antimicrobial and protease-inhibitory activity from cultured cyanobacteria. Pharm. Biol. 47 (1), 53–60.
Dittmann, E., Neilan, B.A., Erhard, M., Von Döhren, H., Börner, T., 1997. Insertional mutagenesis of a peptide synthetase gene that is responsible for hepatotoxin production in the cyanobacterium *Microcystis aeruginosa* PCC 7806. Mol. Microbiol. 26 (4), 779–787.
Dolecek, C., Vrtala, S., Laffer, S., Steinberger, P., Kraft, D., Scheiner, O., et al., 1993. Molecular characterization of Phl p II, a major timothy grass (Phleum pratense) pollen allergen. FEBS Lett. 335 (3), 299–304.
Elbert, W., Weber, B., Burrows, S., Steinkamp, J., Budel, B., Andreae, M.O., et al., 2012. Contribution of cryptogamic covers to the global cycles of carbon and nitrogen. Nat. Geosci. 5 (7), 459–462.
Geh, E.N., Ghosh, D., McKell, M., de la Cruz, A.A., Stelma, G., Bernstein, J.A., 2015. Identification of *Microcystis aeruginosa* peptides responsible for allergic sensitization and characterization of functional interactions between cyanobacterial toxins and immunogenic peptides. Environ. Health Perspect. 123 (11), 1159–1166.
Geh, E., Ghosh, D., Bernstein, J.A., 2016. Sensitization of a child to cyanobacteria after recreational swimming in a Lake. J. Allergy Clin. Immunol. 135 (2), AB104.
Genitsaris, S., Kormas, K.A., Moustaka-Gouni, M., 2011. Airborne algae and cyanobacteria: occurrence and related health effects. Front. Biosci. 3, 772–787 (Elite Ed).
Gobler, C.J., Doherty, O.M., Hattenrath-Lehmann, T.K., Griffith, A.W., Kang, Y., Litaker, R.W., 2017. Ocean warming since 1982 has expanded the niche of toxic algal blooms in the North Atlantic and North Pacific oceans. Proc. Natl. Acad. Sci. 114 (19), 4975–4980.
Heise, H.A., 1951. Symptoms of hay fever caused by algae. 2. *Microcystis*, another form of algae producing allergenic reactions. Ann Allergy. 9 (1), 100–101.
Issa, A.A., Abd-Alla, M.H., Ohyama, T., 2014. Nitrogen Fixing Cyanobacteria: Future Prospect (2014-01-29).
Ivleva, N.B., Golden, S.S., 2007. Protein extraction, fractionation, and purification from cyanobacteria. Methods Mol. Biol. 362, 365–373.
Johansen, J.R., Bohunická, M., Lukešová, A., Hrčková, K., Vaccarino, M.A., Chesarino, N.M., 2014. Morphological and molecular characterization within 26 strains of the genus *Cylindrospermum* (*Nostocaceae*, Cyanobacteria), with descriptions of three new species. J. Phycol. 50 (1), 187–202.
Jordan, B.R., 2004. Carbohydrate-interacting Proteins From Two *Nostoc* (Cyanobacteria) Species. Virginia Polytechnic Institute and State University, Blacksburg, VA.
Knoll, A.H., 2008. Cyanobacteria and Earth History in: The Cyanobacteria: Molecular Biology, Genomics, and Evolution. Horizon Scientific Press, Norfolk, UK.
Komárek, J., 2005. Studies on the cyanophytes (Cyanobacteria, Cyanoprokaryota) of Cuba 11. Freshwater *Anabaena* species. Preslia 77, 211–234.
Komárek, J., Komárková-Legnerová, J., 1992. Variability of some planktic gomphosphaerioid cyanoprocaryotes in northern lakes. Nord. J. Bot. 12 (5), 513–524.
Komarek, J., Kastovsky, J., Mares, J., Johansen, J.R., 2014. Taxonomic classification of cyanoprokaryotes (cyanobacterial genera) 2014, using a polyphasic approach. Preslia 86.
Ku, C.S., Pham, T.X., Park, Y., Kim, B., Shin, M.S., Kang, I., et al., 2013. Edible blue-green algae reduce the production of pro-inflammatory cytokines by inhibiting NF-kappaB pathway in macrophages and splenocytes. Biochim. Biophys. Acta 1830 (4), 2981–2988.
Kuddus, M., Singh, P., Thomas, G., Al-Hazimi, A., 2013. Recent developments in production and biotechnological applications of C-phycocyanin. Biomed. Res. Int. 2013, 742859.
Ladics, G.S., van Bilsen, J.H., Brouwer, H.M., Vogel, L., Vieths, S., Knippels, L.M., 2008. Assessment of three human FcepsilonRI-transfected RBL cell-lines for identifying IgE induced degranulation utilizing peanut-allergic patient sera and peanut protein extract. Regul. Toxicol. Pharmacol. 51 (3), 288–294.
Lang, I., Hodac, L., Friedl, T., Feussner, I., 2011. Fatty acid profiles and their distribution patterns in microalgae: a comprehensive analysis of more than 2000 strains from the *SAG* culture collection. BMC Plant Biol. 11, 124.
Lang-Yona, N., Lehahn, Y., Herut, B., Burshtein, N., Rudich, Y., 2014. Marine aerosol as a possible source for endotoxins in coastal areas. Sci. Total Environ. 499, 311–318.
Lang-Yona, N., Shuster-Meiseles, T., Mazar, Y., Yarden, O., Rudich, Y., 2016. Impact of urban air pollution on the allergenicity of *Aspergillus fumigatus conidia*: outdoor exposure study supported by laboratory experiments. Sci. Total Environ. 541, 365–371.
Le, T.-M., Knulst, A.C., Röckmann, H., 2014. Anaphylaxis to Spirulina confirmed by skin prick test with ingredients of Spirulina tablets. Food Chem. Toxicol. 74, 309–310.
Lenton, T.M., Daines, S.J., 2016. Matworld - the biogeochemical effects of early life on land. New Phytol.
de Leon, M.P., Glaspole, I.N., Drew, A.C., Rolland, J.M., O'Hehir, R.E., Suphioglu, C., 2003. Immunological analysis of allergenic cross-reactivity between peanut and tree nuts. Clin. Exp. Allergy 33 (9), 1273–1280.
Mittal, A., Agarwal, M.K., Shivpuri, D.N., 1979. Respiratory allergy to algae: clinical aspects. Ann. Allergy 42 (4), 253–256.
Morschel, E., Wehrmeyer, W., Koller, K.P., 1980. Biliprotein assembly in the disc-shaped phycobilisomes of *Rhodella violacea*. Electron microscopical and biochemical analysis of B-phycoerythrin and B-phycoerythrin–C-phycocyanin aggregates. J Cell Biol.]–>Eur. J. Cell Biol. 21 (3), 319–327.
Nozzi, N.E., Oliver, J.W.K., Atsumi, S., 2013. Cyanobacteria as a platform for biofuel production. Front. Bioeng. Biotechnol. 1, 7.
Oren, A., 2014. Cyanobacteria: biology, ecology and evolution. Cyanobacteria. John Wiley & Sons, Ltd, pp. 1–20.
Osborne, N.J.T., Webb, P.M., Shaw, G.R., 2001. The toxins of *Lyngbya majuscula* and their human and ecological health effects. Environ. Int. 27 (5), 381–392.
Petrus, M., Culerrier, R., Campistron, M., Barre, A., Rouge, P., 2010. First case report of anaphylaxis to spirulin: identification of phycocyanin as responsible allergen. Allergy 65 (7), 924–925.
Potts, M., 1997. Etymology of the genus name *Nostoc* (Cyanobacteria). Int. J. Syst. Evol. Microbiol. 47 (2), 584.
Rajashankar, K., Bufe, A., Weber, W., Eschenburg, S., Lindner, B., Betzel, C., 2002. Structure of the functional domain of the major grass-pollen allergen Phlp 5b. Acta Crystallogr. D Biol. Crystallogr. 58 (Pt 7), 1175–1181.
Rücker, J., Wiedner, C., Zippel, P., 1997. Factors controlling the dominance of *Planktothrix agardhii* and *Limnothrix redekei* in eutrophic shallow lakes. In: Kufel, L., Prejs, A., Rybak, J.I. (Eds.), Shallow Lakes '95: Trophic Cascades in Shallow Freshwater and Brackish Lakes. Springer, Dordrecht, Netherlands, pp. 107–115.
Schirmer, T., Bode, W., Huber, R., Sidler, W., Zuber, H., 1985. X-ray crystallographic structure of the light-harvesting biliprotein C-phycocyanin from the thermophilic cyanobacterium *Mastigocladus laminosus* and its resemblance to globin structures. J. Mol. Biol. 184 (2), 257–277.
Schlichting Jr., H.E., 1974. Ejection of microalgae into the air via bursting bubbles. J. Allergy Clin. Immunol. 53 (3), 185–188.
Sharma, N.K., Rai, A.K., 2008. Allergenicity of airborne cyanobacteria *Phormidium fragile* and *Nostoc muscorum*. Ecotoxicol. Environ. Saf. 69 (1), 158–162.
Sidler, W.A., 1995. Phycobilisome and phycobiliprotein structures. In: Bryant, D.A. (Ed.), Advances in Photosynthesis: The Molecular Biology of Cyanobacteria. Kluwer Academic Publisher, Tempe, Arizona, U.S.A.
Sonani, R.R., Gupta, G.D., Madamwar, D., Kumar, V., 2015. Crystal Structure of allophycocyanin from marine cyanobacterium *Phormidium* sp. A09DM. PLoS One 10 (4), e0124580.
Stewart, I., Robertson, I., Webb, P., Schluter, P., Shaw, G., 2006a. Cutaneous hypersensitivity reactions to freshwater cyanobacteria - human volunteer studies. BMC Dermatol. 6, 6.
Stewart, I., Seawright, A., Schluter, P., Shaw, G., 2006b. Primary irritant and delayed-contact hypersensitivity reactions to the freshwater cyanobacterium *Cylindrospermopsis raciborskii* and its associated toxin cylindrospermopsin. BMC Dermatol. 6 (1), 5.
Suck, R., Hagen, S., Cromwell, O., Fiebig, H., 2000. The high molecular mass allergen fraction of timothy grass pollen (*Phleum pratense*) between 50–60 kDa is comprised of two major allergens: Phl p 4 and Phl p 13. Clin. Exp. Allergy 30 (10), 1395–1402.
Torokne, A., Palovics, A., Bankine, M., 2001. Allergenic (sensitization, skin and eye irritation) effects of freshwater cyanobacteria - experimental evidence. Environ. Toxicol. 16 (6), 512–516.
Vogel, L., Lüttkopf, D., Hatahet, L., Haustein, D., Vieths, S., 2005. Development of a functional in vitro assay as a novel tool for the standardization of allergen extracts in the human system. Allergy 60 (8), 1021–1028.
Vonshak, A., 1997. Spirulina Platensis Arthrospira: Physiology, Cell-biology and Biotechnology. CRC Press, Salisbury, Wiltshire.
Whitton, B.A., 2012. Ecology of Cyanobacteria II: Their Diversity in Space and Time. Springer Science & Business Media (760 pp.).

Title: Fresh Water, Marine and Terrestrial Cyanobacteria Display Distinct Allergen Characteristics

Supplemental Material

Authors: Naama Lang-Yona[1,*], Anna Theresa Kunert[1], Lothar Vogel[2], Christopher Johannes Kampf[3,1], Iris Bellinghausen[4], Joachim Saloga[4], Anne Schink[1], Kira Ziegler[1], Kurt Lucas[1], Detlef Schuppan[5,6], Ulrich Pöschl[1], Bettina Weber[1], Janine Fröhlich-Nowoisky[1,*]

[1]Max Planck Institute for Chemistry, Multiphase Chemistry Department, Mainz, Germany.
[2]Paul-Ehrlich-Institut, Department of Allergology, Langen, Germany.
[3]Johannes Gutenberg University, Institute of Organic Chemistry, Mainz, Germany.
[4]University Medical Center of the Johannes Gutenberg University, Department of Dermatology, Mainz, Germany.
[5]University Medical Center of the Johannes Gutenberg University, Institute of Translational Immunology and Research Center for Immunotherapy.
[6]Beth Israel Deaconess Medical Center and Harvard Medical School, Boston, MA, USA

*Corresponding author: Naama Lang-Yona (n.lang-yona@mpic.de) and Janine Fröhlich-Nowoisky (j.frohlich@mpic.de)

Table of Contents

Materials and Methods

Table S1. Detailed description of specific IgE levels in different plasma samples.

Sample ID	PL 1	PL 2	PL 3	PL 4	PL 5	PL 6	PL 7	PL N1	PL N2	PL N3
Grasses										
Sweet Vernal Grass	a	a	>100	a	a	a	c	b	b	b
Bermuda Grass	41.0	5.9	89.0	a	a	a	c	b	b	b
Orchard Grass	a	a	>100	a	a	a	c	b	b	b
Meadow Fescue	a	a	>100	a	a	a	c	b	b	b
Perennial Rye Grass	a	a	>100	a	a	a	c	b	b	b
Timothy Grass	>100	90.2	>100	77.8	43.0	20.7	23.7	b	b	b
Common Reed Grass	77.5	15.8	>100	a	a	0.7	c	b	b	b
Meadow Grass (Kentucky Blue)	a	a	>100	a	a	a	c	b	b	b
Red Top	a	a	>100	a	a	a	c	b	b	b
Johnson Grass	63.1	13.4	93.0	a	a	a	c	b	b	b
Brome Grass	a	a	>100	a	a	a	c	b	b	b
Cultivated Rye Grass	a	a	>100	a	a	a	c	b	b	b
Velvet Grass	a	a	>100	a	a	a	c	b	b	b
Cultivated Oat Grass	a	a	>100	a	a	a	c	b	b	b
Cultivated Wheat Grass	a	a	>100	a	a	a	c	b	b	b
Meadow Foxtail Grass	a	a	>100	a	a	a	c	b	b	b
Trees										
Box-elder (Maple)	9.6	4.6	25.1	a	a	a	c	b	b	b
Grey Alder	>100	43.0	6.1	a	a	a	c	b	b	b
Silver Birch	>100	37.2	12.0	>100	5.0	83.0	>100	b	b	b
Hazel	58.9	24.5	12.0	a	a	a	c	b	b	b
American Beech	78.5	26.1	24.8	a	a	a	c	b	b	b
Mountain Juniper (Cedar)	10.2	2.7	13.9	a	a	a	c	b	b	b
Oak	25.0	21.0	25.2	a	a	a	c	b	b	b
Elm	31.7	6.7	23.1	a	a	a	c	b	b	b
Olive	24.3	10.1	32.3	a	3.5	a	c	b	b	b
Walnut	24.7	9.4	24.1	a	a	a	c	b	b	b
Maple Leaf Sycamore, London Plane	33.5	4.2	28.3	a	a	a	c	b	b	b
Willow	14.6	5.8	23.6	a	a	a	c	b	b	b
Cottonwood	15.6	3.3	22.3	a	a	a	c	b	b	b
White Ash	42.7	16.9	24.3	a	a	a	c	b	b	b
White Pine	4.0	1.4	19.9	a	a	a	c	b	b	b
Japanese Cedar	16.6	1.9	20.4	a	a	a	c	b	b	b
Pecan, Hickory	10.3	7.8	20.4	a	a	a	c	b	b	b
Italian/Funeral Cypress	9.4	2.4	15.0	a	a	a	c	b	b	b
Food										
Egg White	0.9	2.7	a	32.2	5.4	b	c	b	b	b
Milk	1.3	0.4	a	a	2.3	a	c	b	b	b
Codfish	68.4	26.5	a	a	b	a	c	b	b	b
Wheat	20.4	1.8	31.8	a	a	a	c	b	b	b
Rye	19.9	2.2	28.4	a	a	a	c	b	b	b
Barley	22.2	2.0	27.5	a	a	a	c	b	b	b
Oat	18.0	4.5	21.4	a	a	a	c	b	b	b
Corn	20.9	1.6	16.2	10.9	a	a	c	b	b	b
Rice	21.4	2.4	27.4	a	a	a	c	b	b	b
Sesame Seed	59.6	8.1	27.0	a	a	a	c	b	b	b

Buckwheat	6.5	2.7	26.7	a	a	a	c	b	b	b
Green Pea	3.8	1.7	11.9	a	a	a	c	b	b	b
Peanut	8.7	a	30.9	>100	2.9	a	c	b	b	b
Soybean	10.1	2.9	21.5	15.2	0.4	1.2	c	b	b	b
White Bean	9.1	0.9	21.7	a	a	a	c	b	b	b
Hazelnut	>100	29.3	20.6	>100	b	a	68.1	b	b	b
Brazil Nut	3.8	1.1	9.9	>100	a	a	c	b	b	b
Almond	4.5	6.3	21.6	57.9	a	a	c	b	b	b
Crab	28.2	5.0	9.2	>100	a	a	c	b	b	b
Shrimp	66.2	17.4	0.9	>100	9.3	a	c	b	b	b
Tomato	23.5	4.3	25.0	a	a	a	c	b	b	b
Pork	3.3	1.9	a	22.3	a	a	c	b	b	b
Beef	0.4	b	a	a	a	a	c	b	b	b
Carrot	20.0	4.7	25.2	a	a	a	c	b	b	b
Orange	20.1	1.9	18.8	a	a	a	c	b	b	b
Potato	19.8	1.9	27.5	a	a	a	c	b	b	b
Coconut	5.7	1.3	13.5	8.1	a	a	c	b	b	b
Blue Mussel	8.2	0.5	0.7	51.0	a	a	c	b	b	b
Tuna	11.4	7.9	a	2.2	a	a	c	b	b	b
Salmon	44.6	25.9	a	a	a	a	c	b	b	b
Strawberry	5.5	4.5	21.1	a	a	a	c	b	b	b
Baker's Yeast	34.8	5.4	1.1	a	a	a	c	b	b	b
Garlic	24.7	3.1	32.3	a	a	a	c	b	b	b
Onion	15.0	4.1	27.9	a	a	a	c	b	b	b
Apple	6.2	11.5	15.7	a	a	a	c	b	b	b
Egg Yolk	0.4	1.3	a	a	a	a	c	b	b	b
Chicken Meat	0.6	0.5	a	50.2	a	a	c	b	b	b
Weeds										
Common Ragweed	26.9	5.3	28.5	14.7	1.9	0.7	c	b	b	b
Western Ragweed	18.1	3.6	28.9	a	a	a	c	b	b	b
Giant Ragweed	17.9	6.6	28.3	a	a	a	c	b	b	b
Wormwood	27.8	3.3	23.8	a	a	a	c	b	b	b
Mugwort	16.8	2.8	22.5	a	b	a	c	b	b	b
Ox-Eye Daisy	10.1	3.4	24.3	a	a	a	c	b	b	b
Dandelion	11.8	2.6	21.4	a	a	a	c	b	b	b
English Plantain	32.9	4.1	26.1	a	a	a	c	b	b	b
Lamb's Quarter	11.0	6.0	27.0	a	a	a	c	b	b	b
Russian Thistle	15.3	9.4	28.6	a	a	a	c	b	b	b
Goldenrod	a	3.1	25.3	a	a	a	c	b	b	b
Cocklebur	24.3	5.2	30.0	a	a	a	c	b	b	b
Common Pigweed	9.67	10.0	25.5	a	a	a	c	b	b	b
Scale, Lenscale	14.4	3.0	27.1	a	a	a	c	b	b	b
Sheep Sorrel	11.1	3.9	37.8	a	a	a	c	b	b	b
Wall Pellitory (Parietaria officinalis)	7.5	6.0	28.0	a	a	a	c	b	b	b
Nettle	6.7	6.0	33.0	a	a	a	c	b	b	b
Parietaria judaica	11.0	4.4	28.8	a	2.4	a	c	b	b	b
Animals										
Cat Dander Epithelium	40.4	28.5	3.3	>100	62.1	2.8	c	b	b	b
Dog Epithelium	a	a	a	a	a	1.3	c	b	b	b
Horse Dander	35.1	14.4	a	a	14.7	a	c	b	b	b
Cow Dander	5.4	10.2	1.2	a	30.1	a	c	b	b	b
Dog Dander	17.9	92.5	2.7	>100	>100	a	c	b	b	b
Guinea Pig Epithelium	5.8	7.1	a	a	7.8	a	c	b	b	b
Pigeon Droppings	9.5	4.9	0.9	a	3.7	a	c	b	b	b
Molds										
Penicillium notatum	2.1	3.0	1.0	a	a	a	c	b	b	b

Cladosporium herbarum	4.9	60.5	0.8	40.2	a	a	c	b	b	b
Aspergillus fumigatus	21.6	13.1	3.5	32.1	10.2	b	c	b	b	b
Mucor racemosus	4.2	2.7	1.5	14.3	a	a	c	b	b	b
Candida albicans	22.7	11.8	5.3	65.4	a	a	c	b	b	b
Alternaria tenuis	3.9	10.7	8.5	16.9	5.0	b	c	b	b	b
Botrytis cinerea	14.2	5.1	2.6	23.6	a	a	c	b	b	b
Setomelanomma rostrata	21.2	12.7	11.8	42.3	a	a	c	b	b	b
Fusarium prolieratum	37.1	8.6	2.4	24.2	a	a	c	b	b	b
Stemphylium herbarum	2.5	8.7	10.7	a	a	a	c	b	b	b
Rhizopus nigricans	14.0	5.7	2.4	27.2	a	a	c	b	b	b
Aureobasidium pullulans	16.5	9.9	2.6	a	a	a	c	b	b	b
Phoma betae	33.0	6.7	15.8	a	a	a	c	b	b	b
Epicoccum purpurascens	10.5	9.7	20.9	a	a	a	c	b	b	b
Trivchoderma viride	6.5	5.0	a	a	a	a	c	b	b	b
Curvularia lunata	2.4	4.2	8.6	a	a	a	c	b	b	b
Insects										
Honey Bee Venom	2.4	b	25.7	a	a	c	c	c	c	c
White-faced Hornet	3.0	0.4	16.8	a	a	c	c	c	c	c
Yellow Jacket Venom	3.7	0.4	11.5	a	a	c	c	c	c	c
Paper Wasp Venom	3.5	0.6	1.1	a	a	c	c	c	c	c
Cockroach	24.2	12.3	14.3	a	1.1	c	c	c	c	c
Mites										
Dermatophagoides pteronyssinus	81.0	31.5	0.7	>100	>100	22	c	b	b	b
Dermatophagoides farinae	70.6	36.8	0.9	a	a	a	c	b	b	b
Dermatophagoides microceras	a	a	2.4	a	a	a	c	b	b	b

a Not detected
b <0.35 kU L^{-1}
c No information available

Mass spectrometry analysis

In parallel to immunostaining, proteins corresponding to the immunoblot bands were detected by staining gel with Coomassie brilliant blue R-250 (Sigma-Aldrich, Darmstadt, Germany). The bands were cut from the SDS-PAGE gel for mass spectrometry (MS) analysis as described previously (1). In short, protein-containing gel pieces were destained, dehydrated and dried. Disulfide bonds were reduced and alkylated. After an additional dehydrating step, proteins were digested with trypsin at 37°C overnight. Peptides were loaded onto a self-prepared C18-layered StageTip (2), washed with 50 mM ABC, 0.1% formic acid (Merck, Darmstadt, Germany), and eluted with 30 µL of 80% ACN, 0.1% formic acid.

For MS analysis of the peptides, samples were injected into a nano-UHPLC (EASY-nLC 1000, Thermo Fisher Scientific, Darmstadt, Germany), with an autosampler and loaded onto a 25 cm capillary (75 µm inner diameter; New Objective, MA, USA) packed in-house with Reprosil C18-AQ 1.9 m resin (Dr. Maisch GmbH, Ammerbuch-Entringen, Germany) for reversed-phase chromatography. Peptide elution from the column was conducted using a 28 min gradient from 2 to 40% ACN with 0.1% formic acid at a flow rate of 250 nL min^{-1}, and the chromatography was stabilized with a 40°C column oven set-up (Sonation, Biberach, Germany).

The processing of the raw files (listed in Table S1) was performed using MaxQuant (version 1.5.2.8) and compared to a subset of the Uniprot database (www.uniprot.org, downloaded on June 27, 2016) using the Andromeda search engine (3) integrated into MaxQuant. Proteins were identified with at least two peptides, based on unmodified unique and razor peptides.

Phycocyanin ELISA

To measure the concentration of phycocyanin in cyanobacterial extracts, we used a similar procedure as in IgE ELISA with some modifications. In short, plates were coated (90% efficiency) with cyanobacterial extracts at a protein concentration of 10 µg mL^{-1} in carbonate buffer. Wells reserved for standards were coated with polyclonal rabbit anti-phycocyanin (BYT-ORB10452, Biorbyt) at a concentration of 10 µg mL^{-1} in carbonate buffer. After blocking, C-PC standard serial dilutions (0.244 - 250 ng mL^{-1}) in 1% BSA-PBS-T, as well as buffer blank, were dispensed to the corresponding wells. Cyanobacteria and pollen extracts (diluted with 1% BSA-PBS-T) were added to the remaining wells with three dilutions per extract (5, 25 and 125 µg mL^{-1}) and incubated at room temperature for 2 h. Bound phycocyanin was detected with HRP conjugated rabbit anti-

phycocyanin antibody (diluted 1:100,000 in 1% BSA-PBS-T) and the experiment was proceeded as described above. Results are reported in ng mL^{-1} of protein extract, as calculated from the linear phase of the dilution to OD curves.

Cell culture growth conditions

Human monocytic THP-1 cells (ATCC code TIB-202; LGC Standards GmbH, Wesel, Germany) were grown in RPMI 1640 medium containing 25 mM D-glucose, 10 mM HEPES, 2 mM L-glutamine, 18 mM sodium bicarbonate, 1 mM sodium pyruvate (Thermo Fisher Scientific, Darmstadt, Germany) supplemented with 10% heat-inactivated fetal calf serum (FCS; Biochrom, Berlin, Germany), 1% penicillin/streptomycin (Thermo Fisher Scientific) and 0.05 mM β-mercaptoethanol (Sigma Aldrich) in a humidified atmosphere of 5% CO_2 at 37°C.

HeLa Toll-like receptor (TLR) 4 reporter cells (Novusbio, Wiesbaden, Germany) were stably transfected with a plasmid for constitutive firefly luciferase expression (pCMB-firefly-luc-hygro, provided by courtesy of Ernst Otto Bockamp, University Medical Center of the Johannes Gutenberg University, Mainz, Germany) by using Lipofectamine 3000 (Thermo Fisher Scientific) following the manufacturer's protocol. The cells were grown in Dulbecco's Modified Eagle's Medium (Thermo Fisher Scientific) containing 25 mM D-glucose, 1 mM sodium pyruvate supplemented with 10% FCS (heat-inactivated) and 1% penicillin/streptomycin, in a humidified atmosphere of 5% CO_2 at 37°C.

TLR4 activation assays

a. Anti-inflammatory activity

The anti-inflammatory abilities of the eight cyanobacteria species were examined by detecting IL-8 levels in the THP-1 cell line. Four x 10^4 THP-1 monocytes were seeded in 100 µL culture medium per well in V-shaped 96-well plates. Cells were incubated at 37°C for 1 h followed by incubation with cyanobacteria at two concentrations for 2 h. Afterwards, the inflammatory signal was induced by 50 ng mL^{-1} lipopolysaccharide (LPS; from *E. coli* O111:B4, Invivogen, San Diego, CA, USA) for 4 h. Incubation with PBS was used as negative control, and 50 ng mL^{-1} LPS served as positive control. The cell supernatant was collected for ELISA and the cells were washed with culture medium before performing Alamar Blue Assay (Thermo Fisher Scientific) to detect cell viability. Human IL-8 protein concentrations in the cell supernatant were measured using the

Human IL-8 ELISA Set (BD Biosciences, San Diego, CA, USA) following the manufacturer's protocol. The supernatant was diluted 6-fold for the measurement. The absorbance was measured using a microplate reader (Synergy Neo, Biotek, Bad Friedrichshall, Germany) at 450 nm. Cell viability was determined by the Alamar Blue assay measuring the fluorescence signal with a microplate reader (Synergy Neo, Biotek) with an excitation wavelength of 560 nm and an emission wavelength of 590 nm.

b. Inflammatory reactivity

Pro-inflammatory potential of seven cyanobacteria species (except *Phormidium* sp.) was tested using the HeLa TLR4 reporter cell-line. The IL-8 dependent renilla luciferase expression was measured in the HeLa TLR4 reporter cell lysate. Two x 10^4 cells per well were seeded in a flat bottom 96-well plate (Greiner, Frickenhausen, Germany) containing 100 µL culture medium and incubated overnight. Next, the cells were treated with different concentrations of cyanobacteria (1-50 µg mL^{-1}), LPS (25 ng mL^{-1}) as positive control or PBS buffer as negative control for 7 h, followed by a washing step with PBS containing calcium and magnesium (Thermo Fisher Scientific). Lysis of cells was conducted using 10 µL of passive lysis buffer (PLB, Promega, Mannheim, Germany), after which cells were stored at -80°C overnight. Analysis of reporter gene activities in cell lysate was performed using a dual-luciferase reporter assay (Promega) according to the manufacturer´s manual. The luminescence was measured on a plate reader (Synergy Neo). The relative luciferase activity was calculated by normalizing each sample's renilla luciferase activity (i.e., TLR4 activation) against the constitutive firefly activity (i.e., viability) measured within the same sample. For data analysis, the value of the negative control (PBS-treated) was set to 1 and other values were scaled accordingly.

Results

Table S2: Uniprot tremble database subsets used for MS protein identification

Name	Entries
uniprot-Anabaena.fasta	32527
uniprot-cylindrospermum.fasta	6288
uniprot-Lyngbya.fasta	26216
uniprot-Microcystis.fasta	98050
uniprot-Nostoc.fasta	40298
uniprot-Phormidium.fasta	8372
uniprot-Planktothrix.fasta	8500

Table S3: Mass spectrometry protein identification for cyanobacterial IgE-reactive bands determined by SDS-PAGE*

Tested species	Fragment size (kDa)	Candidate protein	Identified species	Sum of peptides	Unique peptides	MW (kDa)
Cylindrospermum siamensis	100	**Phycocyanin beta subunit**	*C. siamensis*	4	4	18.2
		Aconitate hydratase B	*C. stagnale*	17	17	95.6
		ATPase with chaperone activity	*C. stagnale*	12	12	91.1
		Protein translocase subunit SecA	*C. stagnale*	10	10	106.1
		Phycobilisome core-membrane linker	*C. stagnale*	8	8	126.4
		Alpha-1,4 glucan phosphorylase	*C. stagnale*	7	7	97.0
		Photosystem II CP47 reaction center	*C. stagnale*	7	7	56.7
		Phycobilisome Linker polypeptide/CpcD/allophycocyanin linker domain	*C. stagnale*	2	2	36.8
	50	**Phycocyanin beta subunit**	*C. siamensis*	5	4	18.2
		60 kDa chaperonin	*C. stagnale*	18	18	58.0
		Glutamine synthetase	*C. stagnale*	17	17	53.1
		Nucleotide sugar dehydrogenase	*C. stagnale*	11	11	49.6
		Nitrogenase protein alpha chain	*C. stagnale*	10	10	56.0
		Glucose-6-phosphate 1-dehydrogenase	*C. stagnale*	9	9	58.2
		Ribulose bisphosphate carboxylase large chain	*C. stagnale*	9	8	53.1
		Photosystem II D2	*C. stagnale*	2	2	39.3
		Phycobilisome Linker polypeptide/CpcD/allophycocyanin linker domain	*C. stagnale*	2	2	36.8
Anabaena ambigua	100	**Phycobilisome linker**	*A. cylindrica*	33	5	126.7
		Photosystem I P700 chlorophyll a apoprotein A2	*A. cylindrica*	4	4	83.1
		Allophycocyanin beta subunit	*A. sp. 90*	2	2	17.3
		UvrB/UvrC protein	*A. variabilis*	5	5	91.4
		Phycocyanin, beta subunit	*A. variabilis*	2	1	18. 4
		Aconitate hydratase B	*Anabaena* sp. wa102	11	3	94.5
	50	Glutamine synthetase	*A. cylindrica*	17	8	53.2
		Phosphoglucosamine mutase	*A. cylindrica*	14	6	51.8
		Glutamate--tRNA ligase	*A. cylindrica*	11	5	53.9
		6-phosphogluconate dehydrogenase, decarboxylating	*A. cylindrica*	5	5	52.3
		Transcription termination/antitermination protein NusA	*A. cylindrica*	4	4	48.1
		Glycogen synthase	*A. cylindrica*	9	4	54.9
		Phycobilisome linker	*A. cylindrica*	2	2	32.3
		3-octaprenyl-4hydroxybenzoate decarboxylase	*A. variabilis*	4	4	55.5
		Phycocyanin, beta subunit	*A. variabilis*	2	2	18.4
		ATP synthase subunit beta	*Anabaena* sp. 90	10	5	51.7
		ATPase domain-containing protein	*Anabaena* sp. 90	7	7	57.0
		60 kDa chaperonin	*Anabaena* sp. wa102	20	3	58.0
Lyngbya lagerheimii	100	Aldehyde-alcohol dehydrogenase	*L. aestuarii*	4	3	97.4
		Allophycocyanin alpha chain	*L. aestuarii*	2	1	17.5
		Phycobiliprotein ApcE	*L. aestuarii*	2	1	102.5
		Alanine--tRNA ligase	*L. confervoides*	4	3	96.5
		Allophycocyanin	*L. confervoides*	5	2	17.5
		Phycocyanin alpha subunit	*L. kuetzingiana*	2	2	10.2
		Photosystem II CP43	*L. sp. (strain PCC 8106)*	3	3	44.8
		Aconitate hydratase B	*Moorea producens* 3L	4	3	93.6
		Phosphoenolpyruvate synthase	*M. producens* 3L	3	3	92.6
	50	60 kDa chaperonin	*L. aestuarii*	5	5	57.9
		Ribulose bisphosphate carboxylase large chain	*L. confervoides*	18	8	52.9
		Allophycocyanin	*L. confervoides*	4	4	17.5
		Phycocyanin alpha subunit	*L. kuetzingiana*	2	2	10.2
		ATPase of the AAA+ class	*M. producens* 3L	5	5	57.8

Tested species	Fragment size (kDa)	Candidate protein	Identified species	Sum of peptides	Unique peptides	MW (kDa)
Planktothrix agardii	100	Clp protease ATP binding subunit	*P. agardhii*	16	11	91.6
		Aldehyde-alcohol dehydrogenase	*P. agardhii*	7	7	97.7
		ApnB	*P. agardhii*	7	5	123.5
		Alpha-1,4 glucan phosphorylase	*P. agardhii*	5	5	97.1
		Leucine--tRNA ligase	*P. agardhii*	5	5	97.5
		1-pyrroline-5 carboxylate dehydrogenase	*P. agardhii*	4	4	111.2
		ATPase, E1-E2 type	*P. agardhii*	4	4	102.1
		Isoleucine--tRNA ligase	*P. agardhii*	3	3	112.1
		Phycobiliprotein (ApcE)	*P. agardhii*	2	2	104.8
		Photosystem II CP47 reaction center	*P. agardhii*	2	2	56.5
	80	Clp protease ATP binding subunit	*P. agardhii*	16	11	91.6
		Aconitate hydratase B	*P. agardhii*	5	5	89.8
		Photosystem I P700 chlorophyll a apoprotein A2	*P. agardhii*	3	3	83.0
		Photosystem I P700 chlorophyll a apoprotein A1	*P. agardhii*	2	2	83.1
		Bile acid beta-glucosidase	*P. agardhii*	2	2	94.0
		ClpC	*P. agardhii*	2	2	87.1
		Photosystem II D2	*P. agardhii*	2	2	41.9
	50	60 kDa chaperonin	*P. agardhii*	11	11	58.2
		Ribulose bisphosphate carboxylase large chain	*P. agardhii*	8	6	53.2
		ATP synthase subunit beta	*P. agardhii*	4	4	51.8
		D-3-phosphoglycerate dehydrogenase	*P. agardhii*	3	3	56.5
		Photosystem II D2	*P. agardhii*	2	2	41.9
		Photosystem II CP43 reaction center	*P. agardhii*	2	2	53.5
***Phormidium* sp.**	50	**Phycoerythrin Beta subunit**	*P. rubidum*	5	5	18.5
		Phycoerythrin Alpha subunit	*P. rubidum*	4	4	17.2
		Allophycocyanin	*P. rubidum*	4	4	16.8
		Allophycocyanin	*P. rubidum*	4	3	16.6
		ATP synthase subunit beta	*P. willei*	4	4	52.3
		ATP synthase subunit alpha	*P. willei*	3	3	54.5
		Ribulose bisphosphate carboxylase large chain	*Phormidium* sp. OSCR	4	4	57.1
		Phycocyanin alpha subunit CpcA	*Phormidium* sp. OSCR	3	2	17.6
***Nostoc* sp.**	110	**Phycobilisome linker polypeptide ApcE**	*N. punctiforme*	26	9	126.2
		DNA-directed RNA polymerase subunit beta	*N. punctiforme*	8	5	123.2
		Carbamoyl-phosphate synthase (glutamine-hydrolyzing)	*N. punctiforme*	5	5	119.2
		Protein translocase subunit SecA	*N. punctiforme*	15	4	106.1
		Putative delta-1-pyrroline-5-carboxylate dehydrogenase	*N. punctiforme*	10	4	109.4
		Phycocyanin, alpha subunit PcyA	*N. punctiforme*	3	3	17.6
		Phycobilisome linker polypeptide CpcC	*N. punctiforme*	2	2	32.0
		Phycocyanin, beta subunit	*Nostoc* sp. (ATCC 29411/PCC 7524)	2	2	18.4
		Phycobilisome protein	*Nostoc* sp. NIES-3756	4	2	126.9
		All3041 protein	*Nostoc* sp. PCC 7107	2	1	116.2
		All3041 protein	*Nostoc* sp. PCC 7107	2	1	116.2
		Allophycocyanin beta subunit	*Nostoc* sp. PCC 7107	2	1	17.3
	50	Peptidase U62	*N. flagelliforme*	10	10	53.3
		6-phosphogluconate dehydrogenase, decarboxylating	*N. punctiforme*	12	12	52.2
		S-adenosylmethionine synthase	*N. punctiforme*	9	9	45.7
		Aldehyde dehydrogenase	*N. punctiforme*	7	6	49.2
		Alpha amylase, catalytic region	*N. punctiforme*	9	5	55.6
		Adenylosuccinate synthetase	*N. punctiforme*	9	5	49.2
		Phycocyanin, alpha subunit PcyA	*N. punctiforme*	2	2	17.6
		Asparagine--tRNA ligase	*Nostoc* sp. (ATCC 29411/PCC 7524)	5	5	52.8
		Photosystem II CP47 reaction center	*Nostoc* sp. (ATCC 29411/PCC 7524)	3	3	56.3
		Long-chain-fatty-acid--CoA ligase	*Nostoc* sp. PCC 7107	4	4	54.9

Tested species	Fragment size (kDa)	Candidate protein	Identified species	Sum of peptides	Unique peptides	MW (kDa)
Mycrocystis aeroginosa	100	**Phycobiliprotein ApcE**	*M. aeruginosa*	40	40	100.9
		DNA-directed RNA polymerase subunit beta	*M. aeruginosa*	30	30	123.9
		Protein translocase subunit SecA	*M. aeruginosa*	26	26	107.3
		HlyB protein	*M. aeruginosa*	20	20	112.4
		Delta-1-pyrroline-5-carboxylate dehydrogenase, putative	*M. aeruginosa*	19	19	109.8
		Glycine dehydrogenase (decarboxylating)	*M. aeruginosa*	16	16	108.6
		Isoleucine-tRNA ligase	*M. aeruginosa*	16	16	107.8
		Genome sequencing data, contig C283	*M. aeruginosa*	12	12	118.9
		UvrABC system protein A	*M. aeruginosa*	12	12	106.3
		Photosystem II CP43 reaction center protein	*M. aeruginosa*	9	9	50.2
		C-phycocyanin beta chain	*M. aeruginosa*	6	6	18.2
		Multidrug transporter MdtC	*M. aeruginosa*	6	6	109.5
		Phycobilisome core-membrane linker	*M. aeruginosa*	7	7	101.06
		phycocyanin alpha subunit	*M. aeruginosa*	5	5	10.0
		Phycobilisome 32.1 kDa linker	*M. aeruginosa*	5	5	32.2
		Phycobilisome rod-core linker	*M. aeruginosa*	4	4	28.7
		Patatin-related protein	*M. aeruginosa*	36	2	116.5
		Allophycocyanin beta chain	*M. aeruginosa*	2	2	17.1
	80	Aconitate hydratase B	*M. aeruginosa*	18	18	93.7
		Photosystem I P700 chlorophyll a apoprotein	*M. aeruginosa*	13	13	82.4
		Negative regulator of genetic competence ClpC/MecB	*M. aeruginosa*	17	12	91.4
		Photosystem I P700 chlorophyll a apoprotein A1	*M. aeruginosa*	11	11	82.5
		1,4-alpha-glucan branching enzyme GlgB	*M. aeruginosa*	9	9	88.1
		Alpha-1,4 glucan phosphorylase	*M. aeruginosa*	24	8	96.5
		Phosphoenolpyruvate synthase	*M. aeruginosa*	8	8	89.9
		Cyanophycin synthetase	*M. aeruginosa*	7	7	95.1
		DNA gyrase subunit A	*M. aeruginosa*	6	6	94.3
	30	ATP synthase subunit beta	*M. aeruginosa*	34	34	51.7
		Phycobiliprotein ApcE	*M. aeruginosa*	25	25	100.9
		ATP synthase subunit alpha	*M. aeruginosa*	25	25	54.0
		Glutamine synthetase	*M. aeruginosa*	26	23	53.0
		4-alpha-glucanotransferase	*M. aeruginosa*	21	21	56.8
		Ribulose bisphosphate carboxylase large chain	*M. aeruginosa*	32	20	52.4
		60 kDa chaperonin	*M. aeruginosa*	19	19	57.6
		Glycogen synthase	*M. aeruginosa*	17	17	54.6
		Ferredoxin--nitrite reductase	*M. aeruginosa*	15	15	57.0
		C-phycocyanin beta chain	*M. aeruginosa*	7	7	18.2
		C-phycocyanin alpha chain	*M. aeruginosa*	7	7	17.5
		Phycobilisome 32.1 kDa linker	*M. aeruginosa*	5	5	32.2
		Allophycocyanin alpha chain	*M. aeruginosa*	3	3	17.4
		Photosystem II CP47 reaction center	*M. aeruginosa*	3	3	51.9
		Photosystem II D2 domain	*M. aeruginosa*	2	2	9.3
		Allophycocyanin beta chain	*M. aeruginosa*	2	2	17.1
		Photosystem II CP43 reaction center	*M. aeruginosa*	2	2	50.2
		Phycobilisome rod-core linker	*M. aeruginosa*	2	2	28.7

* Proteins in bold indicate candidate phycocyanin-related proteins

Table S4: Comparison of IgE-binding* and phycocyanin protein bands detected from different cyanobacterial taxa.**

	IgE-binding bands (kDa)	Phycocyanin bands (kDa)
M. aeruginosa	30, 37, **80**, **110**	20, 23, 45, 50, **80**, **110**
C. siamensis	20, **23**, 30, 37, **110**	**23**, 25, 50, **110**
A. ambigua	20, 50, 80, **110**	**110**
L. lagerheimii	50, 60, 100, **110**, **160**	**110**, 150, **160**
P. agardhii	30, 37, **75**, **100**	**75**, **100**, 150, 240, 250
Synechocystis sp.	10, 25, **37, 40, 150**	**20, 37**, **40**, 50, 75, 85, 110, **150**, 160, 200, 240, 260
Phormidium sp.	**10**, **50**	**10**, 20, **50**, 150
Nostoc sp.	**15, 20**, 30, **50**, **60**, **120**	**20**, 45, **50**, **60**, 110, **120**, 160
C-PC std.	**50**, **60**	18, 21, 37, **50**, **60**, 75, 80, 90, 110
P. pratense	10, 13, 30, 50, 75	--

* Protein reaction with PL 4 as representative plasma.

** IgE-binding and phycocyanin protein bands of identical size are printed in bold letters.

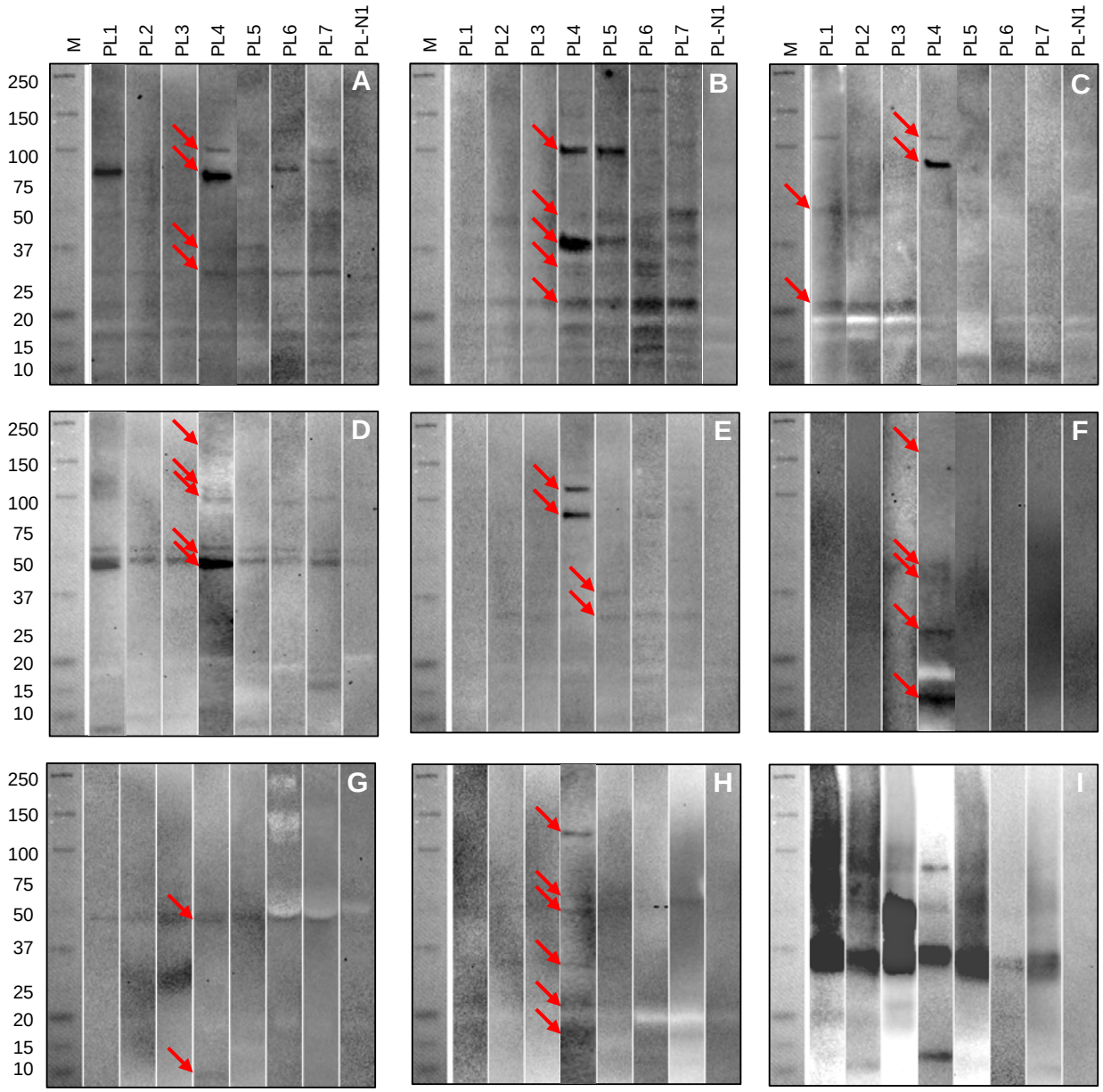

Figure S1: Western blot screen of protein extracts with tested plasma. IgE-reactive bands of *Microcystis aeruginosa* (A), *Cylindrospermum siamensis* (B), *Anabaena ambigua* (C), *Lyngbya lagerheimii* (D), *Planktothrix agardhii* (E), *Synechocystis sp.* (F), *Phormidium sp.* (G), *Nostoc sp.* (H) .and *Phleum pratense* as a positive control (I) with tested plasmas. Data are representative for three independent experimental repeats with specific plasma.

Phycocyanin content in cyanobacteria species

Additional evaluation of the phycocyanin levels in each sample was performed by quantitative ELISA presented in Figure S2. Highest levels were observed in *L. lagerheimii* and *M. aeruginosa* extracts (3272 ± 123 and 2773 ± 39 ng mL^{-1}, respectively). *C. siamensis* (997 ± 76 ng mL^{-1}), *A. ambigua* (629 ± 9 ng mL^{-1}), *P. agardhii* (643 ± 20 ng mL^{-1}) *Nostoc* sp. (988 ± 32 ng mL^{-1}) and *Phormidium* sp. (849 ± 26 ng mL^{-1}) presented intermediate levels, whereas *Synechocystis* sp. (315 ± 4) had relatively low phycocyanin levels. Negative controls included pollen extracts, KLH and PBS buffer blank, and show significantly low levels of phycocyanin.

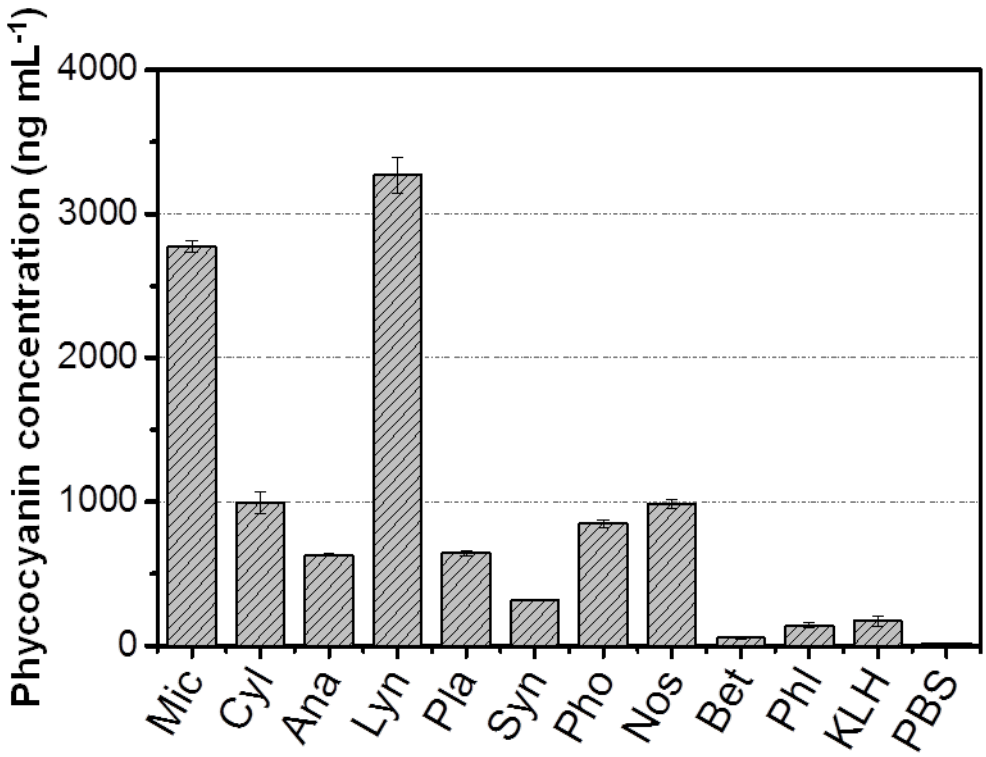

Figure S2: **Quantification of phycocyanin concentration in protein extracts**. Cyanobacteria, *P. pratense* and *Betula pendula* extracts were investigated for phycocyanin content using ELISA, detected with rabbit HRP-labeled anti-phycocyanin antibody. Values of the negative control, Keyhole limpet hemocyanin (KLH) as well as phosphate-buffered saline (PBS) as blank are also presented. Data are representative of two independent experimental repeats. Mean values of triplicates are shown, and $p < 0.01$ compared with control plasma for all samples.

Inflammation and anti-inflammation of cyanobacteria species

Cyanobacterial LPS have different effects on the immune system as compared to *Escherichia coli*-derived LPS due to structural differences in the Lipid-A components (4, 5). It was found to provoke a reduced activation of the TLR4, leading to a lower intensity of inflammation (6). Nevertheless, LPS originating from cyanobacteria can affect the innate immune system by provoking allergies or respiratory and skin diseases (7).

Antibody-driven allergy is regarded as a malfunction of the adaptive immune system (8). Nevertheless, the activation of B-cells depends on innate immune activities. One of the most prominent reactions of innate immunity is the cytokine release after TLR activation. Therefore, we investigated the effect of the cyanobacterial extracts on TLR4, a core receptor in the innate immune system. Activation of TLR4 receptor initiates the expression of various pro-inflammatory cytokines (e.g., Interleukin (IL)-8).

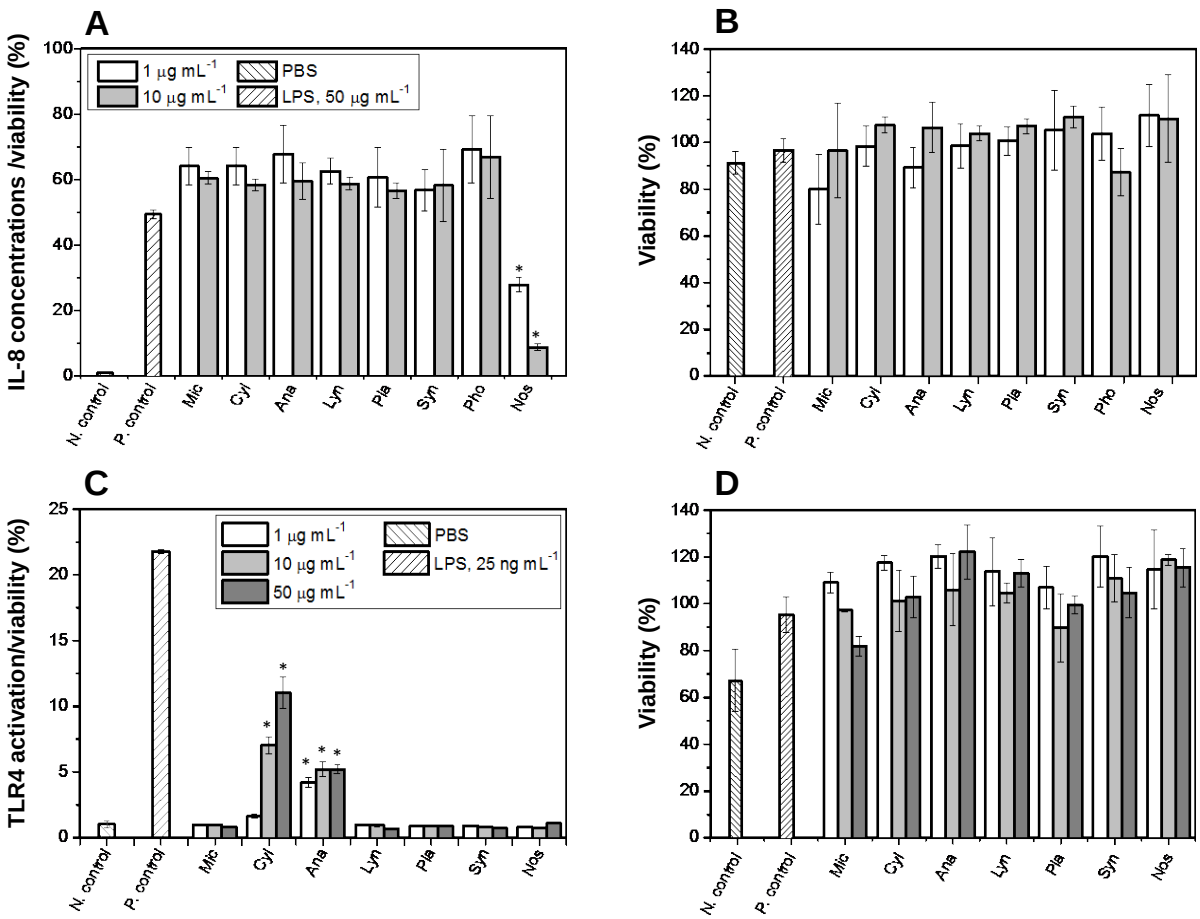

Figure S3: **TLR4 activation by cyanobacterial taxa.** The anti-inflammatory effect of cyanobacterial taxa as assessed by TLR4 activation normalized to cell viability (A,C) and cell viability (B,D) in THP-1 (A,B) and in HeLa TLR4 reporter (C,D) cells. Negative controls represent TLR4 activation of cells exposed to PBS buffer and positive controls the effect of TLR4 activation by LPS. Results are presented as mean values of triplicates with SD, indicated by error bars. Asterisks denote significantly different groups compared to the negative control.

Nostoc spp. were previously reported to possess anti-inflammatory abilities.(9-11) However, to the best of our knowledge, the data presented here are the first report of anti-inflammatory properties for the *Nostoc* sp. (SAG 70.79) used in this study.

Several studies investigated the interaction of cyanobacterial LPS with the TLR4 receptor and its abilities to block TLR4 activation, hence preventing endotoxin shock and cytokine expression (4, 12-14). But the stimulation of TLR4 by cyanobacterial extracts has not been analyzed. LPS levels in all cyanobacterial extracts were found to be high, ranging between $1.09 \times 10^5 - 9.18 \times 10^5$ EU mL^{-1}. However in TLR4-activation experiments (Fig. S1, C + D) out of seven investigated species, only *C. siamensis* and *A. ambigua* protein extracts activated TLR4. We conclude that the LPS variants from these species probably do not significantly activate TLR4 due to varying LPS structure, as was previously discussed for other cyanobacteria (5, 12). Further studies are needed to define the specific triggers of this reaction.

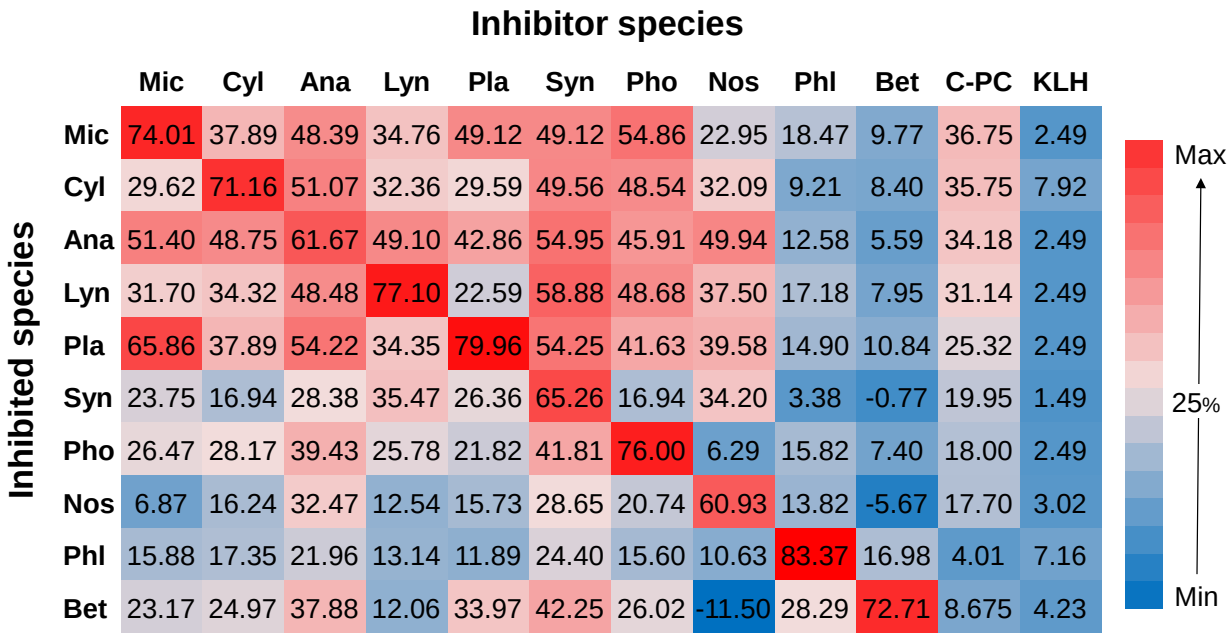

Figure S4: **Heat map of IgE-binding inhibition**. The inhibition indicated as percentages at the maximal inhibitor concentration (125 µg mL^{-1}) are summarized in color scale.

References

1. Bluhm A, Casas-Vila N, Scheibe M, Butter F. Reader interactome of epigenetic histone marks in birds. Proteomics. 2016;16(3):427-36.
2. Rappsilber J, Mann M, Ishihama Y. Protocol for micro-purification, enrichment, pre-fractionation and storage of peptides for proteomics using StageTips. Nat Protoc. 2007;2(8):1896-906.
3. Cox J, Neuhauser N, Michalski A, Scheltema RA, Olsen JV, Mann M. Andromeda: a peptide search engine integrated into the MaxQuant environment. J Proteome Res. 2011;10(4):1794-805.
4. Durai P, Batool M, Choi S. Structure and effects of cyanobacterial lipopolysaccharides. Mar Drugs. 2015;13(7):4217-30.
5. Nijland R, Hofland T, van Strijp JAG. Recognition of LPS by TLR4: potential for anti-inflammatory therapies. Mar Drugs. 2014;12(7):4260-73.
6. Hunter PR. Cyanobacterial toxins and human health. Symposium series (Society for Applied Microbiology). 1998;27:35s-40s.
7. Stewart I, Robertson I, Webb P, Schluter P, Shaw G. Cutaneous hypersensitivity reactions to freshwater cyanobacteria - human volunteer studies. BMC Dermatol. 2006;6:6.
8. Owen JA, Punt J, Stranford SA, Jones PP, Kuby J. Kuby immunology. New York: W.H. Freeman; 2013.
9. Itoh T, Tsuchida A, Muramatsu Y, Ninomiya M, Ando M, Tsukamasa Y, et al. Antimicrobial and anti-inflammatory properties of nostocionone isolated from *Nostoc commune Vauch* and its derivatives against *Propionibacterium acnes*. Anaerobe. 2014;27:56-63.
10. Kapuscik A, Hrouzek P, Kuzma M, Bartova S, Novak P, Jokela J, et al. Novel Aeruginosin-865 from *Nostoc* sp. as a potent anti-inflammatory agent. ChemBioChem. 2013;14(17):2329-37.
11. Romay C, Gonzalez R, Ledon N, Remirez D, Rimbau V. C-phycocyanin: a biliprotein with antioxidant, anti-inflammatory and neuroprotective effects. Curr Protein Pept Sci. 2003;4(3):207-16.
12. Macagno A, Molteni M, Rinaldi A, Bertoni F, Lanzavecchia A, Rossetti C, et al. A cyanobacterial LPS antagonist prevents endotoxin shock and blocks sustained TLR4 stimulation required for cytokine expression. The Journal of Experimental Medicine. 2006;203(6):1481-92.

13. Stewart IS, PJ; Shaw, GR. Cyanobacterial lipopolysaccharides and human health - a review. Environ Health. 2006;5:7.
14. Gemma S, Molteni M, Rossetti C. Lipopolysaccharides in Cyanobacteria: A Brief Overview. Advances in Microbiology. 2016;Vol.06No.05:7.